

Aalborg Universitet



Physical Modelling of Bucket Foundations Subjected to Axial Loading

Vaitkunaite, Evelina

DOI (link to publication from Publisher):
[10.5278/VBN.PHD.ENGSCI.00119](https://doi.org/10.5278/VBN.PHD.ENGSCI.00119)

Publication date:
2016

Document Version
Publisher's PDF, also known as Version of record

[Link to publication from Aalborg University](#)

Citation for published version (APA):
Vaitkunaite, E. (2016). *Physical Modelling of Bucket Foundations Subjected to Axial Loading*. Aalborg Universitetsforlag. <https://doi.org/10.5278/VBN.PHD.ENGSCI.00119>

General rights

Copyright and moral rights for the publications made accessible in the public portal are retained by the authors and/or other copyright owners and it is a condition of accessing publications that users recognise and abide by the legal requirements associated with these rights.

- Users may download and print one copy of any publication from the public portal for the purpose of private study or research.
- You may not further distribute the material or use it for any profit-making activity or commercial gain
- You may freely distribute the URL identifying the publication in the public portal -

Take down policy

If you believe that this document breaches copyright please contact us at vbn@aub.aau.dk providing details, and we will remove access to the work immediately and investigate your claim.

**PHYSICAL MODELLING OF BUCKET FOUNDATIONS
SUBJECTED TO AXIAL LOADING**

**BY
EVELINA VAITKUNAITE**

DISSERTATION SUBMITTED 2016



AALBORG UNIVERSITY
DENMARK

Physical Modelling of Bucket Foundations Subjected to Axial Loading

PhD Dissertation
Evelina Vaitkunaite

Dissertation submitted June 2016

Dissertation submitted: June 12, 2016

PhD supervisor: Prof. Lars Bo Ibsen
Aalborg University, Denmark

Assistant PhD supervisor: Assoc. Prof. Benjaminn Nordahl Nielsen
Aalborg University, Denmark

PhD committee: Associate Professor Johan Clausen (chairman)
Aalborg University, Denmark

Professor Martin Achmus
Leibniz University Hannover, Germany

Dr. Paul Doherty
Gavin & Doherty Geosolutions, Ireland

PhD Series: Faculty of Engineering and Science, Aalborg University

ISSN (online): 2246-1248
ISBN (online): 978-87-7112-726-3

Published by:
Aalborg University Press
Skjernvej 4A, 2nd floor
DK – 9220 Aalborg Ø
Phone: +45 99407140
aauf@forlag.aau.dk
forlag.aau.dk

© Copyright: Evelina Vaitkunaite

Printed in Denmark by Rosendahls, 2016

Thesis Details

Title:

Physical Modelling of Bucket Foundations Subjected to Axial Loading

PhD student:

Evelina Vaitkunaite

Supervisors:

Professor Lars Bo Ibsen

Associate Professor Benjamin Nordahl Nielsen

List of papers included in the thesis:

- Vaitkunaite, E., Ibsen, L. B., Nielsen, B. N., and Devant Molina, S. (2013). Comparison of Foundation Systems for Wave Energy Converters Wavestar. In *10th ewtec 2013 European Wave and Tidal Energy Conference Series: Proceedings of the 10th European Wave and Tidal Energy Conference, Aalborg, Denmark*. Technical Committee of the European Wave and Tidal Energy Conference. No. 10.
- Vaitkunaite, E., Nielsen, B. N., and Ibsen, L. B. (2015). Comparison of design methods for axially loaded buckets in sand. In *Frontiers in Offshore Geotechnics III proceedings of the third international symposium on frontiers in offshore geotechnics (isfog 2015), Oslo, Norway, 10-12 June 2015*. (Vol. 1, pp. 331-342). London: C R C Press LLC.
- Vaitkunaite, E., Ibsen, L. B., and Nielsen, B. N. (2014). New Medium-Scale Laboratory Testing of Bucket Foundation Capacity in Sand. In *Proceedings of the Twenty-fourth (2014) International Ocean and Polar Engineering Conference, Busan, South Korea*. (Vol. 2, pp. 514-520). International Society of Offshore and Polar Engineers.
- Vaitkunaite, E., Ibsen, L. B., and Nielsen, B. N. (2016). *Testing of Axially Loaded Bucket Foundation with Applied Overburden Pressure*. Aalborg: Department of Civil Engineering, Aalborg University. DCE Technical Reports; No. 209.

- Vaitkunaite, E., Ibsen, L. B., and Nielsen, B. N. Bucket Foundation Model Testing under Tensile Axial Loading. *Canadian Geotechnical Journal*. Submitted 14-10-2015 [cgj-2015-0497], Re-submitted 06-06-2016 [cgj-2016-0301].
- Vaitkunaite, E., Nielsen, B. N., and Ibsen, L. B. (2016) Bucket Foundation Response under Various Displacement Rates. *International Journal of Offshore and Polar Engineering*, 26(2), 116-124.
- Vaitkunaite, E. (2015). *Bucket Foundations under Axial Loading: Test Data Series 13.02.XX, 13.03.XX and 14.02.XX*. Aalborg: Department of Civil Engineering, Aalborg University. DCE Technical Reports; No. 199.

Copyright:

This thesis has been submitted for assessment in partial fulfilment of the PhD degree. The thesis is based on the submitted or published scientific papers which are listed above. Parts of the papers are used directly or indirectly in the extended summary of the thesis. As part of the assessment, co-author statements have been made available to the assessment committee and are also available at the Faculty. The thesis is not in its present form acceptable for open publication but only in limited and closed circulation as copyright may not be ensured.

Curriculum Vitae

Evelina Vaitkunaite



Higher Education

- 09/2010-06/2012 **Master of Science in Civil Engineering**
Aalborg University, Aalborg, Denmark
- 09/2006-09/2010 **Bachelor of Science in Civil Engineering**
Vilnius Gediminas Technical University, Vilnius, Lithuania

Professional Experience

- 11/2012-10/2015 **PhD Student** at the Department of Civil Engineering, Aalborg University, Aalborg, Denmark
- 04/2015-05/2015 **Guest PhD Student** at the Norwegian Geotechnical Institute, Oslo, Norway
- 08/2012-10/2012 **Research Assistant** at the Department of Civil Engineering, Aalborg University, Aalborg, Denmark

- 09/2011-06/2012 **Trainee Engineer** at Universal Foundation A/S, Aalborg, Denmark
- 07/2011-08/2011 **Soil Laboratory Assistant** at the Department of Civil Engineering, Aalborg University, Aalborg, Denmark
- 09/2007-08/2009 **Assistant of a Senior Structural Engineer** at UAB Smailiusis Skliautas, Kaunas, Lithuania

Teaching Experience

- Master level - Supervision of the 8th semester project groups in MSc Structural and Civil Engineering
- Supervision of the final project groups in MSc Structural and Civil Engineering

Scientific Publications

Journal papers

- Vaitkunaite, E., Nielsen, B. N., and Ibsen, L. B. (2016) Bucket Foundation Response under Various Displacement Rates. *International Journal of Offshore and Polar Engineering*, 26(2), 116-124.
- Vaitkunaite, E., Ibsen, L. B., and Nielsen, B. N. Bucket Foundation Model Testing under Tensile Axial Loading. *Canadian Geotechnical Journal*. Submitted 14-10-2015 [cgj-2015-0497], Re-submitted 06-06-2016 [cgj-2016-0301]

Conference papers

- Vaitkunaite, E., Nielsen, B. N., and Ibsen, L. B. (2015). Comparison of design methods for axially loaded buckets in sand. In *Frontiers in Offshore Geotechnics III proceedings of the third international symposium on frontiers in offshore geotechnics (isfog 2015), Oslo, Norway, 10-12 June 2015*. (Vol. 1, pp. 331-342). London: C R C Press LLC.
- Gaydadhiew, D.T., Puscasu, I., Vaitkunaite, E., and Ibsen, L.B. (2015). Investigation of Dense Sand Properties in Shallow Depth using CPT and DMT. In *Proceedings of the Third International Conference on the Flat Dilatometer, Rome, Italy, July 2015*. (pp. 223-230).
- Vaitkunaite, E., Ibsen, L. B., and Nielsen, B. N. (2014). New Medium-Scale Laboratory Testing of Bucket Foundation Capacity in Sand. In *Proceedings of the Twenty-fourth International Ocean and Polar Engineering Conference, Busan, South Korea*. (Vol. 2, pp. 514-520). International Society of Offshore and Polar Engineers.

- Vaitkunaite, E., Ibsen, L. B., Nielsen, B. N., and Devant Molina, S. (2013). Comparison of Foundation Systems for Wave Energy Converters Wavestar. In *10th ewtec 2013 European Wave and Tidal Energy Conference Series: Proceedings of the 10th European Wave and Tidal Energy Conference, Aalborg, Denmark*. Technical Committee of the European Wave and Tidal Energy Conference. No. 10.

Technical reports

- Vaitkunaite, E., Ibsen, L. B., and Nielsen, B. N. (2016). *Testing of Axially Loaded Bucket Foundation with Applied Overburden Pressure*. Aalborg: Department of Civil Engineering, Aalborg University. DCE Technical Reports; No. 209.
- Vaitkunaite, E., Ibsen, L.B., and Nielsen, B.N. (2015). *Bucket Foundations under Axial Loading – Test Data Series 13.02.XX, 13.03.XX and 14.02.XX*. Aalborg: Department of Civil Engineering, Aalborg University. DCE Technical Reports; No. 199.
- Vaitkunaite, E., Ibsen, L.B., and Nielsen, B.N. (2015) *Test Procedure for Axially Loaded Bucket Foundations in Sand (Large Yellow Box)*. Aalborg: Department of Civil Engineering, Aalborg University. DCE Technical Memorandum; No. 51.
- Vaitkunaite, E., Thomassen, K., Borup, K., and Nielsen, B.N. (2015). *Safety Instructions in the AAU Geotechnical Laboratory: (Large Yellow Box)*. Aalborg: Department of Civil Engineering, Aalborg University. DCE Technical Report; No. 197.
- Manzotti, E., Vaitkunaite, E., and Ibsen, L.B. (2014). *Laboratory Setup for Vertically Loaded Suction Caisson Foundation in Sand and Validation of Responses*. Aalborg: Department of Civil Engineering, Aalborg University. DCE Technical Memorandum; No. 41
- Manzotti, E., Vaitkunaite, E., and Ibsen, L.B. (2014). *Present knowledge about Laboratory Testing of Axial Loading on Suction Caissons*. Aalborg: Department of Civil Engineering, Aalborg University. DCE Technical Memorandum; No. 42
- Vaitkunaite, E., Devant Molina, S., and Ibsen, L.B. (2012). *Comparison of Calculation Models for Bucket Foundation in Sand*. Aalborg: Department of Civil Engineering, Aalborg University. DCE Technical Memorandum; No. 17.
- Devant Molina, S., Vaitkunaite, E., and Ibsen, L.B. (2012). *Concept Study of Foundation Systems for Wave Energy Converters*. Aalborg: Department of Civil Engineering, Aalborg University. DCE Technical Memorandum; No. 18.

Preface

The present thesis "Physical Modelling of Bucket Foundations Subjected to Axial Loading" is the result of a PhD study in the period November 2012 to June 2016 at the Department of Civil Engineering, Aalborg University, Aalborg, Denmark. The thesis includes introductory chapters, three conference papers, two journal papers and two reports documenting the scientific research performed during the PhD study.

My first insight of working with bucket foundation design was in Universal Foundation A/S in 2011, where I spent one year of my MSc studies. Professor Lars Bo Ibsen was the supervisor of my MSc thesis at that time. Having many years of experience developing mono-bucket foundation concept, he drew my interest to this type of foundations and, later on, gave me the opportunity to do this PhD study.

The PhD project was financially supported by the "Cost Effective Foundation and Installation of Wave Energy converters" project (No. 831052) via the ForskEl-programme. The financial support is gratefully acknowledged.

The first nine months of my PhD study were spent arranging a laboratory testing facility, learning about model testing and attending doctoral courses. The following two years were used for performing laboratory tests and analysing data. Meanwhile, I attended several conferences and participated in exciting workshops. During a short study visit to the Norwegian Geotechnical Institute in Oslo, I met inspiring engineers dedicated to their work and learned about the cyclic foundation behaviour. The final ten months were devoted to writing the thesis and the scientific papers.

Acknowledgements

I would like to thank my supervisor, Professor Lars Bo Ibsen, for his confidence in me and for giving me the opportunity to undertake this PhD study. I also wish to thank my co-supervisor, Associate Professor Benjaminn Nordahl Nielsen, for his insight and constructive guidance.

For their professional technical solutions and help during the testing programme, I would like to say *tusind tak* to the laboratory technicians at the Geotechnical Laboratory of Aalborg University. For their help and ideas in performing the tests, I thank student assistants: Elia, Tomas, Ivaylo, Ionut, Dimitar and Peter.

Furthermore, I would like to thank my PhD student colleagues for enlightening discussions and support throughout: Greta, Kristina, Emil, Søren, Aligi and Giulio.

I am grateful for the support given by my family and friends.

Finally, for being always near, encouraging and for his good sense of humour – essential during all this time – I would like to thank my husband Jaime.

Aalborg, June 2016

Evelina Vaitkunaite

Abstract

Marine renewable energy devices harvest sustainable and safe energy from everlasting sources such as wind and waves. To compete with fossil fuels, the offshore renewables must offer profitable solutions. Consequently, cost savings on foundations are desirable. Bucket foundations are a suitable and cost-effective solution for various offshore structures, and not least marine renewable devices. The present thesis focuses on the tensile axial response of bucket foundations in dense sand. The thesis addresses several critical design problems related to the tensile response. Among those are the soil-structure interface parameters, tensile loading under various displacement rates and tensile cyclic loading.

For the analysis of realistic soil-structure interactions, a physical model was designed. A new laboratory testing facility was built allowing model testing in scale of 1:10 prototype size. Furthermore, an overburden pressure was evenly applied on the sand surface for the simulation of different soil depths. Thus, higher soil stresses were created, diminishing scaling effects and providing more information about the interface parameters. Furthermore, the test set-up allowed examinations of long-term cyclic loading. Up to 40,000 harmonic load cycles were applied with constant mean loads and amplitudes. The test set-up provided high quality data about loads, displacement and pore pressure.

A different test set-up – a pressure tank – was employed for the displacement rate analysis. The pressure tank enabled the simulation of 20 m water depth, allowing for the generation of various pore pressure levels during the examinations.

The extensive testing campaign provides valuable data about bucket foundation behaviour under tensile loading. State of the art analytical methods are employed for the verification and analysis of the data. Back-calculation of the drained tensile capacity shows that the lateral earth coefficient decreases non-linearly with increasing soil depth. An interaction diagram is drawn for a summary of the cyclic loading test results. The diagram indicates the range of mean loads and amplitudes within which the foundation model remains in a stable condition. No excessive upward displacements are accumulated in the range. Finally, the displacement rate tests show that large tensile capacity is available.

Resumé

Vedvarende marine energimaskiner høster bæredygtig og sikker energi fra evige kilder som vind og bølger. For at konkurrere med de fossile brændstoffer, skal vedvarende energimaskiner tilbyde rentable løsninger. Der ønskes derfor besparelser på blandt andet fundamentterne. Bøttefundamenter er en velegnet og omkostningseffektiv løsning til forskellige havkonstruktioner, ikke mindst til de vedvarende energimaskiner. Denne afhandling fokuserer på bøttefundamenternes egenskaber i sand med en høj lejringstæthed ved aksiale trækbelastninger. Afhandlingen henvender sig til kritiske designproblemer relaterede til trækrespons. Blandt dem er parametre, der beskriver berøringsfladen mellem jord og struktur, træklast under forskellige forskydnings-hastigheder og cykliske træklaste.

For at analysere en realistisk interaktion mellem jord og struktur, var en laboratoriemodel designet. En ny forsøgsopstilling som gav mulighed for at undersøge fundamentetsmodeller i en skala på 1:10 var konstrueret, hvor en varierende overfladebelastning på sandet simulerede forskellige jorddybder. Dermed blev skabt højere jordtryk som reducerede skallerings effekterne og indhentede mere information om berøringsfladen. Endvidere tillod laboratoriestyret forsøg med lang tids cyklisk belastning. Bøttemodellen blev udsat for op til 40.000 harmoniske lastcykler med konstant middellast og lastamplitude. Forsøgsopstillingen producerede kvalitetsresultater for laster, flytninger og poretryk.

En anden forsøgsopstilling – en tryktank – blev brugt til undersøgelse af forskydnings-hastigheder. Tryktanken muliggjorde simulering af 20 m vanddybde, som tillod udviklingen af poretryk under forsøgene.

Testkampagnen giver værdifulde data om bøttefundamentets egenskaber ved trækbelastning. Nyeste analytiske metoder er anvendt for verificering og analysering af data. En genberegning af den drænedes trækcapacitet viser, at den vandrette jordtrykskoefficient falder ikkelineært med stigende jorddybde. Et interaktionsdiagram, som sammenfatter resultaterne af de cykliske forsøg, er udarbejdet. Diagrammet viser intervallet for middellaster og amplituder hvori fundamentets model forbliver i en stabil tilstand. Ingen overdrevne flytninger bliver akkumuleret i intervallet. Endelig viser forskydnings-hastighedsforsøg at stor trækcapacitet er tilgængelig.

Contents

1	Introduction	1
1.1	Research projects related to marine renewables	1
1.2	Offshore structures	2
1.3	Offshore loading conditions	3
1.4	Bucket foundations and installation	5
1.5	Overview of the thesis	6
2	Literature Review	9
2.1	The behaviour of coarse grained soils	9
2.2	Bucket foundation behaviour under various axial loading conditions .	10
2.3	Bucket foundation design methods	14
2.3.1	Design practise	14
2.3.2	Analytical expressions for tensile capacity	14
2.3.3	Finite element models (FEM)	15
2.4	Physical modelling of bucket foundations	17
2.4.1	Model size and set-up size (scaling)	18
3	Scope of the Thesis	21
3.1	Main findings of the literature review	21
3.2	Aim and objectives	22
4	Research Outcomes	25
4.1	Overview of the papers	25
4.2	Foundation solutions for the Wavestar wave energy converter	26
4.3	Current design methods for bucket foundations	29
4.4	Design of the "Large Yellow Box" test set-up	34
4.5	Tests performed in the "Large Yellow Box"	38
4.5.1	Main findings	38
4.6	Tests performed in the pressure tank	43
4.6.1	Main findings	43

5	Conclusion and future work	47
5.1	Conclusion	47
5.2	Recommendations for Future Work	49
	References	50
A	Comparison of Foundation Systems for Wave Energy Converters Waves-tar	61
B	Comparison of Design Methods for Axially Loaded Buckets in Sand	81
C	New Medium-Scale Laboratory Testing of Bucket Foundation Capacity in Sand	97
D	Testing of Axially Loaded Bucket Foundation with Applied Overburden Pressure	113
E	Bucket Foundation Model Testing under Tensile Axial Loading	141
F	Bucket Foundation Response under Various Displacement Rates	161
G	Bucket Foundations under Axial Loading – Test Data Series 13.02.XX, 13.03.XX and 14.02.XX	183

CHAPTER 1

Introduction

The current knowledge of offshore geotechnical design stems from experience gained in the offshore oil and gas sector. However, offshore areas are also of interest in the design of wind and wave energy generators. Compared to oil and gas industry structures, they are usually significantly lighter, operate in shallower waters and are subjected to severe cyclic loading and dynamic excitations. These factors result in different structural behaviours. For example, a lightweight structure supported by a tripod will transfer horizontal wind and wave loads to axial components as well as sliding and moment on each of the foundations. Due to the low structural self-weight, the foundations may be exposed to complicated loading combinations, such as cyclic tensile loading. Consequently, the geotechnical design solutions should reflect the real structural behaviour.

The wave energy sector is still experiencing challenges in providing cost competitive solutions compared to other energy sectors, such as fossil fuels and wind. However, the offshore wind energy sector is under continuous development and is able to provide knowledge of relevance to the other green energy devices fixed on the seabed. The present thesis addresses the geotechnical design of offshore foundations for lightweight structures. Cyclic tensile loading on bucket foundations is of particular interest to this research. For investigation of the realistic behaviour of foundations, physical modelling is required. This project describes a reliable modelling technique that can provide knowledge of the interaction between soil and structure.

The following sections of this chapter provide an overview of the research activities related to marine renewable energy generators. Typical offshore structures and their foundations are presented. The last section outlines the structure of the thesis.

1.1 Research projects related to marine renewables

Offshore conditions offer rich opportunities for supporting a greener and more sustainable environment by utilizing the renewable energy that can be provided by wind, waves, tides, currents and sun. At the moment, a large number of research projects

related to such renewable technologies are in progress the world over. A few of them are mentioned here. The projects generally focus on cost-effectiveness, which is essential to success in the marketplace.

A number of research and development projects related to the electricity and gas sector are financed by Energinet.dk (Energinet.dk, 2016). Through the ForskEl-programme, Energinet.dk has financed the Cost Effective Foundation and Installation of Wave Energy Converters project that was developed by three organisations: Aalborg University, Universal Foundations A/S and Wave Star A/S. Essential financial support for this PhD work has been provided by the project.

Mooring Solutions for Large Wave Energy Converters is an ongoing project which concerns cost reduction and structural solutions for the mooring systems of large floating wave energy converters. The project has seven participant organizations and is financed by the EUDP (*in Danish* Energiteknologisk udvikling og demonstration) programme. (Energiforskning.dk, 2016; DAE, 2016)

Innovative Wind Conversion Systems (10-20 MW) for Offshore Applications was an ambitious project that aimed at the design of a 20-MW wind turbine. The project included the analysis of specific technological improvements required to transform the vision of a 20-MW offshore wind turbine into reality. The five-year project involved 27 European partners. (INN WIND.EU, 2015)

The Performance Assessment of Wave and Tidal Array Systems (PerAWaT) project aimed to create software tools for wave and tidal energy device arrays and to assess production costs. The project was developed by seven organizations and financed by the Energy Technologies Institute. (ETI, 2016)

1.2 Offshore structures

The majority of the existing offshore structures were built for the oil and gas industry. Each oil/gas platform is a unique and expensive structure that requires detailed design work. Moreover, for permanently manned structures, attention must be paid to safety and physical working environment. As failure in such a structure may be fatal, the design of offshore platforms is often guided by conservatism and relatively expensive design solutions.

Offshore platforms are usually located in much deeper waters when compared to marine renewable devices. For example, the Perdido platform stands at a water depth of 2450 m, making it the world's deepest oil structure (Shell, 2016). Platforms and terminals can be moored to the seabed or fixed using various types of foundations, e.g. gravity based, pile, skirted foundations, etc. Snorre was the first TLP with multiple caisson foundations in the North Sea (Tjelta et al., 1986). Four bucket foundations were used to support the jacket structures of the Europipe 16/11E and Sleipner T

(Tjelta, 1995).

At present, more than 90% of offshore wind installations are found in the European waters (GWEC, 2016a). In 2014, about 268,000 wind turbines (onshore and offshore) were in operation the world over (GWEC, 2016b). Danish Vindeby, erected in 1991, was the first offshore wind park ever (EWEA, 2016). We are seeing a global expansion in the size and distribution of offshore wind parks. By the end of 2012, 74% of offshore wind turbines were supported by monopiles, 16% by gravity based foundations while the remaining 10% utilized other types of foundations (EWEA, 2016). The design of offshore wind turbines is constantly being improved, leading to increasingly efficient and reliable technology. The sector may currently be characterized as one of the most developed renewable energy sectors.

Wave energy is another promising source of renewable energy. Wave energy converters (WECs) can be divided into three major groups, depending on their structural properties and their method of energy extraction: point absorbers, terminators and attenuators (Jakobsen, 2015). Figure 1.1 shows three examples of WECs:

- Wavestar WECs belong in the point absorber group. Since 2009, a 1:2-scale test section of Wavestar WEC has been in operation in Hanstholm, off the west coast of Denmark (Wavestar, 2016). The structure can be lifted above the sea level during storms for protection from excessive wave loads. Its four gravity based foundations rest on a chalk seabed. A full-scale Wavestar device would be a very large structure which would require the development of a more cost-effective foundation system.
- The floating wave energy device, the Wave Dragon, is characterized as a terminator (Figure 1.1b). A prototype was launched in Denmark in 2003 (WaveDragon, 2009). The position of the device is secured through a system of cables connected to the foundations such as suction anchors.
- Attenuators are exemplified by the Pelamis (Figure 1.1c). In 2004, the first full-scale Pelamis WEC was launched, with a length of 120 m and a diameter of 3.5 m (EMEC, 2016). From a geotechnical point of view, the device requires a similar foundation solution to that of the Wave Dragon.

1.3 Offshore loading conditions

Offshore structures are subjected to structural, operational and environmental loads. Böker (2009) divided the loads into four groups based on their intensity:

- Permanent and quasi-static loads are low frequency loads that may last for hours or days; e.g. mean environmental loads.

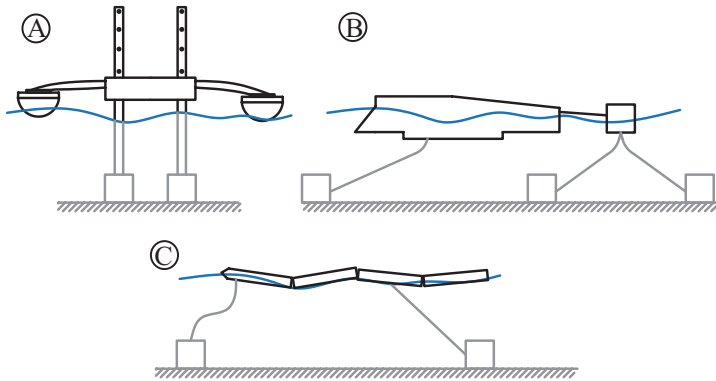


Figure 1.1 Wave energy converters: A) Wavestar (point absorber); B) Wave Dragon (terminator); C) Pelamis (attenuator).

- Cyclic loads are harmonic loads with specific load periods and amplitudes, for example wind and wave loads.
- Stochastic loads are random loads, e.g. from irregular winds.
- Transient loads are brief loads, such as loads from ship collisions and breaking waves.

Loads are transferred through the structure on to the foundation and subsequently to the soil underneath. The frequently very large and heavy oil and gas platforms are typically supported by fixed foundation systems. The large horizontal wind and wave loads to which such structures are exposed create large moment loads that are transferred in several ways: a gravity based foundation has an effective area that resists the moment load, while a system of separate foundations transfers dominating axial components to the soil. Whichever foundation type the platform is supported by, the self-weight of the upper structure results in significant compressive loads.

Offshore wind turbines are significantly lighter compared to offshore platforms. Thus, their foundations may be subjected to tensile loads. However, with sufficient spacing between them, tensile loads will rarely occur. Against such a solution speaks its high cost.

As seen in Figure 1.1, wave energy converters have various shapes and sizes. Consequently, different loading scenarios must be considered. The foundations of the three WECs shown in the figure will need to resist cyclic loadings.

Presently, there are no international standard guidelines that provide detailed instructions on how to deal with cyclic loading on offshore foundations. DNV (1992) mentions cyclic axial loading on the offshore pile foundations:

"The effects of cyclic loading on the axial pile resistance and displacement should be

considered in the design. The main objective is to determine the shear strength degradation along the pile shaft for different loading intensities." (DNV, 1992)

The evaluation of the cyclic loading is a complex task because it presupposes assessments of the cyclic degradation of soil properties and rate effects. A safe foundation design is required to ensure that the structure is able to carry all relevant loads safely and without excessive displacements.

1.4 Bucket foundations and installation

Shallow foundations with a soil-penetrating skirt are generally called skirted foundations. They are used for the support of a variety of offshore structures. Suction buckets, caissons, anchors and skirted plate foundations are synonyms for can-shaped foundations with a lid and a skirt. As shown in Figure 1.2b, the foundations may have different shapes (cylindrical, cubic, multi-shell). Offshore structures may be supported by a single or several skirted foundations (monopods or multipods). The foundations may be made of different materials, such as steel and combined concrete-steel.

Tjelta (2015) briefly describes the Trial Installation Project, which showed that bucket foundations are applicable for any type of seabed, excepting rocks and areas with large boulders in the soil volume. He warns that foundation design, installation technique and preparation for it must be performed by experienced professionals, in particular in locations characterized by stiff clay on a sandy soil (Tjelta, 2015). The author lists limitations on the application of bucket foundations, such as sandy seabed, because of the tensile resistance both in the short and the long-term and the cyclic behaviour under two-way loading.

The installation of a bucket foundation starts with the self-penetration caused by the weight of the structure. After the first 1-2 meters of skirt penetration, a hydraulic seal is created around the tip. Sea water is trapped inside the foundation and can be pumped out creating a hydrostatic pressure difference under the lid. Figure 1.2a shows the installation process, with the water being pumped out and flowing around the tip. Suction pressure may be limited by two factors: pump efficiency, which depends on water depth (cavitation pressure), and piping in sandy soil or a lift-up of soil volume in clay (Houlsby et al., 2005a).

Tjelta (1995) further discusses the geotechnical aspects of bucket foundation installation based on experiences from the Europipe 16/11E project. Houlsby and Byrne (2005a; 2005b) were the first to introduce a theoretical solution for the installation of skirted foundations in various soils. On the basis of empirical data and extensive practical experience, Andersen et al. (2008) suggest that calculations of the installation of skirted foundations need to consider bearing capacity and CPT data in dense sand.

The concept of bucket foundation design has been subjected to considerable research

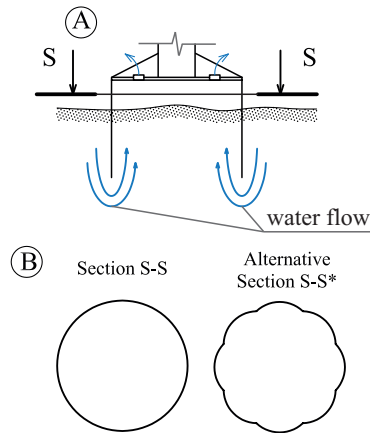


Figure 1.2 Bucket foundation: A) under installation; B) circular and multi-shell skirt section.

efforts since it was introduced by Hogervorst (1980). However, experience with this type of foundation stems mainly from the oil and gas sector where loading conditions differ from those of renewable energy structures, as mentioned in Section 1.3. Standard design guidelines are available for pile and gravity based foundations while knowledge of bucket foundation design is limited.

1.5 Overview of the thesis

Figure 1.3 sketches the usual stages in the design of a bucket foundation. The first step comprises the collection of local soil data and information on loads at the site. When a geotechnical profile has been prepared, the initial dimensioning may start. Analytical design methods are used for the estimation of diameter, skirt length and the calculation of bearing capacity and displacements. Model testing can provide useful empirical equations and clarify design issues related to atypical geotechnical structures, loads and soil-structure interaction. Having done primary geotechnical dimensioning, the suction installation and structural analyses are performed. The later design stages include design verification and scour assessment. This thesis addresses design methods relevant to the topics indicated by yellow in Figure 1.3.

The following outlines the structure of the thesis:

- Chapter 2 presents a short review of the methods developed for offshore foundation design. The division of the review reflects the topics of relevance to tensile loading on bucket foundations in sand.
- Chapter 3 indicates the scope of the thesis. This chapter defines the methods described in Chapter 2 that are used in the thesis and leads to the aim and objectives.

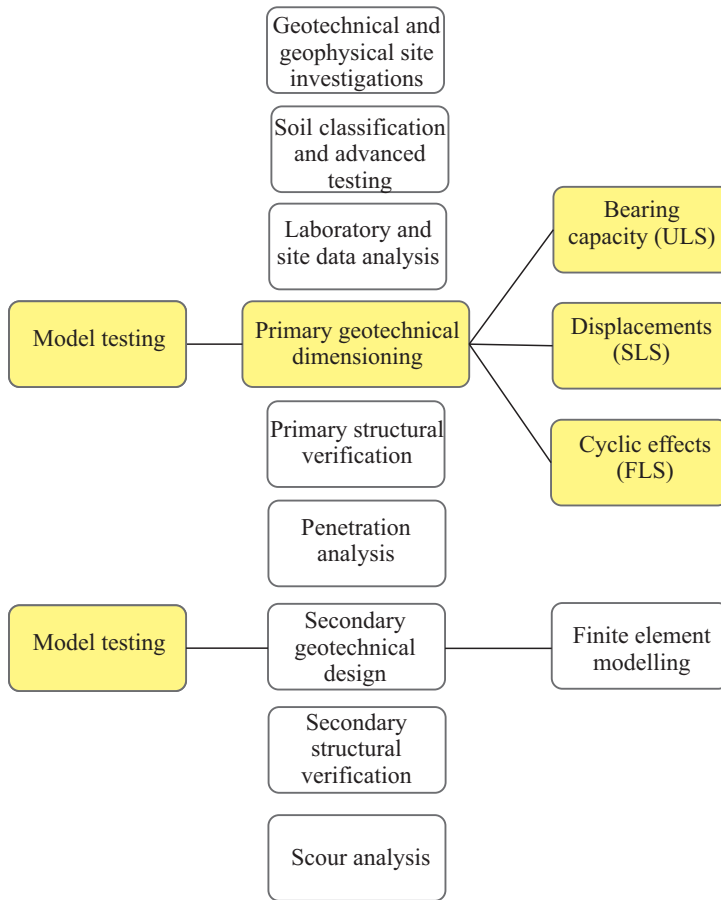


Figure 1.3 Bucket foundation design steps. Sections marked yellow are addressed in this thesis.

- Chapter 4 provides a summary of the research performed during this PhD project.
- Chapter 5 summarizes the main achievements of the work and describes the vision for future work.
- Appendix A: conference paper entitled "Comparison of Foundation Systems for Wave Energy Converters Wavestar".
- Appendix B: conference paper entitled "Comparison of Design Methods for Axially Loaded Buckets in Sand".
- Appendix C: conference paper entitled "New Medium-Scale Laboratory Testing of Bucket Foundation Capacity in Sand".

- Appendix D: technical report entitled "Testing of Axially Loaded Bucket Foundation with Applied Overburden Pressure".
- Appendix E: journal paper entitled "Bucket Foundation Model Testing under Tensile Axial Loading".
- Appendix F: journal paper entitled "Bucket Foundation Response under Various Displacement Rates".
- Appendix G: technical report entitled "Bucket Foundations under Axial Loading – Test Data Series 13.02.XX, 13.03.XX and 14.02.XX".

CHAPTER 2

Literature Review

2.1 The behaviour of coarse grained soils

Various experimental observations with skirted foundations have shown that, under rapid loading conditions, medium- to fine-grained sands do not have enough time to be drained. The drainage level depends on load rate, soil permeability, fluid viscosity and the size of the foundation structure. However, if the loading is quasi-static or static, the fluid drains in the soil. Drainage conditions are extremely important in grained soils since they affect foundation bearing capacity and settlement.

Jafarzadeh and Sadeghi (2012) performed cyclic loading tests in a simple shear apparatus with two uniformly graded sands (Babolsar sand and Toyora sand). The focus of their study was to examine dynamic soil parameters depending on the soil saturation level. The authors found that changes in saturation level significantly affect the dynamic properties of sand, e.g., soil shear modulus G is significantly reduced at saturation level above 75%. The difference in saturated and unsaturated soil shear modulus increases with the number of cycles applied. Damping Δ of loose sand increases with the soil saturation level, while damping of dense sand is nearly the same in saturated and dry soil. Jafarzadeh and Sadeghi (2012) furthermore compared the drained and undrained test results. In both conditions, G increased and Δ dropped due to the increase in the effective vertical stress.

Ibsen and Lade (1998) and Ibsen (1999) found that in static and cyclic loading conditions, the volume changes of dense sands are governed by the characteristic line which is unique for each type of sand. Dense sand behaviour changes when shifting from contraction to dilation, and vice versa. Via a triaxial testing campaign, Ibsen (1995) found that the negative pore pressure is maintained during soil failure, a fact that should be taken into consideration for the foundation design under rapid loading.

Ibsen et al. (2009) analysed test data from laboratory cone resistance tests and drained triaxial tests performed with Aalborg University sand No. 1. Sand classification properties were described by Ibsen and Boedker (1994) and Hedegaard and Borup (1993). Ibsen et al. (2009) related the laboratory cone resistance to the relative soil density. Moreover, they derived the basic soil strength and stiffness parameters, i.e., tangential

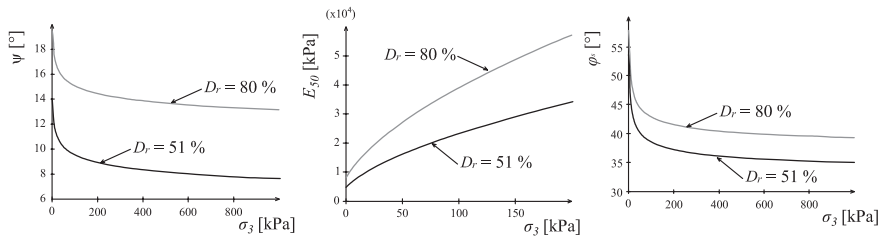


Figure 2.1 Aalborg sand No. 1 parameters dependence on the horizontal stress. Ibsen et al. 2009

φ_t and secant φ_s friction angles, tangential cohesion c_t , angle of dilation ψ and the secant Young's modulus E_{50} . Parameters φ_s and ψ decreased with the increasing horizontal stress σ_3 (especially in the range of [0; 100] kPa), while E_{50} had a tendency to increase with the increasing σ_3 (Figure 2.1).

2.2 Bucket foundation behaviour under various axial loading conditions

A bucket foundation under axial compressive loading behaves like a gravity based foundation. Thus, the usual methodology for bearing capacity and settlements is applicable. The tensile response depends on soil type, water depth and loading intensity. Section 1.3 described four load groups representing different loading intensities.

Figure 2.2 visualizes the bucket foundation response under axial tensile loading. The system acts like a syringe. The upward displacement creates a gap between the soil surface and the lid. As the pressure tends to drop under the lid, water streaming is created through the soil volume to the gap. If the displacement rate is slow enough, the water flows to the gap. But if the rate is high (transient loading), the water cannot fill the gap fast enough and negative pressure is established in the gap and the soil pores.

Permanent and quasi-static tensile loads are carried by the weight of the structure, external skirt friction and the lower of internal skirt friction or plug weight. This corresponds to the drained tensile capacity, with a magnitude of only 1% of the compressive capacity in dense sands.

Cyclic, transient and stochastic loads have higher load rates compared to quasi-static loads. If a bucket foundation is installed in a relatively fine grained soil, partially drained or undrained conditions will arise during rapid tensile loading. The drainage situation depends on several factors: drainage path (proportional to skirt length and diameter), soil hydraulic conductivity and load rate (or displacement rate).

At extremely high loading rates, there is no water flow in the pores which indicates completely undrained conditions. The undrained tensile capacity is a result of external skirt friction and end bearing capacity. The upper limit for the undrained tensile capacity is estimated by the multiplication of the negative pressure under the lid and the inner area of the lid. The negative pressure is limited by water cavitation pressure, that is, water depth.

Deng and Carter (2002) suggested three analytical design models for pull-out capacities under drained, partially drained and undrained conditions in cohesive soils. Accordingly, three different failure modes were given (Figure 2.3): sliding (failure around the internal and external skirt walls), bottom resistance (soil plug plus external wall friction) and reverse bearing capacity (plus external wall friction).

Senders (2009) described two extremes in the theoretical pull-out capacities for bucket foundations in cohesionless soils (Figure 2.4): pure frictional resistance (failure around the internal and external skirt walls), and reverse bearing capacity (corresponding to fully undrained loading). The latter capacity is significantly higher than the first one, but the real foundation response appears to lie somewhere in between of the two limits.

As for any other embedded geotechnical structure, soil-structure interface characteristics are very important for bucket foundation design. Frictional resistance is developed in a narrow contact zone between the structure, e.g. a bucket foundation skirt, and soil. This narrow zone has different properties compared to the rest of the soil body. For granular materials, the interface conditions are dependent on grain size, relative density, relative roughness of the structure (skirt), soil stress conditions, etc.

Under shear loading, granular materials can contract or expand, behaviours that are very important for the interface zone. If dense sand is sheared in the interface, the dilation of grains will increase normal interface stress, resulting in higher frictional response. The behaviour is diminished in higher stress conditions (deeper soil) where the frictional response is more constant. (Boulon and Foray, 1986)

The Coulomb failure criterion for the estimation of friction, such as pile shaft resistance is as follows:

$$\tau = K\sigma'_v \tan\delta, \quad (2.1)$$

Where τ is frictional response, K is earth pressure coefficient relating the effective vertical stress σ'_v to the effective horizontal stress σ'_h and δ is the interface friction angle.

API (2011) provides that δ correlates with the mean particle diameter d_{50} and has an upper limit of 28.8° . δ may be assessed through advanced laboratory tests. Otherwise, API (2011) suggests a product of $K \tan\delta$ that ranges from 0.29 for medium

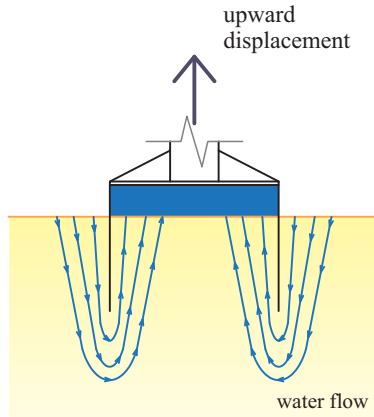


Figure 2.2 Water flow in the soil to the gap between the soil surface and the lid under tensile loading.

dense sand-silt soil to 0.56 for very dense sand.

For pile design, K is between 0.8 and 1 (API, 2011). In bucket foundation design, the expression (2.1) is also applicable, but there are no clear guidelines for K value. Larsen (2008) used $K = 1 - \sin\varphi$, a rather conservative expression, which corresponds to the in-situ lateral pressure coefficient K_0 . Villalobos (2006) showed that K for a bucket foundation under tensile load may be expressed by equation (2.2) where soil arching in the soil-structure interface due to friction on the skirt is taken into consideration. In this case K values increase from 0.2 to 0.6 for φ correspondingly from 55° to 30° . Based on test results and literature review, Boulon and Foray (1986) showed that K changes with sand depth, as given in Figure 2.5. The very high lateral earth pressure coefficient of 3.2 at low soil stress was explained by high dilatation. Based on cone penetration test results performed by Gaydadhiew et al. (2015), Thomassen (2016) showed that K changes from approximately 3 to 0.5 parallel to increasing effective vertical stress from 0 to 100 kPa. Houlsby and Byrne (2005b) explained that $K \tan\delta$ are always used as a coupled term. They showed that in earlier large suction caisson installation projects $K \tan\delta$ values were in the range of 0.48-0.8. Byrne and Houlsby (2002b) commented that $K \tan\delta=0.5$ is a good estimate for most cases of bucket foundations under tensile loading.

$$K = \frac{\cos^2\varphi}{2 - \cos^2\varphi}, \quad (2.2)$$

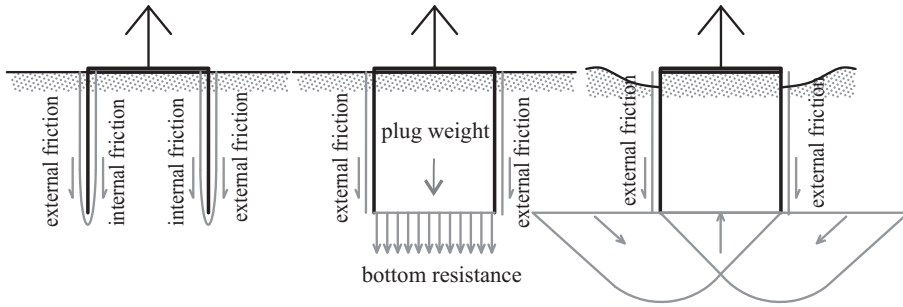


Figure 2.3 Tensile resistance in cohesive soil: (from left) drained response; partially drained response; undrained response. (Deng and Carter, 2002).

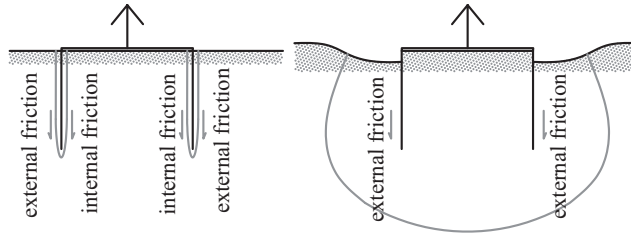


Figure 2.4 Tensile resistance in cohesionless soil: (left) drained response; (right) undrained response. (Senders, 2009).

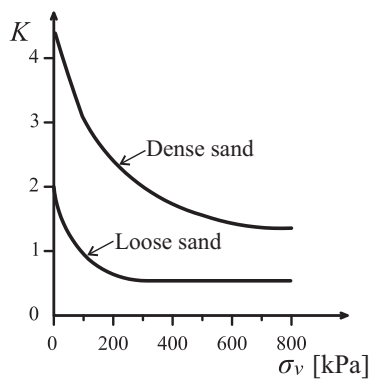


Figure 2.5 Lateral earth stress coefficient vs vertical soil stress. Reproduced from Boulon and Foray (1986).

2.3 Bucket foundation design methods

2.3.1 Design practise

Several standard design guidelines for offshore structures and foundations are acknowledged around the world. Among them DNV (2014), DNV (1992), API (2011) and ISO (2003) should be mentioned. Obviously, the application of standard guidelines depends on local conditions; many countries have standard guidelines that must be taken into account. The following gives a short overview of the foundation types considered in standards:

- DNV (2014) describes offshore foundation concepts for wind turbines: piled, gravity based and skirted (bucket) foundations as well as solutions for moored floating structures. DNV (2014) refers to DNV (1992) regarding the recommended design methodology for gravity based foundations, piles, foundations for jack-up platforms and the prediction of the installation of skirted foundations.
- API (2011) provides the recommended design methodology for shallow and pile foundations, including recommendations for foundations with skirts regarding vertical and horizontal capacity as well as installation with suction application.
- ISO (2003) provides the recommended design methodology for pile and shallow foundations, with general guidelines for foundations with skirts.
- ISO (2007), besides the recommended design methodology for pile and shallow foundations, comments that skirted foundations are able to resist cyclic uplift waves of several seconds' duration, even in sand.

As seen above, standard design guidelines are available for pile and gravity based foundations while information related to bucket foundation design is very limited. Generally, the bucket foundation should be assessed as a gravity based foundation with a skirt. There is ample scope for geotechnical designers choice, for example in using alternative methods for the evaluation of cyclic loading. The assessment of cyclic degradation and the relevant displacements is a complex task as the cyclic properties should be examined under various loading regimes. Moreover, a determined methodology on this topic is unavailable.

2.3.2 Analytical expressions for tensile capacity

Iskander et al. (1993 and 2002) performed tensile loading tests on caisson foundation in sand. The tests led to an analytical method for the calculation of the tensile capacity of caisson foundations in drained and undrained conditions. The drained tensile capacity was found to reflect frictional response on the bucket skirt. The undrained capacity included consideration about the hydraulic gradient induced by the tensile loading.

Houlsby et al. (2005b) introduced a theoretical solution for the skirted foundations

subjected to tensile loading. Their design methodology considered possible pore suction generation due to the tensile loading. The authors proposed a method for the prediction of the suction pressure. The solution was verified by model testing at various scales and in different soils, including field tests (Houlsby et al., 2006).

2.3.3 Finite element models (FEM)

Bye et al. (1995) presented geotechnical design method for bucket foundations in dense sand. Bucket bearing capacity was estimated using undrained soil strength parameters. The proposed method included pore pressure effect estimation according to Andersen and Lauritzsen (1988). Moreover, a method was proposed for the calculation of cyclic bearing capacity.

As a result of their finite element analysis (FEA) of suction caissons in cohesive soil, Deng and Carter (2002) developed and verified simplified solutions for three tensile loading failure modes. Caisson tensile capacity was estimated through displacement controlled calculations in which a load-displacement response was achieved. A non-dimensional parameter T was introduced to evaluate the effects of the displacement rate as follows:

$$T = \frac{c_v}{vD} \quad (2.3)$$

$$c_v = \frac{k}{m_v \gamma_w} \quad (2.4)$$

Where: c_v is the coefficient of soil consolidation, v is displacement rate, D is caisson diameter, k is the hydraulic conductivity of the soil, m_v is the coefficient of 1-dimensional volume decrease and γ_w is the unit weight of pore water.

Thieken et al. (2014) presented FEA for tensile loading on bucket foundations in sand. Different tensile loading rates were applied on a bucket foundation. The analysis showed that under small displacement rates, the drained tensile capacity was mobilized while under high displacement rates, the undrained conditions occurred. In the latter case, large upward displacements occurred.

Cyclic loading analysis using FEM

Cyclic axial loading is extremely important for relatively light offshore structures with multi-pod foundation systems, such as jackets with several foundations. In storm loading, large cyclic loading amplitudes can arise compared to mean cyclic loads. Moreover, it is hard to expect that the cyclic loading would be restricted in the compressive direction as that would inevitably increase the production costs. The best-known testing campaigns for cyclic loading on piles are described by Jardine et al. (2005). According to Abdel-Rahman et al. (2014), axial pile capacity decreases with the number of load cycles due to the loss of the ultimate skin friction. Through a new finite

element calculation for the cyclic tensile loading on piles in dense sand, the authors showed that the reduction of the ultimate skin friction increases with the number of cycles, soil depth (normal stress) and cyclic loading level.

Niemunis et al. (2005) applied a high-cycle accumulation (HCA) model for the prediction of strains and stresses in sand. The model is applicable for large numbers of cycles ($>10^3$) and small strain amplitudes ($<10^{-3}$). The HCA model was based on an extensive laboratory testing programme performed by Wichtmann (2005). Niemunis et al. (2005) implemented the HCA model in a finite element routine. Later, Zachert et al. (2015) compared the HCA finite element model results to a cyclic loading test with a full-scale gravity foundation, showing good agreement for settlement and pore pressure prediction.

A complex design method for cyclic loading on offshore foundations was created by the Norwegian Geotechnical Institute (NGI) (Andersen et al., 1992; Andersen, 2009; Jostad et al. 2014). The method requires triaxial and direct shear tests on relevant soil samples to provide the cyclic soil parameters. It is worth noting that each foundation location requires at least ten cyclic laboratory tests and/or access to rich in-house database for the supplementation of the knowledge of the relevant soil behaviour. In the NGI method, cyclic loading on the structure is systematized to the equivalent loading parcels, after which the data is processed in a finite element program for the calculation of the cyclic capacity and settlements of the foundation. The method is valid also for offshore wind turbine foundations, as argued by Skau and Jostad (2014). While it is estimated to be among best methods for the design of the cyclically loaded foundations, it presupposes high-level expertise and access to a number of design aids, such as advanced laboratory testing data, specific finite element programmes, etc.

2.4 Physical modelling of bucket foundations

Acosta-Martinez and Gourvenec (2008) presented cyclic loading tests on caisson foundations for buoyant offshore structures in overconsolidated soft clay. The foundation model ($d/D = 0.3$) was scaled 167 times. Caisson model was installed by pushing at a constant displacement rate. The installation ended with a predetermined compressive pre-load which nearly reached the primary consolidation. The test results showed that cyclic loading increased the undrained post-cyclic uplift capacity and some consolidation developed after the cyclic loading program. However, the permanent uplift displacement arose when higher cyclic loading amplitudes were applied on the foundation model.

Clukeley et al. (1995) performed cyclic loading tests on caisson foundations in clay. The foundation model ($d/D = 2$) was scaled 100 times. The tests were performed in a centrifuge and showed that the post-cyclic static uplift exceeded the calculated virgin static uplift capacity. On this basis, the authors developed a method for TLP's suction caissons subjected to cyclic loading.

Iskander et al. (1993 and 2002) tested tensile loading of a caisson foundation in dense sand (water saturated). The caisson model had a diameter of 0.11 m and a skirt length of 0.19 m ($d/D = 1.76$). In addition to reporting load, displacement and pore pressure results for monotonic tensile loading, the authors back-calculated the tensile capacity.

Bye et al. (1995) presented field tests on bucket foundations with a height of 1.7 m and diameter of 1.5 m ($d/D = 1.13$) in dense sand locations. The test data were used to verify design methods for bucket foundations for the Europipe 16/11E and Sleipner T. Furthermore, laboratory tests were performed on different size bucket foundation models with $d/D = 0.38$. One model had a diameter of 0.55 m and a skirt length of 0.21 m in skirt length, while another model was 3.5 times smaller. The two model tests showed identical behavioural characteristics. NGI model tests for cyclic loading showed that low frequency cycling increased the undrained cyclic capacity, probably due to the compaction of sand or a stress change.

Feld (2001) performed bucket foundation model tests in a $1g$ test set-up. A half bucket model was constructed to provide visual information about soil behaviour and seepage. The bucket was 0.2 m in diameter and 0.1 m in skirt length ($d/D = 0.5$). The testing programme included pull-out tests with several displacement rates and cyclic loading tests. Feld (2001) showed that tensile resistance increases with increasing displacement rate. Unfortunately, the documentation of the testing programme and the results on the cyclic behaviour were scarce.

Kelly et al. (2003, 2006b) reported cyclic axial loading tests on a model foundation with a diameter of 0.28 m and a skirt length of 0.18 m ($d/D = 0.64$). The tests were performed in a pressure chamber where water depths of up to 20 m could be simulated. The foundation model was installed in dense water saturated sand. Cyclic

loading tests with mean compressive loads were followed by a final tensile pull-out. Later, Houlsby et al. (2006) performed field tests with two large bucket foundations; the first with $D = 3$ m and $d = 1.5$ m ($d/D = 0.5$) for moment loading tests, and the second with $D = 1.5$ m and $d = 1.0$ m ($d/D = 0.67$) for axial loading tests. Finally, Kelly et al. (2006a) compared the data and a proposed methodology for the comparison of the field and laboratory testing data. However, it is worth mentioning that the cyclic axial loading tests had mean compressive load and only a small part of the cyclic amplitudes were on the tension side. Furthermore, Kelly et al. (2006a) compared caisson installation methods of suction and pushing for several caissons of different sizes, documenting that the suction installation disturbed the soil, although it was more evident in the small-scale model tests.

Senders (2009) analysed the response of wind turbine bucket foundations in a tripod combination. Centrifuge tests on model foundations of scale 1:100 were performed. The dimensions were 49-120 mm in diameters and 60-114 mm in skirt lengths ($d/D = 0.5-1$). Various aspects of the testing were documented, including suction and push-installation, the permeability of different soil types, and pull-out and cyclic loading. Frictional resistance during installation and tensile loading were successfully predicted using a cone resistance measurement. Pull-out tests showed that the development of underpressure led to large upward displacements. No cyclic degradation was found where the tensile load did not reach the drained capacity limit.

Thomassen (2016) performed drained tensile loading tests on a segment of pile foundation which had a diameter of 0.5 m and an embedded shaft length of 0.96 m. The pile was installed in dense sand. The author has shown that tensile peak loads were mobilized at upward displacements of about 5 mm.

2.4.1 Model size and set-up size (scaling)

Obtaining a correct scaling of the geotechnical design parameters is one of the main challenges when planning a testing campaign. Corte (1989) provided a useful overview of the scaling laws for small-scale tests (1g and centrifuge). Recently, Byrne (2014) discussed laboratory-scale modelling issues focussing on offshore geotechnics. A set of similarity conditions between the prototype and small-scale test ensures that the results confirm with real physical conditions. However, geotechnical soil parameters are often dependent on the effective stresses, i.e. secant friction and dilation angles decrease with increasing effective stresses and vice versa for the modulus of elasticity (Section 2.1).

Achieving an ideal scaling is therefore often impossible due to equipment or material limitations. For example, a bucket foundation subjected to cyclic loading should be examined in a 1g test set-up. In a scale of 1:10 model, a loading frequency of 1 Hz should be selected to simulate 0.1 Hz load rate in the full-scale. Depending on the test set-up properties, this loading frequency may cause severe damage of the foundation model and the connected measuring equipment. This may give dynamic effects that

are not found in real, full-scale foundation behaviour.

Bye et al. (1995) commented on field and $1g$ laboratory test differences. The field tests were performed with a rather large size foundation model, but difficulties were experienced when considering scaling (in relation to the prototype size) of the soil consolidation parameters and foundation geometry. It is impossible to get the real prototype sand and prepare it to the correct density in the laboratory. Furthermore, the correct consolidation behaviour in the scaled model was unattainable. The authors mentioned that for the smaller laboratory tests with slower loading rates, silicon oil was used instead of water, which resulted in reduced peak friction angle and dilation.

Sørensen et al. (2012) commented on scaling problems in small-scale laboratory tests, where effective stresses are generally low. They proposed a new method for laboratory tests in a pressure chamber which allowed application of water pressure on the soil surface. The effective stresses can only be increased by negative pore pressures in such a test set-up. As the performed tests were quasi-static, no significant change of pore pressures could be expected. Furthermore, the pore pressure results were not commented on (or recorded), it is therefore difficult to see the potential for overcoming low stress parameters. Sørensen et al. (2012) proposed a method for the normalization of laboratory results based on total parameters for the small-scale piles and claimed it to be promising for the scaling to the prototype dimensions.

Buckingham (1914) introduced the dimensionless similitude theory, which may be applied to any physical system. He stated that any physical system can be described by dimensionless units of mass, length and time. Two systems are similar if the physical parameters are similar. The theory was used by Byrne and Houlsby (2002a) for the analysis of bucket foundation models (small-scale only) under cyclic axial loading. Kelly et al. (2006a) successfully applied dimensionless groups for model test results performed with various bucket foundation models subjected to axial and moment loads. The authors made proposed dimensionless groups with regard to load, displacement and stiffness in drained cyclic loading tests.

For comparison of laboratory size and full-scale foundation loading rates, Kelly et al. (2004) used a non-dimensional parameter T (eq. 2.5), which is somewhat the same as expression (2.3). The authors compared the tensile loading rate of a foundation model and a prototype. It is worth mentioning that an assumed prototype case was used for the comparison.

$$T = \frac{c_v t}{H^2} \quad (2.5)$$

Where: c_v is the coefficient of soil consolidation, t is time of 1/4 cycle period, H is the length of the drainage path (equivalent to the skirt length).

Foglia (2014) proposed non-dimensional groups for displacement rate analysis when suction pressure and soil permeability are known as equation (2.6). The non-dimensional

groups were successfully used for a comparison of testing results of two different bucket foundation models.

$$\frac{s}{\gamma_w D} = g\left(\frac{vd}{kD}\right) \quad (2.6)$$

Where: s is pore pressure, γ_w is the fluid unit weight, D is bucket foundation diameter, d is bucket foundation skirt length, v is displacement rate, k is soil hydraulic conductivity and g is a function for the relationship between two models in different scales (can be found by model testing).

CHAPTER 3

Scope of the Thesis

3.1 Main findings of the literature review

The expanding offshore energy sector is demanding increasingly cost effective engineering solutions. Failure in an offshore foundation can result in tremendous financial losses. The pressure for wind turbine generators and waver energy devices to increase their competitiveness compared to other methods of energy extraction also applies to the design of their foundations. As shown in Chapter 1, research on offshore foundations is highly relevant. Standard design guidelines are useful tools for the design of offshore foundations. Section 2.3 gave an overview of several design codes, indicating the need for addressing certain design issues. The response of axially loaded bucket foundations for offshore renewable structures is among the topics to be uncovered in the following.

It is generally accepted that when subjected to compressive loads, bucket foundations behave similarly to gravity based foundations. Section 1.5 indicated some of the critical problems in bucket foundation design, such as the estimation of long- and short-term tensile capacity. In Section 1.4, it was seen how a suction installation creates seepage around the foundation skirt, inevitably reducing the strength of the grained soil surrounding the skirt. Although the frictional interface capacity is affected, this is likely to be regained as a result of the light cyclic loading that compacts the soil interface. But designers are facing difficulties in choosing appropriate parameters for the prediction of the interface resistance (Section 2.2). The usual considerations for the design face two extremes: either the drained capacity (very low) or the undrained capacity with the water cavitation determining the limit (i.e., the highest tensile capacity). However, the real response is somewhere in between the two limits for a design storm loading case.

At present, model testing and advanced finite element modelling may be applied for the investigations. The displacement of axially loaded bucket foundations should be accurately predicted. This concerns in particular foundations that are subjected to tensile loading. While it remains unclear how displacements are influenced by the partial drainage, they should be expected to be larger than under fully drained conditions (Section 2.4).

The evaluation of the cyclic degradation and displacements of bucket foundations under cyclic loading leaves considerable leeway in the design process. The complexity of the assessment of cyclic degradation is due to the necessity of examining the variation of cyclic properties under different loading regimes. This often requires advanced soil laboratory testing or, even more expensive and time consuming, model testing.

3.2 Aim and objectives

It is crucial that the design methods ensure sufficient foundation capacity to prevent the permanent and oscillating loads from causing significant deformation. The cyclic tensile capacity of bucket foundations continues to be a topic of concern. On the one hand, the drained tensile capacity of skirted foundations is generally very low. On the other hand, the negative pore pressure generation may increase the tensile capacity significantly. The key issues are thus to predict the actual drainage conditions during the lifetime of the structure and to evaluate the related settlements.

In the design of bucket foundations in tension, it is typically assumed that the responses can be categorized as drained (low capacity) or undrained (high capacity). However, the real tensile resistance may be expected to lie somewhere in between the two limits for a design storm loading case. Upward displacements related to tensile loading are difficult to predict. Moreover, although the cyclic behaviour of bucket foundation in tension is expected to be very critical, no quantifying prediction analytical methods are available at the moment. The key analysis method is laboratory testing, which is often related to scaling issues (Section 2.4.1). Thus, steps to overcome problems related to low soil stress in laboratory models should be taken.

The aim of the present thesis is to clarify a number of design problems concerning bucket foundations in sand that are subjected to tensile loading (static, rapid and cyclic). The specific objectives of the study are as follows:

- To examine the tensile capacity of bucket foundations under various axial loading conditions.
- To investigate the parameters governing the strength of soil-structure interfaces.
- To investigate the dependency of upward displacements on the tensile loading.
- To assess possible cyclic degradation of axially loaded bucket foundations in tension.
- To evaluate the influence of displacement rate on the ultimate tensile strength.
- To design a new test set-up that is able to provide consistent data for the aforementioned objectives.

The present study provides valuable experimental testing results applicable for the primary foundation dimensioning as well as for advanced finite element model calibration. The novel findings of the thesis include:

- A new laboratory testing facility was designed and built providing consistent results of medium-scale testing. The scale of bucket foundation model was 1:10 compared to prototype size.
- An extensive testing programme of bucket foundations in tension was performed, thoroughly visualizing tensile behaviour under monotonic loads as well as long-term cyclic behaviour with mean tensile loads.
- Pore pressure behaviour was assessed under tensile loading with various displacement rates.
- High-quality displacement measurements were documented.
- Soil-structure parameters were assessed in the new testing facility which allows for the simulation of different soil depths.

CHAPTER 4

Research Outcomes

The thesis is based on seven papers that include three conference papers, two journal papers and two technical reports. The papers cover the aims of the PhD project regarding the scientific analysis and the laboratory testing of bucket foundations in sand subjected to axial loading. Providing an overview of the papers, this chapter indicates the main findings as well as some additional issues that were not addressed in the papers.

4.1 Overview of the papers

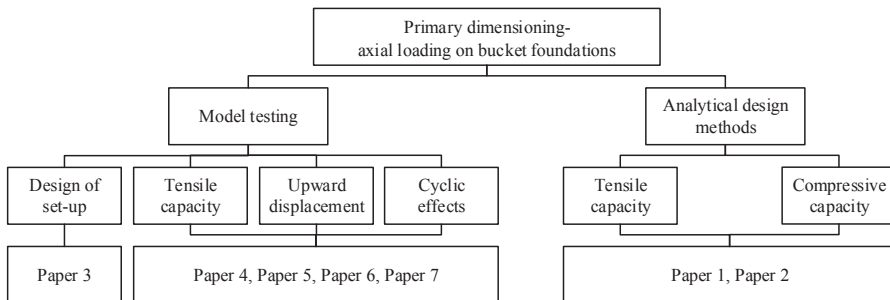


Figure 4.1 Overview of the research and relevant publications.

The aim and objectives were defined in Section 3.2. Figure 4.1 gives an overview of the topics addressed in the thesis. The papers provide the scientific background for the thesis and are as follows:

- *Paper 1*: Vaitkunaite, E., Ibsen, L. B., Nielsen, B. N., and Devant Molina, S. (2013). Comparison of Foundation Systems for Wave Energy Converters Waves-tar. In *10th ewtec 2013 European Wave and Tidal Energy Conference Series: Proceedings of the 10th European Wave and Tidal Energy Conference, Aalborg*,

Denmark. Technical Committee of the European Wave and Tidal Energy Conference. No. 10.

- *Paper 2:* Vaitkunaite, E., Nielsen, B. N., and Ibsen, L. B. (2015). Comparison of design methods for axially loaded buckets in sand. In *Frontiers in Offshore Geotechnics III proceedings of the third international symposium on frontiers in offshore geotechnics (isfog 2015), Oslo, Norway, 10-12 June 2015*. (Vol. 1, pp. 331-342). London: C R C Press LLC.
- *Paper 3:* Vaitkunaite, E., Ibsen, L. B., and Nielsen, B. N. (2014). New Medium-Scale Laboratory Testing of Bucket Foundation Capacity in Sand. In *Proceedings of the Twenty-fourth (2014) International Ocean and Polar Engineering Conference, Busan, South Korea*. (Vol. 2, pp. 514-520). International Society of Offshore and Polar Engineers.
- *Paper 4:* Vaitkunaite, E., Ibsen, L. B., and Nielsen, B. N. (2016). *Testing of Axially Loaded Bucket Foundation with Applied Overburden Pressure*. Aalborg: Department of Civil Engineering, Aalborg University. DCE Technical Reports; No. 209.
- *Paper 5:* Vaitkunaite, E., Ibsen, L. B., and Nielsen, B. N. Bucket Foundation Model Testing under Tensile Axial Loading. *Canadian Geotechnical Journal*. Submitted 14-10-2015 [cgj-2015-0497], Re-submitted 06-06-2016 [cgj-2016-0301].
- *Paper 6:* Vaitkunaite, E., Nielsen, B. N., and Ibsen, L. B. (2016) Bucket Foundation Response under Various Displacement Rates. *International Journal of Offshore and Polar Engineering*, 26(2), 116-124.
- *Paper 7:* Vaitkunaite, E. (2015). *Bucket Foundations under Axial Loading: Test Data Series 13.02.XX, 13.03.XX and 14.02.XX*. Aalborg: Department of Civil Engineering, Aalborg University. DCE Technical Reports; No. 199.

4.2 Foundation solutions for the Wavestar wave energy converter

The section is based on Paper 1:

Comparison of Foundation Systems for Wave Energy Converters Wavestar. In *Proceedings of the 10th European Wave and Tidal Energy Conference, Aalborg, Denmark*.

The Wavestar wave energy converter (WEC) was briefly presented in Section 1.2. Wavestar C6-600kW (Figure 4.2) is designed to operate in water depth of up to 20 m. The structure would be 80 m long and 17 m wide. When Paper 1 was written, the structural design had not been completed. A section of Wavestar C6-600kW is constructed in Hanstholm and is under continuous development. For this WEC to be competitive with other offshore energy devices, more cost-effective technical solutions are needed for various parts of the device, including the suitable foundation.

Paper 1 is a feasibility study considering six possible foundation solutions for the Wavestar C6-600kW. Pile, bucket and gravity based foundations were dimensioned for two-column and four-column combinations. As the structural design details were unknown at the time of analysis, some assumptions were made:

- In the first case of a two-column solution, the foundations had rigid connections to the columns. The foundations thus had to resist large moment loads as well as vertical loads and sliding.
- In the second case of four-column solution, the foundations had hinged connections to the columns. The foundations should therefore be able to resist vertical loads and sliding.

Under storm conditions, the floaters are locked and the WEC is lifted above the water surface. This protects the floaters from large wave loads. Wavestar A/S provided loads for a storm case as follows: wind load on the structure, wave loads on the columns at water surface level and self-weight of the device. The self-weight of the structure was relatively large. Thus, the foundations are exposed to a small portion of the tensile loads. In dimensioning of the foundations, all loads were considered as permanent loads.

A soil profile containing layered sands was assumed for the design. The foundations were designed in three steps considering the ultimate limit state (ULS) and serviceability limit state (SLS) as follow:

- The primary foundation dimensioning in ULS was based on DNV (1992).
- A 2D model was applied for the secondary dimensioning in ULS, employing the commercial LimitState:GEO program.
- A 3D finite element model verified the ULS and SLS conditions. The commercial program Plaxis3D was used in this step.

The last design step was a 3D finite element modelling in which satisfactory ULS and SLS conditions were verified.

The feasibility study shows that even though the two-column case would require larger foundation dimensions, the total amount of material for their manufacture would be smaller than for the foundations in the four-column case. While the installation costs were not assessed, it is expected that the two-column design would be cheaper than the four-column design. When comparing bucket foundations with pile foundations, the latter is found to require about 1.4 times more steel. The bucket foundations thus appear to be a cost-effective solution for the WEC. Even though the two-column design seems to be more profitable, the lifting system of the device might require the four-column design (Figure 4.3). The section of Wavestar C6-600kW in Hanstholm is supported by four columns, which requires a reliable design methodology for the bucket foundation axial capacity, especially with respect to cyclic tensile axial loads.



Figure 4.2 Wavestar C6-600kW wave energy device. (Wavestar, 2011)

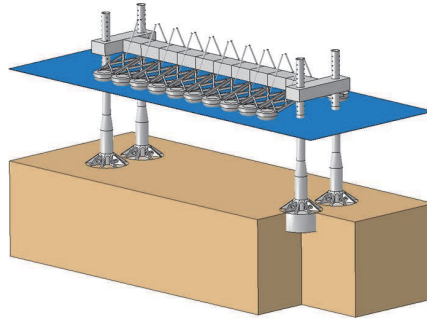


Figure 4.3 Four-column Wavestar with bucket foundations. (Wavestar, 2011)

4.3 Current design methods for bucket foundations

The section is based on Paper 2:

Comparison of design methods for axially loaded buckets in sand. In *Frontiers in Offshore Geotechnics III proceedings of the third international symposium on frontiers in offshore geotechnics (isfog 2015), Oslo, Norway*.

As lightweight marine structures may be subjected to quasi-static loads that result in dominating axial components on the foundations (Chapter 1), the drained axial capacity of a bucket foundation should be determined. Section 2.3 noted that design guidelines in this topic are incomplete. Paper 2 gives an overview of the available methods for the estimation of drained compressive and tensile capacity of bucket foundations. The analysis includes analytical expressions from available design codes and several research institutes and numerical simulations using an axis-symmetric finite element model. The aim of Paper 2 is to investigate the available methods and highlight the differences between them.

The capacities were determined for a hypothetical case study where two bucket foundations of equal diameters (10 m) but with different skirt lengths (5 m and 10 m) were assessed (Figure 4.4). In all the cases, the foundations were analysed as separate units under purely axial loading, either compression or tension. A uniform dense sand was assumed, with the properties given in Table 4.1. As some of the found methods required information on cone resistance, a profile was created based on Baldi et al. (1986) (Figure 4.5).

As it was mentioned in Section 2.2, a bucket foundation behaves as a gravity based foundation under compressive loading. The following list contains the methods (M) used for the estimation of the compressive bearing capacity R_c :

- (M1) Plaxis 2D axis-symmetric Mohr-Coulomb soil model
- (M2) Plaxis 2D axis-symmetric Hardening Soil model
- (M3) Davis and Booker (1971)
- (M4) API (2011)
- (M5) EC-7 (2004)
- (M6) Bolton and Lau (1993)
- (M7) Larsen (2008)
- (M8) Caquot and Kerisel (1953)
- (M9) Brinch-Hansen (1970)
- (M10) Lundgren and Mortensen (1953)

The first two items on the list are finite element calculations. The remaining items are various expressions from research papers and standards addressing bearing capacity factors used in the general Terzaghi's bearing capacity formula. Moreover, Hansen (1979) has suggested using a reduced friction angle φ^{red} in analytical solutions based on the non-associated plasticity theory. The new friction angle accounts for the non-associated plasticity in soils considering friction angle φ and dilation angle ψ (eq. 4.1). Thus, it was included in the methods where possible.

$$\tan\varphi^{red} = \frac{\sin\varphi\cos\psi}{1 - \sin\varphi\sin\psi}, \quad (4.1)$$

Figures 4.6 and 4.7 summarize the results on compressive bearing capacity. It is noted that the ten methods give very different results for the bearing capacity depending on the selected parameters. Indeed, φ^{red} contributes to the estimated R_c values in the sense that the results become more consistent. Methods M3, M5, M7-9 lead to similar estimated capacities. The overall scatter in the results is explainable by considering the exponential increase of the bearing capacity factors N_q and N_γ together with the friction angle. This indicates that the bearing capacity may be significantly overestimated in dense sand locations.

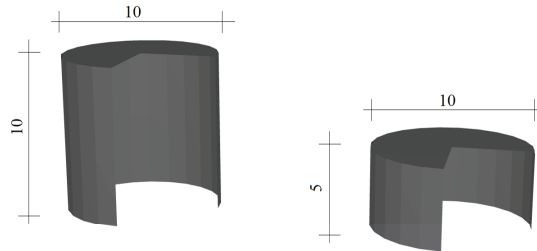
The static tensile capacity was estimated as the sum of external skirt friction and the lowest value of either internal friction or plug weight. Few methods were found to be capable of determining tensile resistance. The methods considered for the tensile capacity R_t calculation were as follows:

- (M1) Plaxis 2D axis-symmetric Mohr-Coulomb soil model
- (M2) Plaxis 2D axis-symmetric Hardening Soil model
- (M11) Senders (2009), CPT based method
- (M12) Houlsby et al. (2005b)
- (M13) DNV (1992) tensile loading
- (M14) API (2011) CPT based method I
- (M15) API (2011) CPT based method II
- (M16) API (2011) CPT based method III
- (M17) API (2011) CPT based method IV

Just as before, the first two items on the list are finite element calculations. Five tensile capacity methods (M11, M14-M17) require data from cone penetration testing (CPT). One CPT based method, M11, is calibrated for tensile loading on bucket foundations, while the other four methods (M14-M17) are used for axially loaded pile design. The latter four were considered purely out of curiosity and, as realized later on, the results indicated that only specially calibrated methods for bucket foundation tensile

Table 4.1 Soil parameters used for the analysis.

Parameter	Unit	Value
Density ratio D_R	[%]	80
Soil unit weight γ	[kN/m ³]	20.25
Triaxial friction angle φ_{triax}	[°]	38.8
Plane friction angle $\varphi_{pl.}$	[°]	42.7
Interface friction angle δ	[°]	32.2
Angle of dilation ψ	[°]	9
Effective cohesion c'	[kPa]	0
Effective Young's modulus E'	[MPa]	39.3
Lateral earth pressure coeff. K	[-]	0.37

**Figure 4.4** Bucket foundations used for the study with dimensions in meters.

response were valid for the design. Methods M12 and M13 are based on the Coulomb failure criterion. The first method includes stress reduction due to frictional loads in the soil-structure interface, while the second is also known as the β -method used for the determination of the axial resistance of piles.

Figure 4.8 shows the calculation results for the tensile loading capacity. The four CPT based methods are excluded from the data presentation in the figure because they resulted in up to 9 times larger capacities. The results of the other methods show some considerable scatter. A comparison between the methods is difficult because they are based on different assumptions. To validate of some of the analysed expressions, a new laboratory equipment was designed for a testing campaign. The results are presented in the following Section 4.4.

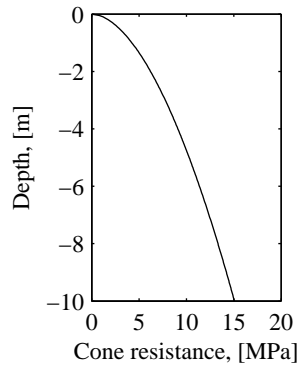


Figure 4.5 An assumed cone resistance profile, based on Baldi et al. (1986).

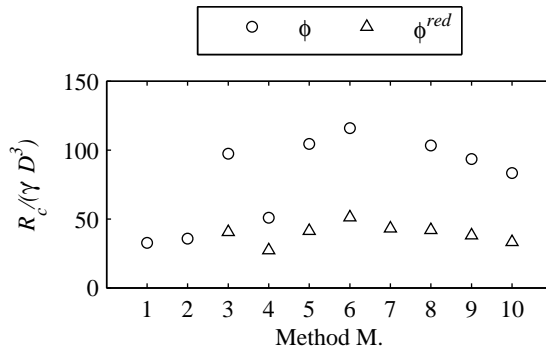


Figure 4.6 Normalized drained bearing capacity for a bucket foundation $d/D=0.5$. (Vaitkunaite et al., 2015)

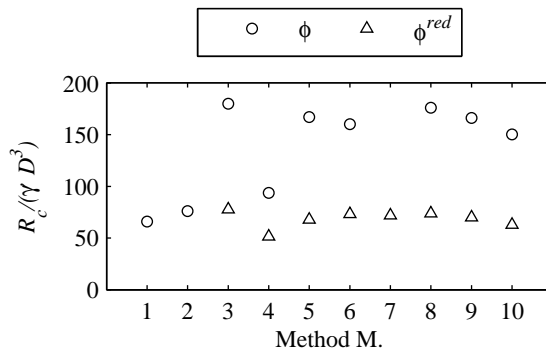


Figure 4.7 Normalized drained bearing capacity for a bucket foundation with $d/D=1$. (Vaitkunaite et al., 2015)

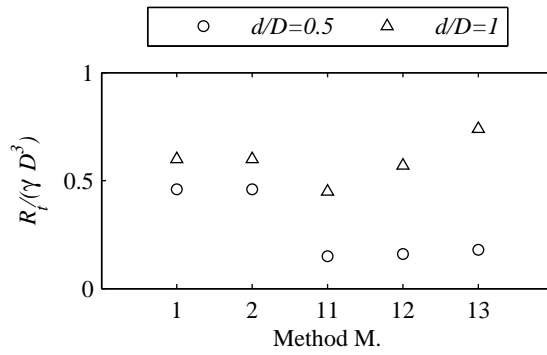


Figure 4.8 Normalized drained tensile capacity for bucket foundations with $d/D=0.5$ and $d/D=1$.

4.4 Design of the "Large Yellow Box" test set-up

The section is based on Paper 3 and Paper 4:

Paper 3: New Medium-Scale Laboratory Testing of Bucket Foundation Capacity in Sand. In *Proceedings of the Twenty-fourth (2014) International Ocean and Polar Engineering Conference, Busan, South Korea*.

Paper 4: *Testing of Axially Loaded Bucket Foundation with Applied Overburden Pressure*. Aalborg: Department of Civil Engineering, Aalborg University. DCE Technical Reports; No. 209.

Vaitkunaite (2015) described the step-by-step test procedure. The report is publicly available on Aalborg University database <http://vbn.aau.dk/>.

Based on the literature study (Chapter 2), several aspects of bucket foundation design remain unclear, e.g., long- and short-term tensile capacity, and tensile cyclic axial response (settlements and cyclic degradation). A new testing facility was designed for the examination of foundation behaviour under tensile loading conditions (Figure 4.9).

The new testing facility was launched in summer 2012, since when it has undergone many improvements. The testing rig consisted of a sand container of 2.5 m diameter and a loading frame supported on four fixed columns. The loading frame carried two hydraulic cylinders of 200 kN and 300 kN loading capacity. One cylinder was used for the push installation of a foundation model while the other cylinder was used for loading.

Two bucket foundation models were designed for the testing campaign. They were 1 m in diameter D and 0.5 and 1 m in skirt lengths d . The skirt material was structural steel that was unprotected from corrosion. The skirt wall thickness was 3 mm. It should be noted that most of the tests were performed on the smaller foundation, whose lower self-weight and shorter skirt length made it much easier to handle (Figure 4.10). Each of the buckets were equipped with a system of narrow steel pipes allowing for inspection of possible pore pressure development at different soil levels around the skirt. The pore pressure transducers were placed on the top of the foundation models, which allowed easy access for adjustments and calibration or re-calibration as needed. An automatic loading system allowed for the application of axial loads or displacements on the bucket foundation model. A successful loading sequence typically resulted in high-quality measurement data with information about time, load, displacements and pore pressures.

The sand container was filled with Aalborg University sand No. 1, as described in detail by Hedegaard and Borup (1993). The sand consisted mainly of fine quartz and a small fraction of feldspar and biotite. The larger particles were rounded, the smaller particles sub-angular. The sand was submerged in water and compacted with a rod vibrator. The same sand specimen was kept in the sand container during the entire testing programme. However, the soil conditions were "reconstructed" before each test, taking the following steps:

1. Loosening sand with an upward water gradient.
2. Compacting it with the rod vibrator.
3. Inspecting sand conditions with a CPT test of our own design, as described by Larsen (2008). Ibsen et al. (2009) suggested a set of equations relating the laboratory cone resistance to the sand properties, such as relative density. Further analysis of the laboratory CPT outside the scope of this thesis.

A bucket foundation model was installed by mechanical pushing. Every installation ended with an elastic compressive pre-load, after which the model was completely unloaded. The pre-load ensured that the procedure is repetitive from test to test. After the installation, the loading sequence started for tests without overburden pressure.

As explained in Section 2.1, Aalborg University sand No. 1 properties changed drastically in the first 0-100 kPa horizontal stress. This creates scaling effects related to the change of the sand properties in low-stress tests. Consequently, the effective stress was increased in the soil to enable analysis of soil-structure interaction under more realistic conditions.

The effective stress was increased using a latex membrane that was specially prepared to cover the surface of the sand and the bucket model. Four narrow pipes were connected to the membrane and used for the suction application on the surface of the sand. A filter layer between the membrane and the sand surface prevented sand particles from being sucked out of the container. By this method, a pressure p_m of 0-70 kPa was uniformly applied on the surface of the sand to simulate the installation of the bucket model installed at different soil depths (Figure 4.11).

Ideally, if the entire volume of sand had contained no air bubbles and the membrane had been perfectly tightened, the suction application would have had resulted in two favourable effects: (1) an increase in effective soil stresses; (2) keeping the sand submerged in water. However, in practise such conditions were very demanding. Any holes in the membrane were regularly expected. It was furthermore cleaned from sand particles before each test. All interfaces of membrane-sand container, membrane-bucket model, membrane-suction hoses were tightened. Despite many attempts for improvements, the tests were performed with a leaky system. As a consequence, the water was sucked out of the sand container, leaving the soil volume just moist (Figure 4.12). Luckily, the effective stresses were successfully increased and, knowing the moist soil unit weight, the testing programme proceeded with the available facilities.



Figure 4.9 "Large Yellow Box" test set-up.



Figure 4.10 Bucket foundation model, 1 m in diameter and 0.5 m in skirt length.

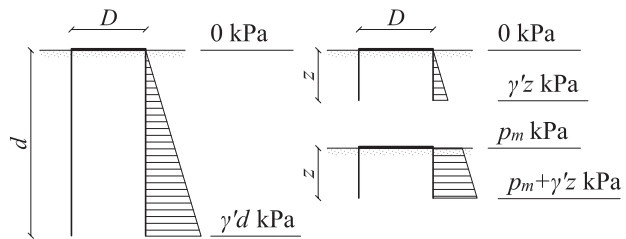


Figure 4.11 Vertical stress distribution on a bucket foundation: prototype (left), model simulations (right). (Vaitkunaite, 2016)



Figure 4.12 Slightly moist sand after a test with the membrane pressure.

4.5 Tests performed in the "Large Yellow Box"

The section is based on Papers 4-7:

Paper 4: *Testing of Axially Loaded Bucket Foundation with Applied Overburden Pressure*. Aalborg: Department of Civil Engineering, Aalborg University. DCE Technical Reports; No. 209.

Paper 5: *Bucket Foundation Model Testing under Tensile Axial Loading*. *Canadian Geotechnical Journal*. Submitted.

Paper 7: *Bucket Foundations under Axial Loading: Test Data Series 13.02.XX, 13.03.XX and 14.02.XX*. Aalborg: Department of Civil Engineering, Aalborg University. DCE Technical Reports; No. 199.

The testing programme performed in the "Large Yellow Box" aimed at showing the behaviour of bucket foundations subjected to axial tensile loading during a normal serviceability situation. Thus, the foundation model was examined under long-term cyclic loading at low intensity. During most tests, drained conditions arose. The testing programme focussed on the development of cyclic displacement and cyclic degradation. The first part of examinations contained slow monotonic pull-out tests that provided reference capacities for the cyclic tests. The bucket was pulled up immediately after the installation with a displacement rate $v=0.002$ mm/s. The second part of examinations contained cyclic loading tests of 20,000-40,000 harmonic cycles N and cyclic frequency f of 0.05-0.1 Hz. The cyclic tests ended with a post-cyclic monotonic tensile load that indicated the level of cyclic degradation (Figure 4.13).

Table 4.2 shows the results of ten monotonic loading tests. For each of the monotonic loading tests, a test ID is given that indicates the membrane pressure level. For example, in a test with the ID M40.1, M indicates a monotonic test, 40 a membrane pressure aiming at 40 kPa and .1 is the attempt number. Reference tensile capacities F_{TR} at various p_m were derived as the average of the corresponding peak tensile resistances. F_{TR} were used for the normalization of cyclic loads.

Table 4.3 shows the results of 18 cyclic loading tests. The test IDs marked the membrane pressure and loading conditions as follows: in test C70A0.24m-0.23, C - cyclic test, 70 - aimed membrane pressure of 70 kPa, A0.24 - cyclic loading amplitude in the test $\xi_A=0.24$ and m-0.23 - the mean cyclic load in the test $\xi_m=-0.23$. The last two coefficients express the corresponding load divided by the reference tensile load F_{TR} .

4.5.1 Main findings

In most monotonic loading tests, the tensile peak resistance was reached at the upward displacement of up to -10 mm. Iskander et al. (2002) examined a caisson of $D=0.1$ m and $d=0.2$ m, which resulted in drained tensile peak load F_T mobilized at a displacement of -4 mm. Thomassen (2016) performed tests with a pile segment of $D=0.5$ m and $d=0.95$ m, which resulted in F_T reached at about -5 mm. Vaitkunaite et al. (2016) performed tests with a bucket foundation model of $D=0.5$ m and $d=0.25$ m, which

resulted in F_T mobilized at displacements of maximum -3.6 mm. All these results indicate that the upward displacement has no correlation neither with diameter nor with skirt/shaft length. Moreover, it may be stated, that the drained tensile capacity is generally reached within a displacement of up to -10 mm in dense sands.

The development of the load and displacement was expressed by peak loading stiffness k_{peak} , which was around 1 MN/m for the monotonic loading tests.

Unit skin friction f_s is analysed for the monotonic loading tests at different levels of surcharge (Figure 4.14). f_s corresponds to the tensile peak load divided by the sum of the inner and outer area of the skirt. f_s is back-calculated according to API (2011) using $K \tan \delta = 0.46$ as recommended for dense sand with D_R in the range of 65-85%. The method under-predicts f_s at surcharges of 2 kPa and 77 kPa, but fits well the other f_s values. Based on performed tests, f_s indicates a non-linear increase of the unit skin friction with the overburden pressure. The non-linear increase of f_s may be explained by the non-linear change of the lateral earth pressure coefficient K (Figures 2.5 and 4.15). The high K value of about 3 at very low soil stress may be generated by the dilative behaviour of dense sand at low stress which is along with findings of Thomassen (2016) and Boulon and Foray (1986).

While most of the cyclic tests resulted in very small cyclic displacements $|w_{cyc}| < 0.01D$, five of them were interrupted because of an excessive development of vertical displacement. In those tests, tensile peak loads reached the reference load or even succeeded it. It was noticed that during the critical tests in saturated sand, namely C0A0.7m-0.4.1 and C0A0.7m-0.4.2, a minor pore suction developed, contributing to the additional capacity of the tensile resistance. Consequently, these tests could resist more cycles compared to the tests where the membrane pressure was applied.

Eight cyclic loading tests finished with a monotonic post-cyclic loading. The peak capacity F_{Pc} was up to 25% lower than the virgin tensile capacity F_T in tests with $p_m = 0$ kPa. Rather few post-cyclic tests were performed with membrane pressures $p_m > 0$ kPa; they did not indicate any cyclic degradation.

Cyclic loading and unloading stiffness were higher than the virgin loading stiffness k_{peak} , with the magnitude depending on the loading amplitude and the mean cyclic load. Post-cyclic monotonic loading tests also resulted in higher peak loading stiffness k_{Pc} than the virgin loading stiffness. The average k_{Pc} was 2.1 MN/m.

Cyclic loading tests showed that mean tensile loads of up to 50% of the tensile drained capacity can be allowed for the design without resulting in excessive accumulated displacement. Figure 4.16 summarizes all cyclic loading test results. The stable zone marks the region where the accumulated displacement was $|w_{cyc}| < 0.01D$.

Table 4.2 Summary of monotonic loading tests. (Vaitkunaite, 2016)

p_m [kPa]	Test ID	d/D	Loading			Installation	
			F_T [kN]	w_T [mm]	v [mm/s]	F_P [kN]	d_{inst} [mm]
0	M0.1	0.5	-5.7	-6.3	0.001	49.6	483
0	M0.2	0.5	-6.3	-5.8	0.001	50.6	474
0	M0.3	0.5	-5.3	-4.6	0.002	49.5	473
0	M0.5	0.5	-5.9	-5.5	0.002	73.0	491
19	M20.1	0.5	-19.0	-24.3	0.001	45.3	486
21	M20.2	0.5	-15.3	-11.4	0.001	46.1	495
20	M20.3	0.5	-23.3	-7.5	0.002	57.3	487
41	M40.1	0.5	-28.2	-5.0	0.001	68.3	487
40	M40.2	0.5	-26.9	-5.2	0.002	72.8	487
73	M70.1	0.5	-96.3	-72.2	0.002	74.0	490

p_m - membrane pressure, F_T - peak tensile load, w_T - displacement at F_T ,
 v - pull-out rate, F_P - installation load, d_{inst} - installation depth.

Table 4.3 Summary of cyclic loading tests. (Vaitkunaite, 2016)

p_m [kPa]	Test ID	Cyclic loading				Post-cyclic load	
		F_{mean} [kN]	F_{cyc} [kN]	w_{cyc} [mm]	N [Hz]	F_{Pc} [kN]	w_{Pc} [mm]
0	C0A0.2m-0.4	-2.11	1.02	-0.88	39,592	-5.34	-3.83
0	C0A0.3m-0.4.1	-2.05	1.93	-1.35	38,227	-5.95	-7.60
0	C0A0.3m-0.4.2	-2.05	1.93	-6.23	39,753	-4.74	-0.53
0	C0A0.7m-0.4.1	-2.05	3.85	-63.76	8,100	-	-
0	C0A0.7m-0.4.2	-2.05	3.85	-65.80	1,285	-	-
0	C0A0.7m0.3.1	1.80	3.85	0.15	28,263	-	-
0	C0A0.7m0.3.2	1.80	3.85	0	39,980	-4.85	-1.30
0*	C0A0.4m0.3	1.91	2.30	0.04	19,629	-5.03	-3.43
0	C0A0.3m-0.1	-0.30	1.66	-0.64	39,729	-	-
0	C0A0.2m0.0	0	1.00	-0.29	40,020	-4.86	-4.84
43*	C40A0.4m0.4	11.76	11.38	0.72	19,900	-31.33	-12.35
41	C40A0.7m-0.5	-13.03	18.37	-67.55	67	-	-
41	C40A0.3m-0.7	20.12	9.33	-63.81	202	-	-
71*	C70A0.3m0.0.1	2.01	29.38	0.74	19,970	-	-
70	C70A0.3m0.0.2	1.92	29.30	1.25	40,867	-93.26	-28.29
73	C70A0.2m-0.2	-22.39	23.08	0.10	31,619	-93.90	-26.53
71	C70A0.3m-0.5	-51.67	24.49	-75.01	19,081	-	-
71	C70A0.5m-0.5	-50.61	45.78	-81.90	5	-	-

*Tests with $f=0.05$ Hz, other tests are with $f=0.01$ Hz

F_{mean} - mean cyc. load, F_{cyc} - cyc. loading amplitude, w_{cyc} - cyc. displacement,
 N - number of cycles, F_{Pc} - peak post-cyc. load, w_{Pc} - displacement at F_{Pc} .

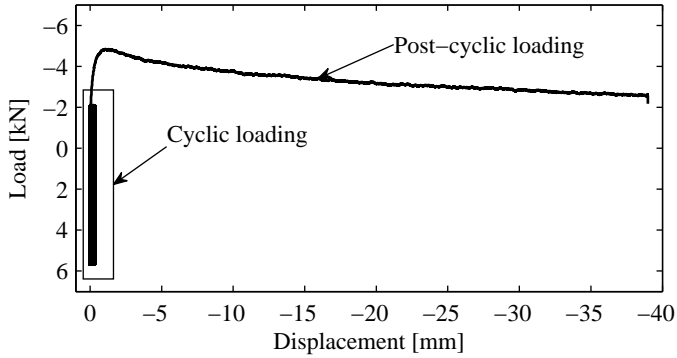


Figure 4.13 Cyclic loading with post-cyclic monotonic pull-out (test C0A0.7m0.3.2). (Vaitkunaite, 2016)

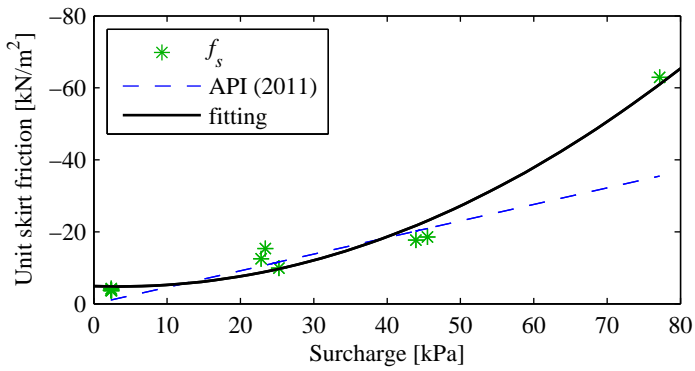


Figure 4.14 Peak tensile load developed at different surcharge levels. (Vaitkunaite, 2016)

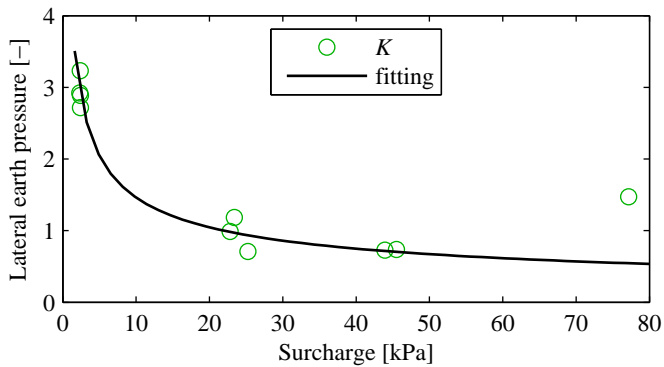


Figure 4.15 Back-calculated lateral earth pressure. (Vaitkunaite, 2016)

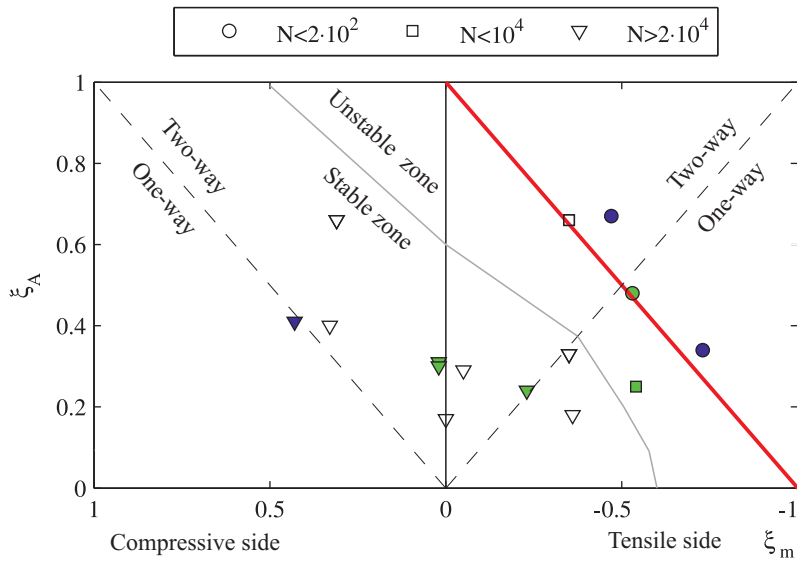


Figure 4.16 Interaction diagram for cyclic loading tests with overburden pressure: 0 kPa (empty marks), 40 kPa (blue) and 70 kPa (green). Red line marks limit of the drained tensile capacity. (Vaitkunaite, 2016)

4.6 Tests performed in the pressure tank

The section is based on Paper 6 and Paper 7:

Paper 6: Bucket Foundation Response under Various Displacement Rates. *International Journal of Offshore and Polar Engineering*, 26(2), 116-124.

Paper 7: *Bucket Foundations under Axial Loading: Test Data Series 13.02.XX, 13.03.XX and 14.02.XX*. Aalborg: Department of Civil Engineering, Aalborg University. DCE Technical Reports; No. 199.

As mentioned in Section 2.2, soil drainage depends on the size of the foundation, loading intensity and soil permeability. Cavitation pressure limits the pore suction that can be induced by loading. When performing cyclic loading tests in the large sand container (see Section 4.5), it was noticed that higher cyclic loading rates induced some negative pore pressures. The drainage conditions are very important for bucket foundation design. The soil below the full-scale bucket foundations would normally experience partial drainage of some degree if permeability is sufficiently low. The test set-up presented in Section 4.4 was not applicable for investigations of condition under higher pore pressures. Thus, the opportunity to test bucket foundation responses in a pressure tank was taken (Figure 4.17).

The test set-up was described by Nielsen et al. (2016) and a short description was given in Paper 6. The aluminium bucket foundation model had dimensions of 0.5 m in diameter and 0.25 m in skirt length. The model had a very smooth skirt wall, which allowed focussing on pore pressure development when subjected to tensile loading. The bucket was installed in dense Aalborg University sand No. 1. The sand sample was prepared in the way as described in Section 4.4 for the previous test set-up.

The bucket was installed by mechanical pushing, compressively pre-loaded and completely unloaded. Afterwards, the tank was closed and a pressure of 200 kPa established (300 kPa including the atmospheric pressure). The bucket model was pulled axially with various displacement rates. Fifteen tests were performed of which ten were documented in Paper 6 showing data with different pull-out rates of 0.01-152 mm/s. The results are summarized in Table 4.4. Tests are numbered according to the pull-out rate; for example, the bucket model has been pulled-out with a velocity of 0.1 mm/ in test v0.1

4.6.1 Main findings

The testing programme showed that the tensile capacity (peak tensile resistance) correlated with the pull-out rate (Figure 4.19). Moreover, the tensile capacity was reached at increasing displacements that were directly dependent on the pull-out rate. Based on the performed tests, it was noticed that much larger than the drained tensile capacity was available even considering the design limit for the upward displacement. Partial drainage in sand should thus be accounted for when estimating tensile capacity.

Table 4.4 Summary of pull-out rate tests in pressure tank. (Vaitkunaite et al., 2016)

p_t [kPa]	Test No.	Loading			Installation		D_R [%]	γ' [kN/m ³]
		F_T [kN]	w_T [mm]	v [mm/s]	F_P [kN]	d_{inst} [mm]		
0	v0.01	(0)	(0)	0.01	31.0	240.5	79	9.3
200	v0.05	-2.7	-0.7	0.05	32.0	239	85	9.6
200	v0.1	-4.08	-0.65	0.10	31.4	240.7	86	9.6
200	v1	-8.02	-3.61	1	37.6	242.0	88	9.7
201	v10	-30.79	-16.01	10	43.7	241.5	90	9.8
200	v22	-44.07	-14.73	21.70	33.0	236.2	83	9.5
200	v27	-48.84	-14.29	27.20	31.5	239.0	85	9.6
200	v47	-65.36	-48.78	46.71	31.5	236.4	83	9.5
200	v98	-71.65	-60.48	98.30	31.0	239.3	82	9.5
200	v152	-75.17	-68.18	152.30	37.0	236.0	84	9.5

Figure 4.18 shows peak pore pressure distribution for four tests. The higher the pull-out rate that was applied, the lower negative pressure was generated. The final test resulted in cavitation pressure, with all inner pore pressure transducers showing nearly identical suction values, indicating undrained behaviour (Figure 4.18, test v152).

Two analytical methods by Iskander et al. (2002) and Houlsby et al. (2005b) were considered for the back calculation of the test data. While the second method gave a very good match with the test data, successful capacity prediction presupposed knowledge of the particular suction induced by the pull-out rate.



Figure 4.17 Pressure tank used for the displacement rate tests.

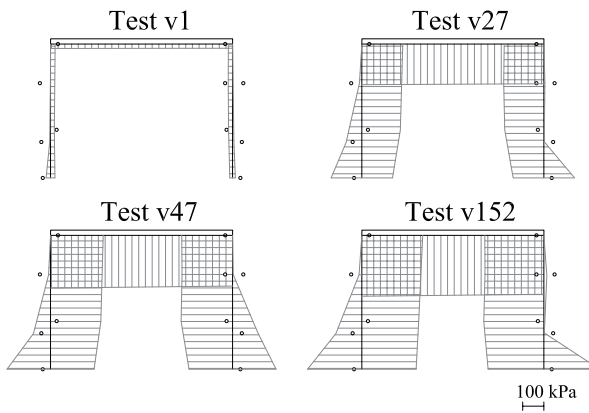


Figure 4.18 Pore pressure distribution around the bucket skirt at peak tensile load for tests with displacement rates v in mm/s. (Vaitkunaite et al., 2016)

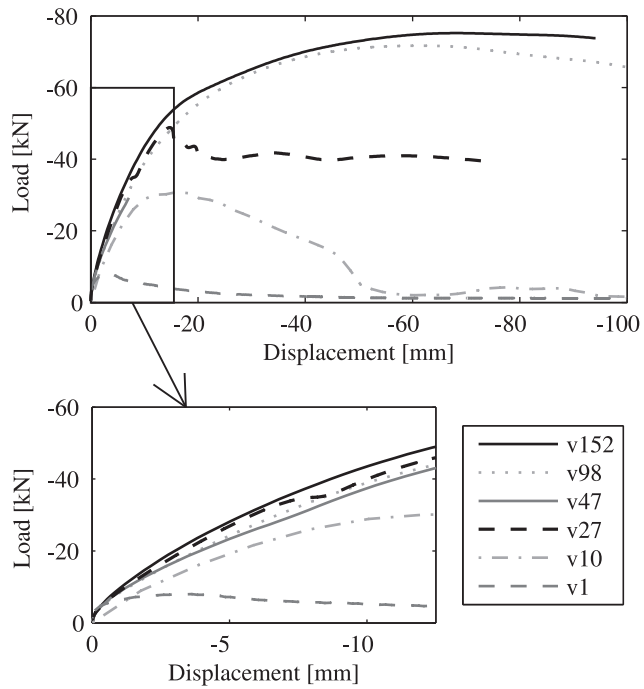


Figure 4.19 Load and displacement results for tests with displacement rates v in mm/s. (Vaitkunaite et al., 2016)

CHAPTER 5

Conclusion and future work

The thesis has addressed a number of critical loading conditions for bucket foundations in sand. Physical modelling was the key tool applied for the analysis as this showed the largest potential for clarifying real bucket foundation behaviour under axial loading. A new test set-up was designed for the analysis of long-term cyclic loading conditions. A pressure tank was furthermore employed for the examination of pore pressure distribution around a bucket foundation model subjected to various pull-out rates. The research work has been documented in seven scientific papers that form the basis of this thesis.

The following Section 5.1 presents the overall outcome of the research, based on its study objectives (Section 3.2). Section 5.2 provides recommendations for future analyses regarding model testing and investigation into the tensile loading on bucket foundations.

5.1 Conclusion

A new laboratory testing facility was designed for the examination of long-term cyclic loading on a bucket foundation model. This allowed for the testing of a large bucket foundation model in laboratory conditions on a 1:10 scale model with a diameter of 1 m and a skirt length of 0.5 m. To the best knowledge of the author, this is the largest model foundation ever tested under laboratory conditions. The model skirt was naturally corroded and installed in fine dense sand providing realistic interface parameters. The size of the sand container was maximally utilized testing mainly tensile loads and minor compressive loads. The boundaries of the sand container thus had no influence on the results. The application of suction under the membrane simulated an evenly distributed overburden pressure, which allowed for the examinations of friction responses at different soil depths. Overall, the design of the test set-up was successful in that it provided high-quality data and consistent results that were essential for the data analysis.

Monotonic displacement controlled tests were performed at various overburden pressure levels. With the slow displacement rate of 0.002 mm/s, drained responses were

obtained. The tensile peak load was achieved within the first 10 mm of upward displacement, followed by an even reduction due to the diminishing area of the soil-structure interface as well as soil softening. The higher the membrane pressure level that was applied, the higher peak resistance was measured, while the stiffness was similar for majority of the tests, at approximately 1 MN/m. The peak resistance values were used for the analysis of interface parameters. It was noticed that the unit skin friction increased non-linearly with the overburden pressure, which may be explained by a non-linear change in the lateral earth pressure. Back-calculation of the lateral earth coefficient K resulted in values from 3 for the low vertical stresses to 0.5 for the higher vertical stresses. The rapid change of K may be expected in the first five meters from the seabed surface. The tests results show that during static tensile loading, lateral earth pressure is higher than may be predicted with the conventional methods.

The next set of examinations involved cyclic load controlled tests at various overburden pressure levels. The mean cyclic loads and amplitudes were normalized with the measured drained tensile capacity. The bucket foundation model was subjected to long-term cyclic loading containing up to 40,000 cycles at a constant frequency of 0.05 or 0.1 Hz. Two-way (compression-tension) and one-way tensile loads were applied in the test programme. It was noticed that mean tensile loads of up to 50% of the tensile drained capacity could be allowed for the design without causing an excessive accumulated displacement during the 40,000 cycles. However, all testing with tensile mean loads resulted in an incremental upward displacement, even though it was as small as -10^{-4} mm. While the cyclic test resulted in very small accumulated displacements $|w_{cyc}| < 0.01D$, the model was exposed to gradual pull-out when peak loads reached the drained tensile capacity.

Values for the cyclic loading and unloading stiffness were higher than those found for virgin loading stiffness. The magnitude depended on the loading amplitude and the mean cyclic load. Post-cyclic monotonic loading showed a stiffer response compared to the virgin loading. The post-cyclic peak tensile capacity was up to 25% lower than the virgin tensile capacity in tests with no membrane pressure. Relatively few post-cyclic tests were performed with membrane pressures $p_m > 0$ kPa; no indication of cyclic degradation was observed.

The final set of tests concerned tensile loadings in a pressure tank. The tank enabled the examination of very low negative pore pressures in a simulation of conditions at 20 m water depth. A bucket foundation model with a diameter of 0.5 m and a skirt length of 0.25 m was installed in dense sand. The smoothness of the model skirt (corrosion free) allowed a focus on the pore pressure distribution and the tensile capacity. The model was subjected to various pull-out rates. A rapid pull-out generated fully undrained behaviour, based on the measurements of the pore pressure transducers. The peak tensile resistance was found to increase with the pull-out rate, as did the upward displacement. The initial loading stiffness showed no clear dependency on the displacement rate. It was found that much larger than the drained tensile capacity is available, even when the limitations of the upward displacement are considered. To

integrate this finding in design practise, a reliable method of negative pore pressure prediction in relation to loading intensity needs to be identified.

Natural seabed conditions are extremely changeable, characterized by complex layering of soils and rich variation in their stiffness, strength parameters and various hydraulic conductivities. Furthermore, offshore loading conditions are complex, with their various loading regimes, amplitudes and mean loads. Model testing provides valuable information about soil and foundation behaviour. But large amounts of data and experimental analysis are still needed before all design aspects are clarified and standardized solutions can be proposed. The data provided in this thesis offer valuable information regarding the behaviour of bucket foundations under tensile cyclic loads in uniform dense sand.

5.2 Recommendations for Future Work

Designing a new model testing facility has been a laborious process. It required much reflection supported by the understanding of physical systems, and not least, imagination. Although the two-year development process of the "Large Yellow Box" testing facility has already yielded significant results, a number of improvements are suggested below:

- The possibility of enabling sand saturation should be investigated if further testing at overburden pressures are to be performed. This is especially relevant for increased loading rates.
- The effect of sand compaction with a rod vibrator on the horizontal stress level should be assessed. This would provide more exact values for the lateral earth pressure coefficient.
- Correct interface properties are essential to successful designing. Further soil-structure interface analysis should be performed considering various sand and gravel types and metal surfaces. Interface tests performed in direct shear box tests may supplement the model test data.
- Even though the main focus of the present project was long-term cyclic loading and drained response, it was observed that small negative pore pressures occurred in a few cyclic loading tests. The pore suction developed gradually during the long-term cyclic loading under constant mean and cyclic loads. In the performed tests, the measuring range of the pore pressure transducers exceeded the needed range at least 50 times, with the result that their accuracy was slightly unsatisfactory (± 2 kPa). Selecting the measuring sensors according to the required measuring range is likely to provide more accurate results.
- The accuracy of cyclic loading interaction diagrams would benefit from cyclic loading tests with different model diameters and skirt sizes. The results would be directly applicable for prototype design.

Bibliography

- Abdel-Rahman, K., Achmus, M., and Thieken, K. (2014). A numerical model for the simulation of pile capacity degradation under cyclic axial loading. In *Proceedings of the 8th European Conference on Numerical Methods on Geotechnical Engineering (NUMGE)*, Delft, Netherlands.
- Acosta-Martinez, H. E. and Gourvenec, S. M. (2008). Response of skirted foundations for buoyant facilities subjected to cyclic uplift loading. *International Journal of Offshore and Polar Engineering*, pages 705–712.
- Andersen, K. H. (2009). Bearing capacity under cyclic loading - offshore, along the coast, and on land. *Canadian Geotechnical Journal*, 46:513–535.
- Andersen, K. H., Dyvik, R., and Schroder, K. (1992). *Pull-out capacity analyses of suction anchors for tension leg platforms*. British Maritime Technology.
- Andersen, K. H., Jostad, H. P., and Dyvik, R. (2008). Penetration resistance of offshore skirted foundations and anchors in dense sand. *Journal of Geotechnical and Geoenvironmental Engineering*, 134(1):106–116.
- Andersen, K. H. and Lauritzsen, R. (1988). Bearing capacity for foundations with cyclic loads. *Journal of Geotechnical Engineering*, 114(5):540–555.
- API (2011). *Geotechnical and foundation design considerations - ANSI/API recommended practise 2GEO*. American Petroleum Institute.
- Baldi, G., Bellotti, R., Ghionna, V., Jamiolkowski, M., and Pasqualini, E. (1986). Interpretation of CPTs and CPTUs; 2nd part: drained penetration of sands. In *Proceedings of the Fourth International Geotechnical Seminar, Singapore*, pages 143–156.
- Böker, C. (2009). *Load simulation and local dynamics of support structures for offshore wind turbines*. PhD Thesis, Leibnitz University Hannover.
- Bolton, M. D. and Lau, C. K. (1993). Vertical bearing capacity factors for circular and strip footings on Mohr-Coulomb soil. *Canadian Geotechnical Journal*, 30(6):1024–1033.

- Boulon, M. and Foray, P. (1986). Physical and numerical simulations of lateral shaft friction along offshore piles in sand. In *Proceedings of the Third International Conference on Numerical Methods in Offshore Piling, Nantes*, pages 127–147.
- Brinch-Hansen, J. (1970). *A revised and extended formula for bearing capacity*. Geotechnisk Institut, Bulletin No. 28, Copenhagen, Denmark.
- Buckingham, E. (1914). On physically similar systems; illustration of the use of dimensional equations. *Physical Review*, 4(4):345–376.
- Bye, A., Erbrich, C., and Tjelta, T. I. (1995). Geotechnical design of bucket foundations. In *Proceedings of the 27th Offshore Technology Conference, Houston, Texas*, pages 869–883. Offshore Technology Conference.
- Byrne, B. W. (2014). Laboratory scale modelling for offshore geotechnical problems. In *CPMG2014—Physical Modelling in Geotechnics: Proceedings of the 8th International Conference on Physical Modelling in Geotechnics 2014 (ICPMG2014), Perth, Australia*, pages 61–75. Taylor & Francis Group, London.
- Byrne, B. W. and Houlsby, G. T. (2002a). Experimental investigations of response of suction caissons to transient vertical loading. *Journal of Geotechnical and Geoenvironmental Engineering*, 128(11):926–939.
- Byrne, B. W. and Houlsby, G. T. (2002b). Investigating novel foundations for offshore windpower generation. In *ASME 2002 21st International Conference on Offshore Mechanics and Arctic Engineering, Oslo*, pages 567–576. American Society of Mechanical Engineers.
- Caquot, A. and Kerisel, J. (1953). Ultimate bearing capacity of a foundation lying on the surface of cohesionless soil. In *Proceedings of the 3rd International Conference on Soil Mechanics and Foundation Engineering, Zurich, Switzerland*.
- Clukeley, E. C., Morrison, M. J., Garnier, J., and Corte, J. F. (1995). The response of suction caissons in normally consolidated clays to cyclic tlp loading conditions. In *Proceedings of Offshore Technology Conference, Richardson, TX*, volume 2, pages 909–918. Offshore Technology Conference.
- Corte, J. F. (1989). General report: Model testing - geotechnical model tests. In *Proceedings of the International Conference on Soil Mechanics and Foundation Engineering*, pages 2553–2571.
- DAE (2016). Danish Energy Agency. <http://www.ens.dk/ny-teknologi/eudp-energiteknologisk-udvikling-demonstration>. Last accessed on Feb 18, 2016.
- Davis, E. H. and Booker, J. R. (1971). The bearing capacity of strip footings from the standpoint of plasticity theory. In *Proceedings of the first Australia-New Zealand Conference in Geomechanics, Melbourne, Australia*, pages 276–282.

- Deng, W. and Carter, J. P. (2002). A theoretical study of the vertical uplift capacity of suction caissons. *International Journal of Offshore and Polar Engineering*, 12(2):89–97.
- DNV (1992). *Foundations. Classification notes No.30.4*. Det Norske Veritas, Oslo, Norway.
- DNV (2014). *Offshore Standard DNV-OS-J101: Design of offshore wind turbine structures*. Det Norske Veritas AS.
- EC-7 (2004). *EN 1997-1:2004, Eurocode 7: Geotechnical design – Part 1: General rules. Dansk Standard*. Dansk Standard, Nordhavn, Denmark.
- EMEC (2016). The European Marine Energy Centre Ltd. <http://www.emec.org.uk>. Last accessed on Jan 13, 2016.
- Energiforskning.dk (2016). Energiforskning.dk. <http://energiforskning.dk/en/node/7973>. Last accessed on Feb 18, 2016.
- Energinet.dk (2016). Energinet.dk. <https://www.energinet.dk/DA/FORSKNING/Sider/default.aspx>. Last accessed on Feb 18, 2016.
- ETI (2016). Energy Technologies Institute. <http://www.eti.co.uk/project/perawat/>. Last accessed on Feb 18, 2016.
- EWEA (2016). European Wind Energy Association. <http://www.ewea.org>. Last accessed on Jan 13, 2016.
- Feld, T. (2001). *Suction Buckets: a new innovative foundation concept, applied to offshore wind turbines*. Ph.D. Thesis, AAU Geotechnical Engineering Papers R0108, Aalborg University, Aalborg, Denmark.
- Foglia, A. (2014). *Bucket foundations under lateral cyclic loading*. DCE Thesis No. 68. Department of Civil Engineering, Aalborg University, Aalborg.
- Gaydadhiew, D., Puscasu, I., Vaitkunaite, E., and Ibsen, L. B. (2015). Investigation of dense sand properties in shallow depth using cpt and dmt. In Marchetti, S., Monaco, P., and Fonseca, V. D., editors, *Proceedings of the Third International Conference on the Flat Dilatometer, Rome, Italy*, 132, pages 223–230.
- GWEC (2016a). Global Wind Energy Council. <http://www.gwec.net/global-figures/global-offshore/>. Last accessed on Jan 10, 2016.
- GWEC (2016b). Global Wind Energy Council. <http://www.gwec.net/global-figures/wind-in-numbers/>. Last accessed on Jan 10, 2016.
- Hansen, B. (1979). Definition and use of frictional angles. In *Proceedings of the International Conference VII ECSMFE, Brighton, Great Britain*.
- Hedegaard, J. and Borup, M. (1993). *Klassifikationsforsoeg med Baskard Sand No. 15*. Department of Civil Engineering, Aalborg University, Aalborg.

- Hogervorst, J. R. (1980). Field trials with large diameter suction piles. In *Offshore Technology Conference, Houston, Texas*.
- Houlsby, G. T. and Byrne, B. W. (2005a). Design procedures for installation of suction caissons in clay and other materials. *Geotechnical Engineering*, 158(2):75–82.
- Houlsby, G. T. and Byrne, B. W. (2005b). Design procedures for installation of suction caissons in sand. *Geotechnical Engineering*, 158(2):135–144.
- Houlsby, G. T., Ibsen, L. B., and Byrne, B. W. (2005a). Suction caissons for wind turbines. In *Frontiers in Offshore Geotechnics I Proceedings of the first International Symposium Frontiers in Offshore Geotechnics (ISFOG), Perth, Australia*, pages 75–93. Taylor & Francis Group, London.
- Houlsby, G. T., Kelly, R. B., and Byrne, B. W. (2005b). The tensile capacity of suction caissons in sand under rapid loading. In *Frontiers in Offshore Geotechnics I Proceedings of the first International Symposium Frontiers in Offshore Geotechnics (ISFOG), Perth, Australia*, page 405–410. Taylor & Francis Group, London.
- Houlsby, G. T., Kelly, R. B., Huxtable, J., and Byrne, B. W. (2006). Field trials of suction caissons in sand for offshore wind turbine foundations. *Géotechnique*, 56(1):3–10.
- Ibsen, L. B. (1995). The static and dynamic strength of sand. In *Proceedings of the 11th European Conference on Soil Mechanics and Foundation Engineering, Copenhagen*.
- Ibsen, L. B. (1999). The mechanism controlling static liquefaction and cyclic strength of sand. In *Proceedings of the Int. Workshop on the Physics and Mechanics of Soil Liquefaction*, pages 29–39. A.A. Balkema, Rotterdam.
- Ibsen, L. B. and Boedker, L. (1994). *Baskarp Sand No. 15: data report 9301*. Department of Civil Engineering, Aalborg University, Aalborg.
- Ibsen, L. B., Hanson, M., Hjort, T., and Thaarup, M. (2009). *MC-Parameter Calibration of Baskarp Sand No.15*. DCE Technical Report No. 62.
- Ibsen, L. B. and Lade, P. V. (1998). The role of the characteristic line in static soil behavior. In *Proceedings of the 4th Int. Workshop on Localization and Bifurcation Theory for Soils and Rocks, Gifu, Japan*, pages 221–230. A.A. Balkema, Rotterdam.
- INN WIND.EU (2015). Innovative Wind Conversion Systems (10-20MW) for Offshore Applications. <http://www.innwind.eu/About-INN WIND>. Last accessed on Jan 13, 2016.
- Iskander, M. G., El-Gharbawy, S., and Olson, R. E. (2002). Performance of suction caissons in sand and clay. *Canadian Geotechnical Journal*, 39(3):576–584.

- Iskander, M. G., Olson, R. E., and Pavlicek, R. W. (1993). Behavior of suction piles in sand. *Design and Performance of Deep Foundations, Piles and Piers in Soil and Soft Rock*, 38:157–171.
- ISO (2003). *Petroleum and natural gas industries — Specific requirements for offshore structures — Part 4: Geotechnical and foundation design considerations*. The International Organization for Standardization. ISO 19901-4:2003.
- ISO (2007). *Petroleum and natural gas industries — Fixed steel offshore structures*. The International Organization for Standardization. ISO 19902:2007.
- Jafarzadeh, F. and Sadeghi, H. (2012). Experimental study on dynamic properties of sand with emphasis on the degree of saturation. *Soil Dynamics and Earthquake Engineering*, 32:26–41.
- Jakobsen, M. M. (2015). *Wave-structure interactions on point absorbers - an experimental study*. Ph.D. Thesis. Department of Civil Engineering, Aalborg University, Aalborg.
- Jara, F. A. V. (2006). *Model testing of foundations for offshore wind turbines*. Ph.D. Thesis, Oxford University, Keble College, Michaelmas Term.
- Jardine, R., Chow, F., Overy, R., and Standing, J. (2005). *ICP design methods for driven piles in sands and clays*. Thomas Telford Publishing, London.
- Jostad, H. P., Grimstad, G., Andersen, K. H., Saue, M., Shin, Y., and You, D. (2014). A FE procedure for foundation design of offshore structures - applied to study a potential OWT monopile foundation in the Korean western sea. *Geotechnical Engineering Journal of the SEAGS & AGSSEA*, 45(4):63–72.
- Kelly, R. B., Byrne, B. W., Houlsby, G. T., and Martin, C. M. (2003). Pressure chamber testing of model caisson foundations in sand. In *Proceedings of the international conference on foundations, Dundee*, pages 421–431.
- Kelly, R. B., Byrne, B. W., Houlsby, G. T., and Martin, C. M. (2004). Tensile loading of model caisson foundations for structures on sand. In *Proceedings of the Fourteenth International Offshore and Polar Engineering Conference, Toulon*.
- Kelly, R. B., Houlsby, G. T., and Byrne, B. W. (2006a). A comparison of field and laboratory tests of caisson foundations in sand and clay. *Géotechnique*, 56(9):617–626.
- Kelly, R. B., Houlsby, G. T., and Byrne, B. W. (2006b). Transient vertical loading of model suction caissons in a pressure chamber. *Géotechnique*, 56(10):665–675.
- Larsen, K. A. (2008). *Static behaviour of bucket foundations: Thesis submitted for the degree of Doctor of Philosophy*. DCE Thesis; Nr. 7, vol. 1. Department of Civil Engineering, Aalborg University, Aalborg.

- Lundgren, H. and Mortensen, K. (1953). Determination by the theory of plasticity of the bearing capacity of continuous footing on sand. In *Proceedings of the third International Soil Mechanics Conference, Zurich, Switzerland*, pages 409–410.
- Nielsen, S. D., Ibsen, L. B., and Nielsen, B. N. (2016). Advanced laboratory setup for testing offshore foundations. *Geotechnical Testing Journal*.
- Niemunis, A., Wichtmann, T., and Triantafyllidis, T. (2005). A high-cycle accumulation model for sand. *Computers and Geotechnics*, 32(4):245–263.
- Senders, M. (2009). *Suction caissons in sand as tripod foundations for offshore wind turbines*. PhD Thesis, University of Western Australia.
- Shell (2016). Shell Global. <http://www.shell.com/about-us/major-projects/perdido.html>. Last accessed on Jan 10, 2016.
- Skau, K. S. and Jostad, H. P. (2014). Application of the ngi-procedure for design of bucket foundations for offshore wind turbines. In *Proceedings of the 24th International Ocean and Polar Engineering Conference, Busan*, pages 514–520.
- Sørensen, S. P. H., Ibsen, L. B., and Foglia, A. (2012). Testing of laterally loaded rigid piles with applied overburden pressure. In *NGM 2012 Proceedings : Proceedings of the 16th Nordic Geotechnical Meeting*.
- Thieken, K., Achmus, M., and Schroder, C. (2014). On the behaviour of suction buckets in sands under tensile loads. *Computer and Geotechnics*, 60:88–100.
- Thomassen, K. (2016). *Experimental investigations of tension piles in sand subjected to static and cyclic loading*. PhD Thesis, Department of Civil Engineering, Aalborg University, Aalborg.
- Tjelta, T. I. (1995). Geotechnical experience from the installation fo the europipe jacket with bucket foundations. In *Proceedings of the 27th Offshore Technology Conference, Houston*, pages 897–908.
- Tjelta, T. I. (2015). The suction foundation technology. In *Proceedings of the Third International Symposium on Frontiers in Offshore Geotechnics, Oslo*, volume 30, pages 331–342.
- Tjelta, T. I., Guttormsen, T. R., and Hermstad, J. (1986). Large scale penetration test at a deepwater site. In *Proceedings of Offshore Technology Conference*.
- Vaitkunaite, E. (2015). *Test procedure for axially loaded bucket foundations in sand (Large Yellow Box)*. DCE Technical Memorandum No. 51, Department of Civil Engineering, Aalborg University, Aalborg.
- Vaitkunaite, E. (2016). *Testing of axially loaded bucket foundation with applied overburden pressure*. DCE Technical Report No. 209, Department of Civil Engineering, Aalborg University, Aalborg.

- Vaitkunaite, E., Nielsen, B. N., and Ibsen, L. B. (2015). Comparison of design methods for axially loaded buckets in sand. In *Frontiers in Offshore Geotechnics III proceedings of the third international symposium on frontiers in offshore geotechnics, Oslo*, pages 331–342.
- Vaitkunaite, E., Nielsen, B. N., and Ibsen, L. B. (2016). Bucket foundation response under various displacement rates. *International Journal of Offshore and Polar Engineering*, 26(2):116–124.
- WaveDragon (2009). Wave Dragon ApS. <http://www.wavedragon.net>. Last accessed on Jan 13, 2016.
- Wavestar (2011). Copyright of “Wavestar A/S”, <http://wavestarenergy.com/>. Last accessed on Jan 10, 2016.
- Wavestar (2016). Wave Star A/S. <http://wavestarenergy.com/projects>. Last accessed on Jan 13, 2016.
- Wichtmann, T. (2005). *Explicit accumulation model for non-cohesive soils under cyclic loading*. Ph.D. Thesis, Soil Mechanics and Foundation Engineering, Ruhr-University Bochum, Issue No. 38.
- Zachert, H., Wichtmann, T., Triantafyllidis, T., and Hartwig, U. (2015). Simulation of a full-scale test on a gravity base foundation for offshore wind turbines using a high cycle accumulation model. In *Proceedings of the Third International Symposium on Frontiers in Offshore Geotechnics, Oslo*, pages 819–824.

Appendix

APPENDIX A

Comparison of Foundation Systems for Wave Energy Converters Wavestar

Vaitkunaite, E., Ibsen, L. B., Nielsen, B. N., and Devant Molina, S. (2013). Comparison of Foundation Systems for Wave Energy Converters Wavestar. In P. Frigaard, J. P. Kofoed, A. S. Bahaj, L. Bergdahl, A. Clément, D. Conley, A. F. O. Falcão, C. M. Johnstone, L. Margheritini, I. Masters, A. J. Sarmento, and D. Vicinanza (Eds.), *10th ewtec 2013 European Wave and Tidal Energy Conference Series: Proceedings of the 10th European Wave and Tidal Energy Conference, Aalborg, Denmark*. Technical Committee of the European Wave and Tidal Energy Conference. (European Wave and Tidal Energy Conference Series; No. 10).

Author's Right

Evelina Vaitkunaite

Fra: EWTEC Secretariat <info@ewtec.org>
Sendt: 20 May 2016 17:28
Til: Evelina Vaitkunaite
Emne: RE: Author's Right

Dear Evelina Vaitkunaite,

EWTEC proceedings are not open access – the copyright of papers in their final form remains with EWTEC, not with authors, as per the copyright agreement (subject to the usual exceptions of Crown and US government copyright). A pre-review version of an author's manuscript (without logos or proceedings' page numbers) may be deposited by the author on an institutional web site or online repository and should therefore be acceptable for inclusion in your thesis.

Kind Regards,

EWTEC Secretariat

From: Evelina Vaitkunaite [<mailto:ev@civil.aau.dk>]
Sent: 18 May 2016 19:50
To: info@ewtec.org
Subject: Author's Right

Dear Sir/Madam,

I have participated in the 10th European Wave and Tidal Conference 2013 with a paper "Comparison of Foundation Systems for Wave Energy Converters Wavestar". I would like to ask for your permission to include the paper in the Appendix of my Ph.D. Thesis.

Sincerely,
Evelina Vaitkunaite
Ph.D. Fellow

Department of Civil Engineering
Aalborg University
Sofieldalsvej 11
DK-9200 Aalborg
Denmark

The pre-review version of the manuscript. The layout has been revised.

Abstract. In order to deliver cost competitive solutions, Wave Energy Converters (WEC) must be optimized in several fields, e.g. transportation, installation, structure, machinery etc. Large expenses lie on the superstructure support, i.e. the offshore foundation. Geotechnical analysis and optimization of six possible foundation solutions for WEC are presented in this article. The study is performed for WEC superstructure supported by two or four foundations. In the four-column system horizontal wind and wave loads are transformed as a pair of vertical forces, acting in tension and compression. When the overturning moment is large, it might be desirable to increase the width distance, achieving smaller vertical forces. For this reason, several distances between the supporting columns are investigated. Additionally, a two-column system is analysed as it is expected to be more cost effective. In such a solution horizontal wind and wave loads are dominant.

Gravity based, pile and bucket foundations are universally applied solutions for the offshore structures. The suitability of these types for a WEC is analysed and commented. The foundations are designed to satisfy ultimate and serviceability limit state requirements. For each of the foundation solutions, three geotechnical design steps are followed, employing analytical calculations, numerical 2D and 3D finite element programs.

Keywords: bucket, pile, gravity based foundation, geotechnical design, wave energy converter, Wavestar.

A.1 Introduction

Wavestar C6-600 kW is a wave energy converter (WEC) designed to deliver 600 kW of electrical power to the grid (Figure A.1). It can operate in up to 20 m water depth including storm surcharge. At present, Wavestar has a grid-connected prototype installed in Hanstholm (Denmark), which is a section of Wavestar C6-600 kW. The prototype has been installed on four concrete foundations in soil predominated by chalk. (Marquis et al. 2012)



Figure A.1 Wavestar wave energy machine (Wavestar, 2011).

The purpose of this paper is to compare and evaluate six foundation solutions for a WEC discussing their applicability and construction materials used. The proposed systems are based on bucket, pile and gravity based foundation. These types are widely used in offshore structures and therefore may be well applicable

There are several different ways to transfer the loads into the foundations. The study is performed for WECs supported by two or four columns, which makes the difference in load

transfer from the structure through the foundation to the soil. The loading phase is explained in details in the following subsections. Six possible foundation solutions are presented and analysed using three geotechnical tools. The programs used are analytical models, the numerical 2D program LimitState:GEO and the finite element program Plaxis 3D.

A.1.1 Dimensioning Procedure

A foundation dimensioning scheme is shown in Figure A.2 and it describes the concept study process of the foundation solutions for the static analysis. The first three steps shown in the scheme are presented in this paper. Primary dimensioning is done with an analytical program, which differs depending on foundation type. Afterwards, a numerical 2D program LimitState:GEO is employed for secondary dimensioning and optimization. Finally, Plaxis 3D is employed for the last optimization and verification in ultimate limit state (ULS) and serviceability limit state (SLS). A completed geotechnical design could be followed by a structural foundation design and the price estimation could be carried out for the foundation and installation costs. The last two parts are not analysed in this article.

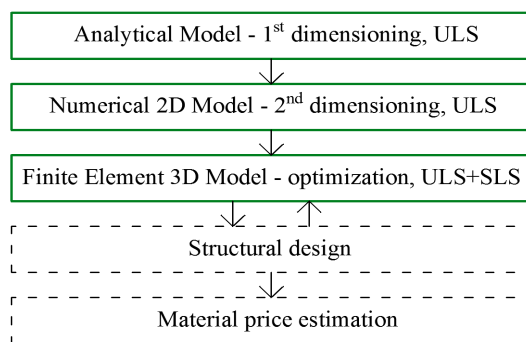


Figure A.2 Design scheme. The first three from top are analysed in this article.

A.1.2 Structural Solutions

As previously mentioned, Wavestar has an active prototype in Hanstholm. The superstructure is supported on four concrete foundations. The distribution of loads on the foundations depends on the overall structural solution. At the time of writing the detailed structural design for the new Wavestar C6-600 kW was unknown. Hence the upper structure is assumed to be perfectly rigid and supported by four pinned foundations, as shown in Figure A.3. In this case vertical compression and tension loads are dominating. It is planned that the new WEC C6-600 kW will be supported on four legs positioned with distances of 17 and 80 m. When the overturning moment is large, it could be desirable to increase the 17 m distance between legs achieving smaller vertical loads and resulting into smaller foundations. That is why the 30 m distance is also investigated, see Figure A.3.

Additionally, a solution with two foundations is considered in this paper because it is expected to be more economical. In such a solution horizontal wind and wave loads dominate, which leads to large moment loading on the foundations, see Figure A.4. However, a rigid foundation connection is assumed here, because it ensures the overall stability of the structure.

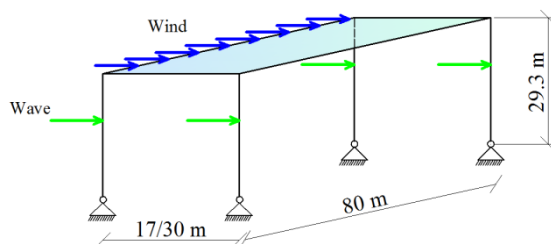


Figure A.3 Pinned support structure for four-column WEC C6-600kW. Wave loads marked in green and wind load marked in blue. The superstructure is assumed to be perfectly rigid.

A.1.3 Load Conditions

Loads on the foundation are provided by Wavestar A/S. This paper presents only calculations in a storm load case, where the superstructure is lifted to the highest position and locked. In such a case, it is expected that the structure will have to resist the highest wind and wave loads creating the least favourable situation.

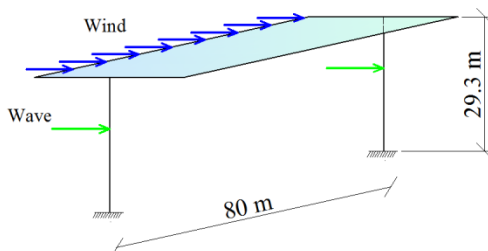


Figure A.4 Rigid support structure for two-column WEC C6-600kW. Wave loads marked in green and wind load marked in blue.

The assumed water depth is 16 m. Loads are estimated for several column diameters, i.e. 2, 3 and 4 m. The loads are presented in Table A.1 and Table A.2. Calculations are performed for the ULS and SLS. Safety factors are taken from DNV (2013) and applied for the characteristic loads and material strength parameters.

A.1.4 Soil Conditions

Seven soil layers up to 33 meters depth are derived from a representative soil profile. The soil parameters: unit weight, γ , friction, ϕ' , dilation, ψ , are presented in Tables A.3 and A.4. The last soil layer is silty clay with a characteristic undrained shear strain strength, $s_u = 563$ kPa.

Table A.1 Characteristic Loads on 1 Column of the 2-Column System.

Description	Units	Column diameter		
		Ø2 m	Ø3 m	Ø4 m
Wind load on WEC	kN	467	467	467
Moment arm for wind load	m	29.3	29.3	29.3
Wave force	kN	1007	1557	2280
Moment arm for wave load	m	15.8	16.0	16.2
Weight of superstructure	kN	7840	7840	7840

Table A.2 Characteristic Loads on 1 Column of the 4-Column System.

Description	Units	Column diameter		
		Ø2 m	Ø3 m	Ø4 m
Pull/compression load, 17 m	kN	2679	3743	5137
Pull/compression load, 30 m	kN	1518	2121	2911
Horizontal load	kN	1241	1791	2514
Weight of superstructure	kN	3920	3920	3920

Table A.3 Characteristic Soil Properties 1.

No.	Alt. [m]	Description	γ	ϕ'	ψ
			[kN/m ³]	[°]	[°]
1	-6.5	Medium Sand	19.5	38	12
2	-7.9	Coarse Sand	19.5	38	12
3	-12	Medium Sand	19.5	35	8
4	-24.8	Gravely Sand	20.0	38	9
5	-26.5	Fine Clayey Sand	19.5	32	4
6	-30.5	Silty Sand	18.0	32	2
7	-33	Silty Clay	18.5	-	-

Table A.4 Characteristic Soil Properties 2.

No.	Alt. [m]	Description	E_{50}^{ref}	E_{oed}^{ref}	E_{ur}^{ref}
			[kN/m ²]	[kN/m ²]	[kN/m ²]
1	-6.5	Medium Sand	88427	70083	265281
2	-7.9	Coarse Sand	128559	101890	385678
3	-12	Medium Sand	72548	63774	217644
4	-24.8	Gravely Sand	130291	103262	390872
5	-26.5	Fine Clayey Sand	77169	75712	231508
6	-30.5	Silty Sand	138459	135844	415376
7	-33	Silty Clay	66766	96435	200297

A.1.5 The Design Criteria

The deformation tolerances are usually derived from the offshore structure's operational requirements. The requirement for WEC is divided into two contributions: one from installation and one from the loads causing deformation. In this case, the requirement is set to a total rotational deformation of 0.50°, where 0.25° originates from the installation and 0.25° is from foundation settlements. According to WEC manufacturer (Wavestar A/S) the machine is able to perform with this inclination, and a limit for the SLS is chosen. Moreover, the requirement was critical for most of the cases, e.g. the inclination of 0.25° in SLS gave the final dimensioning for two-column systems.

A.2 Bucket Foundations

The Bucket Foundation, also known as the Universal Foundation, is found to be a competitive concept for various offshore structures. It provides several positive properties, e.g. short installation time and smaller impact on the natural environment during the installation. The technology was initiated by a research team from Aalborg University, Nielsen and

Ibsen (2011). The dimensioning methodology for bucket foundations is used according to Vaitkunaite et al. (2012).

The WEC C6-600 kW supported by buckets is visualized in Figure A.5. Results are presented in tables for each calculation model. There are two variables: bucket diameter, D , and skirt length, d . It is assumed that the wave impact is on a 2 m diameter column.

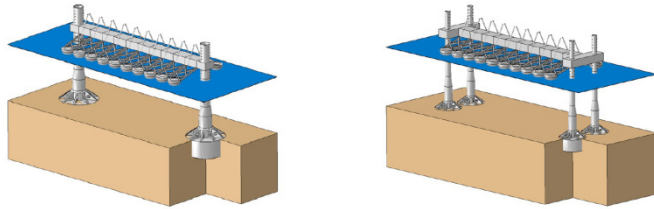


Figure A.5 Wavestar C6-600kW supported by buckets (Aalborg University, 2011)

A.2.1 Analytical Model for Bucket Foundations

Analytical model (Ibsen, 2002) determines the ultimate bearing capacity of bucket foundation subjected to static loads. Wind and wave loads are combined to one horizontal load, H , acting with a corresponding moment arm, h_m . The foundation is also subjected to vertical bucket and superstructure self-weight load, V . It is assumed that the foundation rotates as a solid body around one point in some depth, d_r . The point of rotation can be located below the foundation level or in between the soil surface and the foundation level. In order to calculate the earth pressure, it is assumed that the walls are rotating synchronically around a point in each of them, as shown in Figure A.6.

When calculating the bearing capacity of the bucket foundation, the location of the rotation point is found iteratively. During the iteration process, the vertical, horizontal and moment equilibrium must be ensured. It is done by the use of earth pressures, E , (Figure A.7) as well as friction, F , on the skirt and contribution of the end resistance. The point of rotation which is the centre of the line failure must also be the point of rotation used in the earth pressure calculation. The largest moment capacity is obtained if earth pressures, e_{pre} , are utilized to the full depth. e_{pre} is calculated by the following equations, Ovesen et al. (2012).

$$e'_{pre} = (\gamma'zK_\gamma + p'K_p + c'K_c)D, \text{ drained} \quad (\text{A.1})$$

$$e_{pre} = (\gamma zK_\gamma + pK_p + s_uK_c)D, \text{ undrained} \quad (\text{A.2})$$

Where p is passive earth pressure, kN/m^2 ; γ – soil unit weight, kN/m^3 ; s_u – undrained shear strength, kN/m^2 ; c' – cohesion in kN/m^2 ; K_γ , K_p , and K_c – dimensionless earth pressure factors for the active and passive sides on rough skirt walls, Ovesen et al. (2012); z – soil depth, m; D – bucket skirt diameter, m.

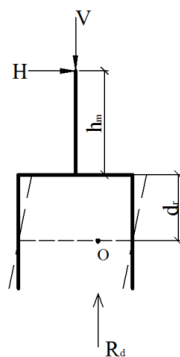


Figure A.6 The assumed rotation of bucket walls around a point O, after (Ibsen, 2002).

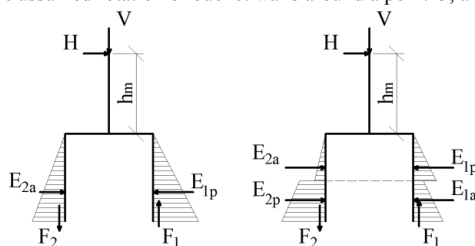


Figure A.7 a) Resultant earth pressure when rotation point is below foundation level; b) earth pressure, rotation point above foundation level, after (Ibsen, 2002).

An extremely eccentric loading is considered. The eccentricity, e , lies within the range $0.3b' < e < 0.5D$. Dimensionless factors (s, i, N) are employed to the bearing capacity (Equation A.3 and Equation A.4) according Appendix G in DNV (2013).

$$\frac{R_d}{A'} = \gamma' b' N_\gamma^e s_\gamma i_\gamma^e + c' N_c^e s_c i_c^e (1.05 + \tan^3 \varphi'), \text{ drained} \quad (\text{A.3})$$

$$\frac{R_d}{A'} = 1.05 s_u N_c^e s_c i_c^e, \text{ undrained} \quad (\text{A.4})$$

Where R_d is bearing capacity, kN; A' – effective area, m^2 ; c is cohesion in kN/m^2 ; γ' – effective soil unit weight, kN/m^3 ; N – bearing capacity factor; s – shape factor; i – inclination factor, b' – width of the effective bearing area, see Figure A.15.

Table A.5 Analytical Model Results, Bucket Foundations, ULS.

Distance	D	d
[m]	[m]	[m]
Two-column support		
-	8	7
Four- column support		
17	8	7
30	9	7

A.2.2 Numerical 2D Model for Bucket Foundations

This software is capable of estimating the ultimate limit state prior to failure of various geotechnical structures as well as retaining wall problems. The program allows 2D calculations. Moreover, it is possible to design pulled and compressed foundations at once for the four-leg supported structure. With several assumptions the program is used for estimation of circular bucket foundation in ultimate limit state.

LimitState:GEO performs numerical analyses utilizing Discontinuity Layout Optimization (DLO). DLO discretises the soil body in a number of nodes. Afterwards, the potential slip-lines discontinuities – sliding blocks – that configure the failure mechanism are assessed through the node connections; see Figure A.8. Results are presented in Table A.6.

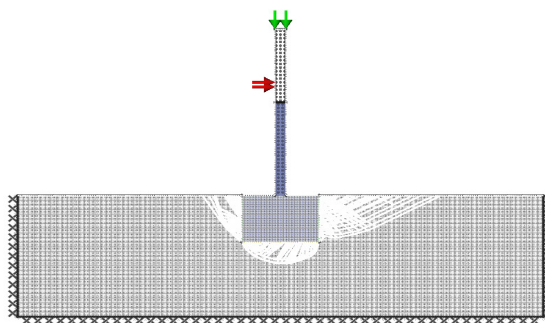


Figure A.8 DLO in LimitState:GEO done for bucket foundation in homogeneous soil layer.

Table A.6 Numerical Model Results, Bucket Foundations, ULS.

Distance [m]	D [m]	d [m]
Two- column support		
-	8	7
Four- column support		
17	6	5
30	4	4

A.2.3 Finite Element Model for Bucket Foundations

Plaxis 3D is a geotechnical software that employs the finite element method (FEM) for the calculations. This numerical technique enables the user to set up a model in three dimensions with the desired geometry and boundary conditions, see Figure A.9. Subsequently, a number of soil constitutive models are available and may well approximate the soil response when the soil properties are well known. In the study presented, Plaxis 3D is used for estimation of the bearing capacity as well as the serviceability conditions.

The Hardening Soil model is an advanced model that is used for analysis of soil behaviour and is selected for the foundation modelling. It directly describes the non-linearity in stress-strain curve as well as stress level dependency. Three elasticity moduli are required, meaning more precise soil stiffness estimations: triaxial loading stiffness, E_{50}^{ref} ; triaxial unloading

stiffness, E_{ur}^{ref} , and the oedometer stiffness, E_{oed}^{ref} , Schanz et al. (1999). All of the mentioned stiffness parameters for the Hardening Soil model are presented in Table A.4.

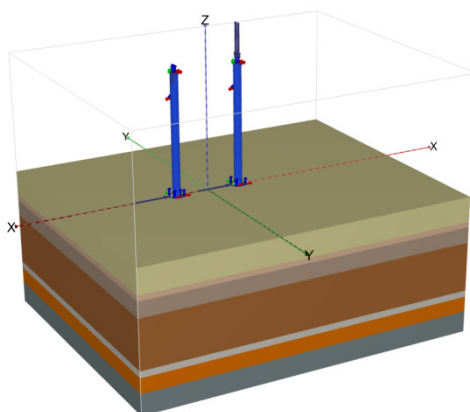


Figure A.9 Plaxis 3D model for two of four bucket foundations. Distance between the buckets 17 m, foundation diameter 5 m, skirt length 4 m.

Table A.7 FEM Results, Bucket Foundations, ULS.

Distance [m]	D [m]	d [m]	Rotation [°]
Two-column support			
-	8	7	0.22
Four-column support			
17	5	4	0.12
30	4	4	0.22

Pulled and compressed foundations are modelled at once for the four-column supported structure. The serviceability limit state is also assessed.

Results are presented in Table A.7, i.e. in 17 m case buckets with diameter and skirt length of 4 meters resulted in maximum rotation of 0.26° , hence, the diameter was increased by a meter and the final dimensioning resulted in rotation of 0.12° . Due to time consuming calculations, the intermediary and more optimal dimensions were not considered. The same procedure was applied to the following foundation types.

A.3 Pile Foundations

Pile foundations have been used for decades to support offshore structures. Steel piles are rather easy to manufacture, and the installation procedure, which requires a hydraulic hammer, is well known. The WEC C6-600 kW supported by piles is visualized in Figure A.10. Results are presented in tables for each calculation model. There are two variables: pile diameter, D_{pile} , and shaft length in the soil, L . It is assumed that the wave impact is on a 4 m diameter in two-column support and 3 m diameter in four-column support.

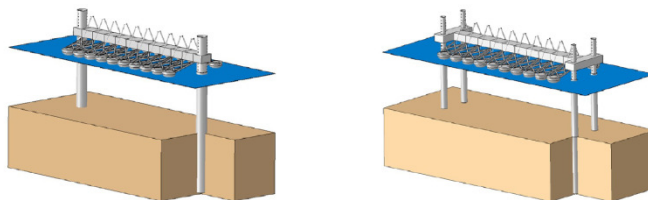


Figure A.10 Wavestar C6-600 kW supported by piles (Aalborg University, 2011).

A.3.1 Analytical Model for Pile Foundations

The analytical method for assessing the required pile dimensions is based on DNV (1992) and API (2000). The ultimate resistance of the pile is determined from the theory of plasticity where lateral and moment loadings are supported by the unit earth pressures developed along the pile shaft. The unit earth pressures estimation is divided into two separate regions, depending on whether the pile is installed in moderate or great depth. Moderate depth, $0 < d < d_t$, is estimated from the soil surface until the level where soil moves to surface when laterally loaded. In the great depth, $d > d_t$, the soil moves around the pile due to lateral loading. The transition point between both calculations is called the transition depth, d_t . Presumably in this point, the unit earth pressure calculated for moderate depth presents the same results as the unit earth pressure calculated for great depth. Detailed estimation is presented in DNV (1992) and API (2000). Additionally, the earth pressures are assessed along the pile for different soil layers. This assessment distinguishes between friction soils where earth pressures are calculated by Equation A.5 and Equation A.6. In case of cohesive soils, the unit earth pressure is calculated by Equation A.7 and Equation A.8.

$$p_u = \left(c_1 \frac{d}{D} + c_2 \right) \gamma' d, \quad \text{for } 0 < d < d_t \quad (\text{A.5})$$

$$p_u = c_3 \gamma' d, \quad \text{for } d > d_t \quad (\text{A.6})$$

$$p_u = 3s_u + \gamma' d + J \frac{d}{D} s_u, \quad \text{for } 0 < d < d_t \quad (\text{A.7})$$

$$p_u = 9s_u, \quad \text{for } d > d_t \quad (\text{A.8})$$

Where p_u is ultimate resistance, kN/m^2 ; c_1 , c_2 and c_3 – coefficients according to DNV (1992), d – depth, m; and D – diameter, m.

The axial resistance is obtained by the skin friction combined with the tip resistance. When the pile is axially loaded after the installation, the total resistance against axial loading, Q , is calculated differently either for pile acting unplugged or plugged manner, corresponding Equation A.9 and Equation A.10. The parameters are illustrated in Figure A.11.

$$Q = 0.9Q_{m,i} + Q_{p,j} + Q_{m,y}, \quad \text{unplugged} \quad (\text{A.9})$$

$$Q = Q_p + Q_{p,j} + Q_{m,y}, \quad \text{plugged} \quad (\text{A.10})$$

Where Q is total resistance against axial loading, kN ; Q_m - inside/outside shaft resistance, kN ; Q_p - tip resistance, kN .

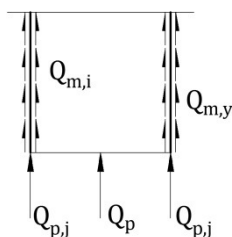


Figure A.11 Parameters for pile axial resistance calculation after (Roesen, 2011).

Term ‘plugged’ specifies that the developed unit skin friction inside of the pile is larger than the tip resistance, $Q_{m,i} > Q_p$. The term $Q_{m,y}$ cannot be utilized when the soil outside the pile is used for lateral loading. Therefore, $Q_{m,y}$ should be set to zero unless additional length is added, which is unwanted as additional length means additional cost. The skin friction, q_m , is calculated for the different soil layers. For drained cases Equation A.11 is used, and for undrained cases Equation A.12. DNV (1992)

$$q_m = K p'_0 \tan \delta < f_l \quad (\text{A.11})$$

$$q_m = \alpha s_u \quad (\text{A.12})$$

Where q_m is the skin friction, kN/m^2 ; K – earth pressure coefficient, 0.8 according to DNV (1992); p'_0 - effective overburden pressure, kN/m^2 ; δ – angle of soil friction in the pile shaft interface, degrees; f_l – the upper limit for skin friction, kN/m^2 ; α – factor, equal or smaller than 1. The end resistance is calculated for drained conditions according to Equation A.13 where the limiting resistance, q_l , corresponds to the resistance at critical depth. The end resistance in undrained case is calculated by Equation A.14.

$$q_p = p'_0 N_q \leq q_l \quad (\text{A.13})$$

$$q_p = 9 s_u F_c \quad (\text{A.14})$$

Where q_p is the end bearing, kN/m^2 ; q_l – resistance at the critical depth, kN/m^2 ; F_c – soil strength correction factor; N_q – bearing capacity factor.

If $Q_{m,i}$ can fulfil Equation A.15, then vertical equilibrium can be achieved without any additional length for the pile.

$$Q_{m,i} \geq V - Q_{p,j} \quad (\text{A.15})$$

Where V is vertical load, kN .

Pile dimensions are estimated by the analytical model and provided in Table A.8, where D_{pile} stands for pile diameter and L for shaft length.

Table A.8 Analytical Model Results, Pile Foundations, ULS.

Distance	D_{pile}	L
[m]	[m]	[m]
Two-column support		
-	4	15.8
Four-column support		
17	3	9.6
30	3	9.6

A.3.2 Numerical 2D Model for Pile Foundations

The same strategy is applied as for bucket foundations in numerical 2D modelling. Results are presented in Table A.9.

Pulled and compressed piles are designed at once for the four-column supported structure, see Figure A.12.

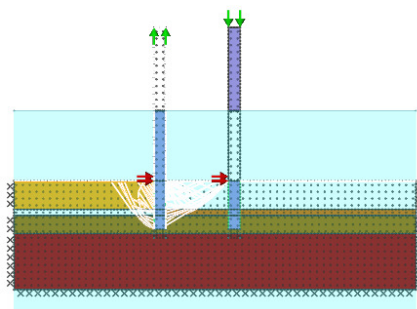


Figure A.12 Two of four piles modelled in LimitState:GEO. Distance between the piles 17 m, pile length in the soil 11 m

Table A.9 Numerical Model Results, Pile Foundations, ULS

Distance	D_{pile}	L
[m]	[m]	[m]
Two-column support		
-	4	15.5
Four-column support		
17	3	11
30	3	10

A.3.3 Finite Element Model for Pile Foundations

With the use of Plaxis 3D, the final dimensions as well as verification for SLS and ULS conditions are achieved. The same strategy as for buckets is followed. Results are presented in Table A.10.

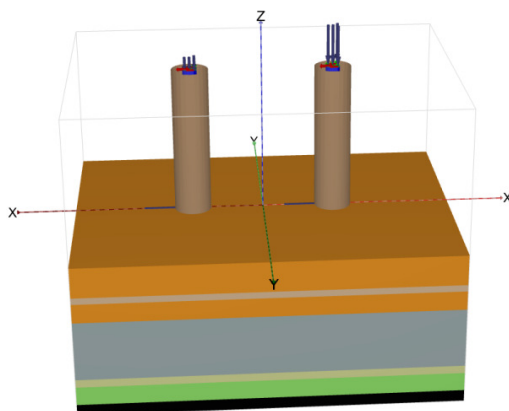


Figure A.13 Two of four piles modelled in Plaxis 3D. Distance between the piles 30 meters, pile length in the soil 7 m, diameter 3 m.

A.4 Gravity Based Foundations

The weight and foot print on the seabed allow gravity foundation to resist environmental loads. They can be produced in various shapes providing advantages in material saving, sustaining ice-loads etc. In this article, gravity foundations are of a very simple square prism shape. The WEC C6-600 kW supported by gravity based foundations is visualized in Figure A.14. Results are presented in tables for each calculation model. There are three variables: length and width, a , and height, h_{grav} . It is assumed that the wave impact is on a 4 m diameter column.

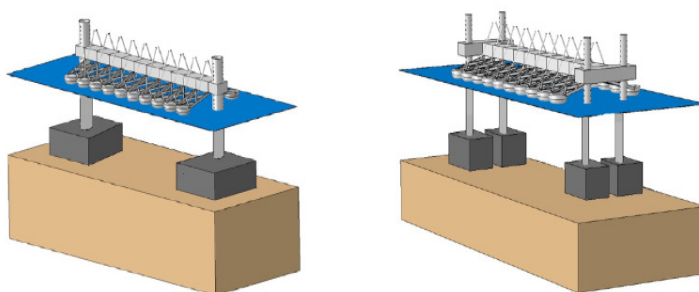


Figure A.14 Wavestar C6-600 kW supported by gravitational foundations (Aalborg University, 2011).

Table A.10 FEM Results, Pile Foundations, ULS & SLS.

Distance [m]	D_{pile} [m]	L [m]	Rotation [°]
Two-column support			
-	4	15	0.18
Four-column support			
17	3	7	0.20
30	3	7	0.18

A.4.1 Analytical Model for Gravity Based Foundations

Bearing capacity formulae for gravity based foundations are taken from Appendix G in DNV (2013). All the external loading and foundation self-weight forces are transformed into design horizontal, H_d , and vertical loads, V_d . The bottom surface of the foundation is in direct contact with the soil in an effective area, A' , calculated by Equation A.17. The size of the effective area depends on the foundation shape and loading eccentricity.

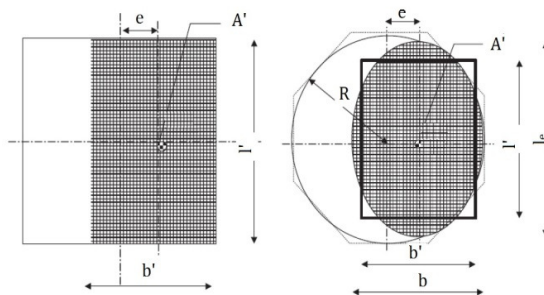


Figure A.15 Effective bearing area (dashed) of square and circular section gravity based foundations (DNV, 2013)

Several possibilities are visualized in Figure A.15. Eccentricity of the foundation is estimated by Equation A.16, and it satisfies the requirement for eccentrically loaded foundation, $e_{max}=0.3b'$.

$$e = \frac{M}{V} \quad (\text{A.16})$$

$$A' = b'l' \quad (\text{A.17})$$

Where M is moment load, kNm; and V – vertical load, kN.

The structure is supported on two or four circle-section concrete columns. Bearing capacity is estimated by Equation A.18, DNV (2013). Layer no. 3 is taken for the calculation. This layer consists of medium sand, see Table A.3. It is chosen because it presents less material strength than the two upper layers and can provide a more conservative dimensioning. Cohesionless fully drained soil is assumed.

$$\frac{R_d}{A'} = 0.5\gamma' b' N_{\gamma} s_{\gamma} i_{\gamma} + p'_0 N_q s_q i_q + c' N_c s_c i_c \quad (\text{A.18})$$

Resistance to sliding is ensured by Equations A.19 and A.20.

$$H < c'A' + V \tan \varphi \quad (\text{A.19})$$

$$\frac{H}{V} < 0.4 \quad (\text{A.20})$$

Where H is horizontal sliding load, kN.

Gravity based foundation dimensions estimated by the analytical model are provided in Table A.11, where a stands for the length and width of the foundation and h_{grav} for the height.

Table A.11 Analytical Model Results, Gravity based Foundations, ULS.

Distance	a	h_{grav}
[m]	[m]	[m]
Two-column support		
-	11	4.5
Four- column support		
17	9	4
30	8	4

A.4.2 Numerical 2D Model for Gravity Based Foundations

The same strategy is applied as for other foundations in numerical 2D model, see Figure A.16. Results are presented in Table A.12.

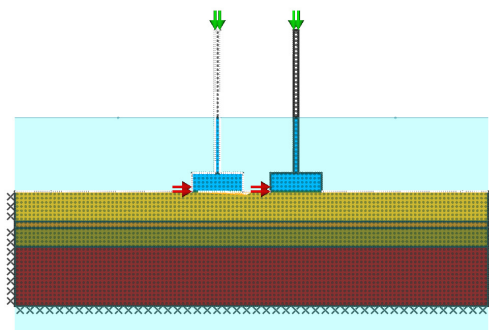


Figure A.16 Two of four gravity based foundations modelled in LimitState:GEO. Distance between the foundations 17 m, foundation height 4 m, width and length 11 m.

Table A.12 Numerical Model Results, Gravity based Foundations, ULS.

Distance	a	h_{grav}
[m]	[m]	[m]
Two- column support		
-	11	4.5
Four- column support		
17	11	4
30	9	4

A.4.3 Finite Element Model for Gravity Based Foundations

With Plaxis 3D the final dimensions as well as verification for SLS and ULS conditions are achieved. The same strategy as for buckets is followed. On the contrary to the previous two types of foundations, the final dimensions of gravity based foundations in four-column case were determined by the ultimate limit state conditions. Results are presented in the following Table A.13.

Table A.13 FEM Results, Gravity based Foundations, ULS & SLS.

Distance	a	h_{grav}	Rotation
[m]	[m]	[m]	[°]
Two-leg support			
-	9	4	0.24
Four-leg support			
17	8	4	0.07*
30	7	4	0.03*

*Rotation due to differential vertical settlement of the foundations

A.5 Limitations

While modelling the four-column case, it was assumed that equal lateral loading would impact both, compressed and pulled, foundations. This assumption is conservative, because during the storm case the wave length is larger than e.g. 17 m, and the waves cannot hit the pile with an equal force. However, the comparison between foundation types is still valid as long as the same conditions are assumed.

In the long-term perspective, cyclic loading influence should be considered. It is noticed that even not large but constantly repeating pull-out loads tend to impact strongly the stability and serviceability of the foundations. This can be another issue for a WEC supported on four foundations. Presently a study on cyclically axially loaded buckets and piles is performed at Aalborg University.

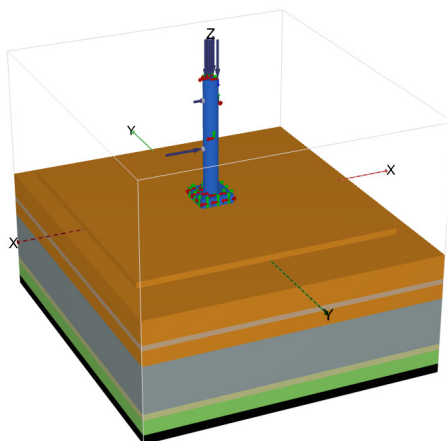


Figure A.17 One of two gravity based foundations modelled in Plaxis 3D.

A.5.1 Discussion about Dimensioning Steps

Significant optimization was performed for the WEC supported by four bucket foundations. This is due to the fact that analytical model Ibsen (2002) is created for buckets subjected to dominating moment loading. The numerical 2D model provided rather good primary results for the WEC supported by four buckets. When support is on two buckets, the analytical Ibsen (2002) model gave a fast and precise result compared to the final estimations in Plaxis 3D.

The dimensioning procedure for piles was followed according to Figure A.1. Small optimization was done for two-column support, when dimensions from the analytical model were minimized by 5%. Larger optimization was not achieved for four-column structure. The analytical model was taken from the monopile foundation calculations, where the pile is subjected to dominating moment loading DNV (2013). That is why it is more suitable for two-column support. However, the analytical model provided a good primary dimensioning, which was optimized by Plaxis 3D afterwards.

The procedure for two-column support with gravity based foundations was rather conservative during the analytical and LimitState:GEO estimations, because it was possible to optimize the dimensions by 40% during the last step. A smaller optimization of maximum 23% was done for four-column support comparing analytical and Plaxis 3D models. Yet for the primary dimensioning the analytical model works better than the present numerical 2D model.

A.6 Comparison

The comparison is done only from the geotechnical point of view. Other influences of installation and structural design would give a better overview. Figure A.18 shows the main dimensions taken into account when comparing the materials used for the foundation.

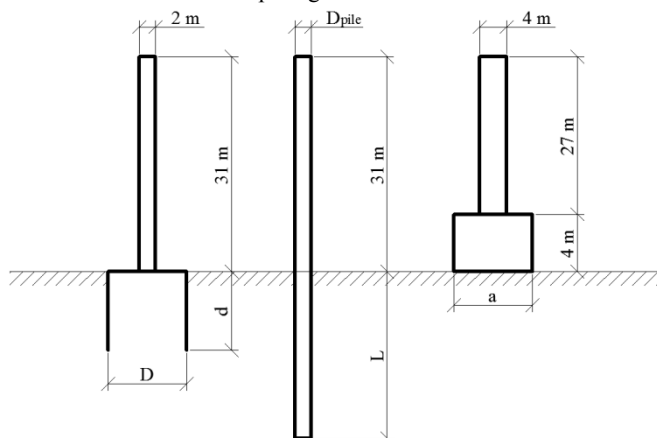


Figure A.18 Dimensions taken into account when estimating the materials used for the manufacturing of the foundation.

A.6.1 Two vs. Four Foundations

With the analysis of the buckets in Table A.7, it can be stated that the dimensions of each foundation unit slightly differs in two and four legs cases. As expected, larger foundations are required for the first case. However, 1.3 times more material would be used for the WEC supported on four foundations. The influence of distance between pulled and compressed foundation is minor too, which is seen only in small fluctuations of rotations in SLS and material used.

With the analysis of the piles in Table A.10, it can be seen that in the two legs case a pile is significantly longer. However, 1.2 times more material would be used for WEC supported on four piles, because the upper column from the seabed to the WEC has to be taken into

account. The influence of distance between pulled and compressed foundation is minor too, which is seen only in small fluctuations of rotations in SLS.

Similarly to the previous types, gravity based foundations in Table A.12 are larger in two legs case. There is a difference between foundations in the four legs cases, where 30 meters distance results in smaller foundation dimensions. It happens due to smaller vertical load. However 1.7 times more material would be used in the four-column case (30 m) compared to the two-column case.

Finally, it can be seen that increasing the distance between the columns from 17 to 30 meters gives small benefits for the foundation size, but requires more complicated upper structure design. Therefore, the smaller distance of 17 m between the supporting columns is more favourable

A.6.2 Buckets vs. Piles

In both two- and four-column cases, 1.4 more steel is required when using piles. However this is just the basic dimensions done from the geotechnical calculations. The structural design should be the following step. The connection to superstructure should be considered in order to estimate more exact results. It is known that piles are connected to the superstructure by the use of transition piece. The bucket foundation does not need this element to be connected to a WEC. However, the production of the foundation itself is rather expensive.

Three foundation concepts for wave energy converters were performed and presented in this paper. The proposed systems are based on foundations widely used to support offshore structures: buckets, piles and gravity based foundations. Dimensioning was done in three steps employing various geotechnical calculation models and providing the optimised results. Analytical models, the numerical 2D program LimitState:GEO and the finite element program Plaxis 3D were used for the design. The comparison showed that two foundations provide a good stability and economical solution in the means of material use. By comparing piles and buckets, it was found that the latter requires less material. A full cost estimation needs a structural analysis, taking fatigue limit state into account, and an installation analysis, where the need for seabed preparation, scour protection and penetration analysis would be estimated.

Acknowledgment. This research is done via the project “Cost Effective Foundation and Installation of Wave Energy converters”, sponsored by Energinet.dk and partners. The financial support is sincerely acknowledged. Moreover, the authors would like to thank Wavestar A/S for supplying the essential information related to the research.

Bibliography

- M. Marquis, M. M. Kramer, J. Kringelum, J. F. Chozas and N. E. Helstrup, “Introduction of Wavestar wave energy converters at the Danish offshore wind power plant Horns Rev 2,” in *Proc. ICOE2012*, 2012.
- L. B. Ibsen, “Analytical model for design of bucket foundations,” Aalborg University, Aalborg, Data Report R0205 – version 1. ISSN 13986465 R0205, 2002.
- DNV *Design of Offshore Wind Turbine Structures*, Offshore Standard DNV-OS-J101, 2013.

- S. A. Nielsen and L. B. Ibsen, "Novel wide-ranging foundation in the range of 30-60 meter water depth," in *EWEA OFFSHORE 2011*, Post No. 159, 2011.
- T. Schanz, P. A. Vermeer and P.G. Bonnier, "The hardening soil model: Formulation and verification," *Beyond 2000 in Computational Geotechnics – 10 Years of PLAXIS*, ISBN 90 5809 040 X, Balkema, Rotterdam, 1999.
- N. K. Ovesen, L. D. Fuglsang, G. Bagge and A. Krogsbøll, *Lærebog i Geoteknik*, 2nd ed., Lyngby, Denmark: Polyteknisk Forlag, 2012.
- DNV C.N. No. 30.4 *Foundations*, Classification Notes No. 30.4, Det Norske Veritas, 1992.
- API *Recommended Practise for Planning, Designing and Constructing Fixed Offshore Platforms – Working Stress Design*, American Petroleum Institute RP 2A-WSD, 21st ed. 2000, Errata and supplement, 2002.
- H. R. Roesen, "Advanced soil mechanics – design of offshore piles," *lecture slides at Aalborg University*, Aalborg, March, 2011.
- Copyright of "Wavestar A/S", <http://wavestarenergy.com/>, 2011.
- Copyright of Aalborg University, <http://www.aau.dk/>, 2011.
- E. Vaitkunaite, S. Devant Molina and L. B. Ibsen , "Comparison of calculation models for bucket foundations in sand," Aalborg University, Aalborg, DCE Technical Memorandum No. 17. ISSN 1901-7278, 2012.

APPENDIX B

Comparison of Design Methods for Axially Loaded Buckets in Sand

Vaitkunaite, E., Nielsen, B. N., and Ibsen, L. B. (2015). Comparison of design methods for axially loaded buckets in sand. In V. Meyer (Ed.), *Frontiers in Offshore Geotechnics III proceedings of the third international symposium on frontiers in offshore geotechnics (isfog 2015), Oslo, Norway, 10-12 June 2015*. (Vol. 1, pp. 331-342). London : C R C Press LLC.

© 2015 Taylor & Francis Group. Used with permission.

Author's Right

The layout has been revised.

Evelina Vaitkunaite

Emne: VS: Author's Right

Fra: Bijnsdorp, Leon [<mailto:Leon.Bijnsdorp@taylorandfrancis.com>]

Sendt: 30 May 2016 12:09

Til: Evelina Vaitkunaite

Emne: RE: Author's Right

Dear Evelina Vaitkunaite,

You have our permission to use the materials. Could you please make sure that proper credit to the source file is made, including a copyright notice ('© 2015 Taylor & Francis Group. Used with permission.')

Kind regards,

Leon Bijnsdorp

Léon Bijnsdorp
Editor Conference Proceedings

CRC Press / Balkema

Taylor & Francis Group - an informa business
Schipholweg 107c, 2316 XC Leiden, The Netherlands
P.O. Box 11320, 2301 EH Leiden, The Netherlands
T: +31 71 524 3089

www.crcpress.com & www.taylorandfrancis.com & www.crcnetbase.com

From: Evelina Vaitkunaite [<mailto:ev@civil.aau.dk>]

Sent: maandag 30 mei 2016 8:57

To: Bijnsdorp, Leon

Subject: Author's Right

Dear Leon Bijnsdorp,

I have participated in the 3rd International Symposium on Frontiers in Offshore Geotechnics (Oslo, Norway) with my paper "Comparison of design methods for axially loaded buckets in sand". I would like to ask for the Publisher's permission to include the paper in the Appendix of my Ph.D. Thesis.

Sincerely,

Evelina Vaitkunaite

Ph.D. Fellow

Department of Civil Engineering
Aalborg University
Sofieldalsvej 11
DK-9200 Aalborg
Denmark

Abstract. A study of the present knowledge about the bucket resistance for axial loading was performed considering analytical and numerical design methods as well as physical models. A case study was performed with two bucket foundations of equal diameter, but different skirt lengths installed in dense sand. It was found that bearing capacity from the surcharge increases approximately twice if the foundation skirt is two times longer. However, the predicted compressive soil capacity can differ by 3.6 times depending on the chosen bearing capacity parameters. Few methods are available for the estimation of the static tensile resistance for a bucket foundation. Furthermore, the predicted tensile resistance can differ up to 12 times indicating that further analysis is needed approaching this issue.

B.1 Introduction

Offshore energy industry is greatly expanding. Wind turbines, wave and tidal energy devices can harvest beneficial and ecological energy. These structures are subjected to strong environmental loads and require some complex support systems. Geotechnical design solutions are often inspired by valuable experience from the oil and gas sector. Suction foundations have been used for decades as a suitable support for various offshore structures worldwide. Recently, the first jacket foundation with three buckets designed for a wind turbine was installed in Borkum Riffgrund wind turbine park in Germany. However, standard guideline for bucket foundations is not yet available.

In 1990s, NGI and Oxford University performed detailed studies of bucket foundations for the Europipe 16/11E and SLT jacket. The campaign included model tests, finite element analysis and a complete foundation design. Comprehensive information regarding the bucket behaviour was provided by Bye et al. (1995), Tjelta (1995) etc. A historical overview of the bucket foundations and NGI developed design procedure are presented by Skau and Jostad (2014).

Oil and gas platforms transfer mainly compressive loads to the foundations. Tensile capacity is considered only for the short-term events such as storms. Compared to the oil and gas platforms, wind turbines are very light. The foundation of a wind turbine has to sustain long-term tensile loads. Consequently, this study focuses on the ultimate tensile and compressive bucket capacities estimated by various analytical methods, found in the available research papers and standards.

Aalborg University started an extensive study about bucket foundations for wind turbines in 2002. The relevant experience is reflected in this paper. It was chosen to perform a case study for two buckets of different embedment ratios illustrating the differences of the methods in a straightforward manner.

B.2 Methods for Compressive Capacity

The compressive capacity of shallow foundations is calculated using the traditional Terzaghi (1943) bearing capacity formula. The formula estimates capacity of shallow onshore strip foundations. It is also applied for offshore shallow foundation calculations when improved by various modification factors to convert the plane strain problem to the axis-symmetric problem. Suction bucket is a skirted shallow offshore foundation of circular shape. The soil that is trapped inside makes the bucket behave as a gravity based foundation. Thus, the bearing capacity of suction bucket can be estimated using the traditional formulae. Bucket compressive capacity R_c consists of four main parts: soil self-weight R_γ , surcharge R_q , effective cohesion R_c and outer skirt friction R_{fric} . Each of these parts can be estimated in various ways which differ slightly from method to method. The skirt friction makes less than one percent of the total compressive capacity. Frictional resistance is addressed in section B.3. For comparison reasons, R_{fric} is ignored in the compressive bearing capacity estimation.

Factor for surcharge N_q increases exponentially with an increase of soil friction angle φ . Most of the methods presented suggest N_q value derived by Prandtl (1920), except Larsen (2008) and Bolton and Lau (1993), who combined modifications for foundation roughness and shape and the bearing capacity factors. Ibsen et al. (2012) has shown how N_q value for bucket foundations is influenced by surface roughness which was analysed using a finite element program. Bearing capacity factor for the self-weight N_γ depends on the values of N_q , φ and surface roughness. Detailed analysis and comparison of bearing capacity factors are done by Ibsen et al. (2012).

Formulae for N_q and N_γ are provided in this paper. Most of the methods require modification factors for foundation shape s , embedment depth d and load inclination i . The specific formulae can be found in the references. A large amount of laboratory tests on axially loaded bucket foundations was performed at Aalborg University. Vertical bearing capacities of rough circular surface footing and buckets of various shapes were tested and analysed by Ibsen et al. (2012, 2013, 2014a and 2014b). These results are discussed in section B.5.1. The tests were followed by a new expression for the bearing capacity of laboratory bucket models.

B.2.1 Design codes

DNV (1992)

DNV (1992) provides (B.1) based on Terzaghi (1943) and describes the calculation of bearing capacity for offshore foundation stability as rough but good estimate for the early stage of design.

$$R_c = A'(0.5\gamma' B' N_\gamma K_\gamma + q' N_q K_q + c' N_c K_c), \quad (\text{B.1})$$

$$N_q = \tan^2(45 + 0.5\varphi) e^{\pi \tan \varphi}, \quad (\text{B.2})$$

$$N_c = (N_q - 1) \cot \varphi, \quad (\text{B.3})$$

$$K_i = s_i d_i i_i, \quad (\text{B.4})$$

where c' is the effective cohesion, q' surcharge, A' effective bearing area of the foundation, B' effective width of the foundation, N_q , N_γ , N_c bearing capacity factors, K_q , K_γ , K_c modification factors to account for foundation shape, embedment and load inclination.

DNV (1992) suggests two methods for N_γ . The first one was found by Brinch-Hansen (1970):

$$N_\gamma = 1.5(N_q - 1)\tan\varphi. \quad (\text{B.5})$$

The second was suggested by Caquot and Kerisel (1953):

$$N_\gamma = 2(N_q + 1)\tan\varphi. \quad (\text{B.6})$$

EC-7 (2004) and API (2011)

Eurocode 7 Geotechnical design EC-7 (2004) and API (2011) adopt equations (B.1) and (B.6). However, the shape and depth factors are different. Eurocode 7 Geotechnical design (EC-7, 2004) is taken into consideration despite that it is intended for onshore foundation design.

B.2.2 Bolton & Lau (1993)

Bolton and Lau (1993) proposed bearing capacity factors N_q^* and N_γ^* . These factors were estimated for the axis-symmetric calculation.

$$R_c = A'(0.5\gamma'DN_\gamma^* + q'N_q^*), \quad (\text{B.7})$$

B.2.3 Larsen (2008)

Larsen (2008) derived new bearing capacity factors N_q and N_γ for the drained bearing capacity. The study was performed using an axis-symmetric numerical model with bucket foundations and lead to equations (B.8) and (B.9). Detailed information is provided in Larsen (2008) and Ibsen et al. (2014b).

$$N_q = c_3 e^{c_4 \pi \tan\varphi} \tan^2(45 + 0.5\varphi), \quad (\text{B.8})$$

$$N_\gamma = c_1 ((N_q - 1) \cos\varphi)^{c_2}, \quad (\text{B.9})$$

where c_i are available for circular and strip foundation with rough and smooth surface in Larsen (2008).

B.2.4 Davis & Booker (1971)

Davis and Booker (1971) performed a rigorous plasticity solution which resulted in N_γ for rough foundation:

$$N_\gamma = 0.1054 e^{9.6\varphi}. \quad (\text{B.10})$$

B.2.5 Lundgren & Mortensen (1953)

Lundgren and Mortensen (1953) estimated N_q based on laboratory tests.

$$N_\gamma = 0.25((N_q - 1)\cos\varphi)^{1.5}. \quad (\text{B.11})$$

B.3 Methods for Tensile Capacity

Applying the theory of anchoring systems, three failure modes for tensile loading on bucket foundation can be considered. When the tensile load is applied rapidly, suction under the lid is generated creating the reverse bearing capacity. However, in long-term loading conditions, two components resist the tensile load: friction on the outer skirt, and the lower value of the soil plug weight and friction on the inner skirt. Obviously, foundation self-weight would be the third component, but it is not considered in this study as mentioned earlier.

Rather few methods are available for the estimation of the long-term tensile capacity of bucket foundations. Houlsby et al. (2005) and Senders (2009) have proposed the tensile capacity estimations for this type of foundation, that are considered in this paper. However, design codes, such as DNV (1992) and API (2011), do not provide guidelines for bucket foundations in tension. This paper includes only β -method, as described in DNV (1992), and four CPT-based methods, as described in API (2011). The CPT-based methods are derived from various slender pile tests and they are not intended to be used for other type of foundation design. However, the applicability of CPT data to bucket foundation design would be ideal as it resembles the seabed soil conditions very well.

B.3.1 DNV (1992)

DNV (1992) recommends the following expression for axially loaded offshore piles.

$$R_t = -((K\tan\delta)_o D_o + (K\tan\delta)_i D_i)\pi \frac{\gamma' d^2}{2}, \quad (\text{B.12})$$

where γ' effective unit weight, D is outer diameter, d skirt length, δ interface friction angle, K coefficient of horizontal stress, indices i and o are indications for the inner and outer skirt correspondingly.

B.3.2 Houlsby et al. (2005)

Houlsby et al. (2005) proposed to take into account the reduced vertical stress down the bucket. The authors stated that if the reduction is not included into the tensile capacity calculations, bucket strength is overestimated.

$$R_t = -\gamma' Z_o^2 y \left(\frac{d}{Z_o} \right) ((K\tan\delta)_o D_o \pi - \gamma' Z_i^2 y \left(\frac{d}{Z_i} \right) ((K\tan\delta)_i D_i \pi, \quad (\text{B.13})$$

where $Z_{i/o}$ are interface parameters with $m = 1.5$.

B.3.3 Senders (2009)

Senders (2009) performed centrifuge model tests with scaled buckets where the foundation behaviour was analysed during the installation, uplift and cyclic loading. Cone resistance q_c was used for the estimation of the tensile bucket capacity. Foundation resistance is expressed as the sum of the inner friction and the outer friction of the skirt.

$$R_t = F_{i,t} + F_{o,t}, \quad (\text{B.14})$$

$$F_{i,t} = \pi D_i k_{f,t} \int_0^d q_c(z) dz, \quad (\text{B.15})$$

$$F_{o,t} = \pi D_o k_{f,t} \int_0^d q_c(z) dz, \quad (\text{B.16})$$

$$k_{f,t} = -0.375C \left[1 - \left(\frac{D_i}{D_o} \right)^2 \right]^{0.3} \tan \delta, \quad (\text{B.17})$$

where $k_{f,t}$ coefficient, C coefficient equal to 0.012 based on back-calculations from the laboratory tests.

B.3.4 API (2011)

API (2011) contains four CPT-based methods for the friction contribution to pile capacity. This paper adopts the four methods for the estimation of the tensile bucket foundation capacity in the main equation (B.18). Authors kindly refer to API (2011) for the formulae and relevant factors.

$$R_t = \pi(D_o + D_i) \int_0^d f_t(z) dz, \quad (\text{B.18})$$

B.4 Finite Element Modelling

Plaxis 2D axis-symmetric Mohr-Coulomb and Hardening-Soil models were used for the research. The first model requires information about triaxial friction angle φ_{triax} , dilation angle ψ , effective cohesion c' , Poisson's ratio ν and effective Young's modulus E' . Whereas, the Hardening-Soil model requires knowledge about the soil stiffness at a reference pressure, i.e. E_{50}^{ref} , E_{ur}^{ref} and E_{oed}^{ref} . The parameters serve to describe the non-linearity in stress-strain curve as well as stress level dependency. The advanced parameters can be estimated, for example, from triaxial test. However, the case study uses assumed, but realistic dense sand parameters.

B.5 Laboratory Testing at Aalborg University

B.5.1 Compressive loading

Recently, Ibsen et al. (2014b) have published data from a number of vertical bearing capacity laboratory tests performed on buckets with diameters of 50-200 mm and embedment ratios d/D from 0 to 1. The buckets were installed in uniform dense sand. The soil conditions were relatively constant from test to test. Ibsen et al. (2014b) have found a new theoretical relationship of the bucket bearing capacity introducing the reduced friction angle φ_{red} for the analysis of the small-scale laboratory results. Hansen (1979) suggested (B.19) to account for non-associated plasticity theory, i.e., considering friction and dilation angle.

$$\tan\varphi_{red} = \frac{\sin\varphi\cos\psi}{1 - \sin\varphi\sin\psi}, \quad (\text{B.19})$$

where φ friction angle and ψ angle of dilation.

Measured bearing capacities of laboratory buckets were normalized and a general bearing capacity equation derived (B.20). This equation is valid for dense saturated Aalborg University sand No. 1 with a mean reduced friction angle $\varphi_{red} = 42^\circ$ for the non-associated plasticity flow. Detailed information about the procedure and analysis employing the reduced friction angle is provided in Ibsen et al. (2014b) and Ibsen et al. (2012), sand properties are reported by Hedegaard and Borup (1993).

$$\frac{R_c}{R_\gamma} = 1 + 2.9 \frac{d}{D}, \quad (\text{B.20})$$

Introduction of reduced friction angle allows realistic interpretation of small-scale test results and possible application to full-scale design. To visualize this, Larsen (2008) method is compared to the laboratory derived equation (B.20). Bearing capacity of full-scale buckets with $D = 10$ m and various embedment ratios d/D is calculated by the two methods. Consequently, dense sand with very high friction angle $\varphi_{red} = 42^\circ$ must be used resembling laboratory conditions. Bearing capacity R_γ of a rough plate with $D = 10$ m was estimated using (B.9) and inserted to (B.19). Estimated capacities (dashed line in figure B.1) fit very well the expression for rough buckets by Larsen (2008).

B.5.2 Tensile loading

Presently, a study about pure axial loading on bucket foundations is in process at Aalborg University. A new medium scale laboratory test set up was designed and installed in 2013. Vaitkunaite et al. (2014) presented the main test set up features and the first results of monotonic tensile loading on bucket foundations. The tested bucket models have a diameter of 1 m and skirt lengths of 0.5 and 1 m. The previously mentioned methods, DNV (1992) and Houlsby et al. (2005), are based on the interface friction angle δ and the coefficient of lateral earth pressure K . If the laboratory findings were

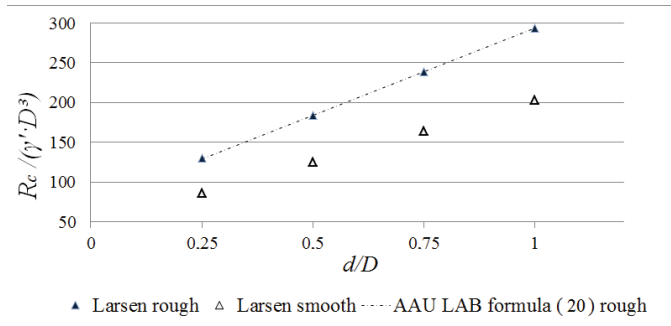


Figure B.1 Normalized vertical bearing capacity vs. bucket embedment.

compared to such methods, K value would be significantly higher than the usual expression $K = 1 - \sin\varphi_{triax}$. However, the CPT based method (Senders, 2009) can be compared to the laboratory results. The cone penetration data is available for every experiment which is a part of the usual procedure at Aalborg University. Normalized measured tensile peak capacities are compared to equation (B.14) and presented in figure B.2.

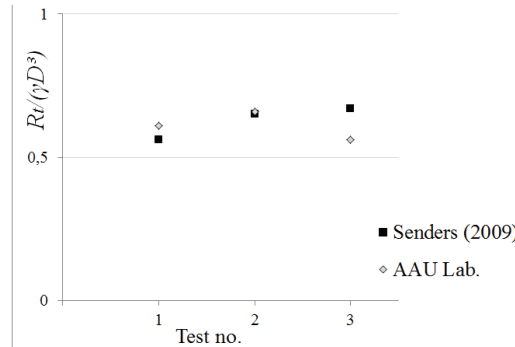


Figure B.2 Laboratory tensile capacity vs. predictions using CPT based method (Senders, 2009).

B.6 Case Study

Some of the best known calculation methods as well as the latest research findings are presented in this paper. In order to compare and visualize the differences of these design tools, an idealized case study is created. In this study, two bucket foundations of different geometries are compared. The comparison is done for the pure axial capacity of a single foundation. For the comparison reasons, any influence of the foundation self-weight is omitted. Table B.1 provides the numbered marking for the previously mentioned methods which is used in the comparison. Each method requires

Table B.1 Methods used for ultimate capacity analysis.

No.	Method	Variables
M1	Plaxis 2D, Hard.-Soil	$\delta, \varphi_{triax}, p_a$
M2	Plaxis 2D, Mohr-Coulomb	$\delta, \varphi_{triax}, p_a$
M3	Davis & Booker (1971)	$\varphi_{pl.}, \varphi_{pl.}^{red}$
M4	API compression	$\varphi_{triax}, \varphi_{triax}^{red}$
M5	EC 7: Geotech. Design	$\varphi_{pl.}, \varphi_{pl.}^{red}$
M6	Bolton & Lau (1993)	$\varphi_{triax}, \varphi_{triax}^{red}$
M7	Larsen (2008)	$\varphi_{triax}, \varphi_{triax}^{red}$
M8	Caquot & Kerisel (1953)	$\varphi_{pl.}, \varphi_{pl.}^{red}$
M9	Brinch-Hansen (1970)	$\varphi_{pl.}, \varphi_{pl.}^{red}$
M10	Lundgren & Mortensen (1953)	$\varphi_{pl.}, \varphi_{pl.}^{red}$
M11	Senders (2009)	δ, q_c
M12	Houlsby et al. (2005)	δ
M13	DNV (1992) tensile loading	δ
M14	API (2011) method 1	δ_{cv}, q_c, p_a
M15	API (2011) method 2	δ_{cv}, q_c, p_a
M16	API (2011) method 3	δ_{cv}, q_c, p_a
M17	API (2011) method 4	δ_{cv}, q_c, p_a

information about skirt length d and soil unit weight γ' , while other variables are given in the table B.1.

B.6.1 Soil Parameters

The assumed seabed contains ideal uniform dense sand with soil parameters given in Table B.2. Horizontal soil stress parameter K is often recommended to be in the range of 0.5-0.8 (DNV (1992), Byrne and Houlsby (2002)). This recommendation originates from the offshore pile design criteria. However, suction bucket installation is slightly different and $K = 1 - \sin\varphi_{triax}$ is used instead in this study according to Larsen (2008). Where possible, the reduced friction angle is introduced, see Table B.1. Furthermore, where the formulae are based on plane strain solution, the plane friction angle $\varphi_{pl.} = 1.1\varphi_{triax}$ is used.

B.6.2 Geometry of the Foundation

Two weightless bucket foundations are considered for the analysis. Both of them have a diameter D of 10 m. The skirt lengths d are 5 m and 10 m, and thickness is 30 mm. During the comparison they are identified by the geometric ratio d/D , which is 0.5 and 1 correspondingly. Foundation surface is rough.

Table B.2 Geotechnical soil parameters.

Parameter	Unit	Value
Triaxial friction angle φ_{triax}	[°]	38.8
Red. triaxial friction angle φ_{triax}^{red}	[°]	34.5
Plane friction angle $\varphi_{pl.}$	[°]	42.7
Red. plane friction angle $\varphi_{pl.}^{red}$	[°]	36.8
Interface friction angle δ	[°]	32.2
Angle of dilation ψ	[°]	9
Density ratio I_D	[%]	80
Soil unit weight γ	[kN/m ³]	20.25
Effective cohesion c'	[kPa]	0
Effective Young's modulus E'	[MPa]	39.3
Triaxial unloading stiffness E_{ur}^{ref}	[MPa]	260.9
Oedometer stiffness E_{oed}^{ref}	[MPa]	43.7
Triaxial loading stiffness E_{50}^{ref}	[MPa]	87
Poisson's ratio ν'	[-]	0.2
Plaxis interface factor R	[-]	0.78
Plaxis factor m	[-]	0.58
Reference pressure p	[kPa]	100
Lateral earth pressure K	[-]	0.37
Cone penetration q_c at 5 m d.	[MPa]	10.3
Cone penetration q_c at 10 m d.	[MPa]	15.1

B.6.3 Comparison

Compression

During the case study, the vertical bearing capacity is estimated according to previously presented analytical and numerical methods. Figure B.3 and figure B.4 present the normalized bearing capacities. The values deviate significantly when the reduced friction angle is included to the calculation. Interestingly, finite element estimations (M1 and M2) are in the same range with the methods where φ^{red} is used. M4 requires using the triaxial friction angle; consequently, the difference between results using φ_{triax}^{red} and φ_{triax} is small, because the difference between the bearing capacity factors N_q and N_γ is smaller comparing to other analytical methods. On the contrary, M3 and M8 for the $d/D=1$ and M5 and M6 for the $d/D=0.5$ are the most sensitive to the change in the friction angle. It can be concluded that the scatter in the bearing capacity estimation is important for the dense or very dense sands, because N_q and N_γ increases exponentially at the higher friction angles and the dilation angle effects the bearing capacity estimation.

As it was shown earlier, the estimation of R_γ and R_q differ from method to method depending on the bearing capacity factors. When analysing the analytical methods, it was found that R_q value increases approximately twice if the skirt is two times longer.

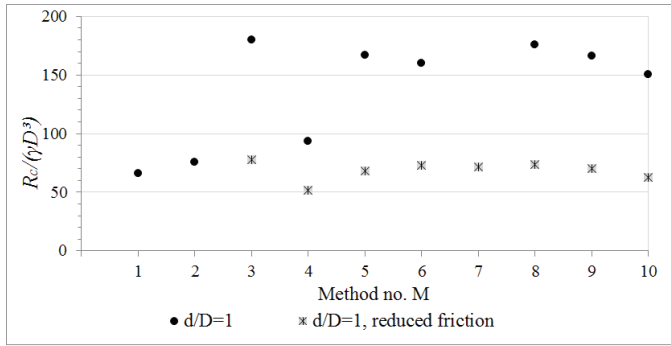


Figure B.3 Normalized compressive capacity for bucket with d/D=1.

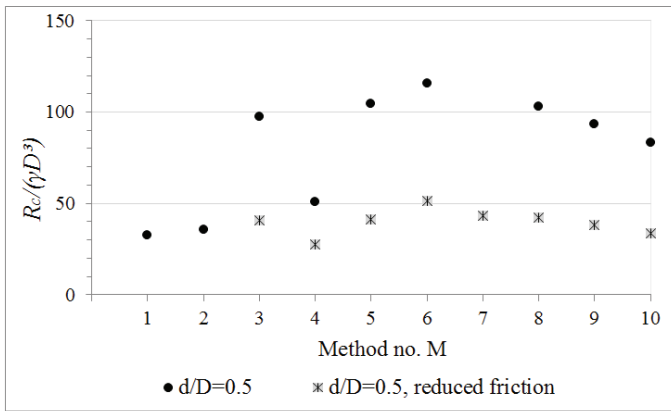


Figure B.4 Normalized compressive capacity for bucket with d/D=0.5.

However, it increased 2.27 times using M10 while only 2 times using M5, M6 and M7. Obviously, R_γ was equal for both foundations as it depends on the foundation area.

Tension

Cone resistance highly depends on location and sand properties. However, an idealized profile is assumed which corresponds to possible cone penetration values for dense sands, as shown in Table B.2. Figure B.5 presents the normalized pull-out capacities. It can be seen that the values deviate significantly from method to method indicating that it is difficult to predict the tensile capacity precisely. M11, M12, M13 are in the same range with the finite element estimation. However, these methods predict quite low tensile capacity for the bucket d/D=0.5 compared to M1 and M2. A great difference in the estimated tensile resistance is seen in the four CPT-based methods (M14-M15). The methods were derived from tests on slender piles and should not

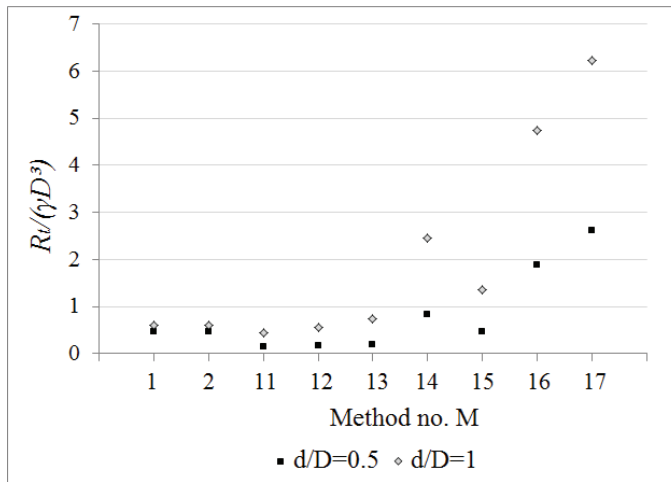


Figure B.5 Normalized tensile capacity.

be used for the bucket design until all relevant adjustments are done. Overall in the selected case, M11 gives the lowest estimate.

B.7 Conclusions

The intention of this article was to collect an up-to-date methodology for the compressive and the tensile bucket bearing capacity estimation. Ten different expressions were used for the estimation of the compressive capacity and nine for the tensile capacity. Quite some scatter between the compressive and tensile capacities was seen, which indicated that more testing and analysis would be favourable to clarify the design of the bucket foundations. Despite the doubts regarding the influence of the non-associated plasticity in the bearing capacity problems (e.g., Davis and Booker (1971)), the influence is significant in dense and very dense soils because of the exponentially increasing bearing capacity factors and high dilation. In the select case study, the precise tensile bucket capacity was complicated to estimate. It was shown that the CPT-based methods from API (2011) can predict very high tensile capacities.

Acknowledgements. This research is sponsored by Energinet.dk and partners. The financial support is sincerely acknowledged.

Bibliography

- API (2011). *Geotechnical and foundation design considerations - ANSI/API recommended practise 2GEO*. American Petroleum Institute.
- Bolton, M. D. and Lau, C. K. (1993). Vertical bearing capacity factors for circular and strip footings on Mohr-Coulomb soil. *Canadian Geotechnical Journal*, 30(6):1024–1033.
- Brinch-Hansen, J. (1970). *A revised and extended formula for bearing capacity*. Geotechnisk Institut, Bulletin No. 28, Copenhagen, Denmark.
- Bye, A., Erbrich, C., and Tjelta, T. I. (1995). Geotechnical design of bucket foundations. In *Proceedings of the 27th Offshore Technology Conference, Houston, Texas*, pages 869–883. Offshore Technology Conference.
- Byrne, B. W. and Houlsby, G. T. (2002). Investigating novel foundations for offshore windpower generation. In *ASME 2002 21st International Conference on Offshore Mechanics and Arctic Engineering, Oslo*, pages 567–576. American Society of Mechanical Engineers.
- Caquot, A. and Kerisel, J. (1953). Ultimate bearing capacity of a foundation lying on the surface of cohesionless soil. In *Proceedings of the 3rd International Conference on Soil Mechanics and Foundation Engineering, Zurich, Switzerland*.
- Davis, E. H. and Booker, J. R. (1971). The bearing capacity of strip footings from the standpoint of plasticity theory. In *Proceedings of the first Australia-New Zealand Conference in Geomechanics, Melbourne, Australia*, pages 276–282.
- DNV (1992). *Foundations. Classification notes No.30.4*. Det Norske Veritas, Oslo, Norway.
- EC-7 (2004). *EN 1997-1:2004, Eurocode 7: Geotechnical design – Part 1: General rules*. Dansk Standard. Dansk Standard, Nordhavn, Denmark.
- Hansen, B. (1979). Definition and use of frictional angles. In *Proceedings of the International Conference VII ECSMFE, Brighton, Great Britain*.

- Hedegaard, J. and Borup, M. (1993). *Klassifikationsforsøeg med Baskard Sand No. 15*. Department of Civil Engineering, Aalborg University, Aalborg.
- Houlsby, G. T., Kelly, R. B., and Byrne, B. W. (2005). The tensile capacity of suction caissons in sand under rapid loading. In *Frontiers in Offshore Geotechnics I Proceedings of the first International Symposium Frontiers in Offshore Geotechnics (ISFOG), Perth, Australia*, page 405–410. Taylor & Francis Group, London.
- Ibsen, L. B., Barari, A., and Larsen, K. A. (2012). Modified vertical bearing capacity for circular foundations in sand using reduced friction angle. *Ocean Engineering*, 47:1–6.
- Ibsen, L. B., Barari, A., and Larsen, K. A. (2013). Calibration of failure criteria for bucket foundations on drained sand under general loading. *Journal of Geotechnical and Geoenvironmental Engineering*, 140:1–16.
- Ibsen, L. B., Barari, A., and Larsen, K. A. (2014a). Adaptive plasticity model for bucket foundations. *Journal of Engineering Mechanics*, 140:361–373.
- Ibsen, L. B., Barari, A., and Larsen, K. A. (2014b). Evaluation of vertical bearing capacity of bucket foundations in saturated sand. *International Journal of Geomechanics, Submitted*.
- Larsen, K. A. (2008). *Static behaviour of bucket foundations: Thesis submitted for the degree of Doctor of Philosophy*. DCE Thesis; Nr. 7, vol. 1. Department of Civil Engineering, Aalborg University, Aalborg.
- Lundgren, H. and Mortensen, K. (1953). Determination by the theory of plasticity of the bearing capacity of continuous footing on sand. In *Proceedings of the third International Soil Mechanics Conference, Zurich, Switzerland*, pages 409–410.
- Prandtl, L. (1920). Über die harte plastischer körper. *Nachrichten von der Gesellschaft der Wissenschaften zu Göttingen, Mathematisch-Physikalische Klasse*, 1920:74–85.
- Senders, M. (2009). *Suction caissons in sand as tripod foundations for offshore wind turbines*. PhD Thesis, University of Western Australia.
- Skau, K. S. and Jostad, H. P. (2014). Application of the ngi-procedure for design of bucket foundations for offshore wind turbines. In *Proceedings of the 24th International Ocean and Polar Engineering Conference, Busan*, pages 514–520.
- Terzaghi, K. (1943). *Theoretical soil mechanics*. John Wiley & Sons, Inc, New York, USA.
- Tjelta, T. I. (1995). Geotechnical experience from the installation fo the europipe jacket with bucket foundations. In *Proceedings of the 27th Offshore Technology Conference, Houston*, pages 897–908.
- Vaitkunaite, E., Ibsen, L. B., and Nielsen, B. N. (2014). New medium-scale laboratory testing of bucket foundation capacity in sand. In *Proceedings of the 24th International Ocean and Polar Engineering Conference, Busan*, pages 514–520.

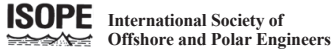
APPENDIX C

New Medium-Scale Laboratory Testing of Bucket Foundation Capacity in Sand

Vaitkunaite, E., Ibsen, L. B., and Nielsen, B. N. (2014). New Medium-Scale Laboratory Testing of Bucket Foundation Capacity in Sand. In *Proceedings of the Twenty-fourth (2014) International Ocean and Polar Engineering Conference, Busan, South Korea*. (Vol. 2, pp. 514-520). International Society of Offshore and Polar Engineers. (International Offshore and Polar Engineering Conference. Proceedings).

Author's Right

The layout has been revised.



ISOPE, 495 North Whisman Road, Suite 300, Mountain View, CA 94043, USA: Website <http://www.isope.org>
Tel 1-650-254-1871; Fax 1-650-254-2038; E-mail isope-2@isope.org

TRANSFER OF COPYRIGHT

Fax or E-mail scanned file to isope-2@isope.org

(Papers will not be published unless this Form is signed and returned.)

Under the terms of the Copyright Law, The Society is required specifically to obtain a written transfer of copyright from all authors in order to hold copyright on the transactions Journal papers and technical papers presented at the conference or symposium. Verbatim reproduction of this paper by anyone or republication by the authors, after the publication or presentation at the meeting below, will be permitted by The Society provided full credit is given to the author(s) and to the conference, symposium or journal, specifically spelled out. The permission does not extend to copying for resale. The purpose in this copyrighting is to control, when necessary, abuses of the privileges. The statements and opinions advanced in papers are understood as individual expressions of their authors, not of The Society or publisher.

Abstract. This article presents a new testing rig for axially loaded bucket foundations. The medium-scale physical model gives the ability to examine the influence of axial loading on bucket foundations subjected to various levels of overburden stress. The properties of the test set-up allow long-term examination. Tests can be done with specimens of up to one meter in diameter and one meter in skirt length. The overburden pressure can be as large as 70 kPa using a tight latex membrane which covers the specimen and the soil surface. In addition to the description of the rig, results from several monotonic tensile tests are presented.

Keywords: Bucket foundation; laboratory test; medium-scale; dense sand; tension; axial loading; overburden pressure.

C.1 Introduction

Offshore structures, such as wind turbines or wave energy machines, require complex support systems in order to withstand the large environmental loading. Due to the size of the structures and the water depth, jacket and tripod foundations supported with three or four suction buckets are often considered by the engineers. Jacket and tripod foundations are mainly subjected to axial loads. Suction caissons can resist large compressive loads. However, monotonic tensile or cyclic capacity can be rather small compared to the compressive capacity.

Environmental loads are greatly variable, and offshore foundations must bear cyclic wind and wave loads. However, the cyclic loads are difficult to model and predict. Real soil behavior is best analyzed by a proper full-scale physical model. Unfortunately, it is also the most expensive and time consuming method. Until today, most of the examined bucket foundations were modelled using small-scale laboratory equipment. Only a few experiments were done in large-scale, but often the results are not publicly available information. Regarding the ultimate tensile capacity of a bucket, loading rate, and the corresponding displacement, several studies were performed.

C.1.1 Physical Models until Today

Feld et al. (2000) performed axially loaded bucket tests. The physical model had a half bucket with diameter of 200 mm and skirt length of 100 mm installed in sand. Several dynamic pull-out tests with velocities of 2 mm/s, 3.7 mm/s, and 5.3 mm/s and several cyclic loading tests were done. It was found that the tensile capacity is very dependent on the displacement rate. The higher pull-out speed, the higher tensile maximum capacity is.

Kelly et al. (2003) tested a bucket with a diameter of 280 mm and a skirt length of 180 mm installed in dense saturated sand in a pressure chamber. The bucket was subjected to some cycles and dynamic tensile load with velocity of 5 mm/s. Cavitation of the pore fluid did not appear. Conclusion was drawn that the ultimate tensile capacity is mobilized at the displacements of 10-20% of the bucket diameter. Further research with the same small-scale testing equipment and pull-out velocity of 100 mm/s showed that the maximum tensile load was mobilized at the displacement of 3.5% of diameter (Kelly et al. 2004).

Houlsby et al. (2006) performed a series of field trials of bucket foundations in sand. The axially loaded specimen had 1500 mm in diameter and in skirt length. The pull-out velocity was low compared to the previous test, approximately 0.23 mm/s. During pull-out tests it was found that a rather high tensile resistance and large displacements were generated.

Senders (2009) performed many tests with axially loaded buckets in dense sand in a centrifuge. The buckets were manufactured on a scale 1:100 which resulted in diameters of

49-120 mm and skirt lengths of 60-114 mm. It was found out that the resistance under drained conditions depends on the skirt friction. It was stated that in drained conditions, the maximum tensile capacity is mobilized at displacement of 0.2% diameter. However, in partially drained conditions, it is much larger, 2-10% of foundation diameter.

To sum up, most of the present experiments were performed on small-scale suction caissons. Knowledge about displacement mobilization during axial loading of a bucket foundation would be valuable. Furthermore, the researchers and engineers are interested in a realistic prediction of the full-scale bucket displacement after long-term cyclic axial loading. Having these goals, a new testing rig for axially loaded bucket foundations was designed (Figure C.2). The design of this test set-up allows long-term examination with more than 40 000 cycles. It is also possible to apply overburden pressures, which simulate different soil depths. The paper describes the main features of the test set-up. Moreover, the results of the first six static tensile tests with various overburden pressures are presented. Attention is paid to the ultimate tensile capacity of a bucket foundation in dense sand and the corresponding displacement.

C.2 Test Set-Up

The test set-up consists of a 2.5 meters diameter sand box, a large installation and loading frame equipped with two hydraulic cylinders and an automatic load regulation system. The tests can be done with bucket specimens of up to 1 meter in diameter and 1 meter in skirt length. Throughout the procedure, loads, displacements and pressures are measured in various points to ensure the knowledge about foundation behavior and influence of the testing equipment. Overburden pressure can be applied as large as 70 kPa using a tight latex membrane which covers the specimen and the soil surface.

C.2.1 Sand Container

A rigid sand container is made of steel with an inner diameter of 2.5 m. Figure C.1 shows the cross-sectional view of the test set-up. The box was filled with 0.3 m of gravel and 1.2 m of sand. The sand was saturated before every test. The bottom of the sand container had a drainage system with equally distributed perforated pipes, draining material (gravel) and a sheet of geotextile. The geotextile ensured that the drainage material was kept clear of sand grains which could potentially block the drainage system. The equally distributed perforated pipes ensured homogenous draining and inflow of water to the entire area.

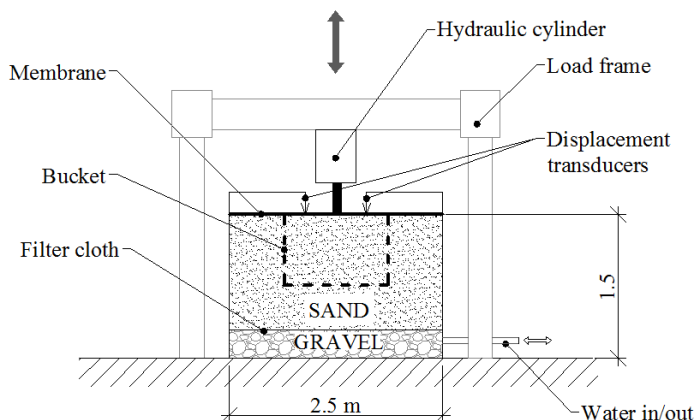


Figure C.1 The cross-sectional view of the test set-up.

The inflow of water to the container came from a water reservoir located in a position higher than the soil surface (Figure C.2). The water level inside the container was regulated by a valve on the inlet pipe, and the level was controlled through a piezometer connected directly to the bottom of the container.

C.2.2 Overburden Pressure

Several research studies regarding the geotechnical testing of offshore foundations has marked the favorability of small-scale testing with overburden pressure (Sørensen et al., 2013; Foglia et al., 2012). The main issues of the small-scale tests are the small soil stresses which result in very high friction angle and elastic Young's modulus. For example, the friction angle in such tests can be as high as 53 degrees. More explanations about the estimation of the friction angle and Young's modulus in the small stresses can be found in Ibsen et al. 2009. Obviously, such properties are different from real offshore soil properties. The problem would be overcome if full-scale foundation was tested. However, this is a very expensive solution. At Aalborg University, a new method was created to increase the soil stresses in the laboratory sand box by applying an overburden pressure. Moreover, the bucket foundation samples were increased to a scale of approximately 1:10, which contributes to larger soil stresses.

Figure C.3 shows air-tight latex membrane specially installed on the sand surface. Four suction hoses were attached to it and used for pumping the excess water out of the sand box creating the differential pressure. A transducer installed on the membrane measured the pressure continuously. The level of the overburden pressure was regulated by a control valve and kept constant during each test.



Figure C.2 The test set-up of axially loaded bucket foundations.

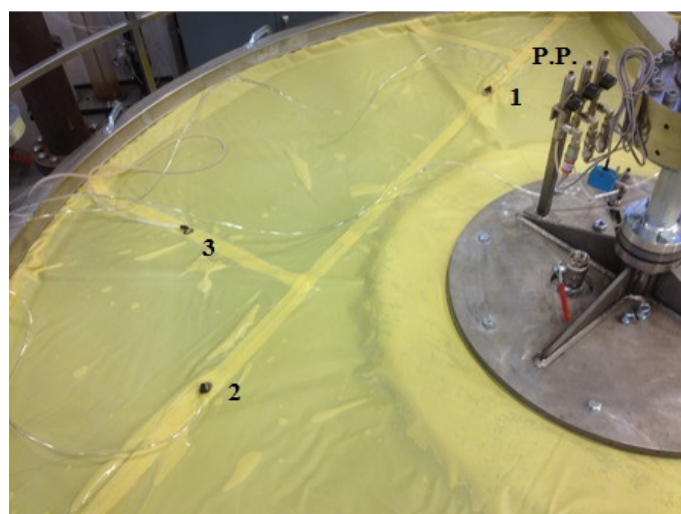


Figure C.3 Yellow latex membrane on the sand surface, suction hoses no. 1 and 2, and three pressure transducers P.P.

C.2.2.1 Measuring System

Every preparation and testing procedure was recorded. Soil preparation, installation, suction application and loading was inspected using various transducers. During the installation, a 250 kN load cell U10M from HBM measured axial resistance. Furthermore, displacement transducer WS17KT from ASM GmbH provided information about the installation depth.

Figure C.4 shows pressure transducers placed on the skirt and under the lid of the specimen. They were used to investigate the pore pressure state. They helped to ensure the state of sand drainage. A rapid pull-out force generates suction under a bucket foundation installed in dense sand. In such a case, the soil experiences undrained condition. However, the pore pressures

are expected to dissipate after the long term cyclic loading. This behavior is difficult to predict, because it depends on the soil type and the dimensions of the foundation. Moreover, during static loading tests, the pore water is able to drain. In such a case, pore pressure sensors should measure no pressure changes. Six transducers PPM-S330A-5 BAR 0-5bar measured pore pressure variations during the test.

An automatic system was designed and installed to regulate and monitor the loading. A powerful hydraulic cylinder, a 250 kN load cell, and a displacement transducer were connected into one system regulated by the MOOG program. The program allows various loading regimes, such as tension/compression and periodic loading with various force/displacement amplitudes and frequencies. The system is able to work continuously for many days or weeks, which is important for the long-term analysis. The program can record the loading information at any moment.

Two external position sensors WS10-125-R1K-L10 from ASM GmbH were placed on the bucket lid, which measured the exact vertical displacements of the specimen during the loading.

All measurement equipment was connected to two data acquisition systems, HBM Spider and MGCplus, which transferred the measured data to the computer. All the sensor signals, such as time and force, were sampled with a rate of 1 Hz during the tests.

C.2.3 Soil Specification

Borup and Hedegaard (1995) defined the material properties of Aalborg University sand No. 1 (Baskarp Sand No. 15), which was used in the tests. The material properties are provided in Table C.1.

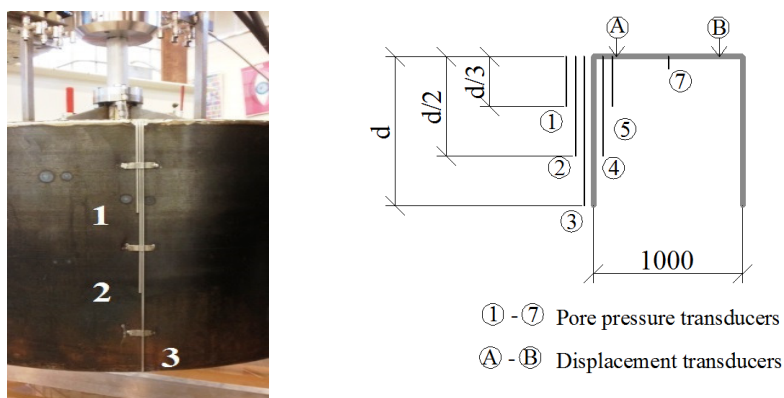


Figure C.4 Pressure and displacement sensors attached to the bucket.

Table C.1 The material properties of Aalborg University Sand No.1.

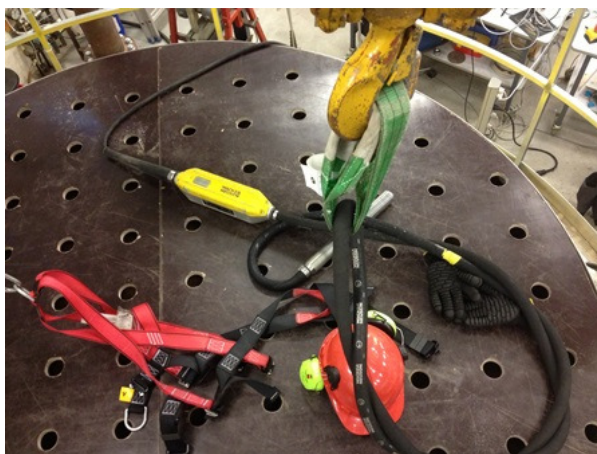
Specific grain density d_s [g/cm ³]	Maximum void ratio e_{max}	Minimum void ratio e_{min}	50%-quantile d_{50} [mm]	Uniformity coefficient $U = d_{50}/d_{100}$
2.64	0.858	0.549	0.14	1.78

Table C.2 The material properties of sand during tests.

Test No.	Relative density I_D [%]
130207	83
130208	83
130211	79
130209	81
130212	79

C.2.4 Preparation of Soil

Prior to each test, the soil was loosened by an upward gradient of 0.9 applied through the drainage system. Systematic mechanical vibration with a rod vibrator ensured the uniform sand compaction and saturated conditions (Figure C.5). The rod vibrator was penetrated to 1.1 meter in the sand. Larsen (2008) has analyzed in details and proved that this preparation method ensures high quality and uniform conditions in the soil. Moreover, the uniformity and soil properties were examined by a laboratory size cone penetration test prior to every test (Figures C.6~7). Table C.2 shows the properties of sand during tests. Sand with a relative density of 79-81% was prepared, corresponding to the sand commonly found in the North Sea.

**Figure C.5** The equipment of sand vibrations.

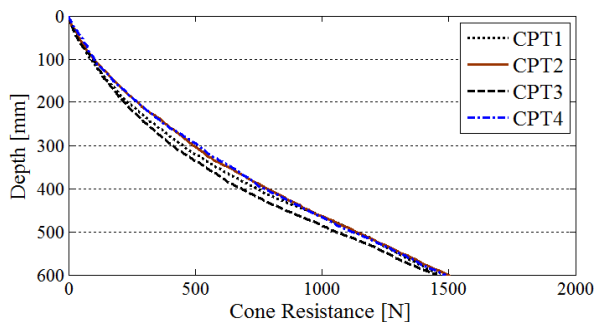


Figure C.6 CPT cone resistance vs. depth (Test 130209).

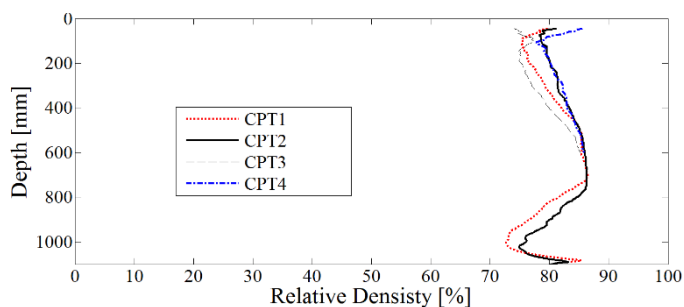


Figure C.7 Relative density vs. depth (Test 130209).

C.2.5 Installation

In offshore sites, a part of the bucket foundation is self-penetrated due to its dead-weight, and another part is installed by suction which generates differential pressure and pushes the foundation into the soil. In the laboratory, the installation was done mechanically by pushing, because it was impossible to apply suction. The installation velocity was 0.2 mm/s. Two valves were attached to the lids of every specimen. They were kept open during installation, which allowed free air flow from the buckets. The valves were closed immediately after the specimen was positioned.



Figure C.8 The installation of bucket $d/D=0.5$.

C.2.5.1 Test Program

The axial tensile capacity of buckets was tested in the geotechnical laboratory of Aalborg University, Denmark. Two steel buckets were used with a diameter D of 1000 mm, skirt lengths d of 500 and 1000 mm, and a skirt wall thickness of 3 mm.

When the sand had been prepared and the bucket installed, the measuring equipment was connected: pore pressure sensors, load cell, and displacement transducers. Afterwards, the loading program was started. During every monotonic pull-out test, the bucket was loaded with displacement rate of 0.002 mm/s. When the tensile capacity had reached the highest value and started to decrease, the test was stopped. The sand was saturated during all the procedure of the tests without the overburden pressure. Drained sand behavior was present during static loading. It was recorded by the pore pressure sensors, which measured no build-up of the pore pressures (Figure C.9). However, the sand was brought to dry condition when suction system was applied.

Table C.3 presents six tensile loading test results with several overburden stress levels. The ultimate capacity and the corresponding displacement are presented.

Table C.3 Laboratory tests with buckets foundations.

Test No.	d/D	d/D^*	Overburden pressure [kPa]	Max. tensile load [kPa]	Displ. [mm]
130207	0.5	0.5	0	10.2	4.2
130208	0.5	0.5	0	9.4	4
130211	0.5	0.75	20	35.7	4
130209	0.5	0.87	40	46.5	8.8
130212	0.5	0.86	40	45.7	6
130210	1	1	0	43.1	3.9

* Equivalent skirt length and diameter ratio

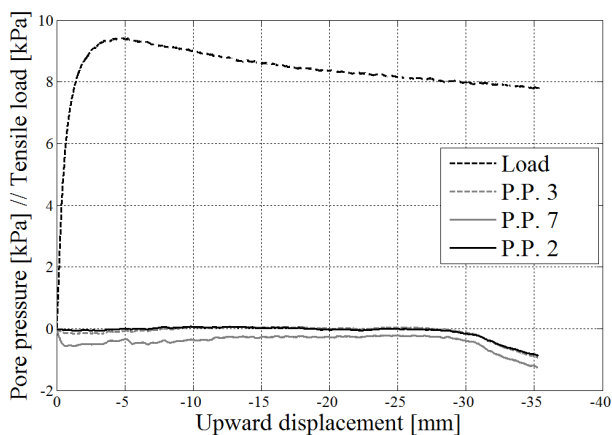


Figure C.9 Pore pressure build-up during loading is less than 1 kPa (Test 130208).

C.2.6 Equivalent Skirt Length

The idea behind the application of the pressure on the soil surface is that it allows investigation of the soil-foundation behavior in larger depths. The stresses created by suction under the membrane can be scaled to the equivalent stresses without overburden pressure, but a deeper soil layer and a greater skirt length. Figure C.10 visualizes the idea of the equivalent overburden pressure to a considerably larger skirt length.

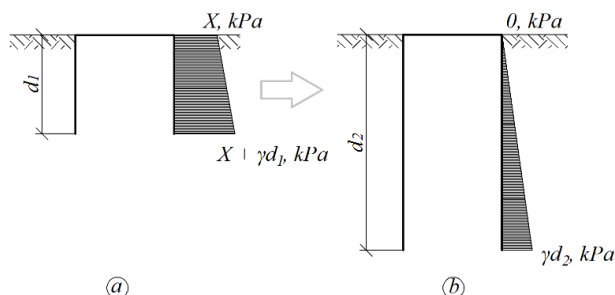


Figure C.10 Overburden pressure used for skirt length simulation: a) real soil stress. b) equivalent soil stress.

The traditional formula for friction induced tensile capacity is used for the scaling of the bucket skirt length. DNV (1992) recommended Eq. C.1 for axially loaded offshore piles. The same equation was used for the estimation of bucket tensile capacity in Byrne and Houlsby (2002).

$$R_t = -((K \tan \delta)_o D_o + (K \tan \delta)_i D_i) \pi \frac{\gamma' d^2}{2}, \quad (\text{C.1})$$

$$\beta = K \tan \delta, \quad (\text{C.2})$$

where R_t is tensile capacity, i and o are indications for the inner and outer skirt correspondingly, D diameter, K coefficient of lateral earth pressure, δ interface friction angle, γ' effective soil weight, d skirt length.

Having the information from the tests with zero overburden pressure, parameter β was calculated. Afterwards, the equivalent skirt length was estimated for the tests with overburden pressure of 20 kPa and 40 kPa. The equivalent skirt lengths are given in the Table C.3.

C.3 Results

Table C.3 presents six static loading tests that were performed in the laboratory: five with specimens of embedment ratio $d/D=0.5$ and one with $d/D=1$. The monotonic tensile capacity was approximately four times higher of $d/D=1$ than $d/D=0.5$ at equal overburden pressure levels, e.g. tests 130207 and 130210. Regardless of the different geometries, the static pull-out capacity tended to increase when larger overburden pressure was applied. Test 130211 with the overburden pressure of 20 kPa showed 3.5 times higher pull-out resistance than test 130207 without any overburden pressure. When the pressure had been increased to 40 kPa, the tensile capacity became approximately 4.6 times higher than the capacity of the tests with

no overburden pressure, e.g. 130207 and 130209. It should be mentioned that the tests with 40 kPa have a slightly larger tensile resistance than the bucket with $d/D=1$ (test 130210). Conclusions regarding this result cannot be drawn at the moment, because many more tests will be performed in the near future. If the tendency of the loading is the same, it may indicate that the method for the scaling of the bucket skirt length should be reconsidered.

In order to visualize the tensile loading influence on displacement and compare it to the previous research of Senders (2009), vertical displacements w were expressed as a percentage part of the bucket diameter D . Figures C.11~12 visualize the loads and displacements in linear graphs. Results of the tests showed that the peak tensile load was reached at the very beginning of the test, within displacement of up to one percent of bucket diameter. This tendency was noticed in the small and the large bucket tests.

C.4 Conclusion

This article presents a novel bucket testing rig. The medium-scale physical model gives the ability to examine the influence of axial tensile, compressive as well as cyclic loading on bucket foundations subjected to various levels of the overburden stress. The test set-up contains a 2.5 meters diameter sand box, a large installation and loading frame equipped with two hydraulic cylinders and an automatic load regulation system. Two bucket foundations were installed in dense sand and subjected to various axial loads. The specimens had depth and diameter ratio d/D of 0.5 and 1. Moreover, several levels of overburden pressure of 0 kPa, 20 kPa and 40 kPa were applied.

Results from the first six tensile loading tests were presented in this article. Tests with the bucket of $d/D=0.5$ resulted in smaller ultimate loads, but similar displacements compared to the test with bucket of $d/D=1$. The peak tensile load was mobilized at the displacements of 0.4-0.9% bucket diameter D . The resultant displacements are a little higher than the displacements found in small-scale laboratory tests done by Senders (2009), where the peak tensile load was mobilized at displacement of 0.2% diameter. The difference in the mobilized displacement can be explained by the scale differences, because the tested buckets were approximately 10 times larger than the buckets tested by previous researchers, among others, Senders (2009). However, more investigations will be performed with the presented testing rig.

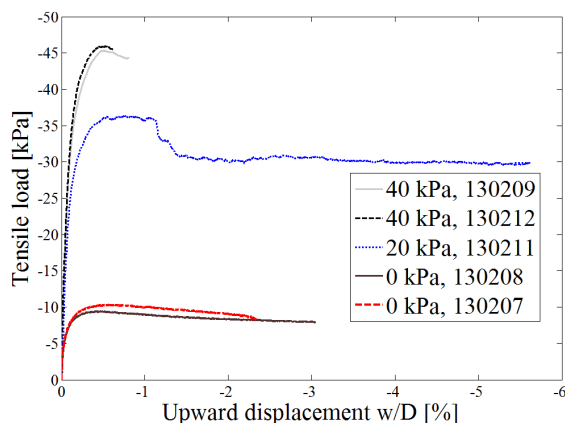


Figure C.11 Static tensile loading vs. upward normalized displacement $d/D=0.5$.

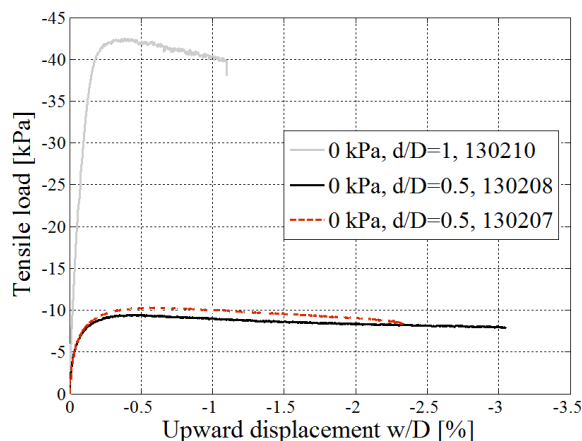


Figure C.12 Static tensile loading vs. upward normalized displacement $d/D=0.5$ and $d/D=1$.

The test set-up has good potential for axially loaded bucket testing. The laboratory work and the analyses of the results presented here provide improved understanding of soil-structure interaction when buckets are subjected to monotonic tensile loading. Using this laboratory equipment, a study about the cyclically axially loaded bucket foundations will be soon published.

Acknowledgment. This research is done via the project “Cost Effective Foundation and Installation of Wave Energy converters”, sponsored by Energinet.dk. The financial support is sincerely acknowledged.

Bibliography

- Borup, M, and Hedegaard, J (1995). Baskarp No. 15: data report 9403. Geotechnical Engineering Group, Aalborg. Data Report, nr. 9403.
- Byrne, BW, and Houlsby, GT (2002). Investigating Novel Foundations for Offshore Wind Power Generation. *Proceedings of OMAE2002-28423*, Oslo, Norway.
- DNV (1992). *Foundations. Classification Notes No.30.4*, Det Norske Veritas, Norway, pp 13.
- Feld, T, Leth, CT, Mikkelsen, H, and Steenfelt, JS (2000). Nyt laboratorieudstyr til simulering af dynamisk påvirkede sugebøttefundamenter. *Proceedings from NGM-2000 : XIII Nordiska Geoteknikermöte*, Helsinki, Building Information Ltd., pp 77-84.
- Foglia, A, Ibsen, LB, and Andersen, LV (2012). An Innovative Physical Model for Testing Bucket Foundations. In *The Nordic Geotechnical Meeting*, pp 323-330.
- Houlsby, GT, Kelly, RB, Huxtable, J, and Byrne, BW (2006). Field trials of suction caissons in sand for offshore wind turbine foundations. *Géotechnique*, 56(1), pp 3-10.
- Houlsby, GT, Kelly, RB, and Byrne, BW (2005). “The tensile capacity of suction caissons in sand under rapid loading,” *Frontiers in Offshore Geotechnics: ISFOG 2005*, Taylor & Francis Group, London, ISBN 0 415 39063 X.

- Ibsen, LB, Hanson, M, Hjort, T, and Tarup, M (2009). MC-Parameter Calibration of Baskarp Sand No. 15. DCE Technical Report No. 62, Department of Civil Engineering, Aalborg University, Aalborg.
- Kelly, RB, Byrne, BW, Houlsby, GT, and Martin, CM (2004). Tensile loading of model caisson foundations for structures on sand. *Proc. ISOPE*, Toulon, 2, pp 638-641.
- Kelly, RB, Byrne, BW, Houlsby, GT, and Martin, CM (2003). Pressure chamber testing of model caisson foundations in sand. *In Proceedings of the international conference on foundations*, Dundee, pp 421-431.
- Larsen, KA (2008). Static behavior of bucket foundations. PhD Thesis, Department of Civil Engineering, Aalborg University, Denmark.
- Senders, M (2009). Suction caissons in sand as tripod foundations for offshore wind turbines. PhD Thesis, University of Western Australia.
- Sørensen, PH, Ibsen, LB, and Foglia, A. (2013). Testing of Laterally Loaded Rigid Piles with Applied Overburden Pressure. *International Journal of Offshore and Polar Engineering*, Vol. 63, pp 17-25, ISSN 1053-5381.

Errata Sheet

Table C.3 Laboratory tests with buckets foundations.

Test No.	d/D	d/D^*	Overburden pressure [kPa]	Max. tensile load [kPa]	Displ. [mm]
130207	0.5	0.5	0	8.0	5.8
130208	0.5	0.5	0	6.8	4.6
130211	0.5	0.70	20	29.7	7.5
130209	0.5	0.77	40	35.9	5.0
130212	0.5	0.76	40	34.3	5.2
130210	1	1	0	35.3	3.9

* Equivalent skirt length and diameter ratio

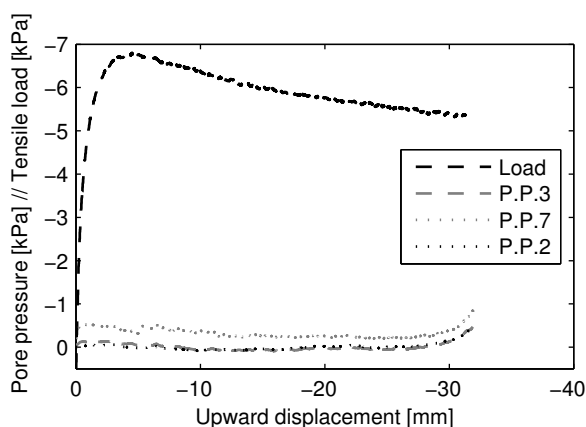


Figure C.9 Pore pressure build-up during loading is less than 1 kPa (Test 130208).

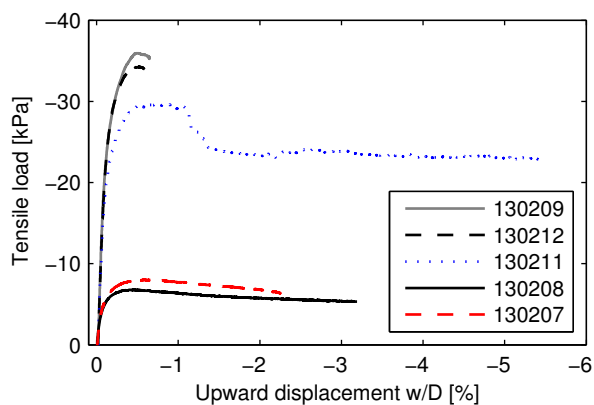


Figure C.11 Static tensile loading vs. upward normalized displacement $d/D=0.5$.

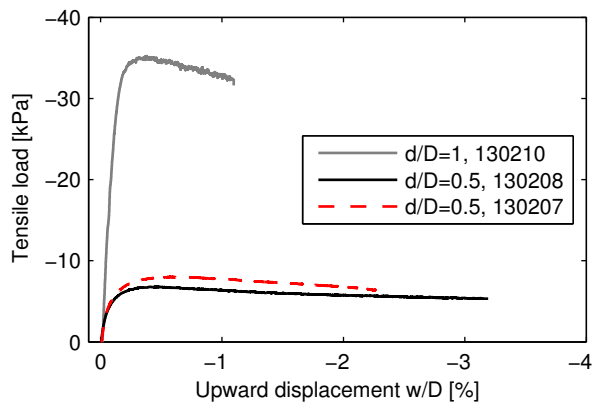


Figure C.12 Static tensile loading vs. upward normalized displacement $d/D=0.5$ and $d/D=1$.

APPENDIX D

Testing of Axially Loaded Bucket Foundation with Applied Overburden Pressure

Vaitkunaite, E., Ibsen, L. B., and Nielsen, B. N. (2016). *Testing of Axially Loaded Bucket Foundation with Applied Overburden Pressure*. Aalborg: Department of Civil Engineering, Aalborg University. (DCE Technical Reports; No. 209).

The layout has been revised.

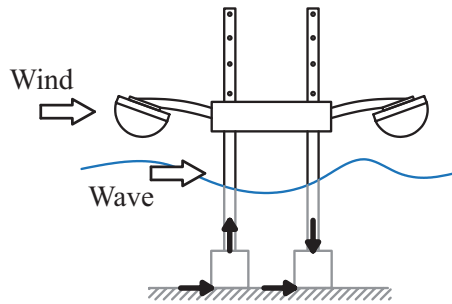


Figure D.1 Loads on the wave energy converter Wavestar in a storm; horizontal wind and wave loads and the axial and horizontal components on a shallow foundation.

D.1 Introduction

This report analyses laboratory testing data performed with a bucket foundation model subjected to axial loading. The examinations were conducted at the Geotechnical laboratory of Aalborg University. The report aims at showing and discussing the results of the static and cyclic axial loading tests on the bucket foundation model. Finally, a cyclic loading interaction diagram is given that can be applied for a full-scale bucket foundation design. This report is based on two previously published reports that contain test data and a detailed description of the test procedure:

- Vaitkunaite, E.: “Bucket Foundations under Axial Loading – Test Data Series 13.02.XX, 13.03.XX and 14.02.XX”. DCE Technical Report, No. 199, Department of Civil Engineering, Aalborg University. 2015. Aalborg, Denmark.
- Vaitkunaite, E.: “Test Procedure for Axially Loaded Bucket Foundations in Sand (Large Yellow Box)”. DCE Technical Memorandum, No. 51, Department of Civil Engineering, Aalborg University. 2015. Aalborg, Denmark.

D.1.1 Aim of the report

In a shallow offshore multi-pod foundation combination, the horizontal wind and wave loads are transferred to the axial loads and sliding. Figure D.1 shows an example of such load transfer in the wave energy converter Wavestar. These load conditions correspond to those of offshore wind turbine foundations standing on a jacket structure.

Suction bucket foundations are shallow skirted geotechnical structures. For bucket foundations in sand, the axial tensile load component can be critical and setting the dimensions. Senders (2009) described the failure mechanisms for bucket foundations in sand (Figure D.2). Constant or static tensile loading on a bucket foundations in sand results in the drained response and lowest capacity. For offshore conditions, cyclic wind and wave loads can create long-term tensile mean loads. Such situation should

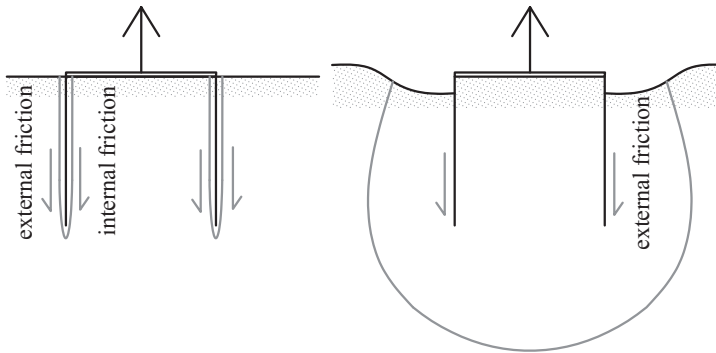


Figure D.2 Bucket foundation tensile resistance in cohesionless soil: (left) drained response; (right) undrained response. After Senders (2009).

be avoided based on the experiences of earlier researches (e.g. Byrne and Houlsby 2006, Kelly et al. 2006a).

If the loading rate is rapid enough, the pore water does not have enough time to drain resulting in an undrained foundation behaviour. A foundation experiences high intensity loading conditions in a storm, where the structure is subjected to large cyclic wind and wave loads. The undrained tensile capacity is significantly larger than the drained capacity because of the suction pore pressure contribution to the resistance. However, such loading conditions can lead to large displacements and tilting of the overall structure (Kelly et al., 2006b). Furthermore, constant cyclic tensile loading with mean tensile load and tensile cyclic amplitude can lead to irreversible upward displacements.

Model testing is an important tool that provides valuable understanding of the real foundation behaviour under various loading conditions. To the knowledge of the authors, no publicly available testing campaign have been performed on bucket foundations subjected to one-way tensile cyclic loading. Thus, the aim of this report is to show the axial behaviour at different effective stress levels and to set the cyclic loading interaction diagram that can be used for bucket foundation design. To fulfil the aim, a new testing facility was employed for bucket foundation testing under axial loading. In this test set-up, an overburden pressure increased the effective stress in the soil. Consequently, the skirt friction of a bucket foundation at different soil depths could be analysed.

The selected cyclic loading program focussed on the axial loading conditions during a normal serviceability situation of an offshore structure. In such case, the foundation is subjected to long-term cyclic loading of small intensity compared to the storm case. Drained conditions are present. Therefore, the target of the testing program was the accumulated cyclic displacement and the cyclic degradation effect on the tensile capacity. The second set of tests started with slow monotonic pull-out tests that provided



Figure D.3 Test set-up for the axial bucket foundation testing with applied overburden pressure.

reference capacities. The testing program continued with low-rate cyclic loading tests corresponding to the drained response. Finally, a post-cyclic monotonic tensile load was applied which was directly comparable to the virgin loading resistance.

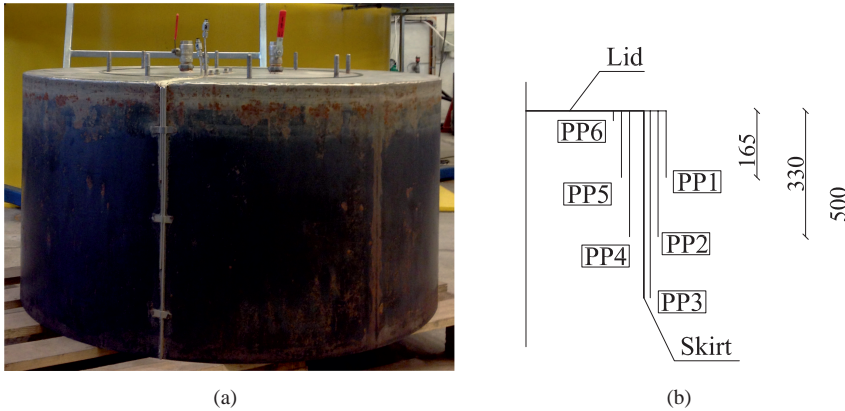


Figure D.4 (a) Bucket foundation model used in the testing campaign. (b) Positions of points for pore pressure measurements and labels of pore pressure transducers PP . Distances in mm.

D.2 Test Set-Up

This chapter presents the principle of the overburden pressure application and provides a short overview of the test set-up facilities. The step-by-step testing procedure can be found in Vaitkunaite (2015).

D.2.1 Testing rig and foundation model

Figures D.3 and D.4 show the testing rig and the bucket foundation model used in the testing campaign. The test set-up consisted of a large container of 2.5 m in diameter and 1.5 m height. The container was filled with 0.3 m of coarse gravel (drainage layer) and 1.2 m of Aalborg University sand No. 1. A rigid structure of four columns and beams was built to support the loading equipment which consisted of two hydraulic cylinders; installation and loading (actuator). Two displacement transducers and two load measuring cells (measuring range 250 kN) were fixed to the hydraulic cylinders.

The bucket foundation model was made of steel. It had a diameter D of 1 m, skirt length d of 0.5 m and skirt thickness t of 3 mm. The skirt was allowed to corrode naturally providing a realistic soil-structure interface. Three inner and three outer narrow pipes were fixed to the bucket foundation model. The pipes were filled with water before the installation of the foundation model to the sand. The pore pressure transducers PP were fixed on the lid and connected to the narrow pipes (Figure D.4). They served for pore pressure measurements at different depths.

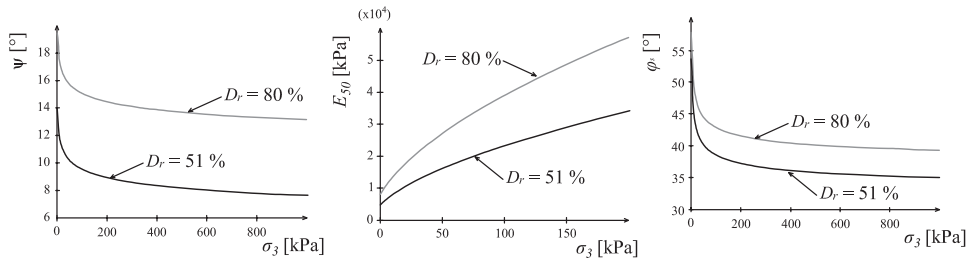


Figure D.5 Aalborg sand No. 1 parameters dependence on the confining stress. (Ibsen et al., 2009)

D.2.2 Soil properties

Aalborg University sand No.1 was used for the testing. Two reports by Hedegaard and Borup (1993) and Ibsen and Boedker (1994) contain sand classification data and triaxial testing data correspondingly. The sand properties are as follows:

- min. void ratio e_{min} 0.549,
- max. void ratio e_{max} 0.858,
- specific grain density d_s 2.64 g/cm³,
- uniformity coefficient U 1.78.

Ibsen et al. (2009) determined Aalborg University sand No.1 parameters for a Mohr-Coulomb material. They showed that the parameters are dependent on confining pressure σ_3 and density index D_R . Results were expressed in the fitted diagrams as given in Figure D.5. As seen, sand properties change strongly in the first 0-100 kPa confining pressure. This visualizes the typical issues related to small-scale testing in low effective stresses, such as a very high friction angle and dilation. Soil-structure interface properties depend on the normal stress, relative surface roughness, soil particle shape and density. To inspect the frictional response at different soil depths, the normal stress on the bucket foundation model had to be increased. Thus, the overburden pressure was applied changing the stress conditions and providing more test results.

D.2.3 Test preparation

This section gives an overview of the preparation for the tests. The step-by-step testing procedure can be found in Vaitkunaite (2015).

Sand preparation

Before each test, water was allowed to flow into the sand box with an upward gradient which loosened and redistributed the sand particles. The sand was compacted

with a rod vibrator to the average $D_R=81\%$ (standard deviation 6%) and the effective unit weight $\gamma'=9.4 \text{ kN/m}^3$. Sand density ratio was found from a laboratory cone penetration test (CPT) specially developed at Aalborg University. Larsen (2008) described the equipment and methodology behind the laboratory CPT. Ibsen et al. (2009) provided the empirical equation for the estimation of D_R based on cone penetration measurements. The procedure was repeated before every installation.

Installation

After the sand preparation, the narrow pipes used for measuring the pore pressure, as mentioned in section D.2.1, were filled with water. The bucket model was placed above the sand surface. Displacement and load transducers were zeroed and the installation started. The installation hydraulic cylinder pushed the model to the sand with a velocity of 0.2 mm/s. The two valves on the model were kept open to let the air flow out during the installation. The installation ended with about 70 kN load F_P that consisted of 50 kN required for the installation and a small compressive pre-load of 20 kN. The elastic pre-load ensured full installation and repetitiveness of the procedure. Due to sand dilation around the circumference of the model, the skirt was installed to approximately 490 mm depth d_{inst} . The installation was followed by connection of the transducers and mounting of the actuator.

Application of the overburden pressure

A latex membrane was laid on the surface of the sand container and the bucket lid. A water pumping system was available by the sand container. Suction was applied in four points on the membrane. A filter layer prevented sand grains from being sucked into the pumping system. Suction application on the membrane evenly pressed the whole surface and simulated overburden pressure p_m . In the atmospheric pressure conditions, the pump unit could apply up to -100 kPa suction. Surcharge of up to -70 kPa was aimed in the testing campaign. In a successful test, the established level of pressure was kept constant with +/- 2 kPa variations. The overburden pressure allowed analysing axial behaviour of the bucket foundation model at different soil depths. Figure D.6 visualizes the idea of the overburden pressure application. On the left side of the figure, vertical stress distribution on a bucket foundation skirt is shown as it is in reality. The right side of the figure shows the bucket model in the test with and without membrane pressure p_m .

This method of the overburden pressure application required a very tight system and de-aired water to saturate the sand. At least 1.5 m^3 of de-aired water would have been necessary to saturate the sand which was unavailable at the time of testing. Tap-water was therefore used for the tests. Although many attempts and special care were taken for the tightening of the system, air was present in the sand. Thus, the suction through the membrane resulted in a reduced amount of water in the sand volume that left the sand moist instead of fully saturated. Furthermore, the sand structure changed - the pores became larger - due to the suction method as shown in Figure D.7. There could

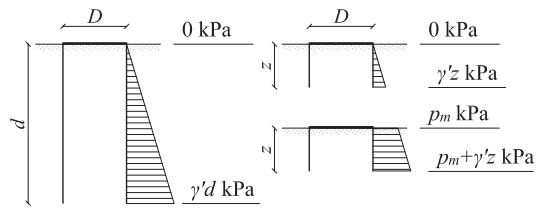


Figure D.6 Vertical stress distribution on a bucket foundation.



Figure D.7 Sand after suction application.

be two reasons for this; water cavitation or expansion due to negative pressure in the air/vapour. Despite this, the testing program continued because it was still possible to apply a constant overburden pressure and to investigate the friction response in the different soil depths. For the result analysis, soil unit weight was measured after several tests with the membrane and was found to be $\gamma=17 \text{ kN/m}^3$.

After a constant membrane pressure was established, the loading could start. During tests with the overburden pressure, load, displacement and membrane pressure were measured. During tests without the overburden pressure, pore pressures were measured too.

D.3 Testing program

In this report, the upward displacement, tensile load and negative pore pressure are drawn on the negative axis and marked with a negative sign.

Monotonic pull-out tests were performed with a constant velocity v of 0.002 m/s. The bucket model was pulled approximately 60 mm which was sufficient to capture the peak load F_T and the corresponding displacement w_T .

Cyclic loading tests were performed with 0.05 or 0.1 Hz frequency f . A testing sequence consisted of 20,000–40,000 harmonic cycles N that were followed by a post-cyclic monotonic tensile load. The post-cyclic load was applied with a displacement rate of 0.002 mm/s until the peak load F_{Pc} and the corresponding displacement w_{Pc} were measured, as shown in Figure D.8. If the accumulated cyclic displacement w_{cyc} reached 60 mm upward displacement, the loading sequence was stopped.

Vaitkunaite et al. (2015) documented the tests performed in the large yellow sand box. Tables D.1 and D.2 provide an overview of the performed tests. The load cell and displacement transducers were zeroed before the beginning of the loading step; thus, the tables provide only the loading response (model self-weight is zero).

Cyclic loading is described using two parameters: ξ_A and ξ_m (eqs.D.1 and D.2). ξ_A is the ratio of cyclic loading amplitude F_{cyc} and the reference tensile load F_{TR} . ξ_m defines the ratio of the mean cyclic load F_{mean} and F_{TR} . The parameter is negative for mean tensile load, and positive for mean compressive load. In the case of perfect two-way loading, ξ_m is 0.

$$\xi_A = -\frac{F_{cyc}}{F_{TR}}, \quad (D.1)$$

$$\xi_m = -\frac{F_{mean}}{F_{TR}}. \quad (D.2)$$

Each test has an ID. For example, a monotonic loading test ID is M20.1, where M stands for monotonic, 20 for the membrane pressure aimed of 20 kPa and .1 marks the test number. A cyclic load loading test ID is, e.g. C70A0.24m-0.23, where C stands for cyclic, 70 for the aimed membrane pressure of 70 kPa, A0.24 marks the cyclic loading amplitude in the test $\xi_A=0.24$ and m-0.23 marks the mean cyclic load in the test $\xi_m=-0.23$.

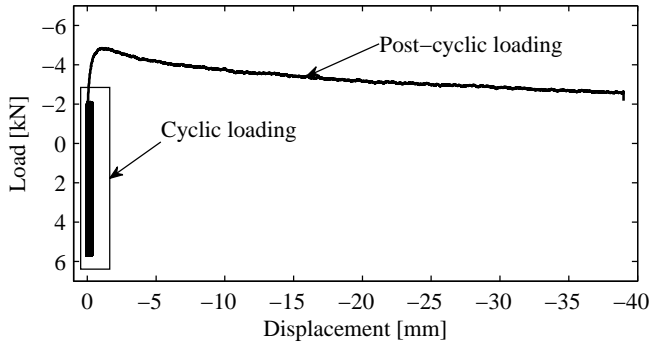


Figure D.8 Cyclic loading with post-cyclic monotonic pull-out (test C0A0.7m0.3.2).

Table D.1 Summary of the monotonic loading tests.

p_m [kPa]	Test ID	d/D	Loading			Installation	
			F_T [kN]	w_T [mm]	v [mm/s]	F_P [kN]	d_{inst} [mm]
0	M0.1	0.5	-5.7	-6.3	0.001	49.6	483
0	M0.2	0.5	-6.3	-5.8	0.001	50.6	474
0	M0.3	0.5	-5.3	-4.6	0.002	49.5	473
0	M0.5	0.5	-5.9	-5.5	0.002	73.0	491
19	M20.1	0.5	-19.0	-24.3	0.001	45.3	486
21	M20.2	0.5	-15.3	-11.4	0.001	46.1	495
20	M20.3	0.5	-23.3	-7.5	0.002	57.3	487
41	M40.1	0.5	-28.2	-5.0	0.001	68.3	487
40	M40.2	0.5	-26.9	-5.2	0.002	72.8	487
73	M70.1	0.5	-96.3	-72.2	0.002	74.0	490

Table D.2 Summary of the cyclic loading tests.

p_m [kPa]	Test ID	Cyclic loading				Post-cyclic load	
		\bar{F}_{mean} [kN]	\bar{F}_{cyc} [kN]	w_{cyc} [mm]	N [Hz]	\bar{F}_{Pc} [kN]	w_{Pc} [mm]
0	C0A0.2m-0.4	-2.11	1.02	-0.88	39,592	-5.34	-3.83
0	C0A0.3m-0.4.1	-2.05	1.93	-1.35	38,227	-5.95	-7.60
0	C0A0.3m-0.4.2	-2.05	1.93	-6.23	39,753	-4.74	-0.53
0	C0A0.7m-0.4.1	-2.05	3.85	-63.76	8,100	-	-
0	C0A0.7m-0.4.2	-2.05	3.85	-65.80	1,285	-	-
0	C0A0.7m0.3.1	1.80	3.85	0.15	28,263	-	-
0	C0A0.7m0.3.2	1.80	3.85	0	39,980	-4.85	-1.30
0*	C0A0.4m0.3	1.91	2.30	0.04	19,629	-5.03	-3.43
0	C0A0.3m-0.1	-0.30	1.66	-0.64	39,729	(-3.49)	-8.66
0	C0A0.2m0.0	0	1.00	-0.29	40,020	-4.86	-4.84
43*	C40A0.4m0.4	11.76	11.38	0.72	19,900	-31.33	-12.35
41	C40A0.7m-0.5	-13.03	18.37	-67.55	67	-	-
41	C40A0.3m-0.7	20.12	9.33	-63.81	202	-	-
71*	C70A0.3m0.0.1	2.01	29.38	0.74	19,970	-	-
70	C70A0.3m0.0.2	1.92	29.30	1.25	40,867	-93.26	-28.29
73	C70A0.2m-0.2	-22.39	23.08	0.10	31,619	-93.90	-26.53
71	C70A0.3m-0.5	-51.67	24.49	-75.01	19,081	-	-
71	C70A0.5m-0.5	-50.61	45.78	-81.90	5	-	-

*Tests with $f=0.05$ Hz, other tests are with $f=0.01$ Hz

D.4 Results

This chapter provides the results of the monotonic and cyclic loading tests. It includes the main results of the load, displacement and stiffness responses. Finally, the chapter presents a cyclic loading interaction diagram applicable to bucket foundation design in dense sand.

D.4.1 Monotonic tensile loading tests

Monotonic tensile loading tests were performed at the overburden pressure levels of 0, 20, 40 and 70 kPa (Figure D.9). The average membrane pressure level p_m varied ± 2 kPa as seen in Table D.1. The four tests with overburden pressure of 0 kPa showed very similar response. Three tests were performed with 20 kPa overburden pressure and showed a bit scattered peak tensile load results. M40 tests were aborted after a displacement of only -8 mm both times due to cracks in the membrane and a sudden pressure loss. However, the peak load was captured and recorded. Only one monotonic tensile loading with 70 kPa was successful. Other attempts failed due to the loss of pressure or other technical issues. As Figure D.9 shows, in most of the cases F_T was reached at upward displacement of up to -10 mm ($0.01D$) except two tests, M20.1 and M70.1 (correspondingly, $0.02D$ and $0.07D$).

The development of peak tensile resistance compared to the corresponding displacement was visualized by the corresponding peak stiffness k_{peak} . It is used as comparison of the resistance development in different tests. Figure D.10 shows k_{peak} values at different surcharge levels. As the tests with the overburden pressure had different soil unit weights (see sections D.2.3 and D.2.3), the surcharge was estimated at the middle of the skirt depth $d/2$. This quantified better the tests with different overburden pressures. Seven k_{peak} values at p_m of 0, 20 and 70 kPa lied around 1 MN/m while the other three tests showed higher stiffness.

As expected, different levels of unit skirt friction f_s were developed in the monotonic loading tests. The skirt friction corresponds to the measured tensile load divided by the sum of the inner and outer areas of the skirt in contact to the soil. According to the testing data, a quadratic fitting resembled best the measured tensile capacities at the different surcharge levels (Figure D.11) which is worth taking a little closer look into. Unit skirt friction f_s can be estimated using equation D.3 that depends on the effective vertical stress σ'_v , lateral earth pressure coefficient K and interface friction angle δ as follows:

$$f_s = \sigma'_v K \tan \delta, \quad (D.3)$$

Obviously, σ'_v increases linearly with depth for a uniform soil layer. Byrne and Houlsby (2002) used $K \tan \delta = 0.5$ for back-calculations of different scale model tests and showed that it is a well applicable value for bucket foundations. Knowing this, the data in Figure D.11 should have had a linear fit. Gaydadhiew et al. (2015) investigated Aalborg University sand No. 1 properties in the same sand container as used in

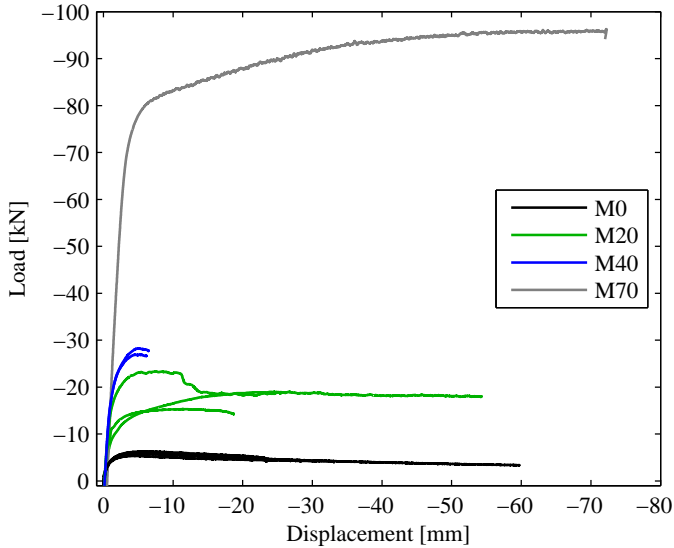


Figure D.9 Monotonic tensile load vs. displacement for tests with 0, 20, 40 and 70 kPa overburden pressure.

this testing program. They used a Marchetti dilatometer (DMT) for the examination of horizontal stress and K values. The lateral pressure coefficients were rather scattered between approximately 0.4 and 4.5 for vertical effective stress between 3 and 9 kPa. The mean value of K was approximately 1.6. However, the testing program was limited to rather few attempts. Boulon and Foray (1986) showed that K value decreases to a constant value together with the increasing confining pressure as seen in Figure D.12. Thus, an attempt was taken to back-calculate the lateral earth pressure value using equation D.3 and assuming that δ is constant and equal to 29° , see Figure D.13. The back-calculated K value has a similar tendency of changing depending on the stress conditions as seen in Figure D.12. At the surcharge of 6 kPa, lateral earth pressure coefficient lies approximately at about 1.8 which is close to 1.6 estimated by Gaydadhzhiew et al. (2015).

D.4.2 Cyclic loading tests

Cyclic loading conditions were modelled taking into consideration the monotonic load results. For each of the overburden pressure levels, the reference monotonic tensile resistance F_{TR} was estimated as the average of the peak tensile resistances F_T . The intention was to test different levels of mean cyclic load and amplitudes and to find the most critical load case. All of the cyclic tests were exposed to peak tensile loads, but the mean loads were various; small compressive, zero (perfect two-way loading) and tensile load. Most of the tests proved to be in a "stable zone". This means that during

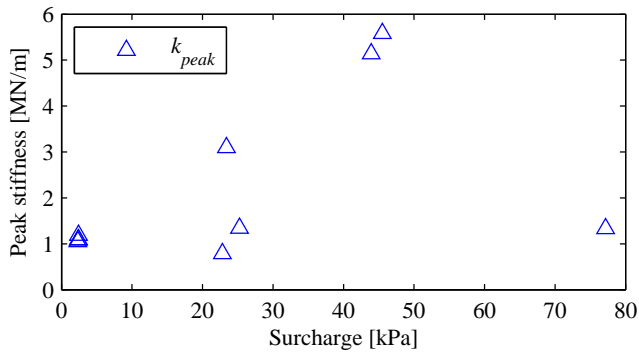


Figure D.10 Peak stiffness at different overburden pressure levels.

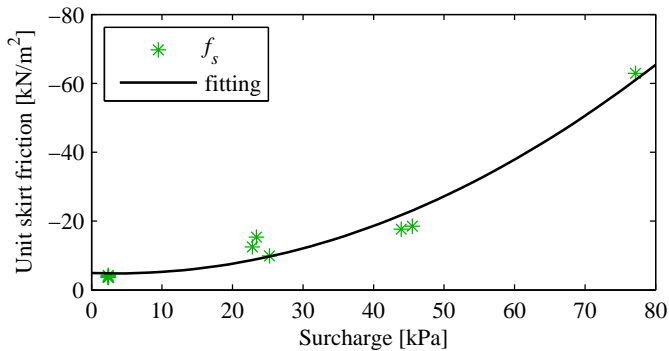


Figure D.11 Peak tensile load developed at different surcharge levels.

the whole cyclic loading sequence of 20,000-40,000 cycles, the vertical displacement was close to zero ($|w_{cyc}| < 0.01D$). Figure D.14 shows some typical examples of this behaviour.

However, as seen in Table D.2, five cyclic loading tests were aborted during the cyclic loading because the upward cyclic displacement developed rapidly and reached the limit of about 65 mm. Figure D.15 shows four of those tests. In all cases, critical tensile loading was applied, where the peak loads reached or even succeeded the reference tensile loads F_{TR} . It was noticed that even under so critical loads, the tests without the overburden pressure and with saturated sand could hold longer than the tests with $p_m > 0$. The reason for this was the development of pore suction that could help the bucket model resist the critical loading. For example, Figure D.16 shows full cyclic loading data for test C0A0.7m-0.4.2. The inner pore pressure transducers (PP4-PP6) measured a small negative suction that at the last part of the cyclic loading reached -8 kPa suction under the bucket model lid. This suction divided by the

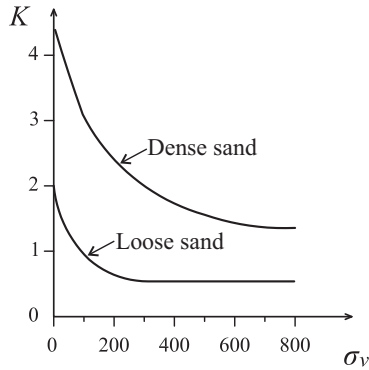


Figure D.12 Lateral earth pressure vs. confining pressure. Reproduced from the figure presented by Boulon and Foray (1986)

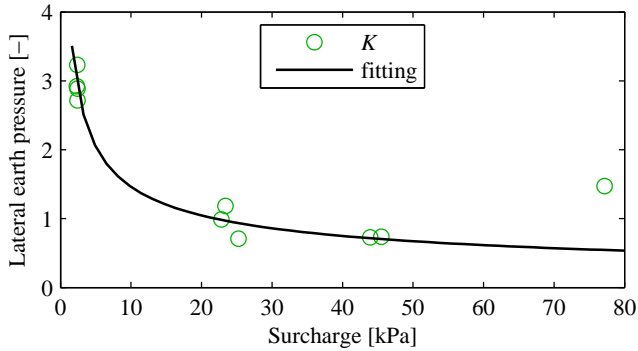


Figure D.13 Back-calculated lateral earth pressure vs. confining pressure.

inner area of the lid provides a resistance suction force of 10 kN which is larger than the peak tensile load applied of -5.9 kN. Even though the loading frequency was low (0.1 Hz), it was sufficient to create partial drainage conditions and generate negative pore suction in the tests with the critical loading.

Eight cyclic loading tests ended up with a post-cyclic monotonic pull-out F_{Pc} . Figures D.17, D.18 and D.19 show the results from tests with different overburden pressures. Virgin monotonic peak load F_T is marked at the corresponding displacement w_T . F_{Pc} values were up to 15% lower than F_T in the tests with 0 kPa overburden pressure (Figure D.17). Very few successful tests with the post-cyclic loading were performed in tests with the overburden pressure of 40 and 70 kPa. From those few tests, it seems that no obvious cyclic degradation was present after the long-term cyclic loading.

Table D.3 shows stiffness results for cyclic loading tests. The following ratios of

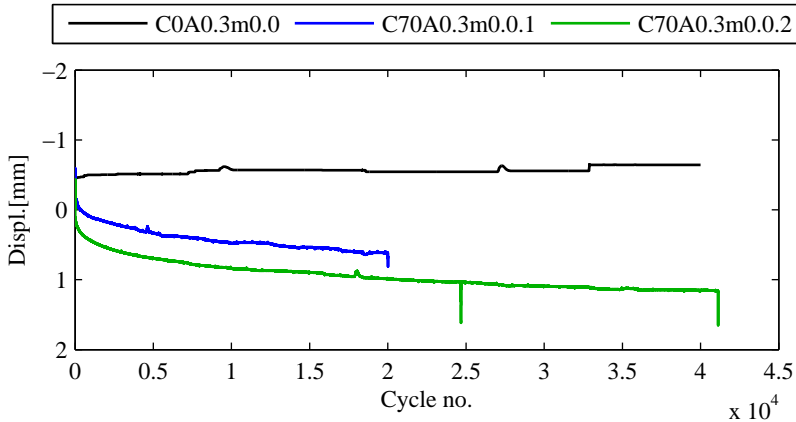


Figure D.14 Accumulated displacement vs. cycle number for three tests.

load and displacement were considered: cyclic unloading stiffness k_{UN} where the trough value was subtracted from the peak value of a cycle, cyclic loading stiffness k where the peak value was subtracted from the trough value of a cycle and peak stiffness k_{Pc} for the post-cyclic monotonic loading part. Three tests developed very small cyclic displacement and had very scattered and extremely high stiffness values, they are marked with a star in Table D.3. Overall, cyclic stiffness was always significantly higher than the virgin loading stiffness k_{peak} (see section D.4.1). By its magnitude, cyclic unloading stiffness was very similar to the loading stiffness except three tests where k_{UN} was higher than k . The post-cyclic peak stiffness k_{Pc} was generally higher than k_{peak} with the mean value of 2.1 MN/m.

Finally, based on the testing data, a cyclic loading interaction diagram was prepared. Figure D.20 shows the results of cyclic loading that led to maximum -50 mm ($0.05D$) upward displacement w_{cyc} . The normalized cyclic amplitude ξ_A and mean load ξ_m were used as the main input to the diagram. The diagram was divided into two zones; stable and unstable. The stable zone contains most of the performed tests, because the displacement developed was close to zero. The response was completely drained in these tests. In the stable zone, a bucket foundation would resist the tensile loading without an excessive upward displacement. As seen, a small mean tensile load of up to $\xi_m = -0.5$ can be allowed for the design. All the tests in the unstable zone resulted in a gradual pull-out of the bucket model. In this case, the foundation would need extra ballast or to be increased in size.

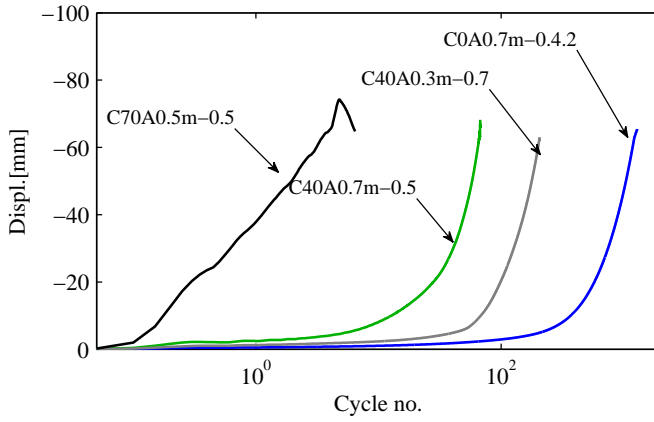


Figure D.15 Accumulated displacement vs. cycle number for four tests where the displacement was developed in less than 20,000 cycles.

Table D.3 Stiffness results for cyclic loading tests.

p_m , [kPa]	Test ID	k_{UN} , [MN/m]	σ , [MN/m]	k , [MN/m]	σ , [MN/m]	k_{PC} , [MN/m]
0	C0A0.2m-0.4	-	-	-	-	1.4
0	C0A0.3m-0.4.1	-	-	-	-	2.6
0	C0A0.3m-0.4.2*	1781	929.1	1705	892	0.7
0	C0A0.7m-0.4.2	21.34	8.68	19.08	7.938	-
0	C0A0.7m0.3.2	228.9	42.0	228.8	42.4	3.7
0	C0A0.4m0.3*	3190	717.9	3150	677.1	1.5
0	C0A0.2m0.0*	5469	2011	5704	2451	-
43	C40A0.4m0.4	17.1	0.5	17.1	0.5	2.7
41	C40A0.7m-0.5	8.8	3.7	7.3	2.9	-
41	C40A0.3m-0.7	183.6	157.2	39.4	5.4	-
71	C70A0.3m0.0.1	39.7	0.3	39.7	0.3	-
70	C70A0.3m0.0.2	41.2	0.4	41.2	0.4	-
73	C70A0.2m-0.2	39.2	0.5	39.2	0.5	-
71	C70A0.3m-0.5	34.8	1.0	34.8	1.0	-
71	C70A0.5m-0.5	13.0	5.5	5.5	0.9	-

*Rough estimate

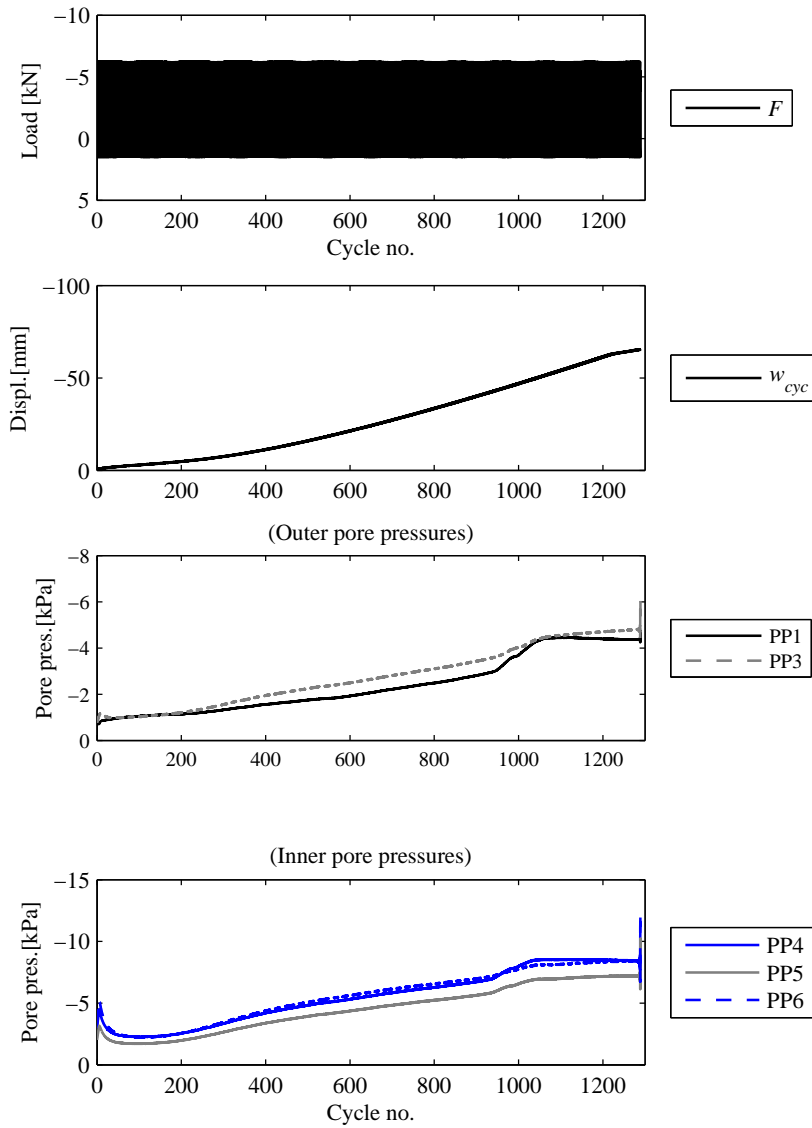


Figure D.16 Full data for the cyclic loading test COA0.7m-0.4.2.

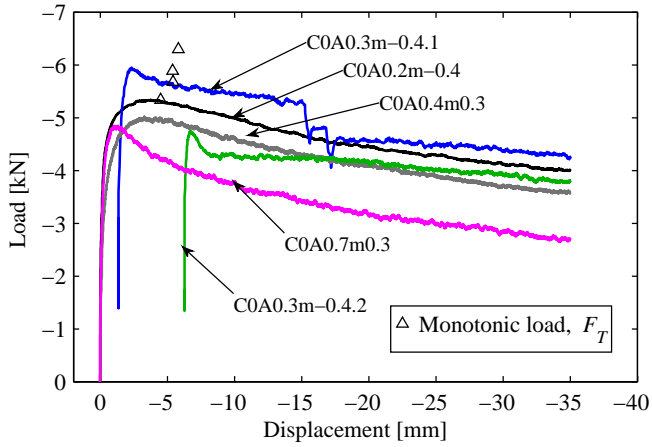


Figure D.17 Post-cyclic tensile loading for two tests vs. vertical displacement for tests with 0 kPa overburden pressure. Triangle marks the peak monotonic tensile load.

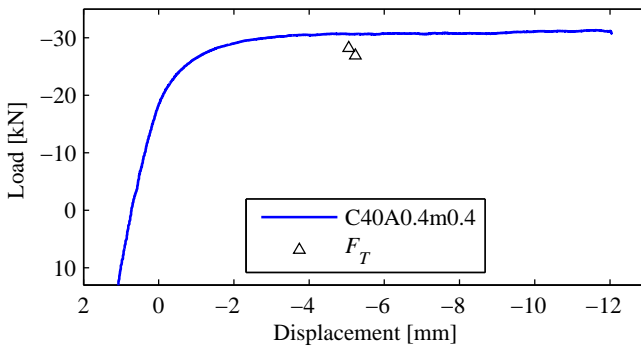


Figure D.18 Post-cyclic tensile loading for two tests vs. vertical displacement for tests with 40 kPa overburden pressure. Triangle marks the peak monotonic tensile load.

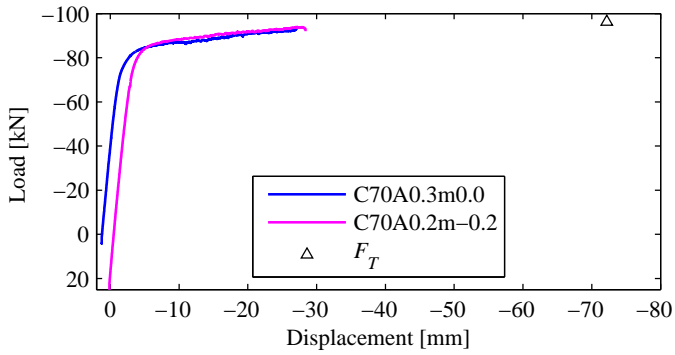


Figure D.19 Post-cyclic tensile loading for two tests vs. vertical displacement. Triangle marks the peak monotonic tensile load.

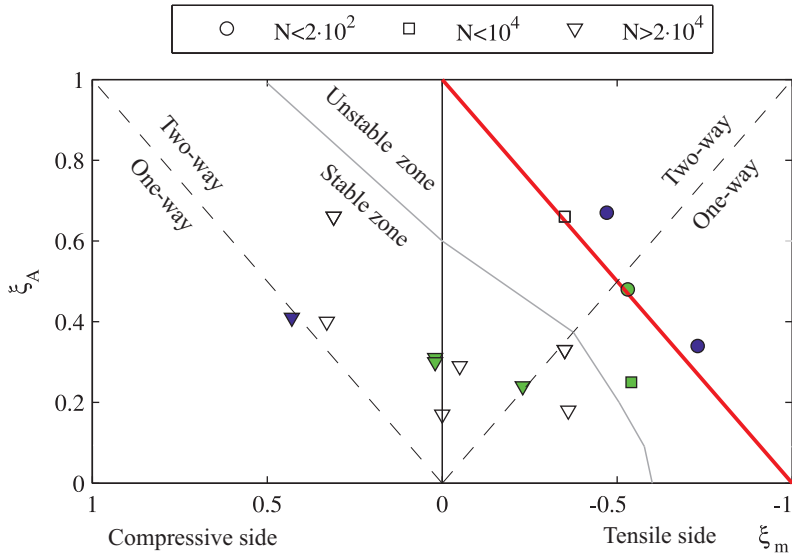


Figure D.20 Interaction diagram for the cyclic loading tests with overburden pressure: 0 kPa (empty marks), 40 kPa (blue) and 70 kPa (green). The red line marks the limit for the drained tensile capacity.

D.5 Conclusion and Recommendations

Conservative assumptions often govern bucket foundation design in sand. Several researchers have recommended that no tensile loading should be allowed for a safe design. But there are no publicly available studies that have focussed on the cyclic behaviour of a bucket foundation subjected to one-way tensile loading. Consequently, this study took a closer look into the cyclic tensile loading on a bucket foundation model. The drained cyclic response was examined by simulating the long-term cyclic loading conditions for an offshore structure under the normal serviceability performance. Cyclic degradation was tested applying post-cyclic pull-out loads on the bucket foundation model. The physical model analysis led to the following observations:

- Unit skin friction increased with the increasing overburden pressure. Interestingly, the measured increase was non-linear which could be explained by a changeable lateral earth pressure coefficient.
- In terms of stiffness, cyclic loading stiffness was much higher than the virgin monotonic loading stiffness. Post-cyclic monotonic loading stiffness was approximately twice as large as the virgin monotonic loading stiffness. However, cyclic unloading and loading stiffnesses were very similar.
- In most of the performed cyclic loading tests, the sand could freely drain and no pore pressure was built up. It was found that mean tensile loads corresponding to ξ_m up to -0.5 can be allowed for long-term loading. For the long-term loading analysis, the tensile drained capacity should never be exceeded, because it would lead to pull-out.
- After long-term cyclic loading, cyclic degradation of up to 15 % was noticed in tests with 0 kPa overburden pressure. Only a few tests with 40 and 70 kPa overburden pressure succeeded, and they showed no cyclic degradation. But more tests are needed to confirm a tendency.

Interface properties were analysed based on the testing data. Variation of the properties, such as different skirt roughness and other types of sand, would provide more information that could be used for a more detailed interface parameter analysis. Moreover, better knowledge about the lateral earth pressure would be very useful and clarifying the soil conditions. Dilatometer may be a suitable tool for the horizontal stress analysis.

The interaction diagram is valid only for a bucket foundation with $d/D=0.5$. Different shapes of foundation model should be tested to provide more data. Rather few tests were successful when testing the post-cyclic monotonic loading with the applied

overburden pressure. More tests would provide a better overview of the results and reduce the scatter in the data.

D.6 List of Symbols

Greek Symbols

γ	Total soil unit weight
γ'	Effective soil unit weight
δ	Soil-structure interface friction angle
ξ_A	Ratio of cyclic loading amplitude and static resistance
ξ_m	Ratio of mean cyclic load and static resistance
σ_3	Confining pressure
σ_v	Vertical stress
σ'_v	Effective vertical stress
φ_s	Secant friction angle
Ψ	Dilation angle

Latin Symbols

D	Bucket model diameter
D_R	Relative soil density
E_{50}	Secant Young's modulus
F	Load
F_{cyc}	Cyclic load amplitude
F_{mean}	Mean cyclic load
F_P	Preload during installation
F_{Pc}	Peak post-cyclic tensile load
F_T	Peak tensile load
F_{TR}	Reference tensile load (average of F_T)
K	Lateral earth pressure coefficient
N	Cycle number
PP	Pore pressure transducer
U	Uniformity coefficient

d	Skirt length
d_{inst}	Installed skirt length
d_s	Specific grain density
e_{max}	Maximum void ratio
e_{min}	Minimum void ratio
f_s	Unit skin friction
f	Loading frequency
k	Cyclic loading stiffness
k_{Pc}	Post-cyclic monotonic loading stiffness
k_{peak}	Monotonic loading stiffness
k_{UN}	Cyclic unloading stiffness
p_m	Membrane pressure
p_t	Tank pressure
v	Tensile load velocity (Pull-out rate)
t	Skirt thickness
w_{cyc}	Displacement during cyclic load
w_T	Displacement at peak tensile load
w_{Pc}	Displacement at peak post-cyclic tensile load

Bibliography

- Boulon, M. and Foray, P. (1986). Physical and numerical simulations of lateral shaft friction along offshore piles in sand. In *Proceedings of the Third International Conference on Numerical Methods in Offshore Piling, Nantes*, pages 127–147.
- Byrne, B. W. and Houlsby, G. T. (2002). Experimental investigations of response of suction caissons to transient vertical loading. *Journal of Geotechnical and Geoenvironmental Engineering*, 128(11):926–939.
- Byrne, B. W. and Houlsby, G. T. (2006). Assessing novel foundation options for offshore wind turbines. In *Proceedings of World Maritime Technology Conference, London*.
- Gaydadhiew, D., Puscasu, I., Vaitkunaite, E., and Ibsen, L. B. (2015). Investigation of dense sand properties in shallow depth using cpt and dmt. In Marchetti, S., Monaco, P., and Fonseca, V. D., editors, *Proceedings of the Third International Conference on the Flat Dilatometer, Rome, Italy*, 132, pages 223–230.
- Hedegaard, J. and Borup, M. (1993). *Klassifikationsforsog med Baskard Sand No. 15*. Department of Civil Engineering, Aalborg University, Aalborg.
- Ibsen, L. B. and Boedker, L. (1994). *Baskarp Sand No. 15: data report 9301*. Department of Civil Engineering, Aalborg University, Aalborg.
- Ibsen, L. B., Hanson, M., Hjort, T., and Thaarup, M. (2009). *MC-Parameter Calibration of Baskarp Sand No.15*. DCE Technical Report No. 62.
- Kelly, R. B., Houlsby, G. T., and Byrne, B. W. (2006a). A comparison of field and laboratory tests of caisson foundations in sand and clay. *Géotechnique*, 56(9):617–626.
- Kelly, R. B., Houlsby, G. T., and Byrne, B. W. (2006b). Transient vertical loading of model suction caissons in a pressure chamber. *Géotechnique*, 56(10):665–675.
- Larsen, K. A. (2008). *Static behaviour of bucket foundations: Thesis submitted for the degree of Doctor of Philosophy*. DCE Thesis; Nr. 7, vol. 1. Department of Civil Engineering, Aalborg University, Aalborg.

- Senders, M. (2009). *Suction caissons in sand as tripod foundations for offshore wind turbines*. PhD Thesis, University of Western Australia.
- Vaitkunaite, E. (2015). *Test procedure for axially loaded bucket foundations in sand (Large Yellow Box)*. DCE Technical Memorandum No. 51, Department of Civil Engineering, Aalborg University, Aalborg.
- Vaitkunaite, E., Nielsen, B. N., and Ibsen, L. B. (2015). Comparison of design methods for axially loaded buckets in sand. In *Frontiers in Offshore Geotechnics III proceedings of the third international symposium on frontiers in offshore geotechnics, Oslo*, pages 331–342.

APPENDIX E

Bucket Foundation Model Testing under Tensile Axial Loading

Vaitkunaite, E., Ibsen, L. B., and Nielsen, B. N. Bucket Foundation Model Testing under Tensile Axial Loading. *Canadian Geotechnical Journal*. Submitted 14-10-2015 [cgj-2015-0497], Re-submitted 06-06-2016 [cgj-2016-0301].

Author's Right

Emne: RE: cgj-2016-0301-Can it be included within a Ph.D. thesis Appendix?

Hi Ms. Vaitkune,

My Managing Editor, Jennifer Stewart, advised that you can include the paper within the Appendix of your Ph.D. thesis, as long as you reference that it "has been submitted to the Canadian Geotechnical Journal" for possible publication.

Sincerely,

Donna

Donna Hartson
Editorial Assistant
Arctic Science &
Canadian Geotechnical Journal
Canadian Science Publishing (NRC Research Press)
65 Auriga Drive, Suite 203, Ottawa, ON K2E 7W6
PHONE NUMBER: 613-656-9846 FAX NUMBER: 613-656-9838
Journals | Website | Facebook | LinkedIn | CSP Weekly Review | The CSP Blog

Please Note: My email has changed, please add me to your contacts and use Donna.Hartson@cdnsiencepub.com for future correspondence.

> Dear Ms. Donna Hartson,
>
> As the manuscript of "Bucket Foundation Model Testing under Tensile Axial Loading" (cgj-2016-0301, re-submission of cgj-2015-0497), has just been re-submitted to the Canadian Geotechnical Journal, I would like to ask you if I may include it to the Appendix of my Ph.D. thesis.
>
>
> Thank you.
>
>
>
> Kind Regards,
>
> Evelina Vaitkune
> Ph.D. Fellow
>
> Department of Civil Engineering
> Aalborg University
> Sofiendalsvej 11
> DK-9200 Aalborg

The layout has been revised.

Abstract. Quasi-static offshore loads, such as mean wave loads, induce drained soil condition. The present study focusses on the bucket foundation behaviour under long-term cyclic loading. The paper analyses model testing results of a bucket foundation model exposed to cyclic tensile loading. The model dimensions are 1 m in diameter and 0.5 m in skirt length. It is installed in dense water-saturated sand. Slow monotonic loading tests and cyclic tensile loading tests are performed (up to 40,000 load cycles) including tests with mean cyclic load in tension which is unique in this sense. High quality data is documented for load, displacement and pore pressure response. Conclusions are drawn regarding static and cyclic loading stiffness, displacement development during the long-term cyclic loading. Four cyclic loading tests induced partially drained soil conditions and showed that pore pressure can accumulate during the long-term loading. Post-cyclic monotonic tensile loading tests showed up to 25% reduction in capacity.

The research results supply valuable information for the design of an upwind bucket foundation under a jacket structure.

Keywords: bucket foundation, tensile loading, axial loading, cyclic loading, long-term loading, 1g testing, dense sand

E.1 Introduction

Bucket foundations have been used for decades as a suitable support for various offshore structures in the oil and gas industry. Tjelta (2015) thoroughly explains the development of suction foundation technology including historical overview and main features. Currently, interest is growing for building extra-large, but still relatively light and very slender wind turbines in deep waters. Compared to an oil platform, a large wind turbine has a small self-weight. To stand in deep water, a wind turbine can be supported on a multi-foundation system. Thus, the large horizontal loading coming from wind and waves would be transferred to dominating axial loads on each foundation. An optimal foundation design solution for extra-large wind turbines should be found, and it is not a straight forward process for two reasons: firstly, the foundations should be cost-effective; and secondly, they should be able to resist tensile loading. In some cases, a long-term cyclic tensile loading would be unavoidable unless the spacing between each foundation is increased or an additional dead-load is placed.

Until today, a significant number of bucket foundation studies were performed at several research institutes and universities, among the best known are Oxford University, Norwegian Geotechnical Institute and Aalborg University. At Aalborg University, monopod bucket foundations were analysed in detail by Feld et al. (1999 and 2000), Larsen et al. (2013), Foglia and Ibsen (2013) and Barari et al. (2015).

An extensive study at Oxford University focussed on axially loaded suction caisson foundations. It included tests with caisson foundation models in different soils in a pressure chamber (Kelly et al. 2003) as well as a large-scale field testing (Kelly et al. 2006a). Most of the times, the performed cyclic loading tests had mean compressive loading and a small part of the loading amplitude was tensile; the highest number of cycles was 1000. It was claimed that, to have a safe design, the highest tensile loading acting on a bucket foundation should be limited to the drained friction resistance (Kelly et al. 2003, 2004, 2006a and 2006b). Thus, the tensile capacity would consist of friction on the outer skirt, self-weight of the structure and the lower of the soil plug weight and the inner skirt friction. Byrne and Houlsby (2006) stated that the tension on the upwind foundation should be generally avoided. However, limited amount of model testing data is publicly available focussing on the cyclic tensile loading on bucket foundations, especially with high cycle number and various mean tensile loads.

A medium-scale bucket foundation model, corresponding to 1:10 prototype size, was used for the testing of load, displacement and pore pressure response in a 1g testing rig. Cyclic loading program consisted of up to 40,000 constant load amplitude cycles followed by a final monotonic pull-out quantifying the cyclic degradation of the frictional resistance. Furthermore, dimensional analysis on stiffness and displacement was applied according to Kelly et al. (2006a). Through the physical model testing, this paper aims at visualizing the bucket foundation behaviour under long-term cyclic loading conditions. The influence of the axial tensile load on the displacement and cyclic degradation is studied.

E.2 Equipment and testing

Quasi-static and permanent loads, such as mean cyclic loads, induce drained conditions in soil. Under drained conditions, the tensile capacity of the bucket foundation corresponds to the dead load of the structure and the frictional resistance generated in the soil-structure interface. Furthermore, it is a lower bound solution for the tensile capacity. This was taken as a starting point in the present model testing program which focussed on the drained response of the bucket foundation model examined by a specially designed laboratory test set-up.

The laboratory test facility was launched in 2013 and presented for the first time by Vaitkunaite et al. (2014). The test set-up consisted of a large sand container, an installation, a loading frame equipped with two hydraulic cylinders and an automatic load regulation system. The tests presented in this article were performed with bucket foundation model of 1 m in diameter D , 0.5 m in skirt length d and 3 mm skirt thickness t , which corresponds to prototype foundation with d/D ratio 0.5. The bucket is made of steel and has a self-weight of 204 kg including the connection flange between the model and the load application point, see Figure E.1.

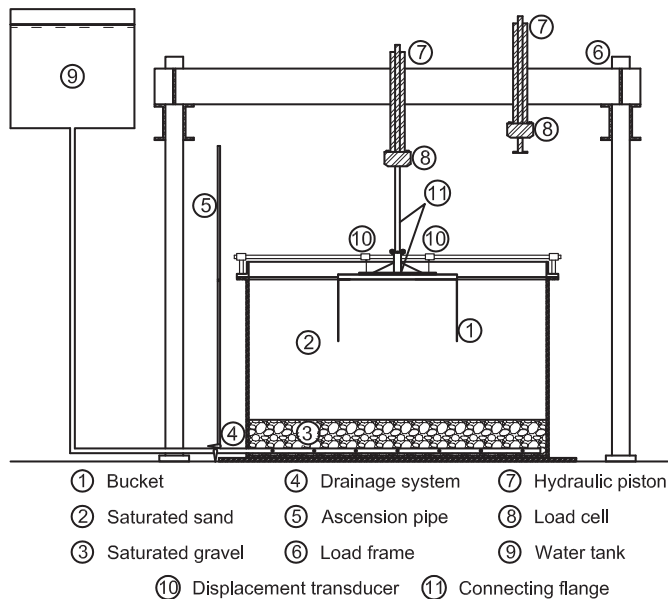


Figure E.1 Test set-up plan (Vaitkunaite 2015).

E.2.1 Sand

The rigid sand container had an inner diameter of 2.5 m. It was filled with 0.3 m of gravel used for drainage and 1.2 m of Aalborg University sand No. 1 (Figure E.1). The latter is quartz sand which contains a small part of biotite and feldspar. The small sand particles are sub-angular while the larger particles are rounded. The main sand properties were as follows: specific grain density 2.64 g/cm^3 , lowest void ratio $e_{min} 0.549$, highest void ratio $e_{max} 0.858$, 50%-quantile 0.14 mm , uniformity coefficient 1.78 . Borup and Hedegaard (1993) and Ibsen and Boedker (1994) thoroughly reported the sand properties. Figure E.3 shows the sieve analysis. The sand was saturated and compacted to a planned density level before every test. Aalborg University sand No. 1 has a hydraulic conductivity of $8 \cdot 10^{-5} \text{ m/s}$ when prepared to relative density $D_R = 80\%$. Sjelmo (2012) performed a permeability analysis of Aalborg University sand No. 1 through a falling head apparatus.

E.2.2 Testing procedure and data sampling

Vaitkunaite et al. (2014) described testing procedure that was applied for this program. To begin with, the sand was loosened with an upward gradient. Afterwards, the sand volume was compacted by a rod vibrator. Later on, at least four small-scale laboratory cone penetration tests (CPT) were performed to inspect soil conditions. Larsen (2008) described the laboratory CPT device and the methodology for the CPT interpretation. Ibsen et al. (2009) estimated D_R from the laboratory cone resistance. Tests presented in this article were performed in dense sand with $D_R \approx 80\%$, see Table E.1.

Table E.1 Testing program.

Test ID	D_R [%]	γ' [kN/m ³]	F_T / F_{Pc} [kN]	$F_{mean} \pm F_{cyc} \cdot f$ [kN, Hz]	LR , [kN/s]	ζ_m	ζ_d	N [x10 ³]
St.1	80	9.3	-5.7 / -	-	0.02**	-	-	-
St.2	80	9.5	-6.3 / -	-	0.02**	-	-	-
St.3	84	9.6	-5.3 / -	-	0.02**	-	-	-
St.4	85	9.6	-5.9 / -	-	0.02**	-	-	-
A0.2m-0.4	78	9.3	- / -5.3	-2.1±1.0, 0.1	0.41	-0.4	0.2	40.0
A0.3m-0.4:1	77	9.2	- / -5.7	-2.1±1.9, 0.1	0.77	-0.4	0.3	38.2
A0.7m-0.4:1	79	9.3	pulled	-2.1±3.9, 0.1	1.54	-0.4	0.7	8.1
A0.7m0.3:1*	85	9.6	-	1.8±3.9, 0.1	1.54	0.3	0.7	28.3
A0.4m0.3	78	9.3	- / -5.0	1.9±2.3, 0.05	0.46	0.3	0.4	19.6
A0.3m-0.4:2	-	9.1	- / -4.7	-2.1±1.9, 0.1	0.77	-0.4	0.3	39.7
A0.7m-0.4:2	-	9.1	pulled	-2.1±3.9, 0.1	1.54	-0.4	0.7	1.3
A0.7m0.3:2	81	9.4	- / -4.9	1.8±3.9, 0.1	1.54	0.3	0.7	40.0
A0.2m0	81	9.4	- / -4.9	0±1.00, 0.1	0.40	0	0.2	40.0
Where: D_R – density ratio, γ' – soil unit weight, $F_{T/Pc}$ – monotonic tensile peak load, F_{mean} – mean cyclic load, F_{cyc} – cyclic amplitude, f – load frequency, LR – load rate, N – cycle number.								
*Test stopped after cycle No. 28,263; loading program was repeated in test A0.7m0.3:2.								
**Max. load rate.								

Mechanical push installation of bucket foundation models was used by Kelly et al. (2003), Kelly et al. (2006a) and Foglia (2015). Kelly et al. 2006a compared installation by suction and pushing and documented that the soil disturbance due to suction installation was more visible in small-scale model tests, probably, because of local soil disturbances which do not increase in proportion to caisson diameter. It is expected that suction installation loosens soil in the inner interface zone and reduces the strength properties of soil-structure interface in a short-term. However, the properties are probably regained after some time due to small cyclic wave loading which is typical in summer weather conditions. Nielsen (2016) performed

laboratory tests with bucket foundation models. He showed that a bucket foundation model gained 1.6 times larger bearing capacity when pre-loaded with small load cycles. This study dealt with the foundation model installed by mechanical pushing, because the focus was operational loading discharging the installation impact.

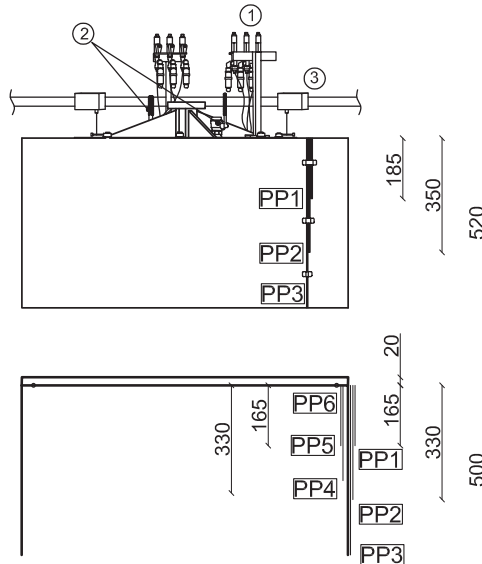


Figure E.2 Bucket model used for the testing: pressure transducer (1), valves (2), displacement transducers (3), positions for the pore pressure measurements (PP1-PP7); dimensions in mm.

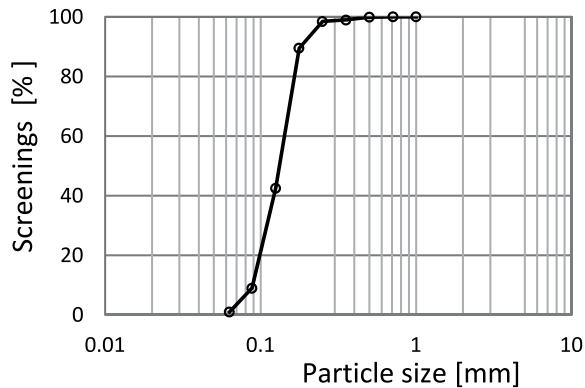


Figure E.3 Sieve analysis of Aalborg University Sand No. 1. performed in 2012.

Installation started with positioning the bucket right on the soil surface level, zeroing the signal of the load cell and penetrating the bucket skirt down to the soil with 0.2 mm/s velocity. Two large valves were kept open during the installation to let the air flow out. The installation ended when approximately 70 kN force was reached. Right after that, the model was completely unloaded. The installation required about 50 kN force from the hydraulic cylinder. An elastic compressive preload of 20 kN ensured that the bucket was fully installed

and kept the procedure repetitive (Figure E.4). In most of the cases, during the installation, the water table was about 3 cm above sand surface. During installation procedure, it was noticed that the load cell reacted to the lid contact with the water table. In a few tests, were the water table was at the same level of the sand surface, only one change in the response was noticed corresponding to the level of the soil surface. This means that the installation rate was slightly higher than would be required for completely drained soil response. However, the installation velocity was limited by the equipment and could not be lower than 0.2 mm/s. Thus, bucket model was left to rest in the sand at least 2 hours allowing pore pressure dissipation. Load and position signals were measured during the installation process with sampling frequency of 1 Hz.

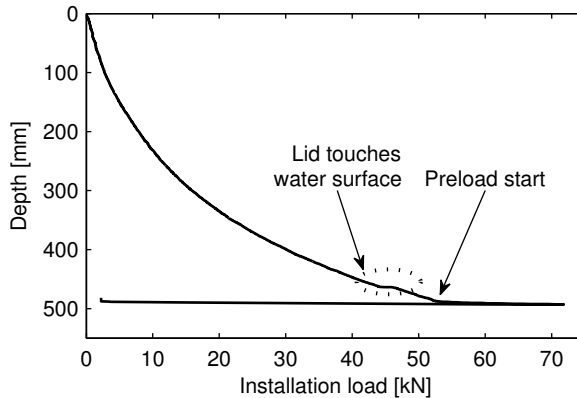


Figure E.4 Model installation with preload and elastic unload, test A0.7m0.3:1.

The testing program of the monotonic tensile loading and cyclic loading tests is presented in details in section 2.3. Load, displacement and pore pressure responses were measured during the tests. Load cell had a capacity of 250 kN and was positioned right above the foundation model. Position of the hydraulic cylinder piston was measured with a displacement transducer. Additionally, two displacement transducers were placed on the lid of the foundation model; they could measure displacements of up to 125 mm. To analyse the drainage conditions, pore pressure response was measured at different levels on the model skirt. Pore pressure transducers were placed above the bucket model and connected to measuring positions via narrow water-filled pipes. As the cyclic tests typically took up to five days, the atmospheric pressure changes were also measured and separated from the pore pressure measurements. Figure E.2 shows all the mentioned transducers. Data sampling rate depended on the type of loading, i.e. 1 Hz frequency was chosen for monotonic loading tests and 2 Hz frequency for cyclic loading tests.

MOOG modular test controller was used to control and monitor various loading regimes; for example, tension, compression and periodic loading with various force or displacement amplitudes and frequencies. The system was able to work continuously for several days, which was important for the high cycle number loading tests.

E.2.3 Loading program

Before describing the loading program, it is worth mentioning that tensile loading, upward displacement and suction pore pressure are marked with a negative sign or drawn on the negative axis.

For the presentation of the load cases, two parameters were used to characterise the cyclic axial loading, i.e. ζ_A and ζ_m . Ratio ζ_A (eq. E.1) describes the cyclic loading amplitude F_{cyc} normalized with reference monotonic tensile load F_{TR} . ζ_A takes a value from 0 to 1, where F_{cyc} equal to F_{TR} results in $\zeta_A=1$ and the smaller F_{cyc} results in $\zeta_A<1$. The second parameter (eq. E.2) expresses the ratio between the mean cyclic load F_{mean} and the reference monotonic tensile capacity F_{TR} . ζ_m takes a value from -1 to 1, where mean tensile cyclic load equal to F_{TR} results in $\zeta_m=1$ while mean compressive cyclic load equal to $|F_{TR}|$ results in $\zeta_m=-1$. A perfect two-way cyclic loading with $F_{mean}=0$ results in $\zeta_m=0$. Figure E.5 visualizes the mentioned loading parameters.

$$(E.1) \quad \zeta_A = -\frac{F_{cyc}}{F_{TR}}$$

$$(E.2) \quad \zeta_m = -\frac{F_{mean}}{F_{TR}}$$

In the first set of tests, the monotonic tensile capacity was measured. The tests were position controlled with maximum vertical pull-out velocity of 0.002 mm/s which ensured that the soil response was drained.

The second set of tests focussed on drained behaviour of bucket foundation subjected to cyclic axial loading. Sinusoidal cyclic loading with constant amplitude and mean load was applied on the model. Loading frequency f was 0.1 Hz, except in one test presented in this paper where the frequency was 0.05 Hz. Each time, the testing program consisted of more than 20,000 load controlled cycles followed by a position controlled monotonic pull-out F_{pc} .

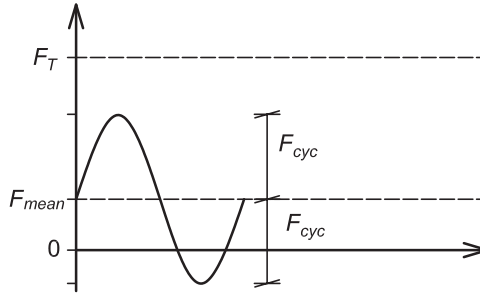


Figure E.5 The definition of loading parameters.

E.3 Test results

All monotonic tensile loading tests showed very similar behaviour and similar tensile peak resistance. Pore pressures did not exceed 1.3 kPa during the loading sequence (Figure E.6), which was within the measuring accuracy of the transducers. Two different displacement rates were applied in the four monotonic tests: two tests with 0.001 mm/s and two with 0.002 mm/s. No influence on the pore pressure transducers was seen for the different displacement rate tests. The displacement rate was extremely low for water saturated sand and it took 1.4-2.8 hours to lift the model only 10 mm. Thus the response was assumed to be drained.

It was noticed that the peak tensile load F_T was reached within the first 6 mm upward displacement ($0.006D$), which was followed by a continuous decrease in load resistance due

to a decrease in the soil-structure interface area and softening behaviour of the soil. The reference monotonic tensile resistance F_{TR} was chosen as the average of F_T .

This paper presents five cyclic loading tests with mean tensile load, three tests with mean compressive load and one with zero mean load. Figure E.7 shows a cyclic loading test followed by a post-cyclic monotonic pull-out. The bucket foundation model was allowed to move up to -65 mm upwards ($0.065D$). In Table E.1, two tests are marked as “pulled”; it refers to vertical upward displacement of -65 mm.

If no significant displacement rate and pore pressure change were seen, then it was expected that there was no cycle that could exceed the drained tensile capacity. However, during four cyclic loading tests, i.e. A0.3m-0.4:1, A0.3m-0.4:2, A0.7m-0.4:1 and A0.7m-0.4:2, pore pressure build up during the loading sequence was noticed. Loading rate analysis showed that the pore pressure build up was present in the tests where the loading rate was higher than 0.77 kN/s and mean tensile load was applied in the loading sequence (see Table E.1). Pore water pressure during cyclic loading is addressed in section 3.3.

Some of the tests are referred as critical loading tests or tests where a critical load is reached. The critical load in this loading program is the drained tensile resistance F_{TR} . The drained soil response is normally assumed for long-term loading conditions. As the main subject of this testing program is drained soil response, the loads reaching F_{TR} are referred as critical.

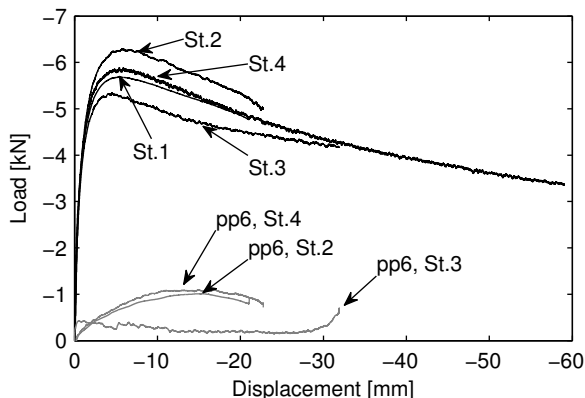


Figure E.6 Monotonic tensile loading tests and pore pressure development under the bucket model lid vs. upward displacement (tests St.1, St.2, St.3 and St.4).

E.3.1 Displacement vs. cycles

All the tests had a tendency to either keep the bucket in the initial position or develop upward displacement. During tests with $\zeta_m=0.3$ and $\zeta_A \leq 0.7$, the foundation model stayed in the initial position (A0.4m0.3, A0.7m0.3:1, A0.7m0.3:2). Very small upward displacements ($<0.006D$) developed in tests with $\zeta_m \in [-0.4, 0]$ and $\zeta_A \leq 0.3$ (A0.2m0, A0.3m-0.4:1 and A0.3m-0.4:2). Figure E.8 clearly shows that when critical loading was applied - the tensile load reached F_{TR} - the bucket eventually was pulled out (A0.7m-0.4:1, A0.7m-0.4:2). However, the foundation model had to be subjected to more than 1,000 cycles of such critical loading to be lifted up to $0.05D$.

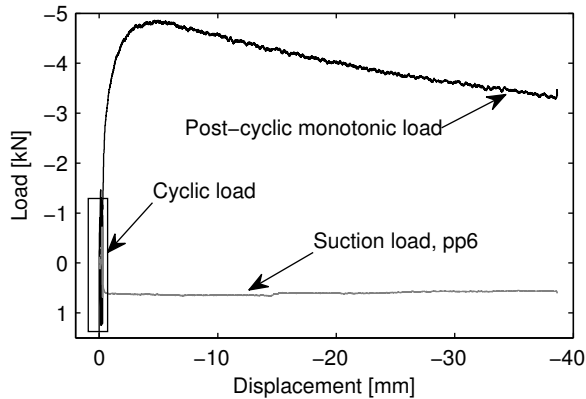


Figure E.7 Full loading program for test A0.2m0: Load and pore pressure vs. upward displacement.

Tests A0.7m-0.4:1 and A0.7m-0.4:2 had identical loading conditions, but slightly different behaviour, the first test required 8 times more cycles to lift the bucket model to -60 mm (Figure E.8). Obviously, the displacement rate was changeable in the tests A0.7m-0.4:2 while in A0.7m-0.4:1 was rather constant. Furthermore, the inner pore pressure in test A0.7m-0.4:2 decreased constantly (Figure E.13) whereas in the test A0.7m-0.4:1 it was around 0 kPa during the first 5,000 cycles (Figure E.14). This indicated that the accumulation of negative pore pressure resulted in higher displacement. As the loading rate was identical, it should be expected that slightly lower soil permeability (thus, higher D_R) could result in the lower negative pore pressure of test A0.7m-0.4:2 compared to test A0.7m-0.4:1. Unfortunately, the density ratio was not estimated for the test A0.7m-0.4:2 due to technical issues.

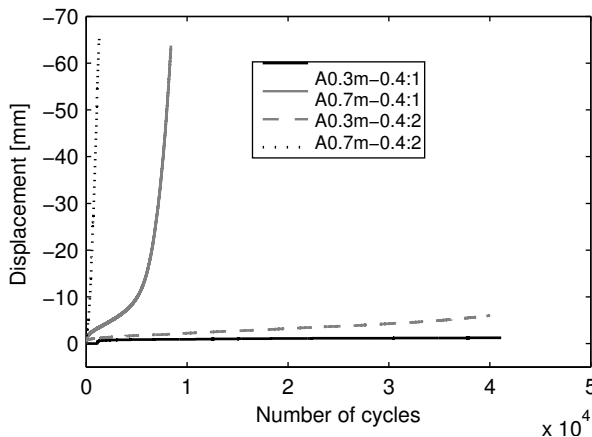


Figure E.8 Accumulated displacement vs. number of cycles (tests A0.3m-0.4:1, A0.3m-0.4:2, A0.7m-0.4:1, and A0.7m-0.4:2).

Kelly et al. (2006b) analysed incremental and cumulative cyclic displacement during one test with mean compressive load (referred as Test15) and showed that the incremental displacement decreased within the first 200 cycles and, afterwards, kept constant with a small positive value pushing the bucket model down to the soil at a constant rate. Positive

incremental displacement indicates a safe foundation design range, because the bucket cannot be lifted due to the loading conditions.

Table E.2 Displacement analysis.

Test ID	ξ_m	ξ_A	N	Comment for displacement
A0.7m0.3:1	0.3	0.7	160	Developed constant $w_{i,d}$ of 10^{-6} mm
A0.7m0.3:2	0.3	0.7	200	Developed constant $w_{i,d}$ of 10^{-6} mm
A0.4m0.3	0.3	0.4	1100	Developed constant $w_{i,d}$ of 10^{-6} mm
A0.2m0	0	0.2	40	Developed stable $w_{i,d}$ of -10^{-7} mm
A0.3m-0.4:2	-0.4	0.3	188	Developed stable $w_{i,d}$ of -10^{-4} mm
A0.7m-0.4:1	-0.4	0.7	-	Large displ. during all cycles
A0.7m-0.4:2	-0.4	0.7	-	Average $w_{i,d}$ of $-5 \cdot 10^{-2}$ mm

Where: D_R – density ratio, $w_{i,d}$ – incremental displ., N – cycle number to reach a constant $w_{i,d}$.

During the present testing campaign it was seen that in most of the examined cases the incremental displacement $w_{i,d}$ became constant within the first 200 loading cycles. Figure E.9 shows accumulated and incremental cyclic displacement during test A0.7m0.3:2. The incremental displacement changed within the first 200 cycles and continued almost constant with a very small positive increment of 10^{-6} mm until the end of the test. Within the first 200 cycles, the model reached the uppermost position and, afterwards, it was slowly pushed downwards to the initial position (0 mm). The accumulated displacement during this long-term cyclic loading test was very small ($<10^{-3}D$). Similar behaviour was seen in tests A0.7m0.3:1 and A0.4m0.3.

However, all tests with $\xi_m \leq 0$ resulted in negative incremental displacements, where average $w_{i,d}$ was in the range from -10^{-7} mm to -10^{-2} mm depending on loading conditions (Table E.2). Furthermore, under the critical tensile loading, the displacement increment varied during the loading sequence, as seen in Figure E.10. Overall, the negative incremental displacements are small, but they would eventually lead to an inadmissible accumulated displacement of the foundation.

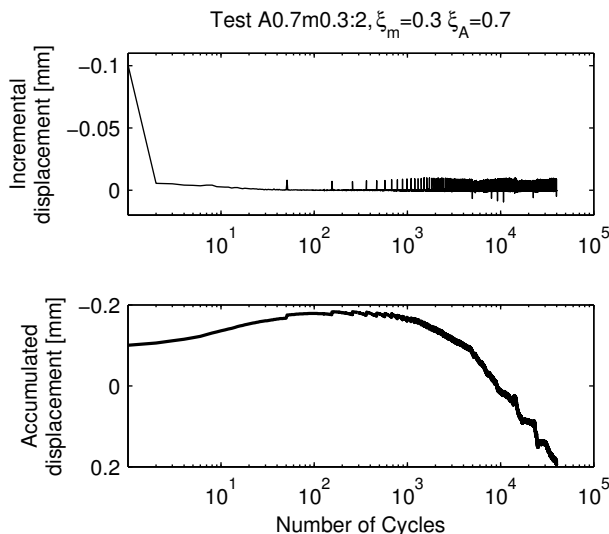


Figure E.9 Incremental and accumulated displacement vs. number of cycles, test A0.7m0.3:2.

E.3.2 Post-cyclic load

Cyclic degradation is a very important factor that should be evaluated when designing offshore foundations. In this testing program, the cyclic degradation was evaluated comparing the virgin loading response and the post-cyclic loading response. The measured monotonic load decreased continuously due to a decrease in the soil-structure interface area and softening behaviour. Thus, the corresponding shaft friction was calculated dividing the measured load by the area of the shaft in contact to soil (Figure E.11). The peak post-cyclic shaft friction was very similar to or lower than the virgin shaft friction; in the performed tests, up to 25% difference in the peak capacity. The peak resistance was reached within the upward displacement of -10 mm, which corresponded to $0.01D$.

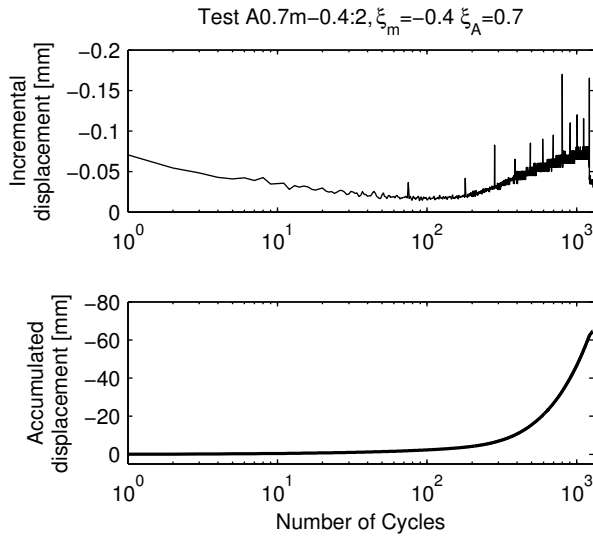


Figure E.10 Incremental and accumulated displacement vs. number of cycles, test A0.7m-0.4:2.

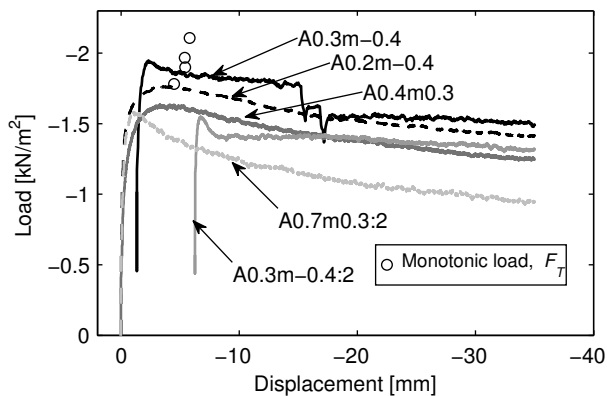


Figure E.11 Virgin and post-cyclic monotonic shaft friction vs. upward displacement.

E.3.3 Pore pressure vs. cycles

Shear and dilation occur when dense sands are subjected to external loads. Negative pore pressure occurs if water is unable to flow into the pores when the soil dilates. Dilation is especially high in low soil stresses (shallow depth). As mentioned earlier, the negative pore pressure is limited by the cavitation.

Until now, no tensile high cycle number tests were performed measuring pore pressure behaviour at different depths of the bucket model skirt. In this testing campaign, it was noticed that pore pressure depends not only on loading rate, but can also change/develop during long-term cyclic loading as seen in Figure E.12 (test A0.3m-0.4:2). It should be noted that any influence from the atmospheric pressure change during the tests was removed from data, so it shows only the pore pressure state in the soil contact to the foundation model, see also Figure E.2 for the pore pressure measuring positions.

No pore pressure development (thus, fully drained response) was seen during full loading program in tests A0.2m-0.4, A0.7m0.3:1, A0.7m0.3:2, A0.4m0.3 and A0.2m0. Small suction accumulation during cyclic loading was visible in tests A0.3m-0.4:1 and A0.3m-0.4:2 that were subjected to a higher loading rate of 0.77 kN/s and mean tensile load (Table E.1). The highest measured pore pressure reached -8.5 kPa in test A0.7m-0.4:2 which was small compared to the cavitation limit of -100 kPa (Figure E.12 and Figure E.13). However, the generated suction pressure of -8.5 kPa under the bucket lid resulted in 6.7 kN resistance to tensile load which was larger than F_{TR} . As seen in Figure E.13, negative pore pressure was continuously generated through all the loading sequence. Due to measuring accuracy of the pore pressure transducers (± 2 kPa) it is hard to say the exact time when drained behaviour changed to partially drained and the tensile resistance was induced by negative pore pressure additionally to the interface friction. Moreover, the pore pressure transducers measured different suction in different levels on the bucket skirt, i.e. the inner part of the bucket was subjected to more suction than the outer indicating partial drainage conditions, see Figures E.2 and E.13. As mentioned in section 3.1, the accumulation of the negative pore pressures influenced the displacements. Vaitkunaite et al. (2016) performed experimental analysis with a bucket foundation model in a pressure tank. The analysis confirmed that pore suction level is closely related to upward displacement rate. More analysis of this matter was out of the focus of the present research.

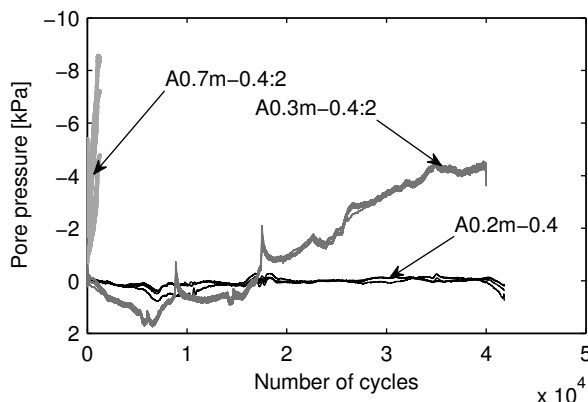


Figure E.12 Pore pressure development during cyclic loading (tests A0.2m-0.4, A0.3m-0.4:2 and A0.7m-0.4:2).

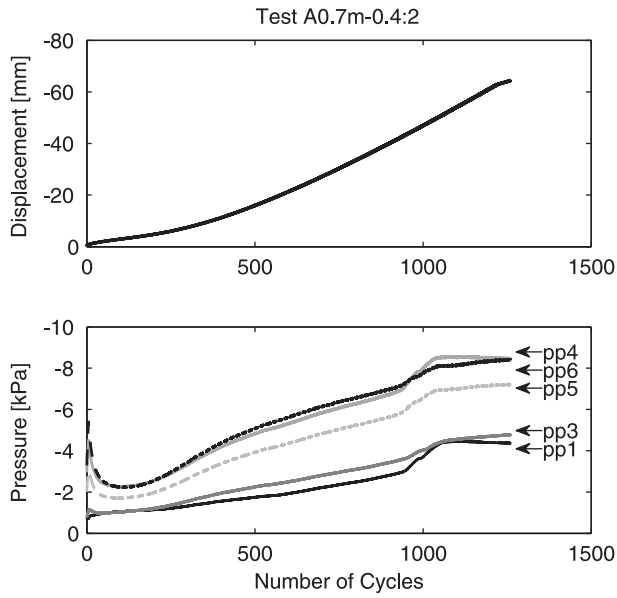


Figure E.13 Accumulated displacement and pore pressure vs cyclic loading in test A0.7m-0.4:2.

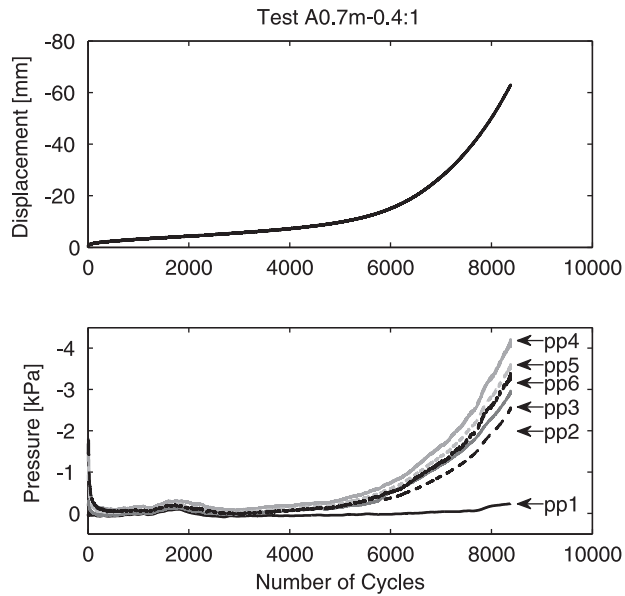


Figure E.14 Accumulated displacement and pore pressure vs cyclic loading in test A0.7m-0.4:1.

E.3.4 Stiffness during monotonic and cyclic loading

Monotonic loading stiffness during the first 10% of load, $k_{10\%}$ was about 11 MN/m, see Figure E.15 for the definition of stiffness. Peak loading stiffness k_{peak} , from the beginning to the peak of the load, was 1.1 MN/m. Post-cyclic tensile load resulted in rather high stiffness. Here $k_{10\%}$ was very high, i.e. from 46 MN/m to 3300 MN/m, while the peak loading stiffness k_{peak} was from 1.0 to 7.3 MN/m.

It was noticed that cyclic loading and unloading stiffness were significantly higher than the monotonic loading stiffness and it had similar values to post-cyclic pull-out values of $k_{10\%}$. Moreover, the stiffness was rather constant during the loading sequence except tests A0.3m-0.4:2 and A0.7m-0.4:2, where the stiffness dropped at some point. Figure E.16 shows that test A0.7m0.3:2 unloading stiffness k_{cyc} was about 230 MN/m (mean). On the contrary, k_{cyc} was quite low (only 24 MN/m) in test A0.7m-0.4:2 where large tensile loading dominated. Clear stiffness degradation during cyclic loading was visible only when critical tensile cyclic loading was applied and no degradation in other loading cases.

Kelly et al. (2006a) performed cyclic loading tests with mean compressive load and showed that unloading cyclic stiffness had no degradation during cyclic loading, i.e. it was constant or increasing during the loading sequence. Such tendency is confirmed with the present tests, except when critical tensile cyclic loading was applied (tests A0.7m-0.4:1 and A0.7m-0.4:2).

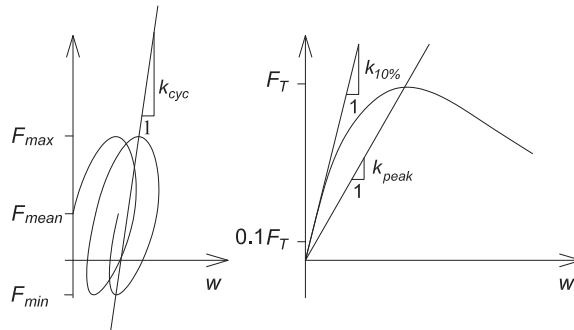


Figure E.15 Cyclic unloading stiffness (a), Monotonic loading stiffness (b).

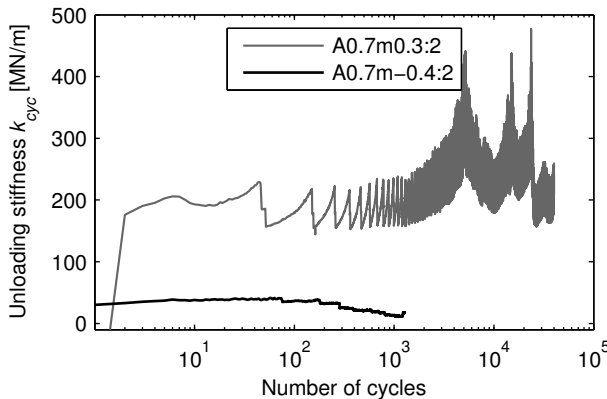


Figure E.16 Unloading stiffness vs cycles for tests A0.7m-0.4:2 and A0.7m0.3:2.

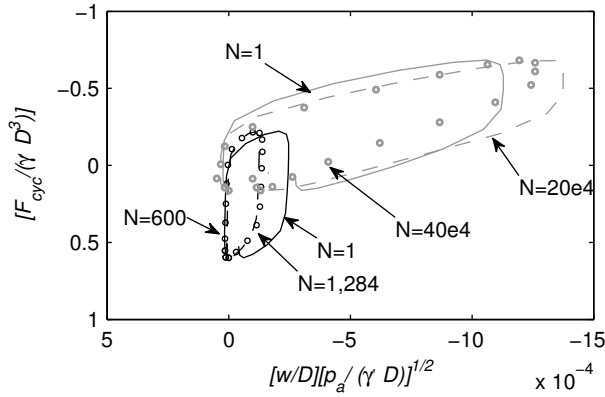


Figure E.17 The normalized cycles of tests A0.7m0.3:2 (black) and A0.7m-0.4:2 (grey).

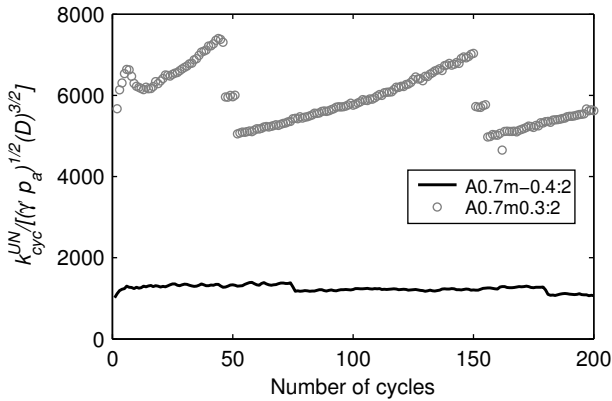


Figure E.18 Normalized unloading stiffness vs. cycle number during the first 200 cycles.

E.3.5 Dimensional analysis

Kelly et al. (2006a) provided equations for comparison of laboratory and field tests which indicated that the method used for data normalization was very successful. Indeed, the study showed good comparability of stiffness in any of the cycles. However, accumulation of deformation during the cyclic loading (90 cycles) had smaller similarity when comparing laboratory and field test data. Analysis of vertically loaded caissons showed that disturbance due to suction installation was less important for field caisson. It is worth mentioning that the dimensional analysis was applied to test data with foundation models having 0.15, 0.2 and 1.5 m diameter while the present study analyses a foundation model with 1 m in diameter. Moreover, the loading conditions were quite different compared to the present study, since herein more attention is given to the tensile loading. Model testing data provides valuable knowledge for the full-scale foundation design. Therefore, the application of the theoretical background is of interest.

Figure E.17 shows the first, middle and last cycles of the corresponding loading sequence in the normalized space. It is clearly seen that test with mean compressive loading (A0.7m0.3:2) presented significantly stiffer behaviour compared to test with mean tensile loading

(A0.7m-0.4:2). Softer behaviour of an axially loaded bucket foundation model in tension was also noticed by Kelly et al. (2006a). Actual unloading stiffness is plotted in Figure E.18 which shows that the unloading stiffness was approximately 6.5 times higher in test A0.7m0.3:2. It is impossible to compare directly Kelly et al. (2006a) results to the present data, because the load amplitudes herein are much smaller. The softer behaviour of tensile loading tests with negative F_{mean} resulted in progressive uplift of the foundation mode is as seen in Figure E.19.

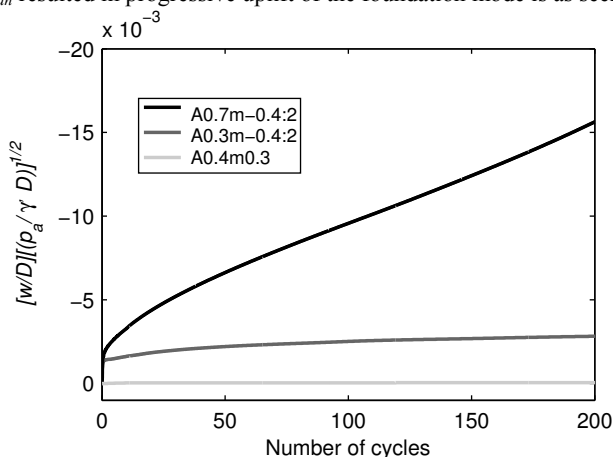


Figure E.19 Normalized accumulative displacements vs. cycle number during the first 200 cycles.

E.4 Conclusions

The study drew attention to the cyclic tensile loading on a bucket foundation model. The paper presented results from four monotonic and nine cyclic loading model tests where several tests had a mean tensile load which has not been publically documented until now. The medium scale bucket foundation model, corresponding to 1:10 prototype size, was subjected to large number of load cycles with various mean loads. Continuous measurements of load, displacement and pore pressures visualized the actual tensile loading behaviour. Based on the performed laboratory tests, the following findings can be drawn:

- Displacement during long-term cyclic loading: All the tests had a tendency to either keep the bucket in the initial position or develop upward displacement. During tests with ξ_m from -0.4 to 0.3 and $\xi_A \leq 0.3$, the accumulated displacement was smaller than $0.006D$. Tests with $\xi_m = -0.4$ and $\xi_A = 0.7$ resulted in gradual pull-out. However, the foundation model had to be subjected to more than 1,000 cycles of such critical loading to be lifted up to $0.05D$.
- A constant negative incremental displacement developed in the tests with $\xi_m \leq 0$ which indicated that the bucket foundation would be eventually moved to an inadmissible upward displacement.
- Pore pressure during long-term cyclic loading: Negative pore pressures developed during four tests indicating partially drained behaviour. Consequently, it was noticed that pore pressure can continuously accumulate during long-term cyclic.
- Cyclic loading stiffness during long-term cyclic loading: During tests where the mean compressive loading dominated, the cyclic unloading stiffness was higher compared to tests where mean tensile loading dominated. Generally, cyclic stiffness was much higher than monotonic loading stiffness. Clear stiffness degradation during cyclic loading was visible only when critical tensile cyclic loading was

applied and no degradation in other loading cases. Unloading stiffness was slightly higher compared to loading stiffness.

- Cyclic degradation: The peak post-cyclic shaft friction was very similar to or lower than the virgin shaft friction; in the performed tests, up to 25% difference in the peak capacity. The peak tensile resistance was reached within upward displacement of 1% of bucket diameter ($0.01D$).
- Dimensional analysis by Kelly et al. 2006a was applied and visualized well the different trends in the tests for load, displacement and cyclic stiffness development. The dimensional analysis can be validated only performing similar loading program on bucket foundation models of different size.

Acknowledgment. The research was sponsored by project “Cost Effective Foundation and Installation of Wave Energy Converters” through the program ForskEl. The financial support is sincerely acknowledged.

References

- Barari, A. 2012. Characteristic Behavior of Bucket Foundations. DCE Thesis; No. 36. Department of Civil Engineering, Aalborg University, Aalborg.
- Barari, A., Ibsen, L.B., and Foglia, A. 2015. Effect of Load Shape on Impedances of Laterally Loaded Suction Caissons. *Canadian Geotechnical Journal*. (In press)
- Byrne, B.W., and Houlsby, G.T. 2006. Assessing novel foundation options for offshore wind turbines. *In Proceedings of World Maritime Technology Conference, London*.
- Feld, T., Rasmussen, J.L., and Sørensen, P.H. 1999. Structural and Economic Optimization of Offshore Wind Turbine Support Structure and Foundation. *In Proceedings of OMAE-99, 18th International Conference on Offshore Mechanics and Arctic Engineering, St. Johns Nfld.*
- Feld, T., Leth, C.T., Mikkelsen, H., and Steenfelt, J.S. 2000. Nyt laboratorieudstyr til simulering af dynamisk påvirkede sugebøttefundamenter. *In Proceedings of NGM-2000: XIII Nordiska Geoteknikermötet, Helsinki, p.p. 77-84.*
- Foglia, A., and Ibsen, L.B. 2013. A Similitude Theory for Bucket Foundations Under Monotonic Horizontal Load in Dense Sand. *Geotechnical and Geological Engineering, 31(1): 133-142.*
- Hedegaard, J., and Borup, M. 1993. Klassifikationsforsøg med Baskard Sand No. 15. Aalborg University, Aalborg.
- Ibsen, L.B., and Bødker, L. 1994. Baskarp Sand No. 15: data report 9301. Aalborg University, Aalborg.
- Ibsen, L.B., Hanson, M., Hjort, T., and Thaarup, M. 2009. MC-Parameter Calibration of Baskarp Sand No. 15, DCE Technical Report No. 62, Department of Civil Engineering, Aalborg University, Aalborg.
- Kelly, R.B., Byrne, B.W., Houlsby, G.T., and Martin, C.M. 2003. Pressure chamber testing of model caisson foundations in sand. *In Proceedings of the international conference on foundations, Dundee, p.p. 421-431.*
- Kelly, R.B., Byrne, B.W., Houlsby, G.T., and Martin, C.M. 2004. Tensile loading of model caisson foundations for structures on sand. *In the Fourteenth International Offshore and*

- Polar Engineering Conference. Toulon, 23-28, May 2004. International Society of Offshore and Polar Engineers.
- Kelly, R.B., Houlsby, G.T., and Byrne, B.W. 2006a. A comparison of field and laboratory tests of caisson foundations in sand and clay. *Géotechnique*, **56**(9): 617-626.
- Kelly, R.B., Houlsby, G.T., and Byrne, B.W. 2006b. Transient vertical loading of model suction caissons in a pressure chamber. *Géotechnique*, **56**(10): 665-675.
- Larsen, K.A. 2008. Static Behaviour of Bucket Foundations: Thesis submitted for the degree of Doctor of Philosophy. DCE Thesis; Nr. 7, vol. 1. Department of Civil Engineering, Aalborg University, Aalborg.
- Larsen, K.A., Ibsen, L.B., and Barari, A. 2013. Modified Expression for the Failure Criterion of Bucket Foundations Subjected to Combined Loading. *Canadian Geotechnical Journal*, **50**(12): 1250-1259.
- Nielsen S.D. 2016. Transient Monotonic and Cyclic Load Effects on Mono Bucket Foundations. Ph.D. Dissertation. Department of Civil Engineering, Aalborg University, Aalborg. ISSN: 2246-1248, ISBN: 978-87-7112-552-8
- Sjelmo, A. 2012. Soil-structure Interaction in Cohesionless Soils due to Monotonic Loading. M.Sc. Thesis, Civil Engineering Department, Aalborg University.
- Thieken, K., Achmus, M., and Schroder, C. 2014. On the behaviour of suction buckets in sands under tensile loads. *Computer and Geotechnics*, **60**: 88-100.
- Tjelta, T.I. 2015. The suction foundation technology. *In* Proceedings of the Third International Symposium on Frontiers in Offshore Geotechnics, Oslo, 10-12 June 2015. CRC Press LLC, London, pp. 331-342.
- Vaitkunaite, E. 2015. Test Procedure for Axially Loaded Bucket Foundations in Sand (Large Yellow Box). DCE Technical Memorandum, No. 51, Department of Civil Engineering, Aalborg University, Aalborg.
- Vaitkunaite, E., Ibsen, L.B., and Nielsen, B.N. 2014. New Medium-Scale Laboratory Testing of Bucket Foundation Capacity in Sand. *In* the Twenty-fourth International Ocean and Polar Engineering Conference, Busan, 15-20 June 2015. International Society of Offshore and Polar Engineers, pp. 514-520.
- Vaitkunaite, E., Nielsen, B.N., and Ibsen, L.B. 2016. Bucket Foundation Response under Various Displacement Rates. *International Journal of Offshore and Polar Engineering*. *In Press*.
- Vaitkunaite, E., Nielsen, B.N., and Ibsen, L.B. 2015. Comparison of design methods for axially loaded buckets in sand. *In* Proceedings of the Third International Symposium on Frontiers in Offshore Geotechnics, Oslo, 10-12 June 2015. CRC Press LLC, London, pp. 331-342.

APPENDIX F

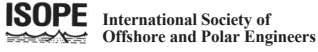
Bucket Foundation Response under Various Displacement Rates

Vaitkune*, E., Nielsen, B. N., and Ibsen, L. B. (2016) Bucket Foundation Response under Various Displacement Rates. *International Journal of Offshore and Polar Engineering*, 26(2), [JC-R-47], In-Press.

Vaitkune - married name, Vaitkunaite - birth name.

Author's Right

The layout has been revised.



495 N. Whisman Road, Suite 300, Mountain View, CA 94043-5711, USA: Website <http://www.isopec.org>
Tel 1-650-254-1871; Fax 1-650-254-2038; E-mail editor@isopec.org

TRANSFER OF COPYRIGHT

(Papers will not be published unless this Form is signed and returned.)

Under the terms of the Copyright Law, The Society is required specifically to obtain a written transfer of copyright from all authors in order to hold copyright on the transactions Journal papers and technical papers presented at the conference or symposium. Verbatim reproduction of this paper by anyone or republication by the authors, after the publication or presentation at the meeting below, will be permitted by The Society provided full credit is given to the author(s) and to the conference, symposium or journal, specifically spelled out. The permission does not extend to copying for resale. The purpose in this copyrighting is to control, when necessary, abuses of the privileges. The statements and opinions advanced in papers are understood as individual expressions of their authors, not of The Society or publisher.

Abstract. The present testing program aims at showing the pore pressure response around a bucket foundation skirt as well as the load and displacement change due to ten different displacement rates. Research findings are useful for a numerical model calibration focussing on the design of the upwind foundation in a multi-bucket foundation system. The foundation model is in a scale of approximately 1:20 prototype foundation size. The tests are performed in a pressure tank with the foundation model installed in dense sand. Based on the data, the conclusion is that bucket foundation design in storm case should allow accounting for partial drainage in sand.

Keywords: Bucket foundation, tension load, axial load, displacement rate, pore pressure, model testing, pressure tank.

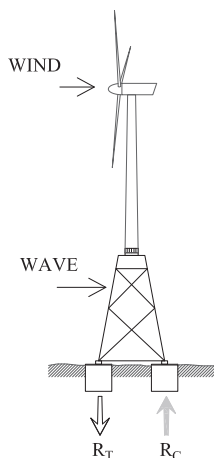


Figure F.1 A wind turbine on a jacket with several bucket foundations with reactions to tensile loading (R_T) and to compressive loading (R_C).

F.1 Introduction

If a jacket with several bucket foundations supports a wind turbine, the upwind foundation should be able to resist tensile loading in the short or long term. Drained tensile capacity of a bucket foundation corresponds to the self-weight of a structure and the frictional resistance on the inner and the outer skirt. If the tensile load is applied rapidly enough, undrained conditions can arise, resulting in high tensile resistance even in a sandy soil. Drainage conditions depend on the size of the foundation, soil permeability and loading intensity. Cavitation pressure limits the pore suction induced by the tensile loading; the cavitation pressure is approximately -100 kPa in atmospheric pressure conditions and temperatures of about 0-35°C.

When estimating bucket foundation response during a storm loading, it is important for the foundation to resist the large wave loads. In a jacket case, the horizontal wave loads would be transferred to the dominating tensile and compressive components on the foundations. A well-known case with the “monster wave” in Draupner E jacket with four bucket foundations proved, that the pore pressure dissipation during the large wave (wave period 11.2 s) was very low (Hansteen et al. 2003, Tjelta 2015). Thus, in a storm loading, the loads on a full-scale bucket foundation would most probably create partial drainage conditions and the tensile

response would be somewhere between the drained and undrained even in sandy soils. Pore suction induced due to rapid loading increases the tensile bucket foundation capacity. The tendencies of the tensile capacity dependence on the loading rate were also noticed by Bye et al. (1995), Feld et al. (2000), Kelly et al. (2006) etc. Clearly, a successful numerical model would be preferable for the foundation design. In the best case, a suitable numerical model should be calibrated with a large-scale model test. As the latter is very expensive, laboratory tests can provide useful information.

Iskander et al. (1993) performed tensile loading tests on a model suction pile which had an outer diameter of 0.11 m and a shaft length of 0.19 m. The foundation model was installed in water saturated dense sand. The authors investigated suction installation and its influence on the frictional resistance. The study included four pull-out tests: each of different type according to the installation method and type of tensile loading. An analytical method predicting the tensile capacity was proposed according to the test data. Feld et al. (2000 and 2001) performed laboratory tests on a small-scale bucket foundation and concluded that large tensile capacity could be generated by suction. Housby et al. (2005) presented an analytical method evaluating the tensile resistance of a bucket foundation when suction is present. They stated that friction along the skirt reduces vertical stresses and proposed a method to include this reduction in the tensile capacity calculation. Housby et al. (2005) validated their analytical method comparing it to laboratory tests performed in a pressure chamber with a suction caisson installed in water saturated dense sand. The bucket dimensions were: diameter of 0.28 m and skirt length of 0.18 m. Housby et al. (2006) performed a large-scale field testing and remarked that large tensile capacity at large displacements could be generated during pull-out tests. Kelly et al. (2003, 2004 and 2006) performed laboratory tests and concluded that the bucket foundation tensile capacity should be limited to the self-weight of the structure, frictional resistance and plug weight (if applicable). Byrne and Housby (2006) stated that tension of the upwind foundation should be avoided to have a safe structure. To follow such recommendations, the spacing between each of the bucket foundations should be increased, which would increase the manufacturing costs.

Bye et al. (1995) presented a design methodology for Sleipner T and Europipe 16/11E jackets on bucket foundations. The design included model testing and finite element modelling. By numerical simulation, Cao et al. (2002) analysed the passive suction and displacement development of a suction caisson installed in clay. The model showed close agreement with centrifuge test results. Thieken et al. (2014) and Achmus and Thieken (2014) presented a finite element model for the design of axially loaded bucket foundations in sand. The model was compared to several test results (including Iskander et al., 1993) and gave rather good results. Tang et al. (2015) implemented a finite volume model of a poro-elasto-plasticity soil model where they simulated a suction caisson under vertical tensile loads applied with several displacement rates.

The present testing program aims at showing the pore pressure response all around the foundation structure as well as the load and displacement change due to a variety of different displacement rates. A pressure tank was used allowing the generation of lower negative pore pressures. The bucket foundation model was at least two times larger than the previously mentioned laboratory models. It was installed in water saturated dense sand. Finally, the results were compared to the analytical methods proposed by Iskander et al. (2002) and Housby et al. (2005).

F.2 Testing Equipment and Program

Figure F.2 shows the bucket foundation model used for the testing. It had a diameter D of 0.5 m, skirt length d of 0.25 m and skirt thickness t of 2 mm, which was approximately 1:20 prototype size. Pore pressure transducers were fixed to the lid of the model and connected to measuring positions via narrow water-filled pipes.

The test set-up was previously used by Sørensen and Ibsen (2012) for pile foundation testing. The test set-up consisted of a large steel pressure tank, a hydraulic cylinder (actuator) and an automatic load regulation system (Figure F.3). The pressure tank had an inner diameter of 2.1 m and the height of 2.1 m. Figure F.3 shows the plan of the pressure tank and the bucket model installed in sand. It is expected that the pressure tank is large enough for the tensile loading tests with low pull-out rates. If the reverse end bearing failure aroused, the size of the tank might be insufficient resulting in lower measured tensile capacity. However, the authors did not perform a detailed assessment of the boundary effects.

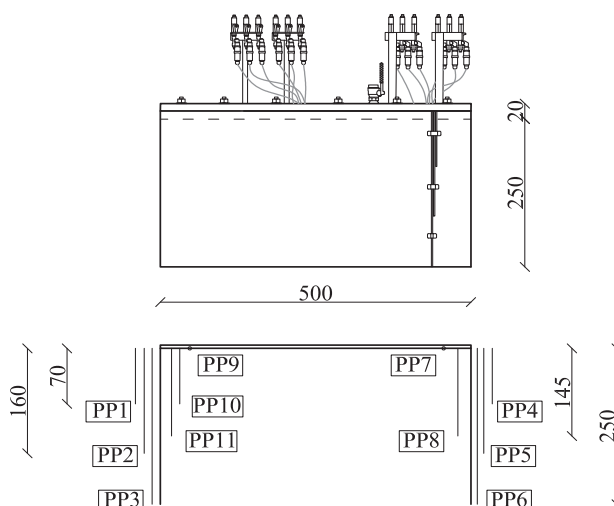


Figure F.2 Bucket foundation model with pore pressure transducers PP1-PP11. Dimensions in mm. (Vaitkunaite, 2015)

F.2.1 Properties of sand

The soil sample consisted of 0.6 m of Aalborg University sand No. 1. Hedegaard and Borup (1993), Ibsen and Boedker (1994) provided a detailed study about the sand properties. Hydraulic conductivity k was $7.4 \cdot 10^{-5}$ m/s and the effective soil unit weight γ' was 9.6 kN/m³ when the sand was prepared to relative density D_R of 85%. The permeability of Aalborg University sand No. 1 was tested in a falling head apparatus by Sjelmo (2012). Figure F.4 shows the hydraulic conductivity dependence on the void ratio for Aalborg University sand No. 1.

The summary of the sand properties:

- min void ratio e_{min} 0.549,
- max void ratio e_{max} 0.858,
- specific grain density d_s 2.64 g/cm³,

- uniformity coefficient U 1.78.

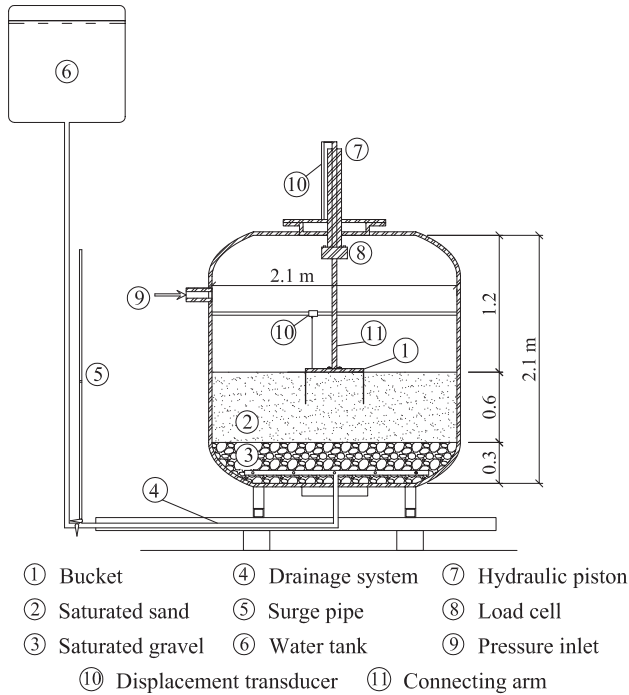


Figure F.3 In-scale plan of the test set-up for the axially loaded bucket foundation model. After Vaitkunaite, 2015.

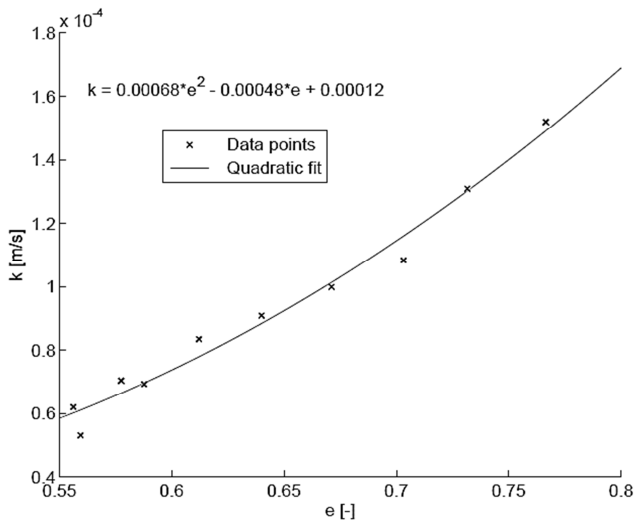


Figure F.4 Hydraulic conductivity vs. void ratio for Aalborg University sand No. 1. (Sjelmo, 2012)

F.2.2 Preparation and testing

Before proceeding with the testing description and results, it should be noted that tensile loading, upward displacement and suction pressure are negative in this paper. The peak tensile load is marked as F_T and the corresponding displacement at the peak load is w_T . Suction pressure s shows the differential pressure between the absolute p_{abs} and the atmospheric pressure p_{atm} as:

$$s = p_{abs} - p_{atm}. \quad (F.1)$$

In the case with the applied pressure p_t in the tank, the suction pressure corresponds to:

$$s = p_{abs} - p_{atm} - p_t. \quad (F.2)$$

Sand preparation and laboratory CPT testing

Every test started with soil preparation: loosening the sand with an upward gradient and compacting it with a rod vibrator as explained by Vaitkunaite et al. (2014). Afterwards, at least four CPT tests were performed with a small-scale and custom-built device to inspect soil conditions. Larsen (2008) developed this laboratory CPT testing procedure and provided the methodology behind it (Larsen 2008, Appendix A). Ibsen et al. (2009) provided an expression for the estimation of the relative soil density D_R based on the cone resistance from the laboratory CPT device:

$$D_R = 5.14 \left(\frac{\sigma'_{v0}}{q_c^{0.75}} \right)^{-0.42}, \quad (F.3)$$

where σ'_{v0} – vertical effective stress, q_c – laboratory cone resistance.

Figure F.5 shows the typical CPT results, i.e. cone resistance and relative density. It should be noted, that the first 100 mm are not considered for the interpretation of data. That is due to a different failure figure in the very shallow depth, where the laboratory CPT interpretation cannot be applied (Larsen, 2008). In the performed tests, the relative soil density D_R was on the average 85% with the standard deviation of 5%.

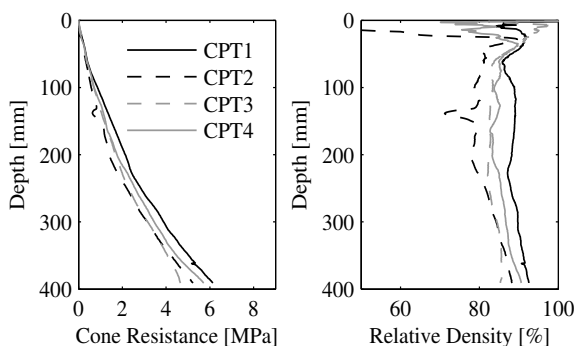


Figure F.5 Cone resistance and relative density measured with the laboratory CPT in test v27.

F.2.2.1 Installation

Installation started with positioning the bucket right on the soil surface level, zeroing the signal of the load cell (measuring capacity 100 kN) and mechanically pushing the bucket down in the soil with a velocity of 0.05 mm/s. Two displacement transducers were used: one on the actuator and another on the bucket lid. A valve on the bucket lid was kept open during the installation to let the air flow out. At an installation depth d_{inst} of about 240 mm, the installation load response changed, meaning that the bucket lid was in contact with the soil surface. During the installation, a compressive force of 32 kN was reached. Immediately after it, the bucket model was completely unloaded (Figure F.6). The push installation required about 10 kN load to penetrate the skirt 240 mm. The additional 22 kN were used for the compressive preloading. This preloading was purely elastic and ensured that the testing program was repetitive and the model was completely installed.

During the installation, the sand dilated slightly around the skirt circumference. Thus, the foundation model could not be installed to full depth ($d=250$ mm). In small-scale testing, every millimetre of the model dimensions is important. Thus, the installation depth d_{inst} was carefully measured and noted after every installation (Table F.1). Furthermore, it was taken into account in the data analysis.

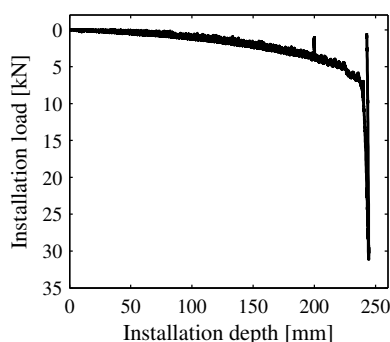


Figure F.6 Installation load vs. installation depth in test v27. (Vaitkunaite, 2015)

F.2.2.2 Testing program

After the installation, the pressure tank was tightly closed and p_t of 200 kPa ($p_{abs}=300$ kPa) was established allowing the simulation of 20 meters water depth. The pressure in the tank provided a possibility of lower negative pore pressure generation during loading. Displacement controlled tests with a pull-out velocity v (in mm/s) were conducted on the bucket foundation model. The testing program contained ten tests, which were numbered according to the displacement rate, e.g. v47 stands for velocity $v = 47$ mm/s (Table F.1). The aim of the testing program was to capture the lowest and the highest tensile capacity. Furthermore, the program had to show the change of the tensile behaviour in between those two limits, especially the change in pore pressures, development of peak resistance and displacements. The needed displacement rates were unknown without actually testing them. As a result, ten different pull-out rates were used in this campaign. Table F.1 gives an overview of the performed tests.

Table F.1 Overview of the performed tests

p_t , [kPa]	Test No.	F_T , [kN]	w_T , [mm]	v , [mm/s]	d_{inst} , [mm]	D_R , [%]
0	v0.01	-	-	0.01	241	79
200	v0.05	-2.7	-0.7	0.05	239	85
200	v0.1	-4.1	-0.7	0.10	241	86
200	v1	-8.0	-3.6	1	242	90
201	v10	-30.8	-16.0	10	242	90
200	v22	-44.1	-14.7	22	236	83
200	v27	-48.8	-14.3	27	239	85
200	v47	-65.4	-48.8	47	236	83
200	v98	-71.7	-60.5	98	239	82
200	v152	-75.2	-68.2	152	236	84

where p_t – pressure in the tank, F_T – peak tensile load, w_T – upward displacement at F_T , v – pull-out rate, d_{inst} – installed skirt length, D_R – sand density ratio.

F.2.3 Scaling law

Small-scale experimental studies can provide useful information about various design issues. In the case of this testing program, the main interest is brought to the pore pressure change and distribution during tensile loading of a bucket foundation. Dimensional analysis is often employed as a good tool to visualize the influence of various parameters on the specific model test. Foglia et al. (2013) proposed non-dimensional groups for the analysis of pore pressure development around a bucket foundation model. The same test set-up was used as in the present campaign, but the bucket foundation models were loaded laterally.

In the proposed method all the relevant parameters are reduced to combinations of force [F], length [L] and time [T]. Thus, suction pressure s [FL⁻²] depends on the unit weight of pore fluid γ_w [FL⁻³], drainage length L [L], soil hydraulic conductivity k [LT⁻¹] and displacement rate v [LT⁻¹] as follows:

$$s = f(\gamma_w, L, k, v). \quad (\text{F.4})$$

The drainage length is presumed to be directly proportional to bucket foundation skirt d and diameter D . Consequently, the non-dimensional group is as follows:

$$\frac{s}{\gamma_w D} = g\left(\frac{vd}{kD}\right), \quad (\text{F.5})$$

Eq. F.5 contains one unknown function g which can be foundation from the laboratory experiments. If the non-dimensional groups are expressed correctly, the non-dimensional pore water behaviour should resemble the prototype behaviour. The analysis can be validated comparing the non-dimensional patterns of experiments performed with different soil and

geometry parameters, various model scales and other types of modelling, such as finite element modelling.

Foglia et al. (2013) conducted small-scale experiments with two bucket foundation models that differed in skirt lengths. The non-dimensional pore water behaviour had a good match. In this model analysis only one bucket foundation is used and it is subjected to tensile loading, however, it is expected that the method holds.

F.3 Results

The following sections are intended for the presentation of the testing results. Load, displacement, stiffness and pore pressure responses are considered in this part. It should be noted that the self-weight of the bucket model and displacements were zeroed, thus, the diagrams with the results show the pure response of the tensile loading.

F.3.1 Load vs. displacement

Figure F.7 shows loading response when tension was applied with six different displacement rates from 1 mm/s to 152 mm/s. Table F.1 shows two tests with displacement rates below 1 mm/s that resulted in very small tensile capacity. F_T increased together with increasing v . The peak tensile capacity was 9.4 times higher in the tests with $v=152$ mm/s compared to $v=1$ mm/s.

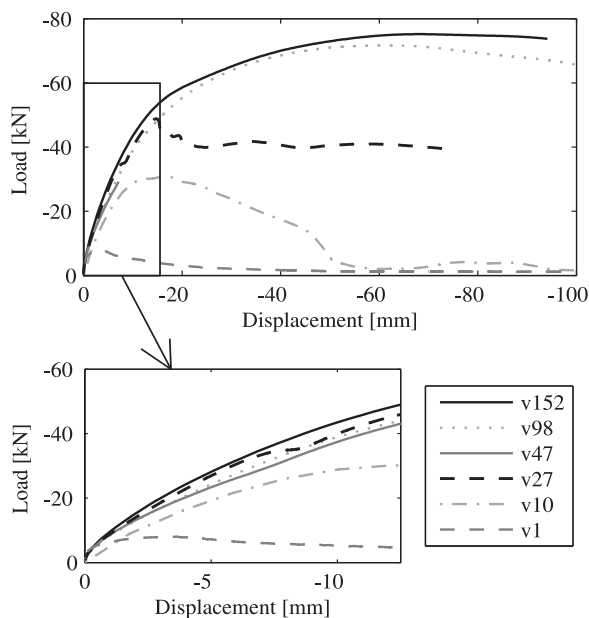


Figure F.7 Load vs. displacement response for tests v1, v10, v27, v47, v98 and v152.

The higher the peak tensile resistance F_T , the higher the displacement w_T was developed. It was noticed that test v152 developed peak load at -68.2 mm ($0.136D$) while test v1 developed peak load at -0.7 mm ($0.0014D$). Upward displacement in test v152 clearly indicates problems

with serviceability limit state. However, assuming that a bucket foundation in a design case can have the maximum upward displacement of only $0.05D$, the tensile resistance is still considerably higher for the faster pull-out tests than for the slower pull-out tests. Thus, the tensile capacity can be up to 7.8 times higher, see Figure F.7. In other words, the pore pressure response should be considered when designing the upwind foundation since it can have significantly higher tensile capacity compared to the drained tensile capacity.

F.3.2 Stiffness

Figure F.8 shows the definition of the initial stiffness k_i and the peak stiffness k_{peak} that were calculated for each of the performed tests. The stiffness defines how the tensile load developed compared to the displacement. The highest measured k_{peak} was 7.13 MN/m in the test v0.1, while the lowest measured k_{peak} was 1.01 MN/m in test v152. Figure F.9 shows that some scatter was noticed in k_{peak} for displacement rates 0-27 mm/s. However, in this range, peak stiffness had higher values compared to the faster pull-out rate tests. The testing data showed that the peak load was reached at higher upward displacements for the higher pull-out rates. Thus, the decrease of stiffness was expected. As seen in Figure F.9, the fitted expression $k_{peak} = 3.11198v^{0.221}$ gives a satisfactory resemblance of the measurements.

The initial stiffness k_i was rather scattered for all the tests and no clear dependency on the pull-out velocity was noticed. Mean value of k_i was 8.23 MN/m with the uppermost value of 20.85 MN/m and the lowermost value of 1.00 MN/m discharged. As seen, the mean initial stiffness was higher than any of the peak stiffness values and did not depend on the displacement rate.

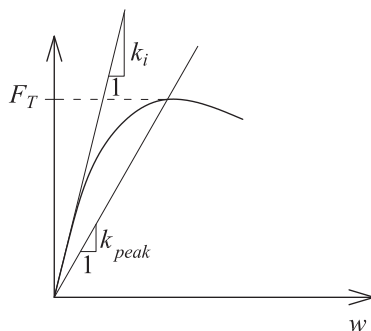


Figure F.8 Peak stiffness k_{peak} and initial stiffness k_i definition in the load-displacement graph.

F.3.3 Poor pressure development

The following comments and illustrations refer to the suction pressure s (see Eq. F.2). In all of the performed tests, the inner pore pressures (transducers PP7-PP11, see Figure F.2) were lower compared to the outer pore pressures (PP1-PP6); Figure F.10 shows an example of such response in test v10. Figure F.11 shows the peak pore pressures during four different tests. In test v98 the inner transducers measured peak pressure of about -272 kPa. The displacement rate was increased to 152 mm/s in test v152, but the pressure development was not more significant. The lowest pore pressures generated had peak pressure of about -288 kPa.

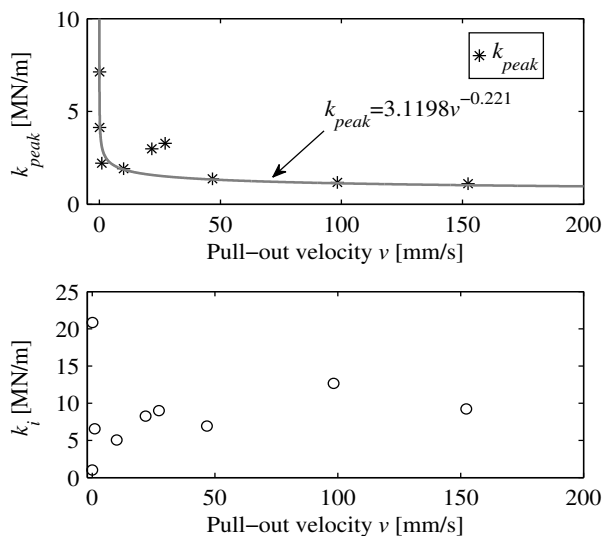


Figure F.9 Peak and initial stiffness vs. pull-out velocity.

Higher than 152 mm/s pull-out velocity attempts were unsuccessful, because the velocity could not be kept constant during several seconds due to the limitations of the actuator. However, it was assumed that the measured peak pressure in test v152 reached cavitation. Ideally, the cavitation should be reached at $s = -300$ kPa, but deviations from this value can be influenced by imperfect saturation of the narrow water-filled pipes, air bubbles in the sand and measurement accuracy of the pressure transducers. Lower cavitation level was earlier noticed in triaxial cell tests (Ibsen, 1995) and centrifuge tests (Senders, 2008).

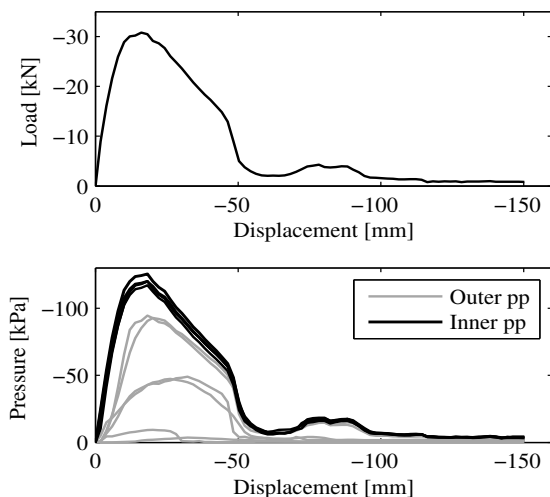


Figure F.10 Load and pore pressure vs. displacement in test v10.

Moreover, as the inner transducers in test v152 showed almost identical measurement, it should be understood that the response was fully undrained since no inner water flow was present.

Figure F.12 shows the peak suction pressure results expressed in the non-dimensional groups. Pore pressure measurements from the skirt tip and under the bucket lid are shown in the figure. The pore pressures drop with the increasing pull-out rate following a non-linear path. Suction on the skirt tip is slightly higher than the suction developed right under the lid. However, when the pull-out rate is fast enough to cause cavitation, the developed suction becomes very similar in all the transducers indicating the undrained behaviour.

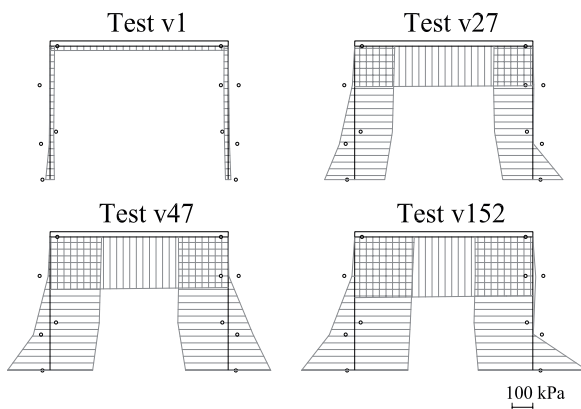


Figure F.11 Peak suction distribution along the bucket model in tests v1, v27, v47 and v152.

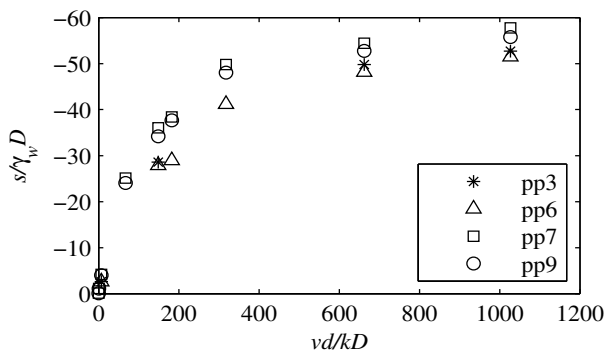


Figure F.12 Non-dimensional group results for pore pressure transducers pp3, pp6, pp7 and pp9.

F.3.4 General remarks

Figure F.13 and Table F.1 prove that very small tensile resistance and no significant suction pore pressure development were measured during the test with the lowest displacement rate (v0.01). The tensile loading resulted in completely drained response, the bucket skirt was

rather smooth, and thus, this behaviour was expected. However, oscillations in load and pore pressure responses are seen in Figure F.13. This is due to the noise of the system and vibrations in the loading equipment. During the testing, it was noticed that the loading equipment experienced some sort of vibrations when very low displacement rates were applied (as seen in Figure F.13). Unfortunately, it was impossible to tune these vibrations. However, the tuning of higher displacement rates was much easier as seen in the response in Figure F.7. Furthermore, Figure F.13 shows slightly drifting pore pressure measurements in the range of [0.5; -1.7] kPa. Such drift and measuring error was noticed during calibration of the pore pressure transducers and, in this case, should be treated as zero pore pressure measurement.

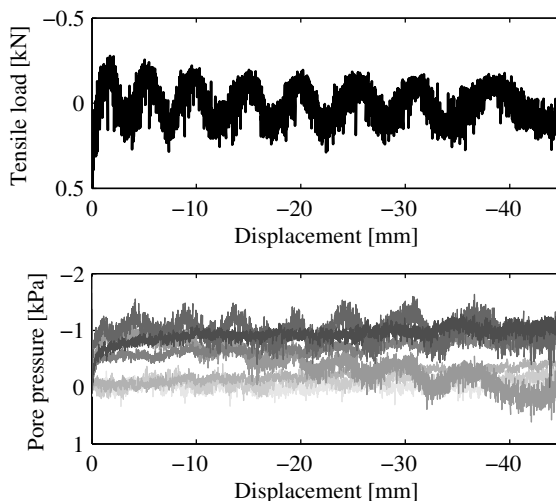


Figure F.13 Slow pull-out test v0.01. Total load and pore pressure vs. displacement.

Before model installation

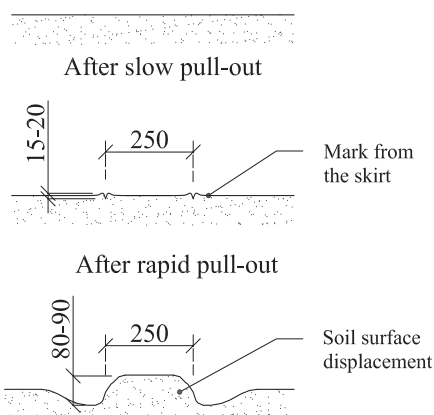


Figure F.14 Approximate surface elevations after slow (v0.05) and rapid (v152) pull-out tests.

The submerged weight of the soil volume inside the bucket was 0.45 kN, corresponding to the soil unit weight ($\gamma' = 9.6 \text{ kN/m}^3$) multiplied by the inner volume of the bucket model. The soil surface was visually inspected after every extraction of the foundation model. It was noted that during slow pull-out tests (v0.01-v0.1), the soil surface was rather flat and only marks of the skirt were visible. However, after the fast pull-outs (v98, v152), the soil under the bucket formed an 80-90 mm hill and was completely disturbed indicating that the soil volume was actually lifted up. Figure F.14 shows the changes of the soil surfaces after the tests.

F.4 Back-Calculation

Figure F.15 shows total measured tensile load and suction load (pressure under the lid times the inner lid area) for four tests. The difference between the F_T and peak suction load F_s increases together with increasing v . In some cases, such as tests v27 and v47, it was noticed that the F_s was larger than F_T which is physically impossible. In both tests, this response is visible after -100 mm of the upward displacement. One of the reasons for it could be some sudden loss of saturation in the water filled pipes connecting the pore pressure transducers (Figure F.2). That could result in unexpected and wrong pore pressure measurements. Clearly, data where $F_s > F_T$ should be discharged from analysis.

The suction force under the lid gives a significant contribution to the total tensile resistance as shown in Figure F.15. Two analytical methods were considered for the back-calculation of the test results. Both of them include the contribution of pore suction to the tensile capacity.

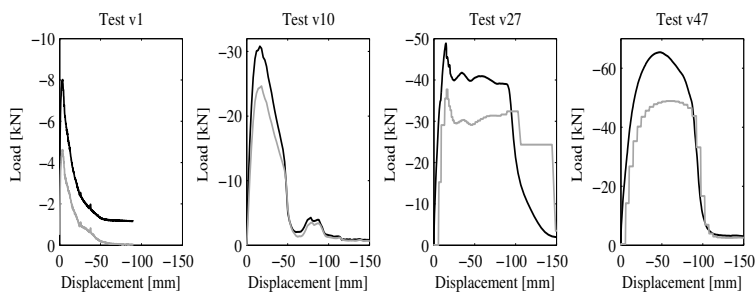


Figure F.15 Load vs displacement: Total measured tensile load (black line) and suction load (grey line).

The first method by Iskander et al. (2002) requires the knowledge about the pore suction. Thus, the measured pore suction was used for the prediction. In the second method by Houlsby et al. (2005), firstly the suction under the bucket lid is predicted and then the tensile capacity is estimated.

F.4.1 Method by Iskander et al. (2002)

Table F.2 gives an overview of the load response in the tests where clear soil disturbance and elevation were noticed after the foundation model was pulled out (see also Figure F.14). It was assumed that the soil plug was lifted up and contributed to the total tensile capacity, which was expressed in Eq. F.6 by Iskander et al. (2002):

$$F_T = F_s + W_b + W_{plug} + F_{f,o}, \quad (\text{F.6})$$

where F_T is the total tensile capacity, F_S is the suction force (pore pressure times the internal area of the lid), W_b is the self-weight (in these tests zeroed before testing, 0 kN), W_{plug} is the soil plug weight (estimated earlier, 0.45 kN) and $F_{f,o}$ is the outer friction.

From the test results, $F_{f,o, test}$ was determined for the peak values by:

$$F_{f,o, test} = F_T - F_S - W_b - W_{plug}. \quad (F.7)$$

$F_{f,o, test}$ in Table F.2 increases together with the increasing displacement rate (and suction pressure). Iskander et al. (1993 and 2002) explained this by an increase in side shear due to the downward vertical gradient i acting outside the skirt:

$$F_{f,o, eq. 8} = -\frac{d}{2}(\gamma' + i\gamma_w)K \tan(\delta)A_o, \quad (F.8)$$

where K is the coefficient of lateral earth pressure, δ interface friction angle, γ_w water unit weight, d skirt length penetrated to the soil (equal to d_{inst}), A_o outer area of the skirt. For this and the following calculations $K \tan \delta = 0.5$ was taken as typical value according to Byrne and Houlsby (2002).

As the pore pressures were actually measured in this testing program, it was possible to evaluate the hydraulic gradient and estimate $F_{f,o, Eq. F.8}$ using Eq. F.8 (Table F.2). Peak load and peak pore pressure under the bucket model lid were used in Table F.2.

Table F.2 Load overview for tests, where the soil plug was displaced.

Test No.	v , [mm/s]	F_T , [kN]	F_S , [kN]	$F_{f,o, test}$, [kN]	i	$F_{f,o, Eq. F.8}$, [kN]
v10	10	-30.79	-24.64	-5.70	-9.6	-2.39
v22	22	-44.07	-35.37	-8.25	-14.4	-3.46
v27	27	-48.84	-37.71	-10.68	-14.7	-3.54
v47	47	-65.36	-48.87	-16.04	-20.8	-4.93
v98	98	-71.65	-53.45	-17.75	-24.7	-5.81
v152	152	-75.17	-56.71	-18.01	-26.3	-6.16

where F_S – suction force, $F_{f,o, test}$ – measured outer friction, $F_{f,o, Eq. F.8}$ – estimated according to Eq. F.8 outer friction.

F.4.2 Method by Houlsby et al. (2005)

Houlsby et al. (2005) proposed an analytical method for calculation of the tensile capacity of a bucket foundation under the presence of suction:

$$F_T = -sA \left(1 + \frac{4Z_o^2}{Dd} y_o \left(\frac{d}{Z} \right) K \tan \delta \right), \quad (F.9)$$

$$Z_o = \frac{D(m^2 - 1)}{4(K \tan \delta)_o},$$

$$y_o(x) = (\exp(-x) - 1 + x),$$

$$m = 1.5.$$

Four different loading conditions were analysed: slow rate tensile load, liquefaction without cavitation, cavitation without liquefaction and cavitation with liquefaction. It was noted that friction contributes to reducing the vertical stress further down the foundation skirt. An expression for estimation of suction s was proposed as:

$$s = -\frac{\pi}{4F} \frac{D\gamma_w}{k_o} \frac{dh}{dt}, \quad (\text{F.10})$$

where s – suction pressure, F – dimensionless flow factor, γ_w – water unit weight, k_o – hydraulic conductivity, dh/dt – displacement rate.

Eq. F.10 requires knowledge about the hydraulic conductivity k_o , which changes depending on flow conditions in the soil. Back-calculating the measured suction pressure with the initial $k=7.4\cdot 10^{-5}$ m/s, leads to a significant overestimation of suction for tests with $v>10$ mm/s (Figure F.16). Thus, for the tensile load prediction, the measured suction was used and k_o was back-calculated using Eq. F.10 as shown in Figure F.17.

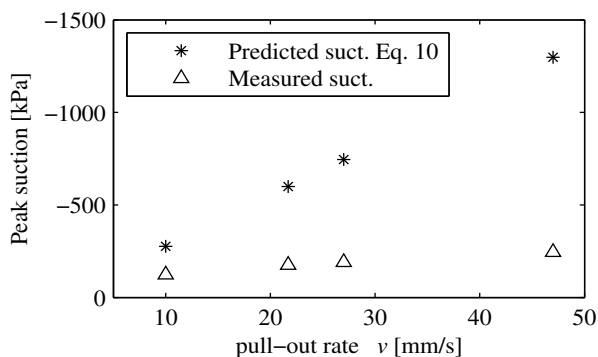


Figure F.16 Back-calculated peak suction s using Eq. F.10 and measured peak suction.

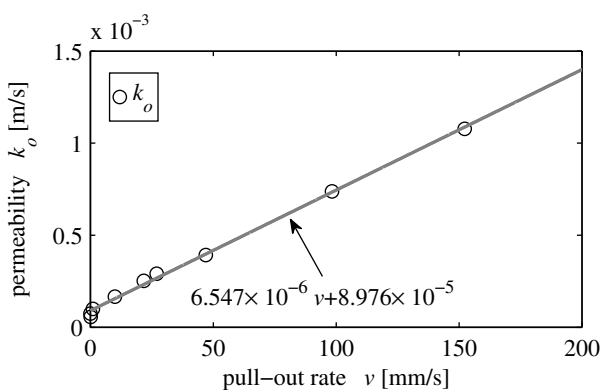


Figure F.17 Back-calculated permeability k_o using Eq. F.10.

F.4.3 Comparison

Tensile capacity was estimated using two mentioned methods: Iskander et al. (2002) (Eq. F.8 introduced to Eq. F.6) and Houlsby et al. (2005) (Eq. F.9). Figure F.18 shows the measured peak resistances and predicted tensile resistances taking into consideration the upward displacements w_T . Obviously, the suction under the lid F_s makes the largest part of the measured as well as the predicted loads. Thus, Figure F.19 shows the outer interface strength and the plug weight part ($F_T - F_s$) for the methods.

Comparing the measured and predicted tensile response, Houlsby et al. (2005) method gives a very good agreement if the suction under the lid is known. The pore suction according to Eq. F.10 was highly overestimated for $v > 10$ mm/s compared to the present testing data. Therefore, it was back-calculated according to the measured suction. It should be noticed that Houlsby et al. (2005) had to use somewhat higher hydraulic conductivity than was measured in their testing program to get a fair match.

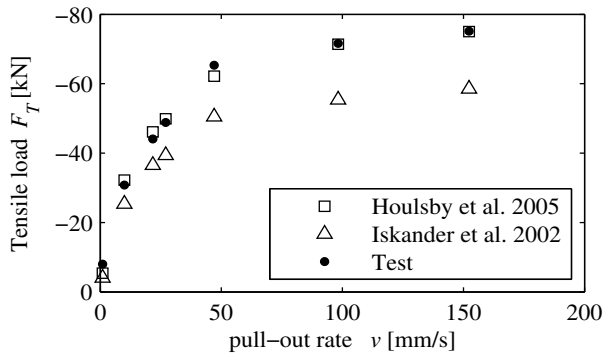


Figure F.18 Predicted and measured tensile resistance with the different pull-out rates.

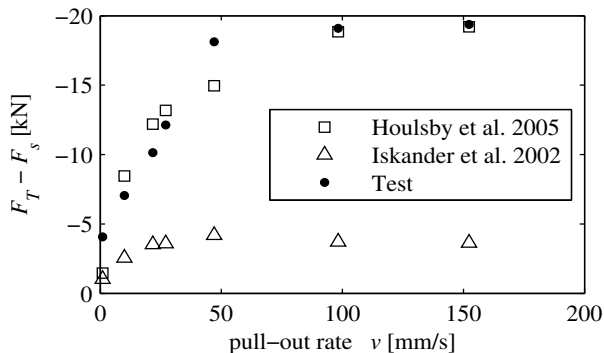


Figure F.19 Predicted and measured contribution to the tensile loading $F_T - F_s$ with the different pull-out rates.

F.5 Conclusion

Traditionally, the tensile capacity of a bucket foundation in sand is designed taking very conservative assumptions. This study drew attention to the pore pressure distribution around the bucket foundation skirt when it is subjected to tensile loading. The response was tested under axial tensile loads applied at various displacement rates. The paper presented results from 1g model tests performed in a pressure tank. One bucket foundation model was used in this testing campaign. To the knowledge of the authors, the foundation model was at least twice larger than previously tested laboratory models. Load, displacement and pore pressures visualized the tensile behaviour of the bucket foundation model. Pore pressures were measured all around the bucket skirt providing valuable information about the flow in the soil due to the tensile loading. Moreover, ten different pull-out rates were applied (displacement controlled). This gave a good overview of the tensile behaviour starting with the drained tensile capacity and ending with the undrained tensile capacity in sand. Finally, the results were compared to the analytical methods proposed by Iskander et al. (2002) and Houlsby et al. (2005). After the testing program, it was clarified that pore pressures contribute highly to the tensile capacity. Bucket foundation design in storm case should allow accounting for partial drainage in sand. Overall, the outcome of the performed tests was as follows:

- Tensile capacity increased parallel to the increasing displacement rates. The increased capacity was reached at higher displacements of the foundation model, indicating serviceability problems when utilizing the full capacity. However, even if only using part of the capacity, the real tensile capacity was much higher including the effect of the pore pressure than estimating only the drained capacity. Thus, based on the performed tests, the pore pressure response should be considered when designing the upwind foundation since it can have much higher tensile capacity compared to the drained capacity. Though, knowledge about the soil permeability (which changes according to loading conditions) is essential for the correct tensile resistance estimations.
- Peak loading stiffness was high in slow monotonic pull-out tests, but it dropped significantly when the displacement rate increased. On the other hand, initial loading stiffness did not show any clear dependency on the displacement rate and was generally higher than the peak loading stiffness.
- The inner transducers in test v152 (152 mm/s) showed almost identical measurement. The response was fully undrained since no inner water flow was present. The rapid pull-out load generated cavitation.
- Non-dimensional groups were suggested for the analysis of the pore pressure behaviour that can be used for further comparisons with other model tests or finite element models.
- Iskander et al. (2002) and Houlsby et al. (2005) analytical methods were compared to the testing data. The second method gave a very good agreement with the measured response, but the knowledge about the soil permeability (or possible suction) was essential.

In nature, soil conditions are very variable: soil is often layered and have variable permeability. It would be favourable to have a numerical model that is capable of calculating tensile capacity under various soil drainage conditions. The data provided in this paper supplies valuable information for the calibration of numerical models.

Bibliography

- Achmus, M, and Thieken, K (2014). "Numerical Simulation of the Tensile Resistance of Suction Buckets in Sand," *J of Ocean and Wind Energy*, 1 (4), 231–239.
- Bye, A, Erbrich, C, Rognlien, B, and Tjelta, TI (1995). "Geotechnical Design of Bucket Foundations," *Proc of the 27th Offshore Technology Conference*, OTC, 869-883.
- Byrne, BW, and Houlsby, GT (2002). "Experimental Investigations of Response of Suction Caissons to Transient Vertical Loading," *J of Geotechnical and Environmental Eng*, ASCE, 128(11), 926-939.
- Byrne, BW, and Houlsby, GT (2006). "Assessing Novel Foundation Options for Offshore Wind Turbines," *Proc of World Maritime Technology Conf*, London.
- Cao, J, Phillips, R, Popescu, R, Audibert, JME, and Al-Khafaji, Z (2002). "Numerical Analysis of the Behavior of Suction Caissons in Clay," *Proc 12th Int Offshore and Polar Engineering Conf*, Kitakyushu, Japan. ISOPE, 795-799.
- Feld, T, Leth, CT, Mikkelsen, H, and Steinfeld, JS (2000). "Nyt Laboratorieudstyr til Simulering af Dynamisk Påvirkede Sugebøttefundamenter," *Proc of NGM-2000: XIII Nordiska Geoteknikermötet*, Helsinki, 77-84.
- Feld, T (2001). "Suction Buckets: a New Innovative Foundation Concept, Applied to Offshore Wind Turbines," Ph.D. Thesis, AAU Geotechnical Engineering Papers R0108, Aalborg University, Aalborg, Denmark.
- Foglia, A, Ibsen, LB, Nielsen, SK, and Mikalauskas, L (2013). "A Preliminary Study on Bucket Foundations under Transient Lateral Loading," *Proc 23rd Int Offshore and Polar Engineering Conf*, Anchorage, USA. ISOPE.
- Hansteen, OE, Jostad, HP, and Tjelta, TI (2003). "Observed Platform Response to a "Monster Wave"," *Field Measurements in Geomechanics*, Oslo, Norway, 15–18.
- Hedegaard, J, and Borup, M (1993). "Klassifikationsforsøg med Baskarp Sand No. 15," Aalborg University Center, Aalborg.
- Houlsby, GT, Kelly, RB, and Byrne, BW (2005). "The Tensile Capacity of Suction Caissons in Sand under Rapid Loading," *Proc Int Symp Front Offshore Geotech (ISFOG)*, Perth, Australia, 405–410.
- Houlsby, GT, Kelly RB, Huxtable, J, and Byrne, BW (2006). "Field Trials of Suction Caissons in Sand for Offshore," *Géotechnique*, 56(1), 3-10.
- Ibsen, LB, and Bødker, L (1994). "Baskarp Sand No. 15: Data Report 9301," Geotechnical Engineering Group, Aalborg University, Aalborg.
- Ibsen, LB (1995). "The Static and Dynamic Strength of Sand," *Proc of the 11th European Conf on Soil Mechanics and Foundation Engineering*, Copenhagen.
- Iskander, MG, Olsen, RE, and Pavlicek, RW (1993). "Behavior of Suction Piles in Sand," *Design and Performance of Deep Foundations, Piles and Piers in Soil and Soft Rock*. ASCE, GSP No 38, 157–171.
- Iskander, MG, El-Gharbawy, S, and Olson, R (2002). "Performance of Suction Caissons in Sand and Clay," *Canadian Geotechnical Journal*, 39, 576-584.
- Kelly, RB, Byrne, BW, Houlsby, GT, and Martin, CM (2003). "Pressure Chamber Testing of Model Caisson Foundations in Sand," *Proc of the Int Conf on Foundations*, Dundee, 421-431.
- Kelly, RB, Byrne, BW, Houlsby, GT, and Martin, CM (2004). "Tensile Loading of Model Caisson Foundations for Structures on Sand," *Proc 14th Int Offshore and Polar Engineering Conf*. Toulon. ISOPE.
- Kelly RB, Houlsby, GT, and Byrne, BW (2006). "Transient Vertical Loading of Model Suction Caissons in a Pressure Chamber," *Géotechnique*, 56(10), 665-675.

- Larsen, KA (2008). "Static Behaviour of Bucket Foundations: Thesis submitted for the degree of Doctor of Philosophy," Department of Civil Engineering, Aalborg University, Aalborg. DCE Thesis, 1 (7).
- Senders, M (2009). "Suction Caissons in Sand as Tripod Foundations for Offshore Wind Turbines," PhD Thesis, University of Western Australia.
- Sørensen, SPH, and Ibsen, LB (2012). "Experimental Comparison of Non-Slender Piles under Static Loading and under Cyclic Loading in Sand," *Proc 22nd Int Ocean and Polar Engineering Conf*, Rhodes, Greece. ISOPE
- Tang, T, Hededal, O, and Cardiff, P (2015). "On Finite Volume Method Implementation of Poro-Elasto-Plasticity Soil Model," *Int J for Numerical and Analytical Methods in Geomechanics*, Wiley Online Library (wileyonlinelibrary.com). DOI: 10.1002/nag.2361
- Vaitkunaite, E, Ibsen, LB., and Nielsen, BN (2014). "New Medium-Scale Laboratory Testing of Bucket Foundation Capacity in Sand," *Proc 24th Int Ocean and Polar Engineering Conf*, Busan, South Korea. ISOPE, 2, 514-520.
- Vaitkunaite, E (2015). "Bucket Foundations under Axial Loading – Test Data Series 13.02.XX, 13.03.XX and 14.02.XX," Department of Civil Engineering, Aalborg University, Aalborg. DCE Technical Report No. 199. ISSN 1901-726X.
- Sjelmo A (2012). "Soil-structure Interaction in Cohesionless Soils due to Monotonic Loading," M.Sc. Thesis, Aalborg University.
- Tjelta, TI (2015). "The Suction Foundation Technology," *Proc Int Symp Front Offshore Geotech (ISFOG)*, Oslo, Norway, 85–93.
- Thieken, K, Achmus, M, and Schröder, C (2014). "On the Behavior of Suction Buckets in Sand under Tensile Loads," *Comput Geotech*, 60, 88–100.

APPENDIX G

Bucket Foundations under Axial Loading – Test Data Series 13.02.XX, 13.03.XX and 14.02.XX

Vaitkunaite, E. (2015). *Bucket Foundations under Axial Loading: Test Data Series 13.02.XX, 13.03.XX and 14.02.XX*. Aalborg: Department of Civil Engineering, Aalborg University. (DCE Technical Reports; No. 199).

The layout has been revised.

Contents

G	Bucket Foundations under Axial Loading – Test Data Series 13.02.XX, 13.03.XX and 14.02.XX	185
G.1	List of Symbols	189
G.2	Test Series 14.02.XX Overview	190
G.2.1	Test 14.02.01	193
G.2.2	Test 14.02.02	196
G.2.3	Test 14.02.03	198
G.2.4	Test 14.02.04	200
G.2.5	Test 14.02.05	202
G.2.6	Test 14.02.06	204
G.2.7	Test 14.02.07	206
G.2.8	Test 14.02.08	208
G.2.9	Test 14.02.09	210
G.2.10	Test 14.02.10	212
G.2.11	Test 14.02.11	214
G.2.12	Test 14.02.12	216
G.2.13	Test 14.02.13	219
G.2.14	Test 14.02.14	221
G.2.15	Test 14.02.15	223
G.3	Test Series 13.02.XX Overview	226
G.3.1	Test 13.02.01	229
G.3.2	Test 13.02.02	231
G.3.3	Test 13.02.03	233
G.3.4	Test 13.02.04	235
G.3.5	Test 13.02.05	237
G.3.6	Test 13.02.06	239
G.3.7	Test 13.02.07	241
G.3.8	Test 13.02.08	243
G.3.9	Test 13.02.09	245
G.3.10	Test 13.02.10	247
G.3.11	Test 13.02.11	249
G.3.12	Test 13.02.12	251

G.3.13	Test 13.02.13	253
G.3.14	Test 13.02.14	255
G.3.15	Test 13.02.15	257
G.3.16	Test 13.02.16	259
G.3.17	Test 13.02.17	261
G.4	Test Series 13.03.XX Overview	263
G.4.1	Test 13.03.01	264
G.4.2	Test 13.03.02	267
G.4.3	Test 13.03.03	270
G.4.4	Test 13.03.05	273
G.4.5	Test 13.03.06	275
G.4.6	Test 13.03.08	277
G.4.7	Test 13.03.09	280
G.4.8	Test 13.03.10	282
G.4.9	Test 13.03.11	285
G.4.10	Test 13.03.12	287
G.4.11	Test 13.03.13	290
G.4.12	Test 13.03.14	292
G.4.13	Test 13.03.15	294
G.4.14	Test 13.03.16	296
G.4.15	Test 13.03.17	298
G.4.16	Test 13.03.19	300
G.4.17	Test 13.03.20	303
G.4.18	Test 13.03.21	306
References		309

G.1 List of Symbols

Greek Symbols

γ	Total soil unit weight
γ'	Effective soil unit weight
σ	Standard deviation

Latin Symbols

D	Bucket model diameter
D_R	Relative soil density
F	Load
F_{cyc}	Cyclic load amplitude
F_{mean}	Mean cyclic load
F_P	Preload during installation
F_{Pc}	Peak post-cyclic tensile load
F_T	Peak tensile load
N	Cycle number
PP	Pore pressure transducer
d	Skirt length
d_{inst}	Installed skirt length
f_s	Data sampling frequency
f	Loading frequency
p_m	Membrane pressure
p_t	Tank pressure
v	Tensile load velocity (Pull-out rate)
t	Skirt thickness
w_{cyc}	Displacement during cyclic load
w_T	Displacement at peak tensile load
w_{Pc}	Displacement at peak post-cyclic tensile load

G.2 Test Series 14.02.XX Overview

Series 14.02.XX present tensile loading tests on a bucket foundation model performed with different pull-out rates. This chapter provides the data of tests performed in the pressure tank. Bucket model dimensions were: 0.50 m in diameter D , 0.25 m in skirt length d and 2 mm in skirt thickness t . Figure G.3 shows the positions of the laboratory CPT samplings. Sørensen and Ibsen 2012 have shortly described the test set-up. Hedegaard and Borup 1993, Ibsen and Boedker 1994 have studied the Aalborg University sand No.1. properties.

Table G.1: Test series 14.02.XX summary.

p_t [kPa]	Test No.	Loading			Installation		D_R [%]	γ' [kN/m ³]
		F_T [kN]	w_T [mm]	v [mm/s]	F_P [kN]	d_{inst} [mm]		
163	14.02.01	-3.91	-0.46	0.05	-	-	75	9.1
177	14.02.02	-2.03	-0.81	0.10	36.2	244.2	88	9.7
197	14.02.03	-2.74	-2.66	0.25	33.2	240.0	92	9.9
200	14.02.04	-8.02	-3.61	1	37.6	242.0	88	9.7
201	14.02.05	-30.79	-16.01	10	43.7	241.5	90	9.8
199	14.02.06	-36.94	-22.30	17.80	31.9	242.3	88	9.7
200	14.02.07	-44.07	-14.73	21.70	33.0	236.2	83	9.5
200	14.02.08	-48.84	-14.29	27.20	31.5	239.0	85	9.6
200	14.02.09	-65.36	-48.78	46.71	31.5	236.4	83	9.5
200	14.02.10	-	-	0.05	32.3	246.6	86	9.6
200	14.02.11	-4.08	-0.65	0.10	31.4	240.7	86	9.6
200	14.02.12	-2.67	-0.70	0.05	32.0	239.2	85	9.6
200	14.02.13	-71.65	-60.48	98.30	31.0	239.3	82	9.5
200	14.02.14	-75.17	-68.18	152.30	37.0	236.0	84	9.5
0	14.02.15	(0)	(0)	0.01	31.0	240.5	79	9.3

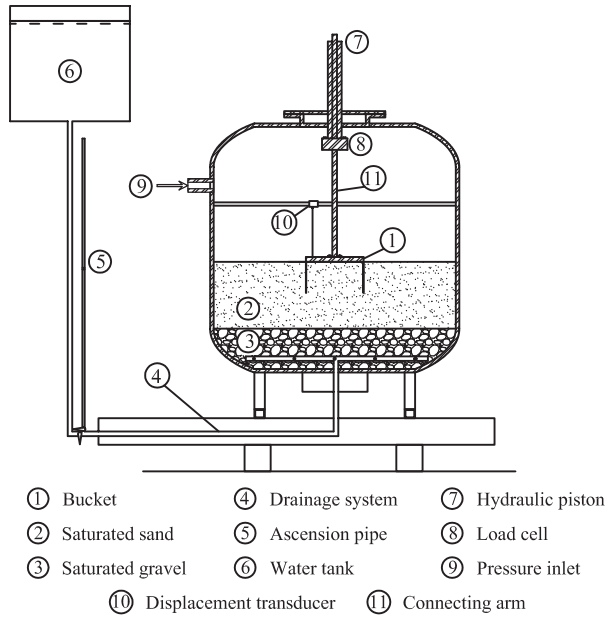


Figure G.1: Test set-up for testing program 14.02.XX.

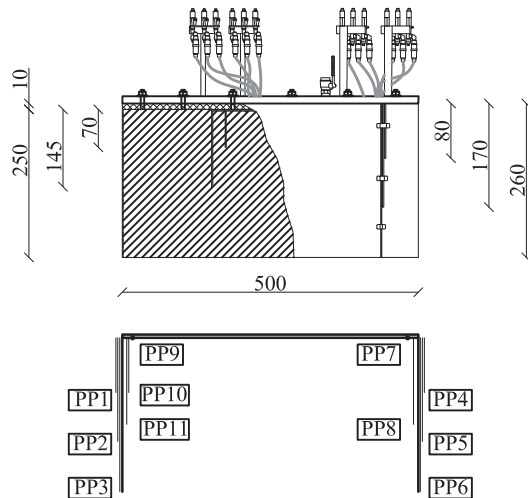


Figure G.2: Bucket foundation model for testing program 14.02.XX.

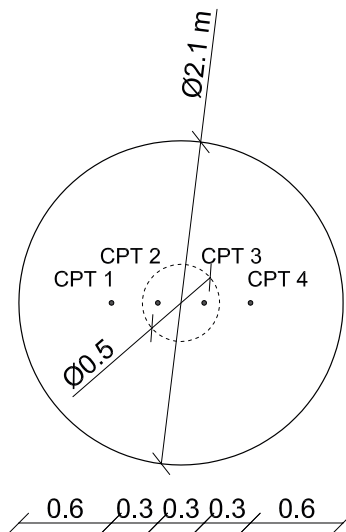


Figure G.3: CPT positions.

G.2.1 Test 14.02.01

Soil properties			Loading			Installation		
D_R	[%]	75.2	f_s	[Hz]	5	F_P	[kN]	-
σ of D_R	[%]	2.6	F_T	[kN]	-3.91	d_{inst}	[mm]	-
γ	[kN/m ³]	19.1	w_T	[mm]	-0.46	Tank pressure		
γ'	[kN/m ³]	9.1	v	[mm/s]	0.05	p_t	[kPa]	163

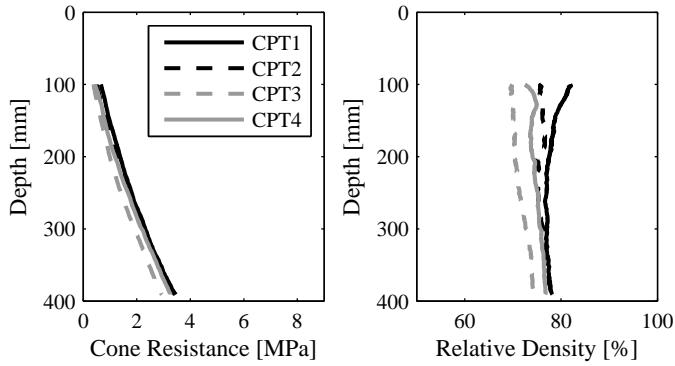


Figure G.4: CPT testing 14.02.01.

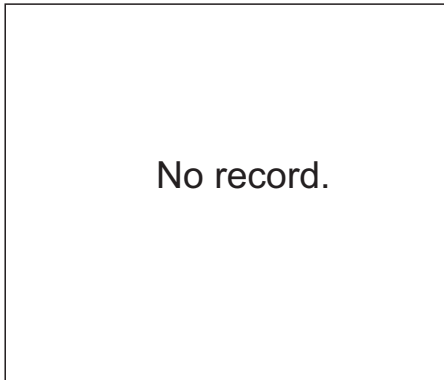


Figure G.5: Installation 14.02.01.

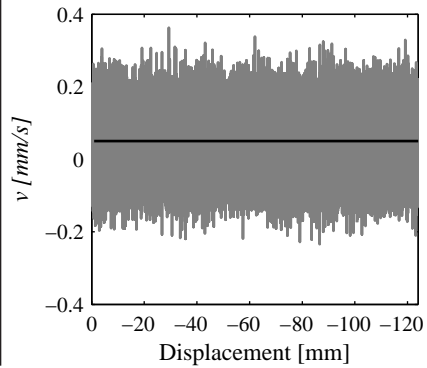


Figure G.6: Pull-out velocity 14.02.01.

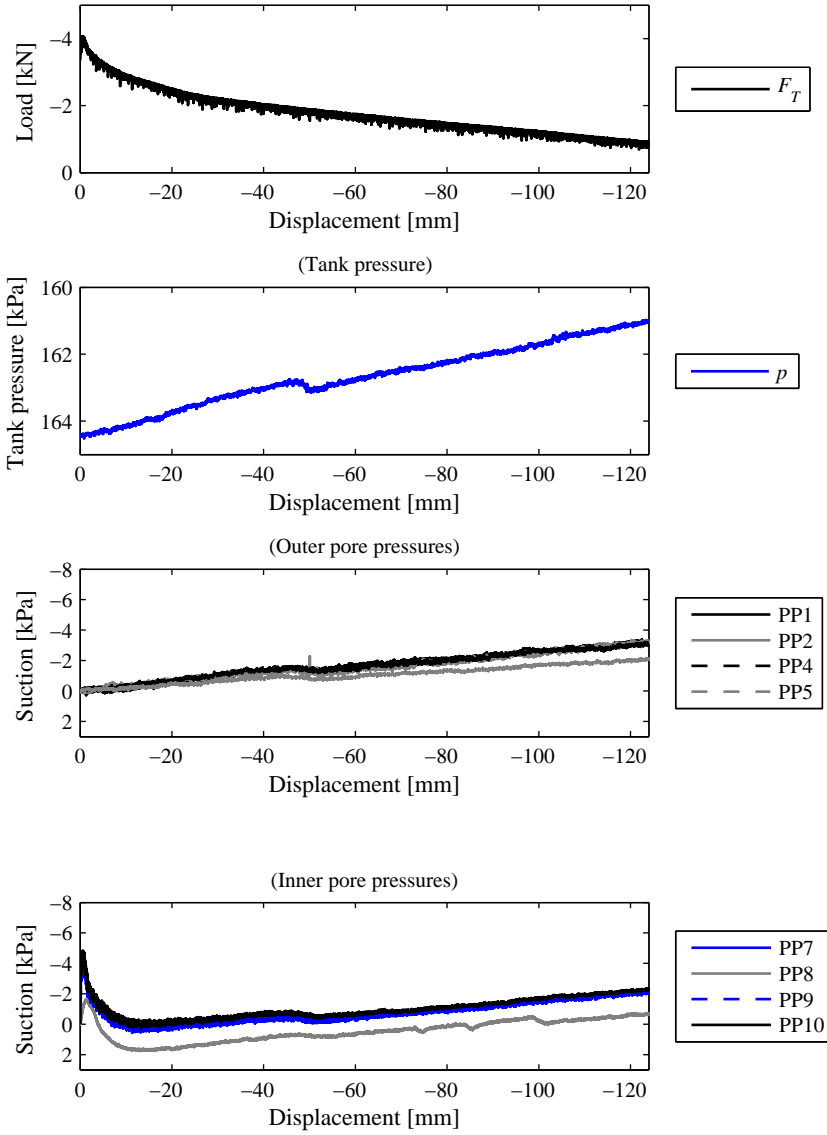


Figure G.7: Loading 14.02.01.

Comments:

The first test with very disturbed sand from previous testing. Load cell was not zeroed before the installation. Tank pressure was unstable due to pressure leakage from the tank. The test is discharged from any analysis. Pressure transducers PP3, PP6, PP11 did not function. Improvements to the test set-up followed: tightening of the pressure tank, tightening and calibrating pressure transducers.

G.2.2 Test 14.02.02

Soil properties			Loading			Installation		
D_R	[%]	87.6	f_s	[Hz]	5	F_P	[kN]	36.2
σ of D_R	[%]	5.7	F_T	[kN]	-2.03	d_{inst}	[mm]	244.2
γ	[kN/m ³]	19.7	w_T	[mm]	-0.81	Tank pressure		
γ'	[kN/m ³]	9.7	v	[mm/s]	0.10	p_t	[kPa]	177

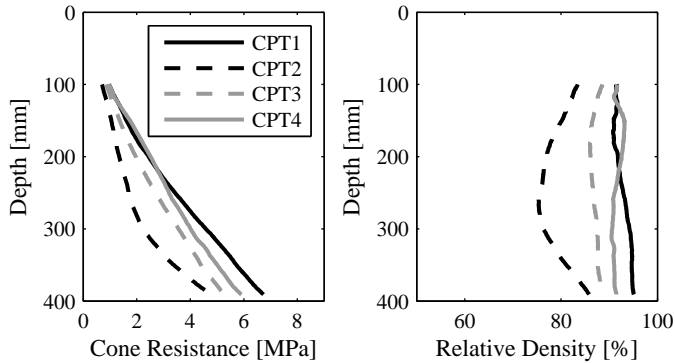


Figure G.8: CPT testing 14.02.02.

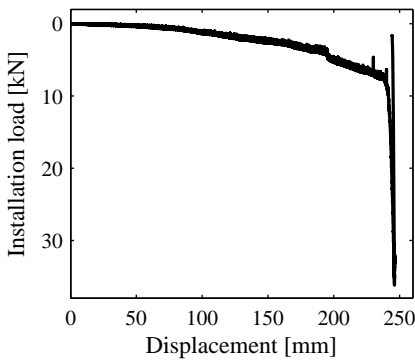


Figure G.9: Installation 14.02.02.

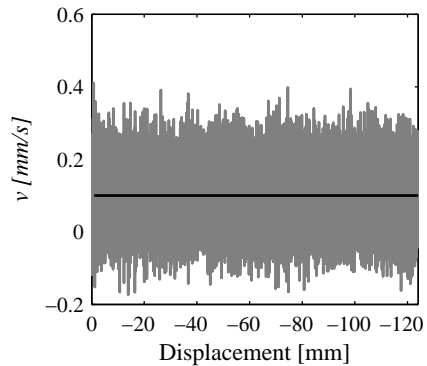


Figure G.10: Pull-out velocity 14.02.02.

Comments:
 Tank pressure did not reach the wanted value (200 kPa). Pressure transducer PP3 did not function.

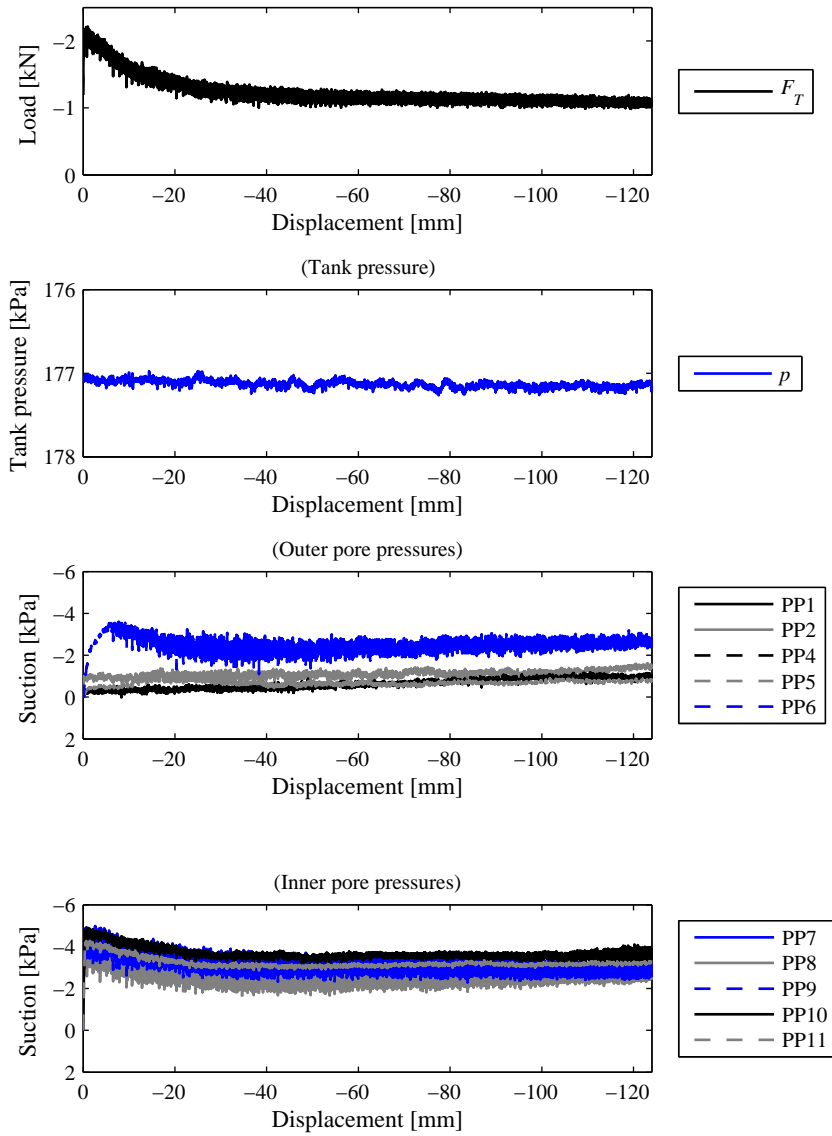


Figure G.11: Loading 14.02.02.

G.2.3 Test 14.02.03

Soil properties			Loading			Installation		
D_R	[%]	91.6	f_s	[Hz]	5	F_P	[kN]	33.2
σ of D_R	[%]	3.1	F_T	[kN]	-2.74	d_{inst}	[mm]	240.0
γ	[kN/m ³]	19.9	w_T	[mm]	-2.66	Tank pressure		
γ'	[kN/m ³]	9.9	v	[mm/s]	0.25	p_t	[kPa]	197

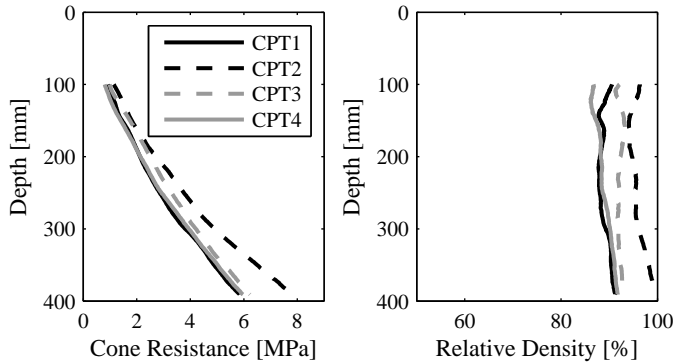


Figure G.12: CPT testing 14.02.03.

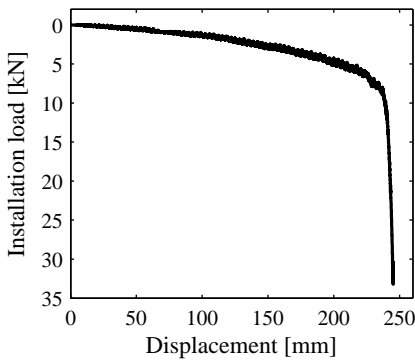


Figure G.13: Installation 14.02.03.

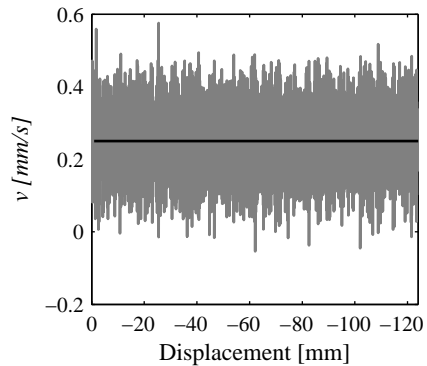


Figure G.14: Pull-out velocity 14.02.03.

Comments:
 Secondary peak in load and pore pressure response probably due to a small sudden deviation in loading velocity (possibly, higher than recorded).

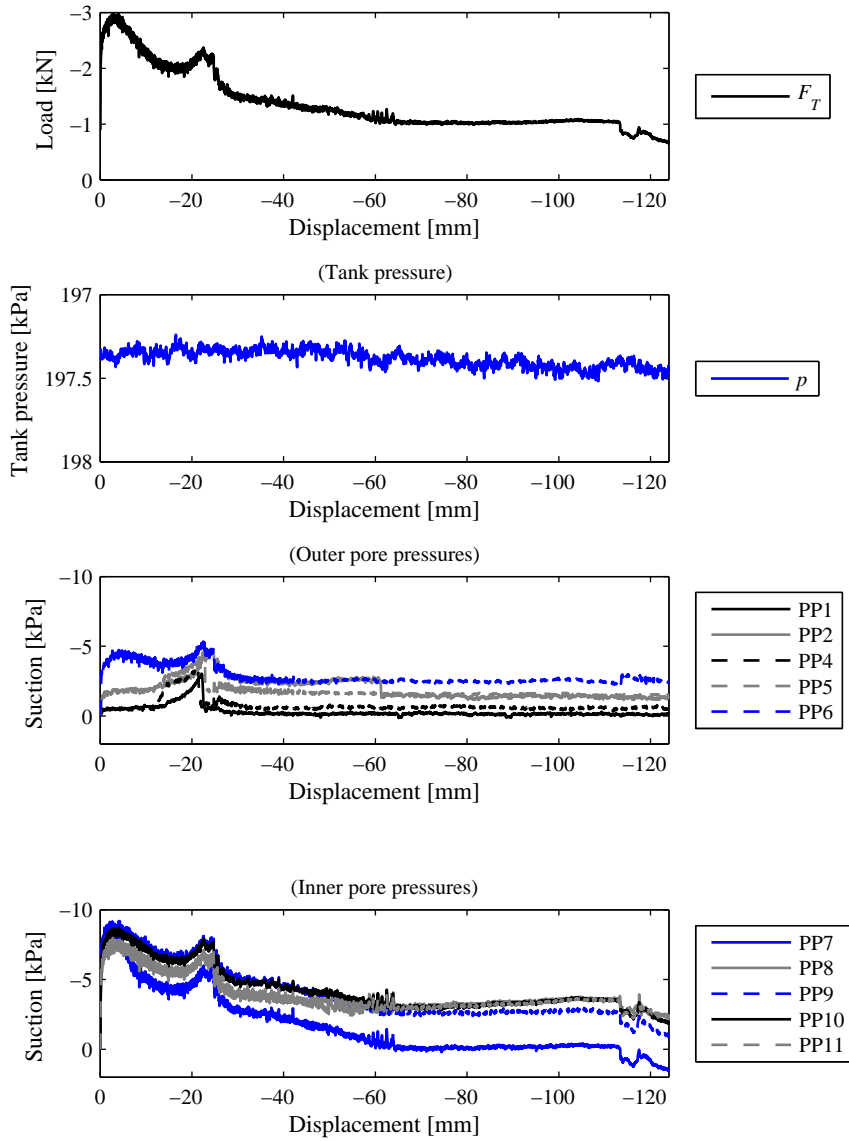


Figure G.15: Loading 14.02.03.

G.2.4 Test 14.02.04

Soil properties			Loading			Installation		
D_R	[%]	88.0	f_s	[Hz]	5	F_P	[kN]	37.6
σ of D_R	[%]	3.3	F_T	[kN]	-8.02	d_{inst}	[mm]	242
γ	[kN/m ³]	19.7	w_T	[mm]	-3.61	Tank pressure		
γ'	[kN/m ³]	9.7	v	[mm/s]	1	p_t	[kPa]	200

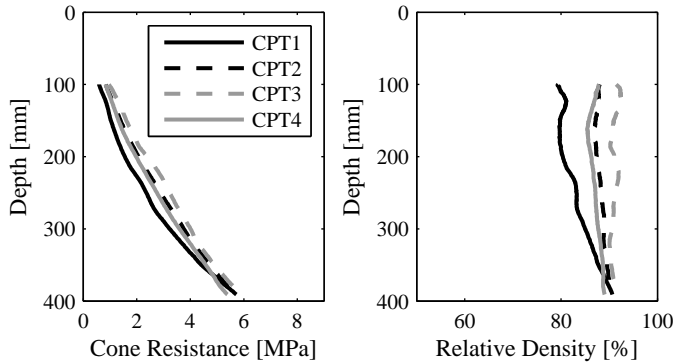


Figure G.16: CPT testing 14.02.04.

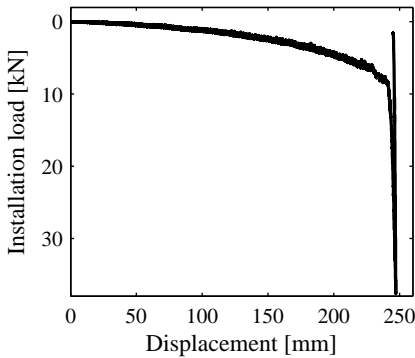


Figure G.17: Installation 14.02.04.

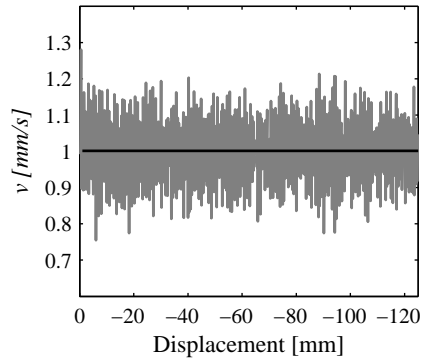


Figure G.18: Pull-out velocity 14.02.04.

Comments:
Pressure transducer PP2 did not function.

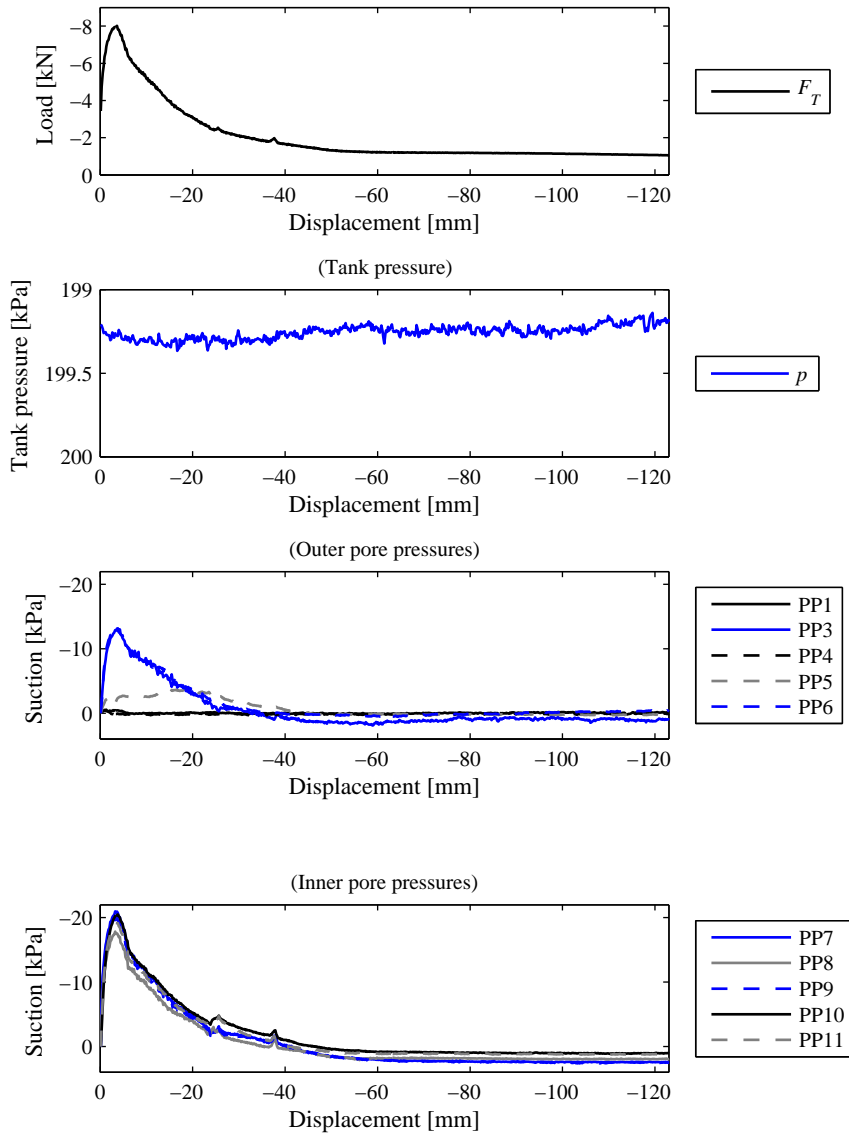


Figure G.19: Loading 14.02.04.

G.2.5 Test 14.02.05

Soil properties			Loading			Installation		
D_R	[%]	90.0	f_s	[Hz]	5	F_P	[kN]	43.7
σ of D_R	[%]	4.9	F_T	[kN]	-30.79	d_{inst}	[mm]	241.5
γ	[kN/m ³]	19.8	w_T	[mm]	-16.01	Tank pressure		
γ'	[kN/m ³]	9.8	v	[mm/s]	10	p_t	[kPa]	200.9

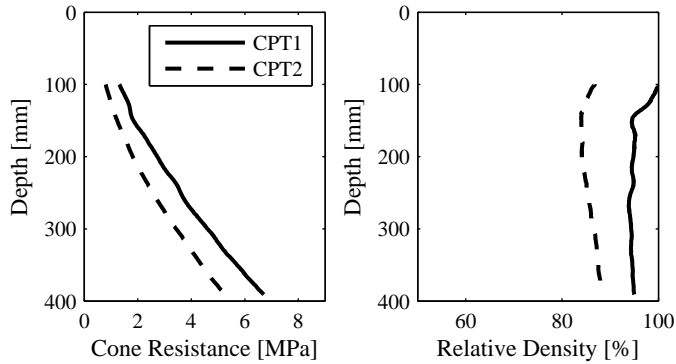


Figure G.20: CPT testing 14.02.05.

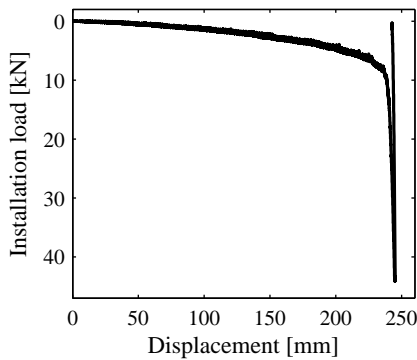


Figure G.21: Installation 14.02.05.

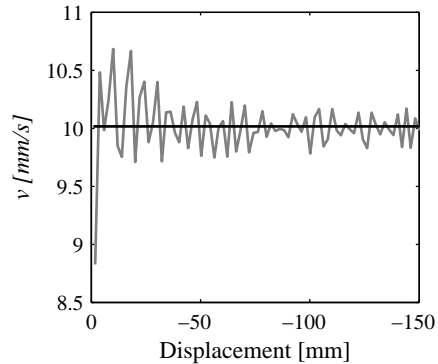


Figure G.22: Pull-out velocity 14.02.05.

Comments:

Pore pressure response is delayed. Peak pore pressure measurement was recorded approximately 0.5 s after the peak load measurement.

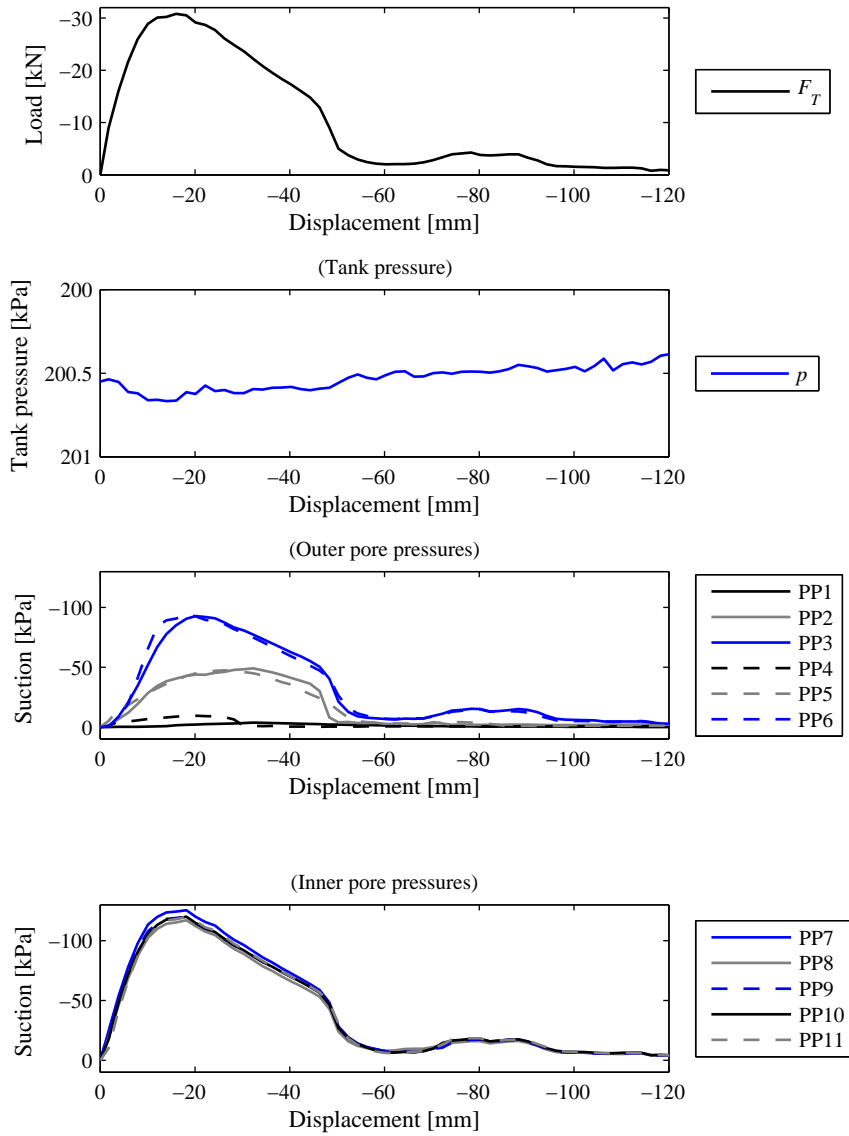


Figure G.23: Loading 14.02.05.

G.2.6 Test 14.02.06

Soil properties			Loading			Installation		
D_R	[%]	87.8	f_s	[Hz]	5	F_P	[kN]	31.9
σ of D_R	[%]	3.0	F_T	[kN]	-36.94	d_{inst}	[mm]	242.3
γ	[kN/m ³]	19.7	w_T	[mm]	-22.30			
γ'	[kN/m ³]	9.7	v	[mm/s]	17.80	p_{tank}	[kPa]	199.0

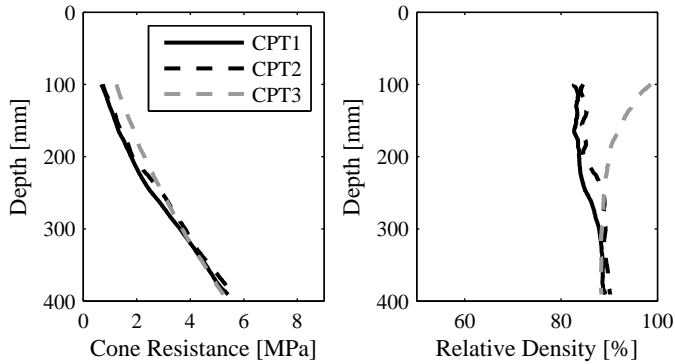


Figure G.24: CPT testing 14.02.06.

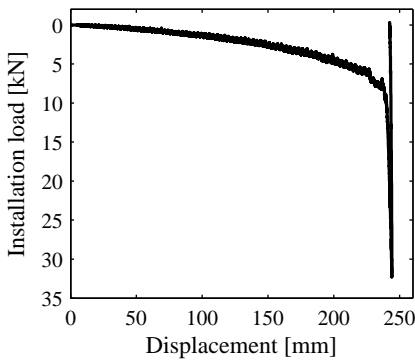


Figure G.25: Installation 14.02.06.

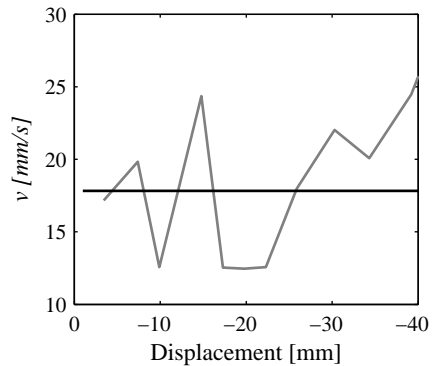


Figure G.26: Pull-out velocity 14.02.06.

Comments:
Sampling rate was rather low for this pull-out velocity.

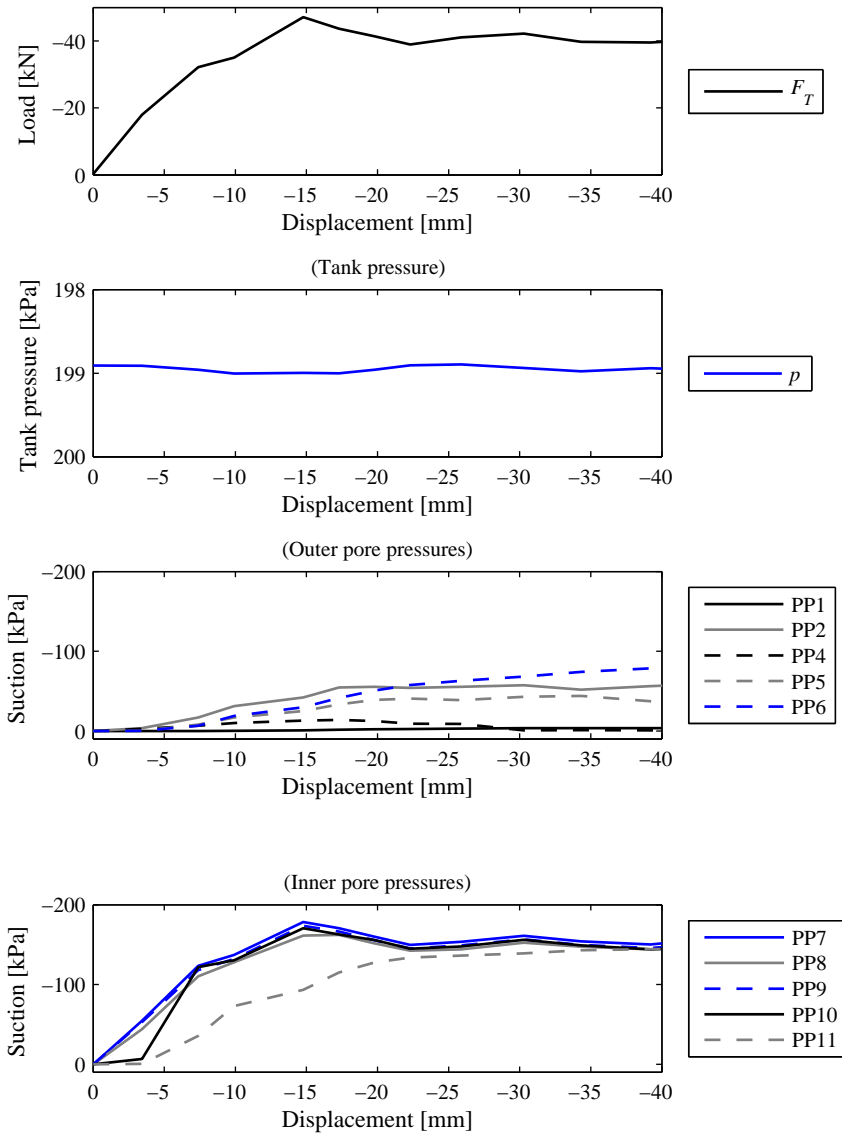


Figure G.27: Loading 14.02.06.

G.2.7 Test 14.02.07

Soil properties			Loading			Installation		
D_R	[%]	83.0	f_s	[Hz]	50	F_P	[kN]	33
σ of D_R	[%]	4.9	F_T	[kN]	-44.07	d_{inst}	[mm]	236.2
γ	[kN/m ³]	19.5	w_T	[mm]	-14.73	Tank pressure		
γ'	[kN/m ³]	9.5	v	[mm/s]	21.70	p_t	[kPa]	200

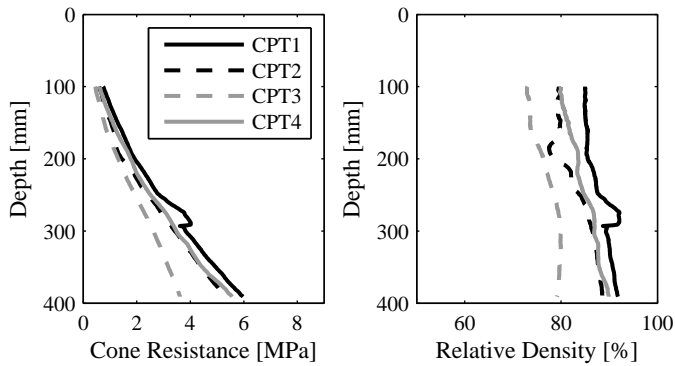


Figure G.28: CPT testing 14.02.07.

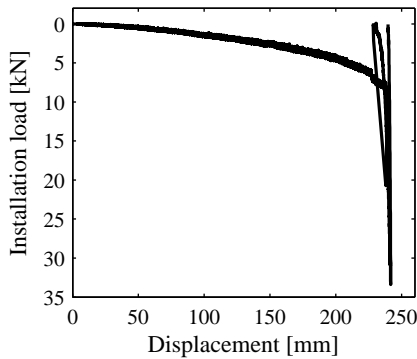


Figure G.29: Installation 14.02.07.

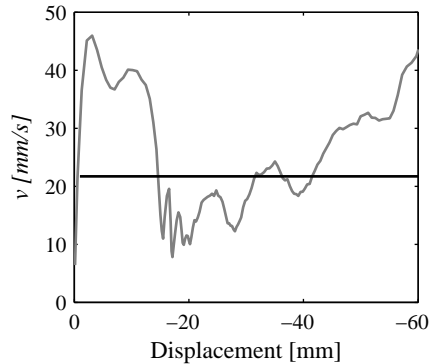


Figure G.30: Pull-out velocity 14.02.07.

Comments:
 Saturation problems in transducers: PP2, PP3, PP7, PP8, PP9, PP10. Peak pore pressure measurement was recorded approximately 0.5 s after the peak load measurement.

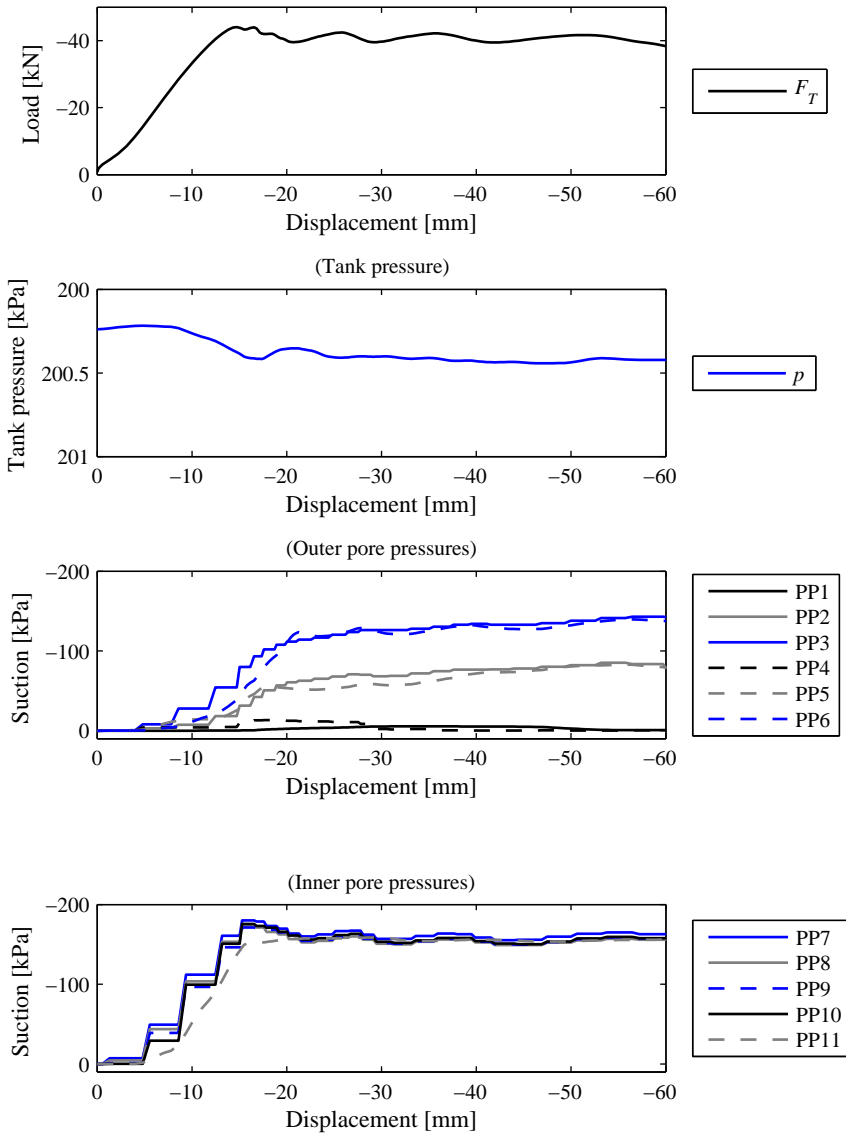


Figure G.31: Loading 14.02.07.

G.2.8 Test 14.02.08

Soil properties			Loading			Installation		
D_R	[%]	85.0	f_s	[Hz]	100	F_P	[kN]	31.5
σ of D_R	[%]	3.7	F_T	[kN]	-48.84	d_{inst}	[mm]	239
γ	[kN/m ³]	19.6	w_T	[mm]	-14.29	Tank pressure		
γ'	[kN/m ³]	9.6	v	[mm/s]	27.2	p_t	[kPa]	200

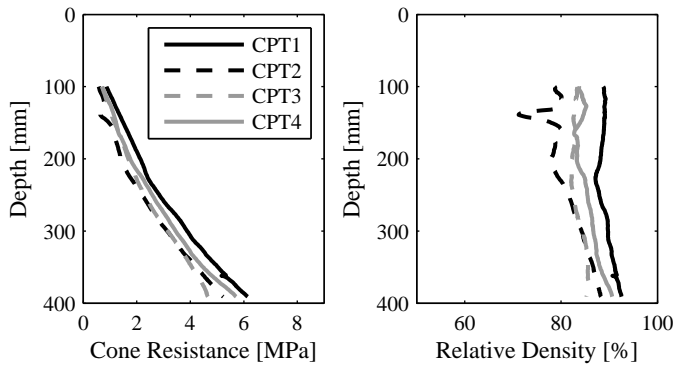


Figure G.32: CPT testing 14.02.08.

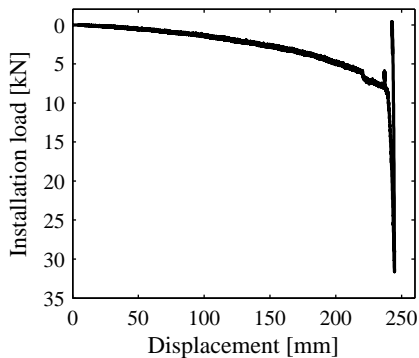


Figure G.33: Installation 14.02.08.

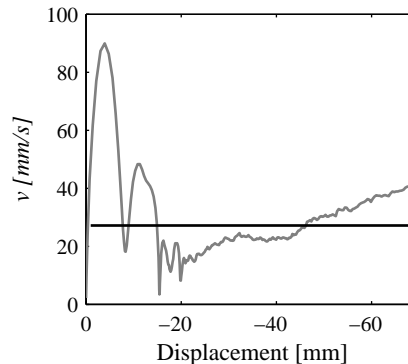


Figure G.34: Pull-out velocity 14.02.08.

Comments:

Saturation problems in transducers: PP4, PP7, PP8, PP9, PP10. Peak pore pressure measurement was recorded approximately 0.5 s after the peak load measurement.

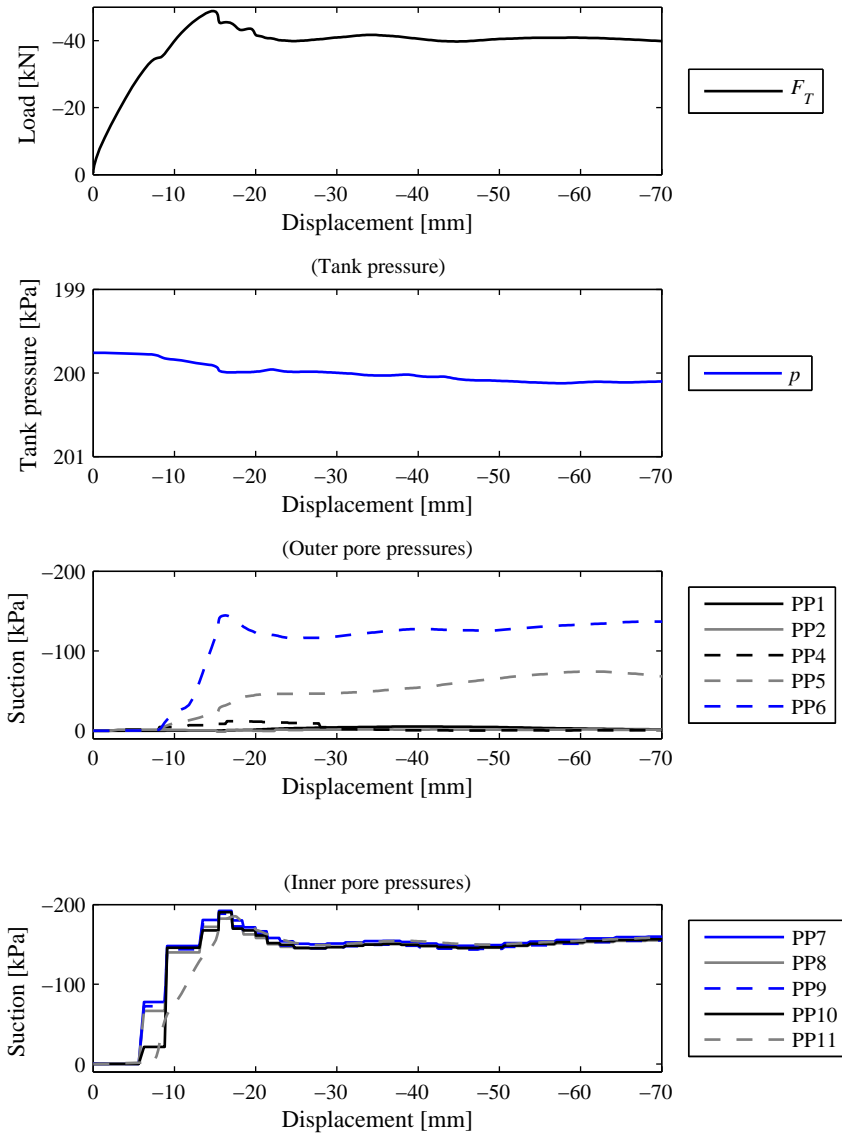


Figure G.35: Loading 14.02.08.

G.2.9 Test 14.02.09

Soil properties			Loading			Installation		
D_R	[%]	83.0	f_s	[Hz]	100	F_P	[kN]	31.5
σ of D_R	[%]	5.4	F_T	[kN]	-65.36	d_{inst}	[mm]	236.4
γ	[kN/m ³]	19.5	w_T	[mm]	-48.78	Tank pressure		
γ'	[kN/m ³]	9.5	v	[mm/s]	46.71	p_t	[kPa]	200.4

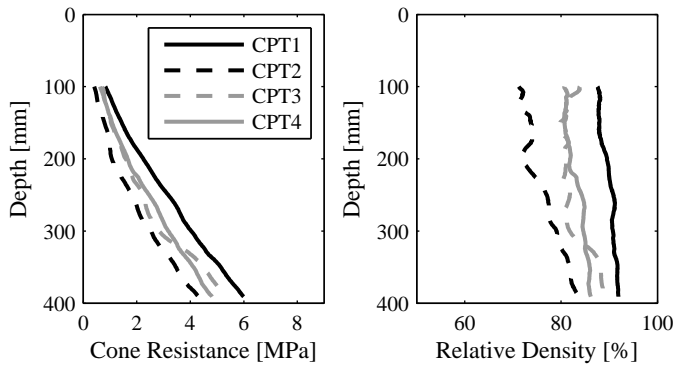


Figure G.36: CPT testing 14.02.09.

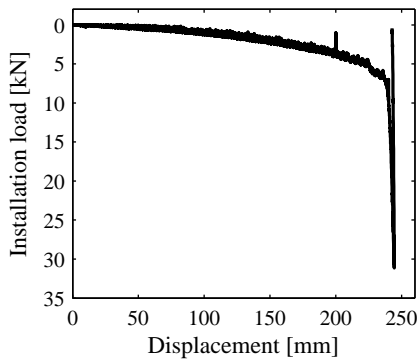


Figure G.37: Installation 14.02.09.

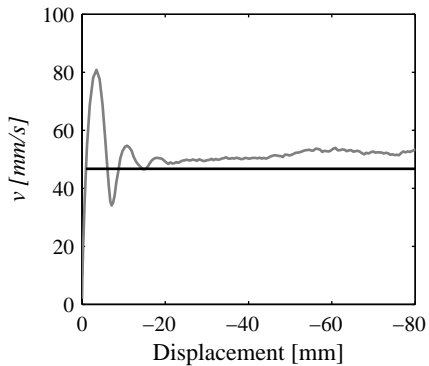


Figure G.38: Pull-out velocity 14.02.09.

Comments:
 Saturation problems in transducers: PP2, PP7, PP8, PP9, PP10. Peak pore pressure measurement was recorded approximately 0.5 s after the peak load measurement.

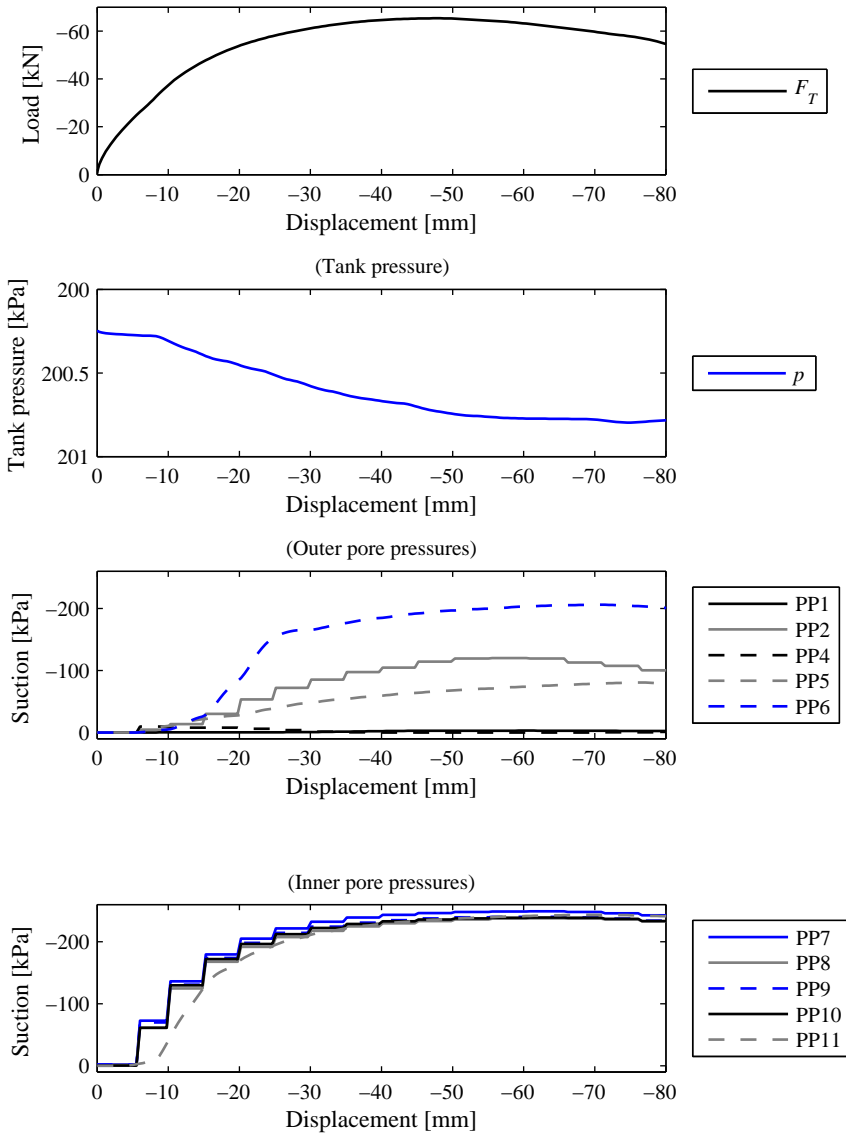


Figure G.39: Loading 14.02.09.

G.2.10 Test 14.02.10

Soil properties			Loading			Installation		
D_R	[%]	85.8	f_s	[Hz]	5	F_P	[kN]	32.3
σ of D_R	[%]	5.2	F_T	[kN]	-	d_{inst}	[mm]	246.6
γ	[kN/m ³]	19.6	w_T	[mm]	-	Tank pressure		
γ'	[kN/m ³]	9.6	v	[mm/s]	0.05	p_t	[kPa]	200

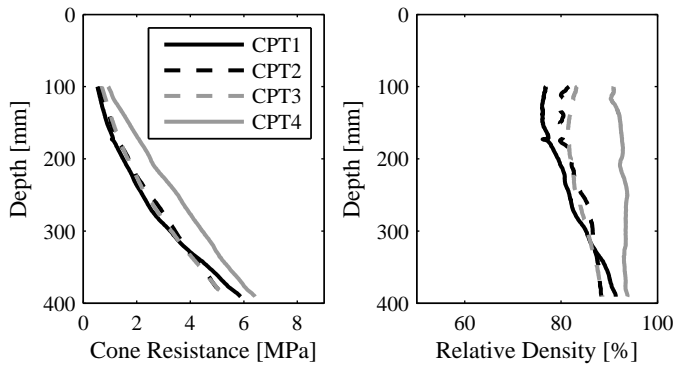


Figure G.40: CPT testing 14.02.10.

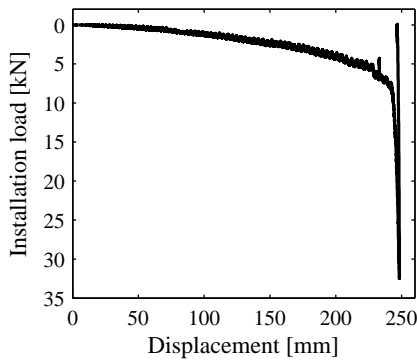


Figure G.41: Installation 14.02.10.

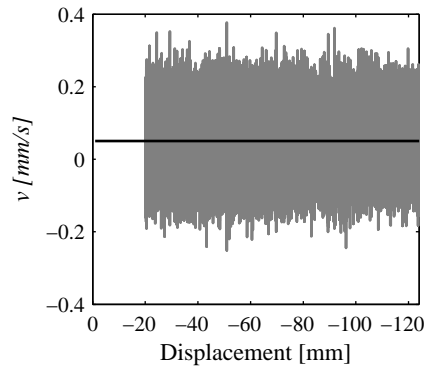


Figure G.42: Pull-out velocity 14.02.10.

Comments:

First centimetres were not recorded. Secondary peak in load and pore pressure response probably due to a small sudden deviation in loading velocity (possibly, not recorded).

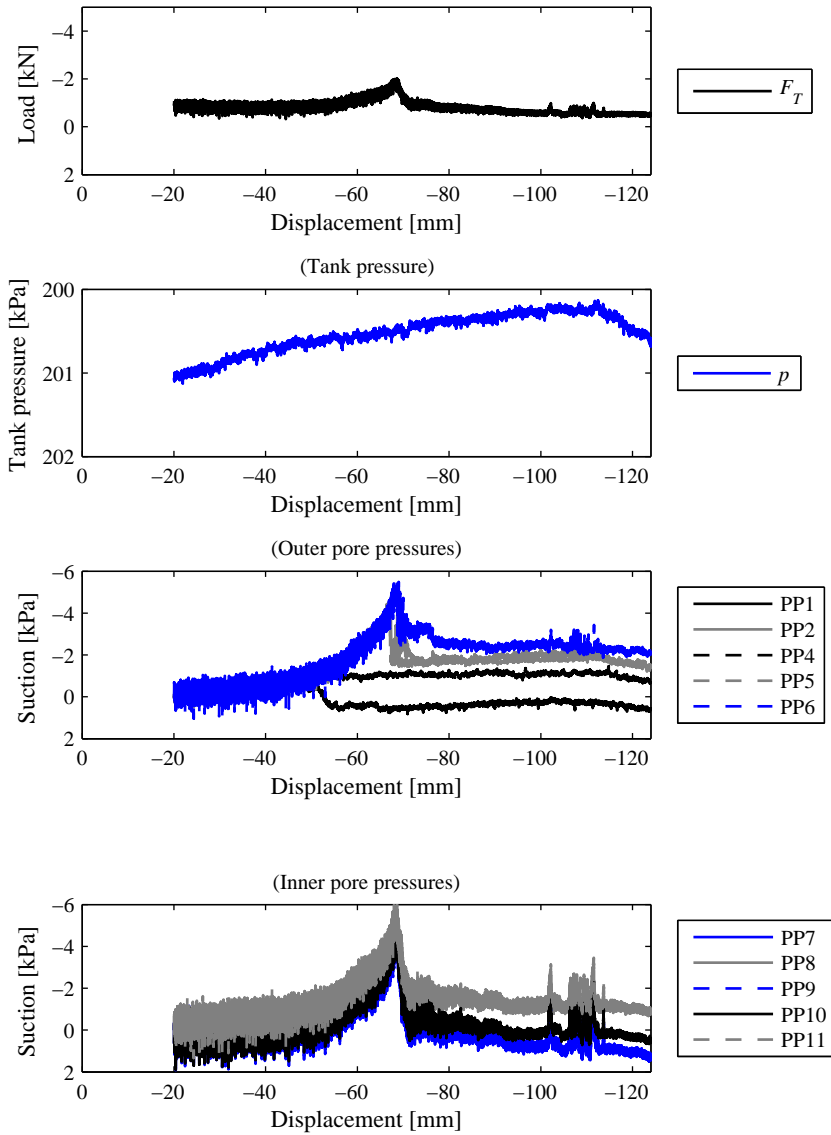


Figure G.43: Loading 14.02.10.

G.2.11 Test 14.02.11

Soil properties			Loading			Installation		
D_R	[%]	86.0	f_s	[Hz]	5	F_P	[kN]	31.4
σ of D_R	[%]	4.9	F_T	[kN]	-4.08	d_{inst}	[mm]	240.7
γ	[kN/m ³]	19.6	w_T	[mm]	-0.65	Tank pressure		
γ'	[kN/m ³]	9.6	v	[mm/s]	0.1	p_t	[kPa]	199.7

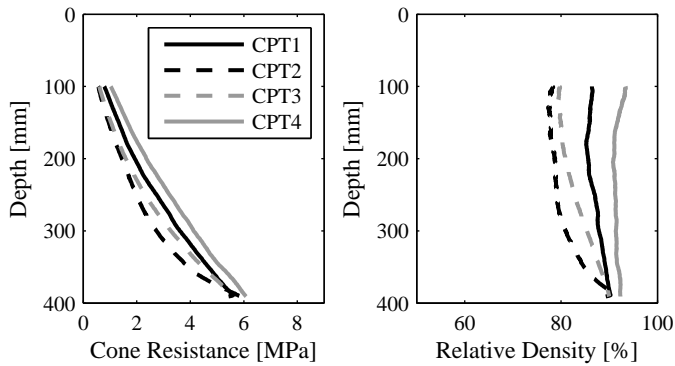


Figure G.44: CPT testing 14.02.11.

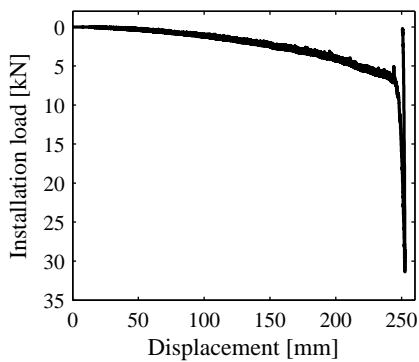


Figure G.45: Installation 14.02.11.

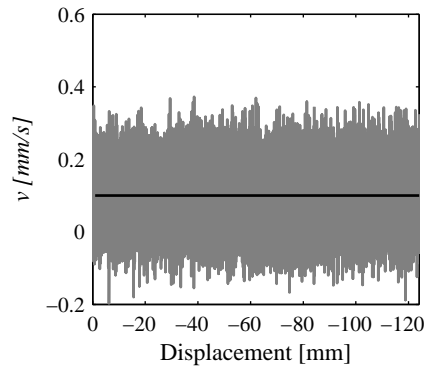


Figure G.46: Pull-out velocity 14.02.11.

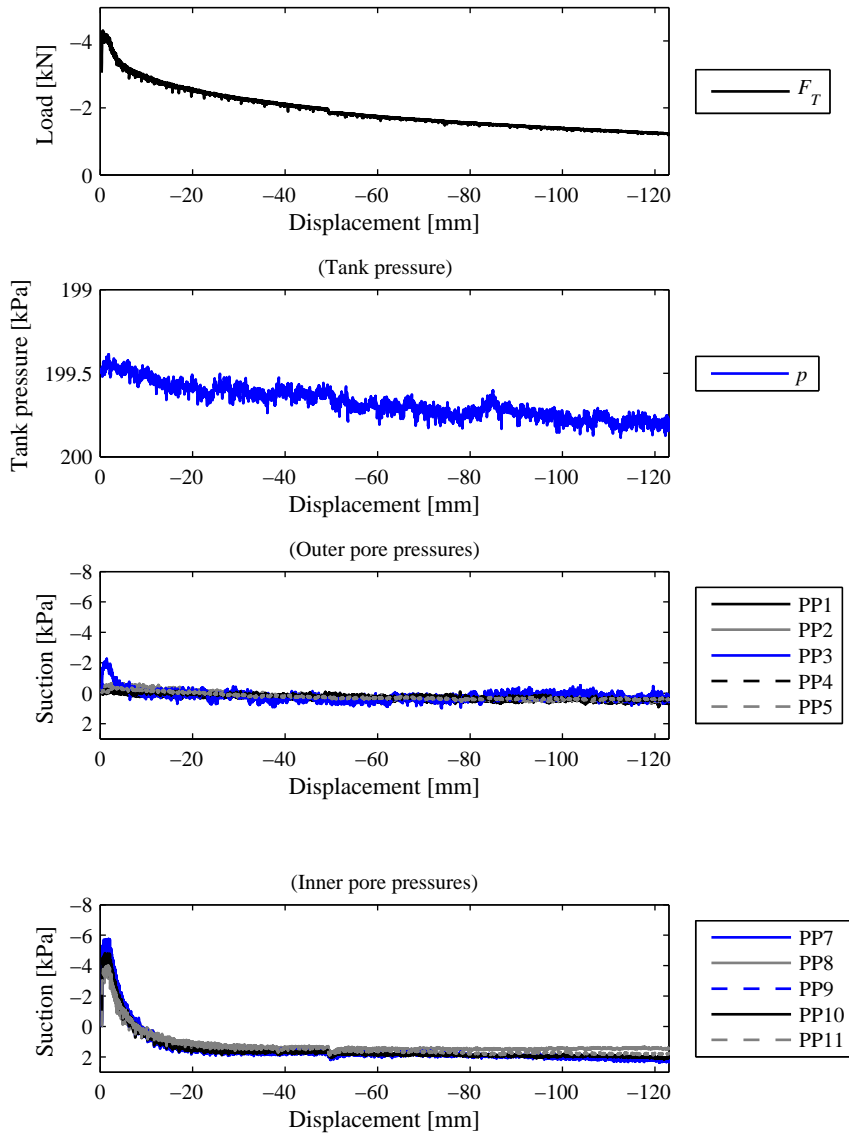


Figure G.47: Loading 14.02.11.

G.2.12 Test 14.02.12

Soil properties			Loading			Installation		
D_R	[%]	85.0	f_s	[Hz]	2	F_P	[kN]	32
σ of D_R	[%]	6.4	F_T	[kN]	-2.67	d_{inst}	[mm]	239.2
γ	[kN/m ³]	19.6	w_T	[mm]	-0.70	Tank pressure		
γ'	[kN/m ³]	9.6	v	[mm/s]	0.05	p_t	[kPa]	199.6

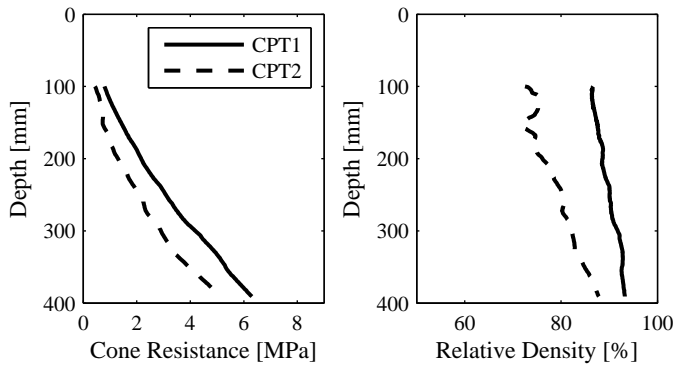


Figure G.48: CPT testing 14.02.12.

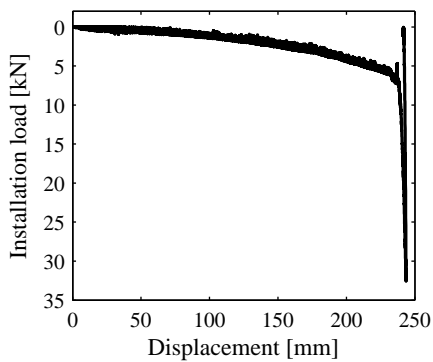


Figure G.49: Installation 14.02.12.

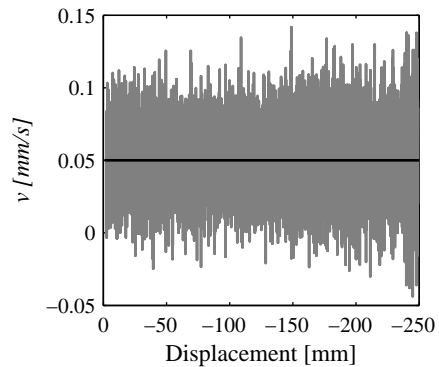


Figure G.50: Pull-out velocity 14.02.12.

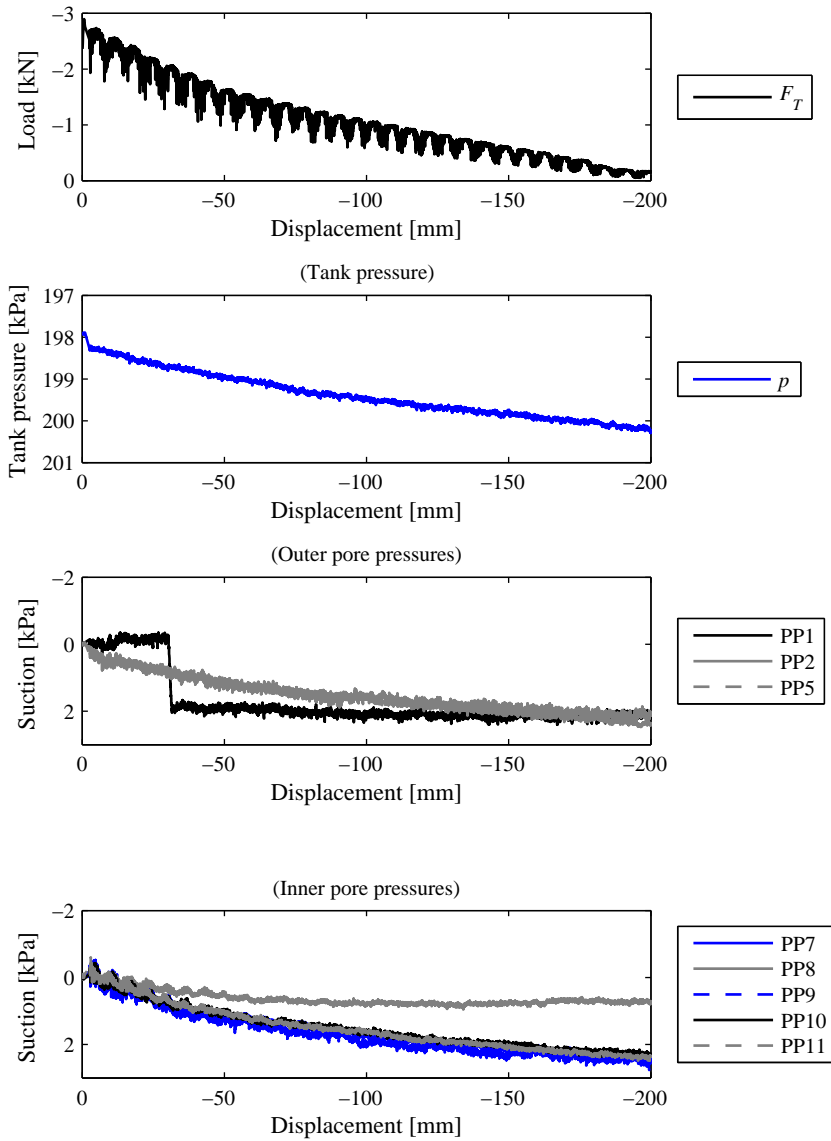


Figure G.51: Loading 14.02.12.

Comments:

CPT tool was accidentally broken after the first two samplings. Visible change in frequency in load and pore pressure response, while the loading velocity was stable. Possibly, the vibrations were due to external works in the laboratory that affected the whole system. Pressure transducer PP1 did not function.

G.2.13 Test 14.02.13

Soil properties			Loading			Installation		
D_R	[%]	82.0	f_s	[Hz]	200	F_P	[kN]	31
σ of D_R	[%]	6.8	F_T	[kN]	-71.65	d_{inst}	[mm]	239.3
γ	[kN/m ³]	19.5	w_T	[mm]	-60.48	Tank pressure		
γ'	[kN/m ³]	9.5	v	[mm/s]	98.3	p_t	[kPa]	200.4

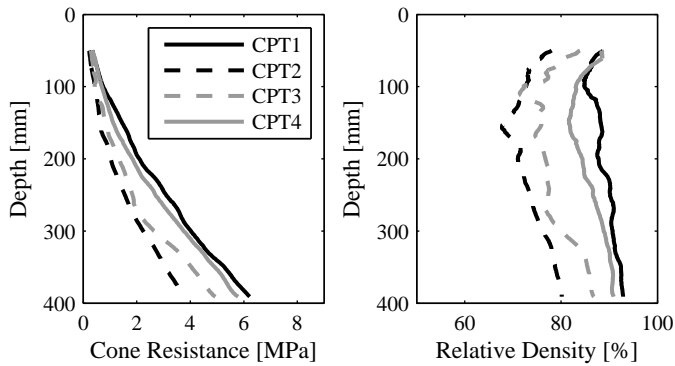


Figure G.52: CPT testing 14.02.13.

No record.

Figure G.53: Installation 14.02.13.

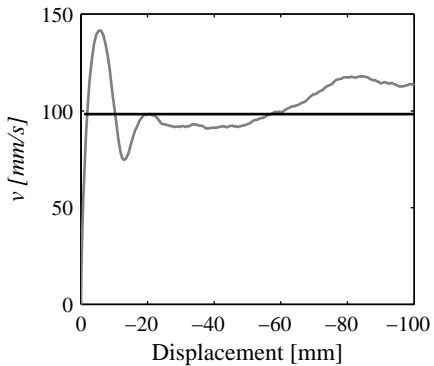


Figure G.54: Pull-out velocity 14.02.13.

Comments:
 Saturation problems in transducers: PP2, PP7, PP8, PP9, PP10. Peak pore pressure measurement was recorded approximately 0.5 s after the peak load measurement.

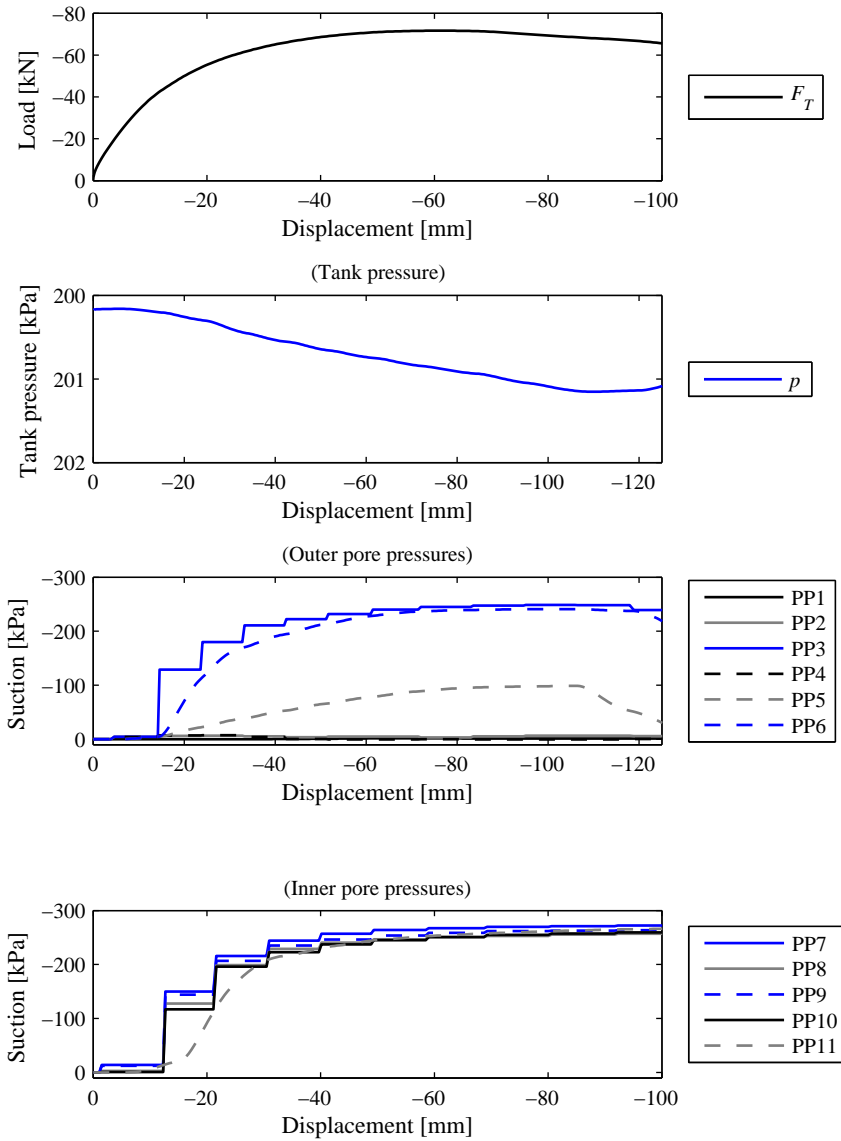


Figure G.55: Loading 14.02.13.

G.2.14 Test 14.02.14

Soil properties			Loading			Installation		
D_R	[%]	83.5	f_s	[Hz]	500	F_P	[kN]	37
σ of D_R	[%]	3.4	F_T	[kN]	-75.17	d_{inst}	[mm]	236
γ	[kN/m ³]	19.5	w_T	[mm]	-68.18	Tank pressure		
γ'	[kN/m ³]	9.5	v	[mm/s]	152.3	p_t	[kPa]	199.7

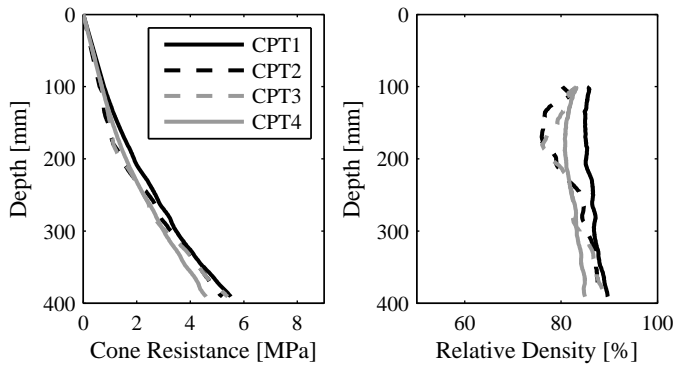


Figure G.56: CPT testing 14.02.14.

No record.

Figure G.57: Installation 14.02.14.

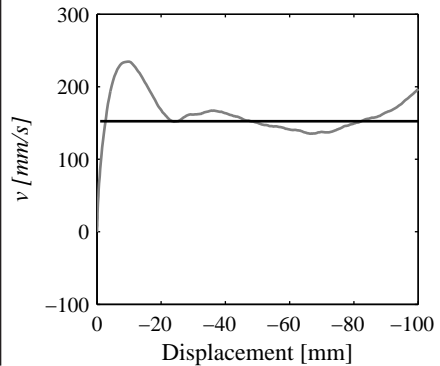


Figure G.58: Pull-out velocity 14.02.14.

Comments:
 Saturation problems in transducers: PP2, PP3, PP7, PP8, PP9, PP10. Peak pore pressure measurement was recorded approximately 0.5 s after the peak load measurement.

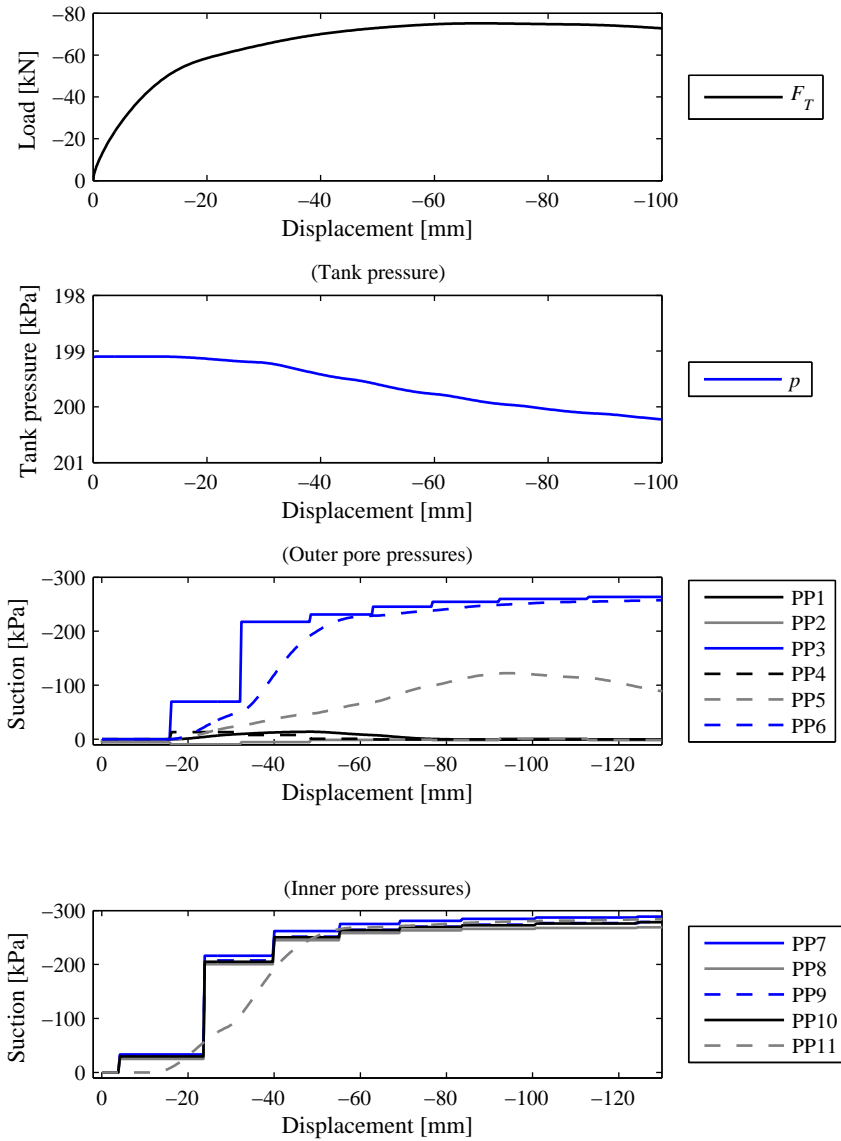


Figure G.59: Loading 14.02.14.

G.2.15 Test 14.02.15

Soil properties			Loading			Installation		
D_R	[%]	78.6	f_s	[Hz]	1	F_P	[kN]	31
σ of D_R	[%]	6.0	F_T	[kN]	(0)	d_{inst}	[mm]	240.5
γ	[kN/m ³]	19.3	w_T	[mm]	(0)	Tank pressure		
γ'	[kN/m ³]	9.3	v	[mm/s]	0.01	p_t	[kPa]	0

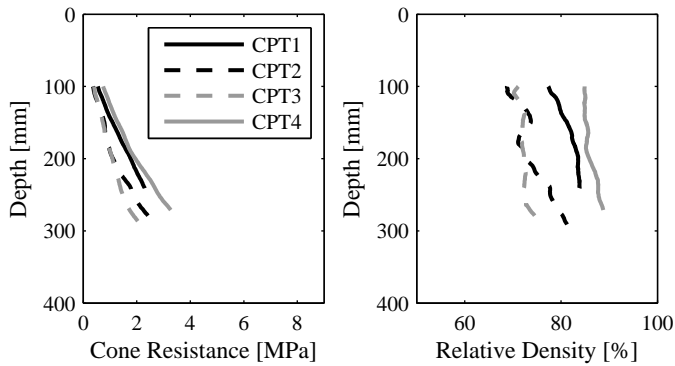


Figure G.60: CPT testing 14.02.15.

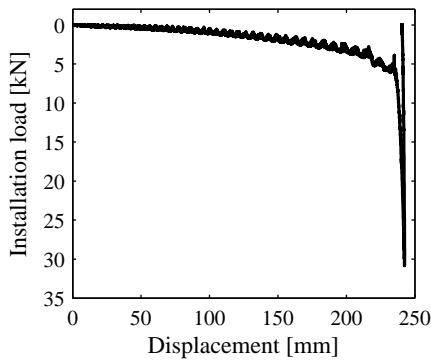


Figure G.61: Installation 14.02.15.

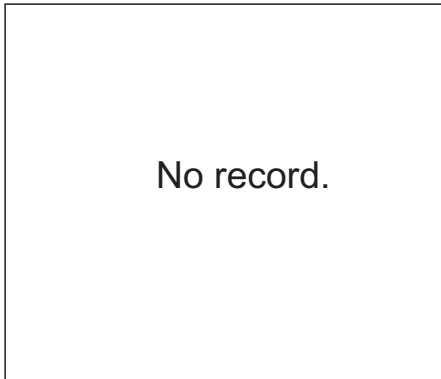


Figure G.62: Pull-out velocity 14.02.15.

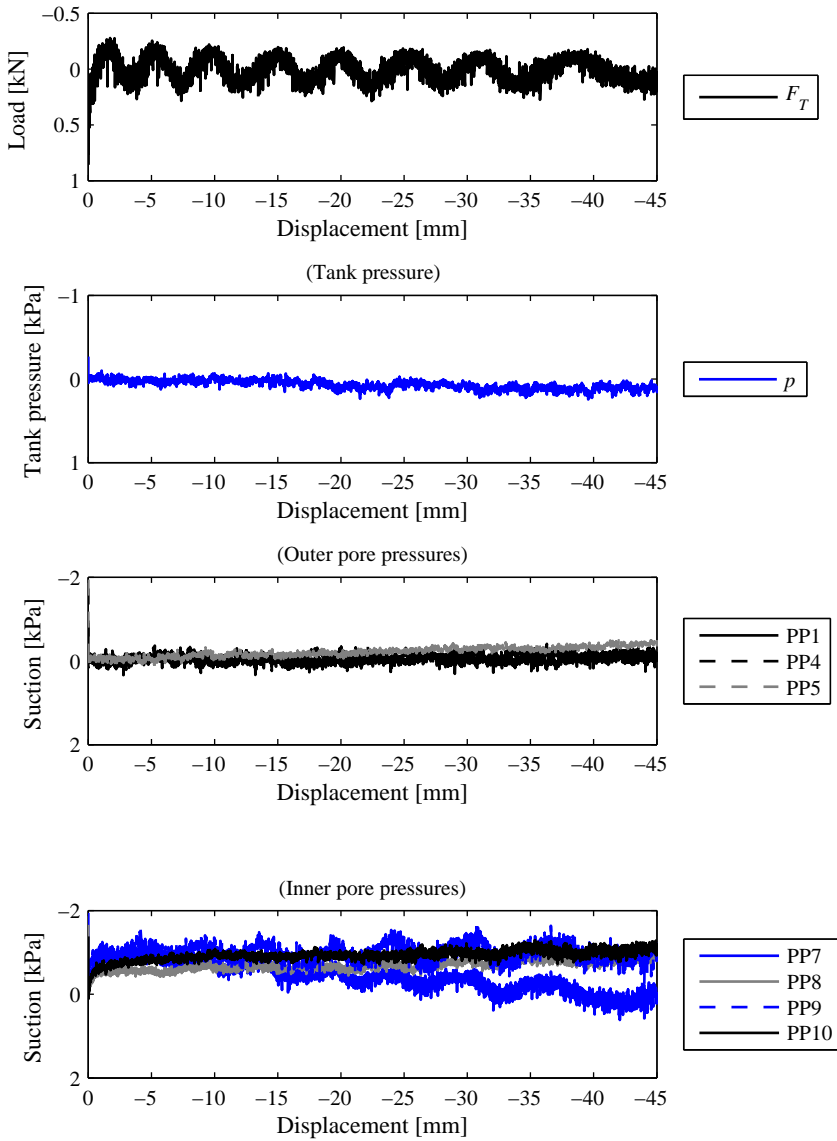


Figure G.63: Loading 14.02.15

Comments:

No significant tensile resistance was recorded. Visible change in frequency in load and pore pressure response, while the loading velocity was stable. Possibly, the vibrations were due to external works in the laboratory that affected the whole system.

G.3 Test Series 13.02.XX Overview

Series 13.02.XX present slow monotonic tensile loading tests on a bucket foundation model. This chapter provides the data of tests performed in the large yellow sand box (Figure G.64). Two bucket models were used with the dimensions as follows: (1) 1.0 m in diameter D , 0.5 mm in skirt length d and (2) 1.0 m in diameter D , 1.0 mm in skirt length d . Both models had skirt thickness $t = 3$ mm. Figure G.65 shows the positions of the laboratory CPT samplings. Figures G.66 and G.67 show the bucket foundation models. Vaitkunaite 2015 described the testing procedure. Hedegaard and Borup 1993, Ibsen and Boedker 1994 have studied the Aalborg University sand No.1 properties.

Table G.2: Test series 13.02.XX summary.

p_m [kPa]	Test No.	d/D	Loading			Installation		D_R [%]	γ' [kN/m ³]
			F_T [kN]	w_T [mm]	v [mm/s]	F_P [kN]	d_{inst} [mm]		
12	13.02.01	0.5	-26.4	-11.7	0.021	47.5	490	82.4	9.5
65	13.02.02	0.5	-53.6	-20.0	0.039	42.0	490	82.7	9.5
18	13.02.03	0.5	-	-	0.002	55.2	492	74.8	9.1
19	13.02.04	0.5	-19.0	-24.3	0.001	45.3	486	79.0	9.3
21	13.02.05	0.5	-15.3	-11.4	0.001	46.1	495	82.3	9.5
0	13.02.06	0.5	-5.7	-6.3	0.001	49.6	483	79.9	9.3
0	13.02.07	0.5	-6.3	-5.8	0.001	50.6	474	83.1	9.5
0	13.02.08	0.5	-5.3	-4.6	0.002	49.5	473	84.3	9.6
41	13.02.09	0.5	-28.2	-5.0	0.001	68.3	487	81.3	9.4
0	13.02.10	1.0	-27.7	-3.9	0.001	203.0	980	85.5	9.6
20	13.02.11	0.5	-23.3	-7.5	0.002	57.3	487	79.3	9.3
40	13.02.12	0.5	-26.9	-5.2	0.002	72.8	487	79.3	9.3
68	13.02.13	0.5	-43.2	-10.7	0.002	70.1	493	82.9	9.5
0	13.02.14	1.0	-29.8	-4.5	0.001	220.0	990	83.0	9.5
0	13.02.15	0.5	-5.9	-5.5	0.002	73.0	491	85.0	9.6
0	13.02.16	0.5	-14.9	-4.8	0.002	70.5	493	77.2	9.2
73	13.02.17	0.5	-96.3	-72.2	0.002	74.0	490	83.4	9.5

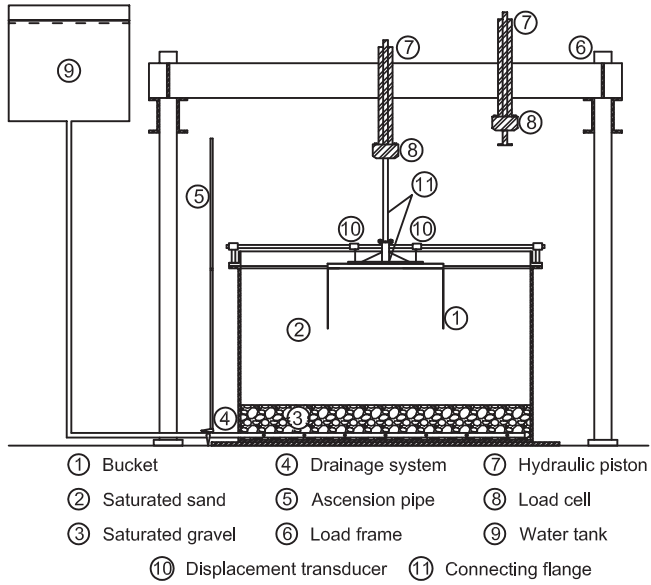


Figure G.64: Test set-up. Vaitkunaite (2015)

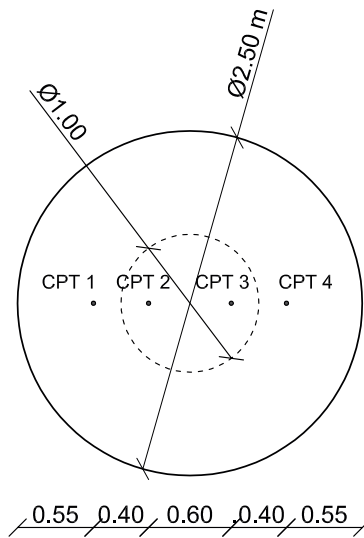


Figure G.65: CPT positions.

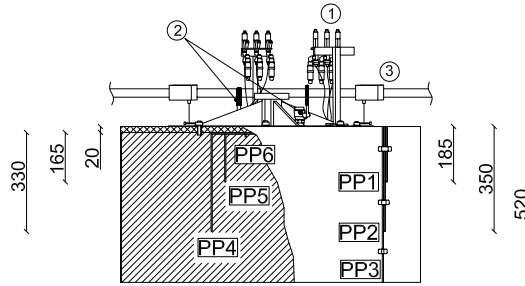


Figure G.66: Bucket foundation model $d/D = 0.5$: (1) pressure transducers, (2) valves, (3) displacement transducers. Vaitkunaite (2015)

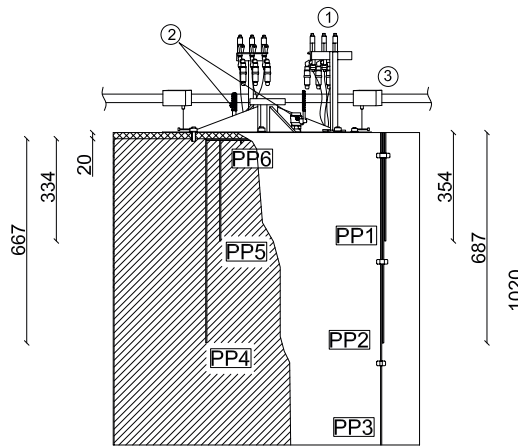


Figure G.67: Bucket foundation model $d/D = 1.0$: (1) pressure transducers, (2) valves, (3) displacement transducers. Vaitkunaite (2015)

G.3.1 Test 13.02.01

Soil properties			Loading			Installation		
D_R	[%]	82.4	F_T	[kN]	-26.4	F_P	[kN]	47.5
σ of D_R	[%]	3.3	w_T	[mm]	-11.68	d_{inst}	[mm]	490.0
γ	[kN/m ³]	19.5	v	[mm/s]	0.021	Membrane pressure		
γ'	[kN/m ³]	9.5				p_m	[kPa]	12

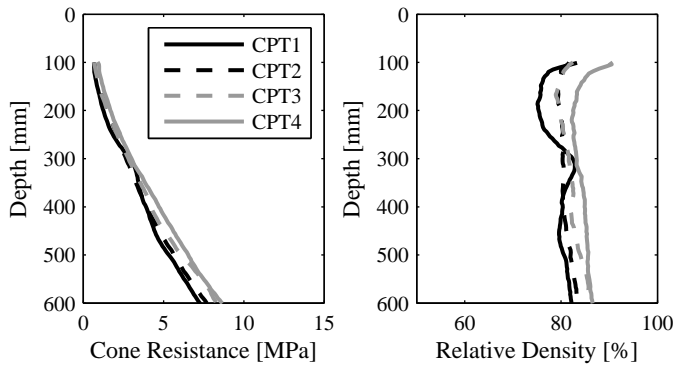


Figure G.68: CPT testing 13.02.01.

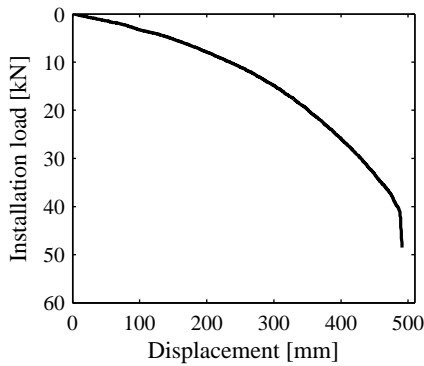


Figure G.69: Installation 13.02.01.

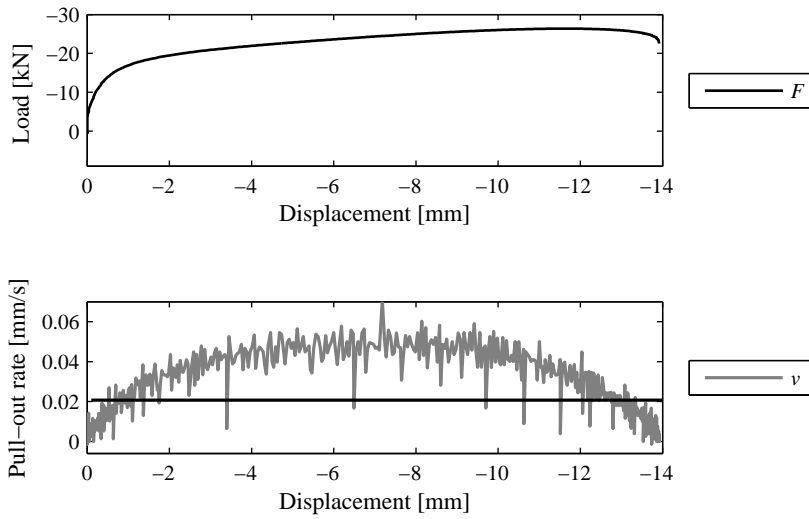


Figure G.70: Loading 13.02.01.

G.3.2 Test 13.02.02

Soil properties			Loading			Installation		
D_R	[%]	82.7	F_T	[kN]	-53.6	F_P	[kN]	42.0
σ of D_R	[%]	3.8	w_T	[mm]	-20.0	d_{inst}	[mm]	490.0
γ	[kN/m ³]	19.5	v	[mm/s]	0.039	Membrane pressure		
γ'	[kN/m ³]	9.5				p_m	[kPa]	65

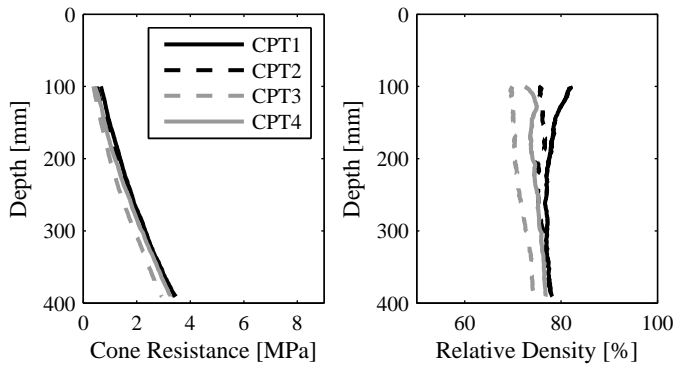


Figure G.71: CPT testing 13.02.02.

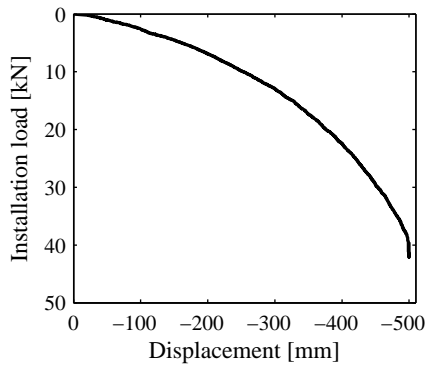


Figure G.72: Installation 13.02.02.

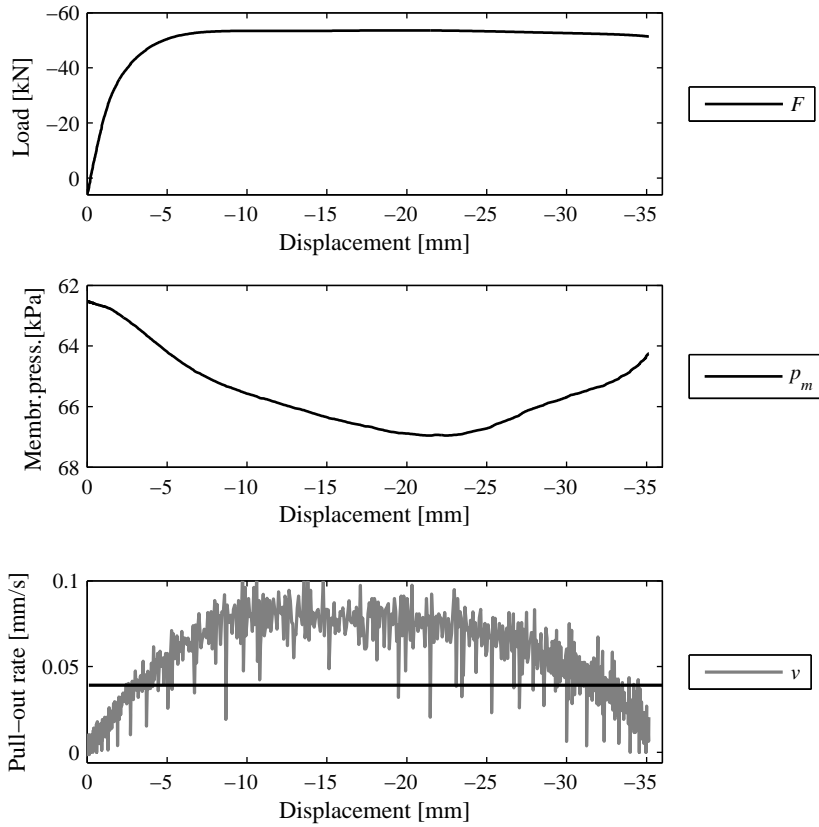


Figure G.73: Loading 13.02.02.

G.3.3 Test 13.02.03

Soil properties			Loading			Installation		
D_R	[%]	74.8	F_T	[kN]	-	F_P	[kN]	55.2
σ of D_R	[%]	3.4	w_T	[mm]	-	d_{inst}	[mm]	491.8
γ	[kN/m ³]	19.1	v	[mm/s]	0.002	Membrane pressure		
γ'	[kN/m ³]	9.1				p_m	[kPa]	18

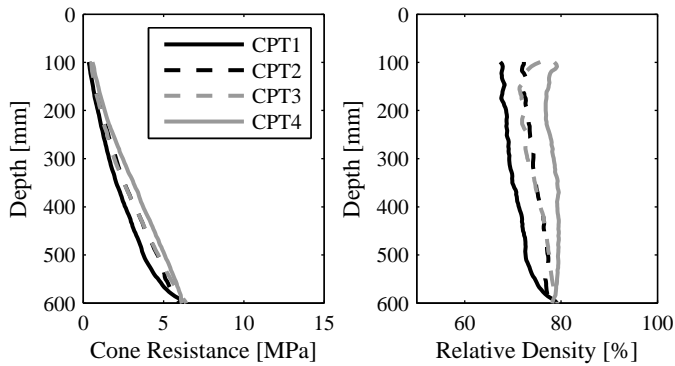


Figure G.74: CPT testing 13.02.03.

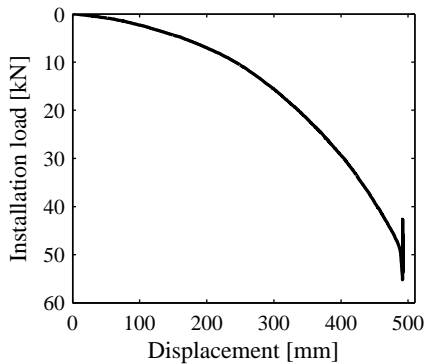


Figure G.75: Installation 13.02.03.

Comments:

Loading was attempted to times.

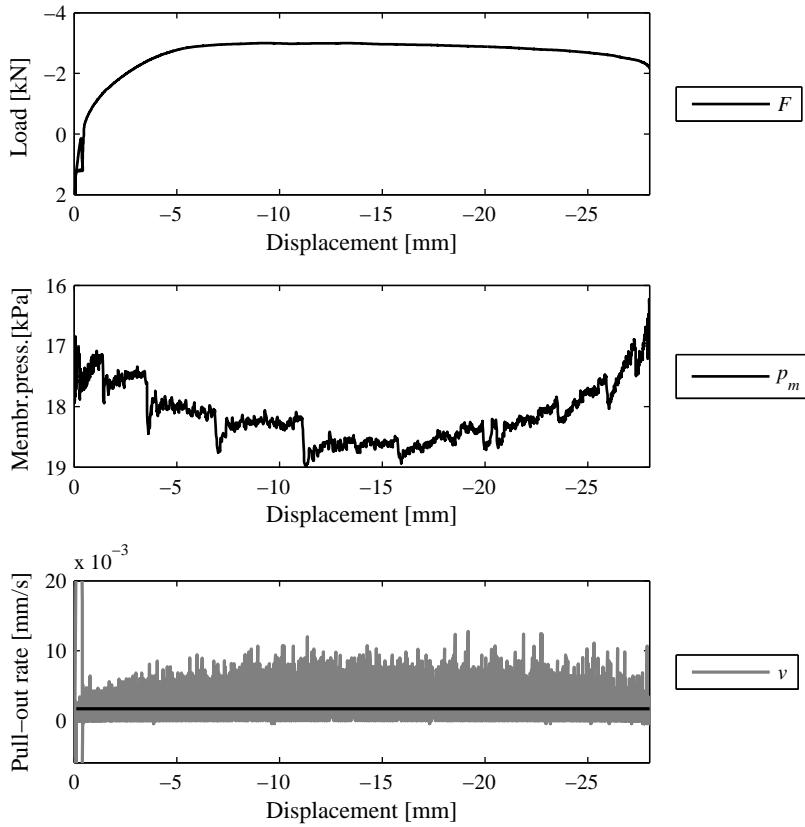


Figure G.76: Loading 13.02.03.

G.3.4 Test 13.02.04

Soil properties			Loading			Installation		
D_R	[%]	79.0	F_T	[kN]	-19.0	F_P	[kN]	45.3
σ of D_R	[%]	4.4	w_T	[mm]	-24.3	d_{inst}	[mm]	486.0
γ	[kN/m ³]	19.3	v	[mm/s]	0.001	Membrane pressure		
γ'	[kN/m ³]	9.3				p_m	[kPa]	19

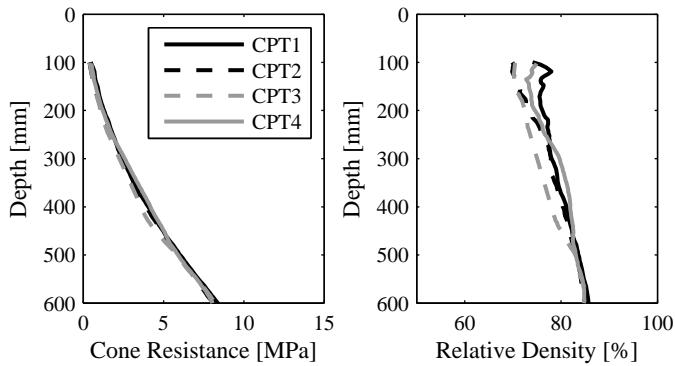


Figure G.77: CPT testing 13.02.04.

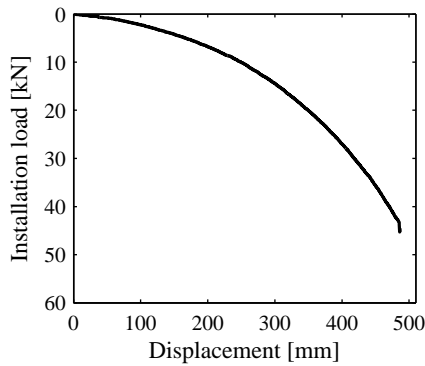


Figure G.78: Installation 13.02.04.

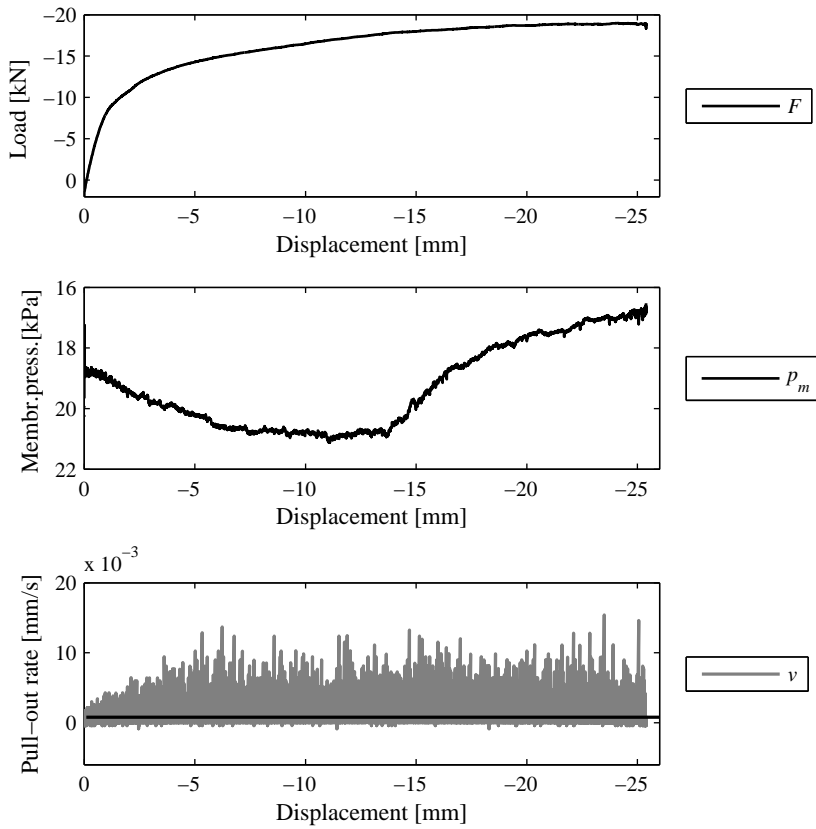


Figure G.79: Loading 13.02.04.

G.3.5 Test 13.02.05

Soil properties			Loading			Installation		
D_R	[%]	82.3	F_T	[kN]	-15.3	F_P	[kN]	46.1
σ of D_R	[%]	4.2	w_T	[mm]	-11.4	d_{inst}	[mm]	495.0
γ	[kN/m ³]	19.5	v	[mm/s]	0.005	Membrane pressure		
γ'	[kN/m ³]	9.5				p_m	[kPa]	21

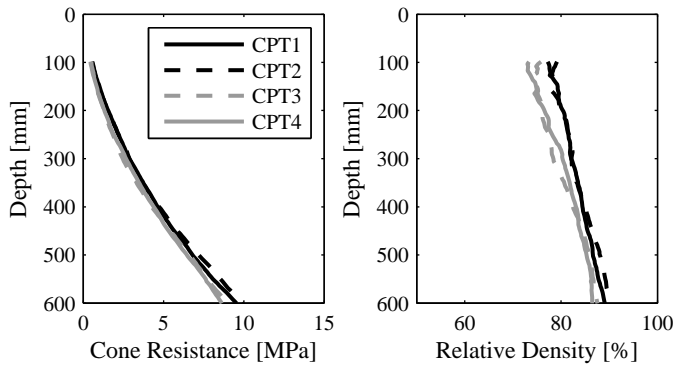


Figure G.80: CPT testing 13.02.05.

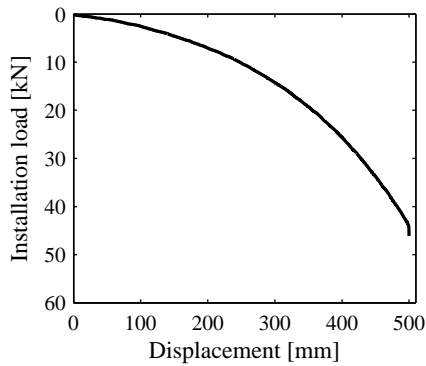


Figure G.81: Installation 13.02.05.

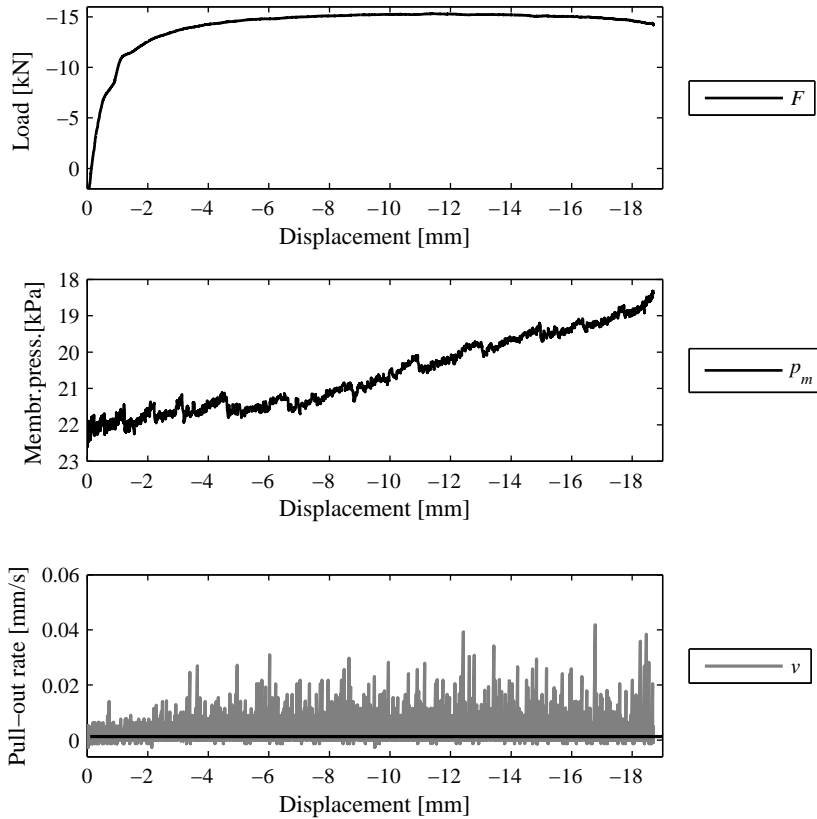


Figure G.82: Loading 13.02.05.

G.3.6 Test 13.02.06

Soil properties			Loading			Installation		
D_R	[%]	79.9	F_T	[kN]	-5.7	F_P	[kN]	49.6
σ of D_R	[%]	4.3	w_T	[mm]	-6.3	d_{inst}	[mm]	483.0
γ	[kN/m ³]	19.3	v	[mm/s]	0.001	Membrane pressure		
γ'	[kN/m ³]	9.3				p_m	[kPa]	0

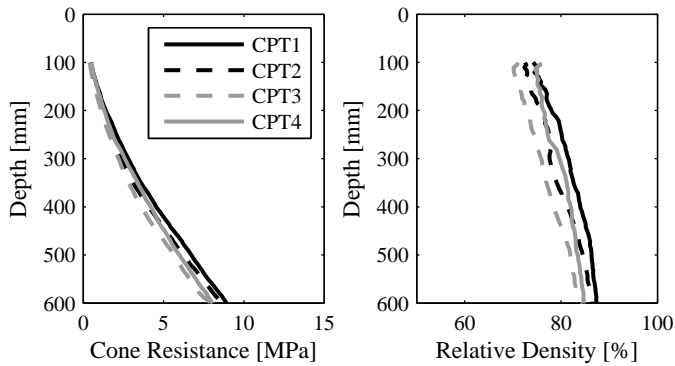


Figure G.83: CPT testing 13.02.06.

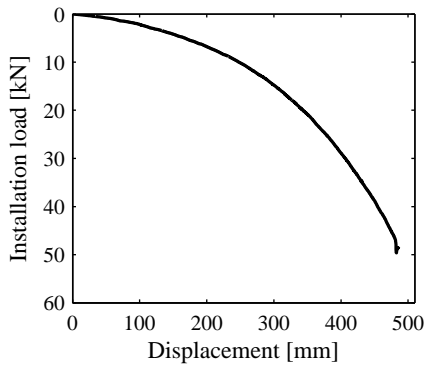


Figure G.84: Installation 13.02.06.

Comments:

Pore pressure transducer PP1 did not function.

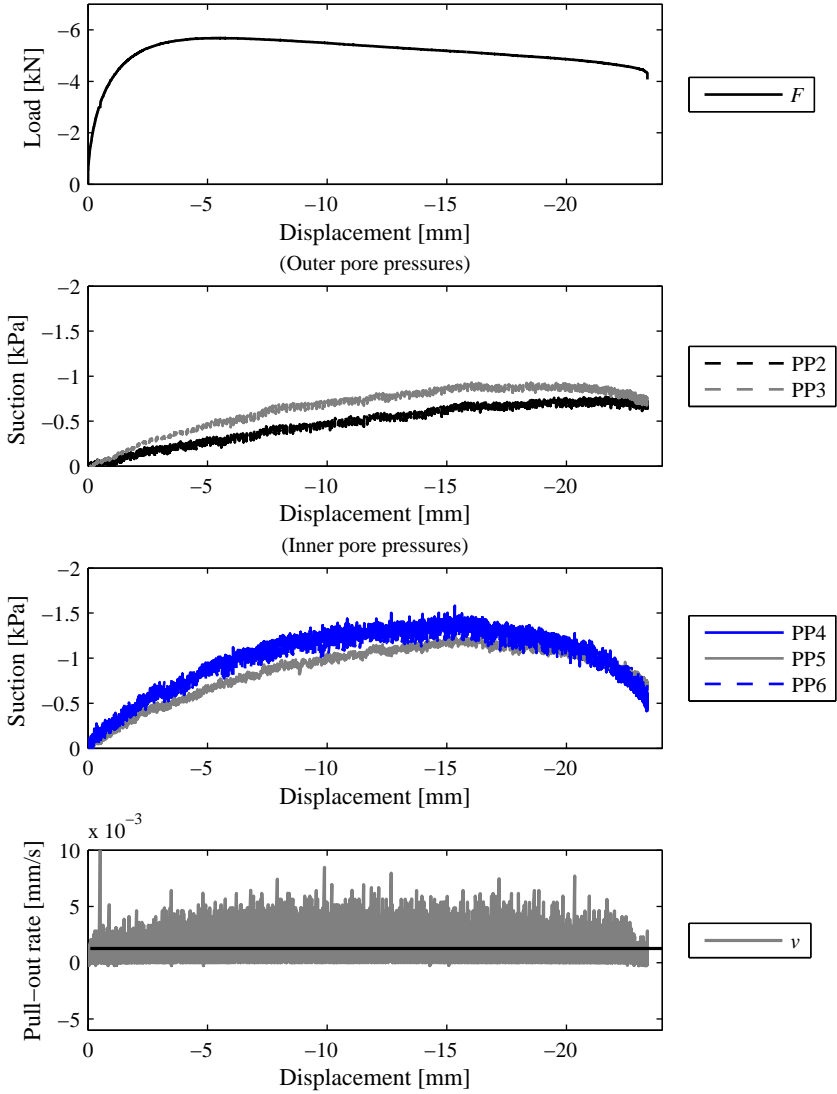


Figure G.85: Loading 13.02.06.

G.3.7 Test 13.02.07

Soil properties			Loading			Installation		
D_R	[%]	83.1	F_T	[kN]	-6.3	F_P	[kN]	50.6
σ of D_R	[%]	4.4	w_T	[mm]	-5.8	d_{inst}	[mm]	474.0
γ	[kN/m ³]	19.5	v	[mm/s]	0.001	Membrane pressure		
γ'	[kN/m ³]	9.5				p_m	[kPa]	0

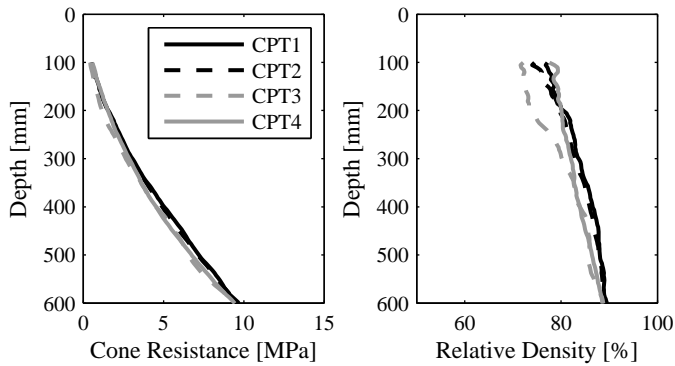


Figure G.86: CPT testing 13.02.07.

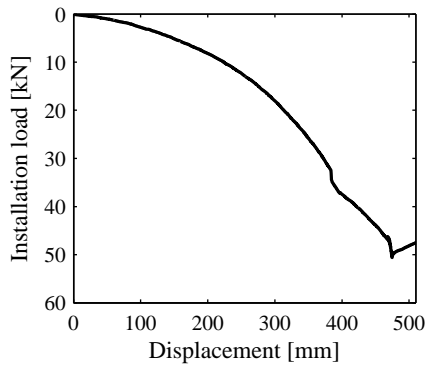


Figure G.87: Installation 13.02.07.

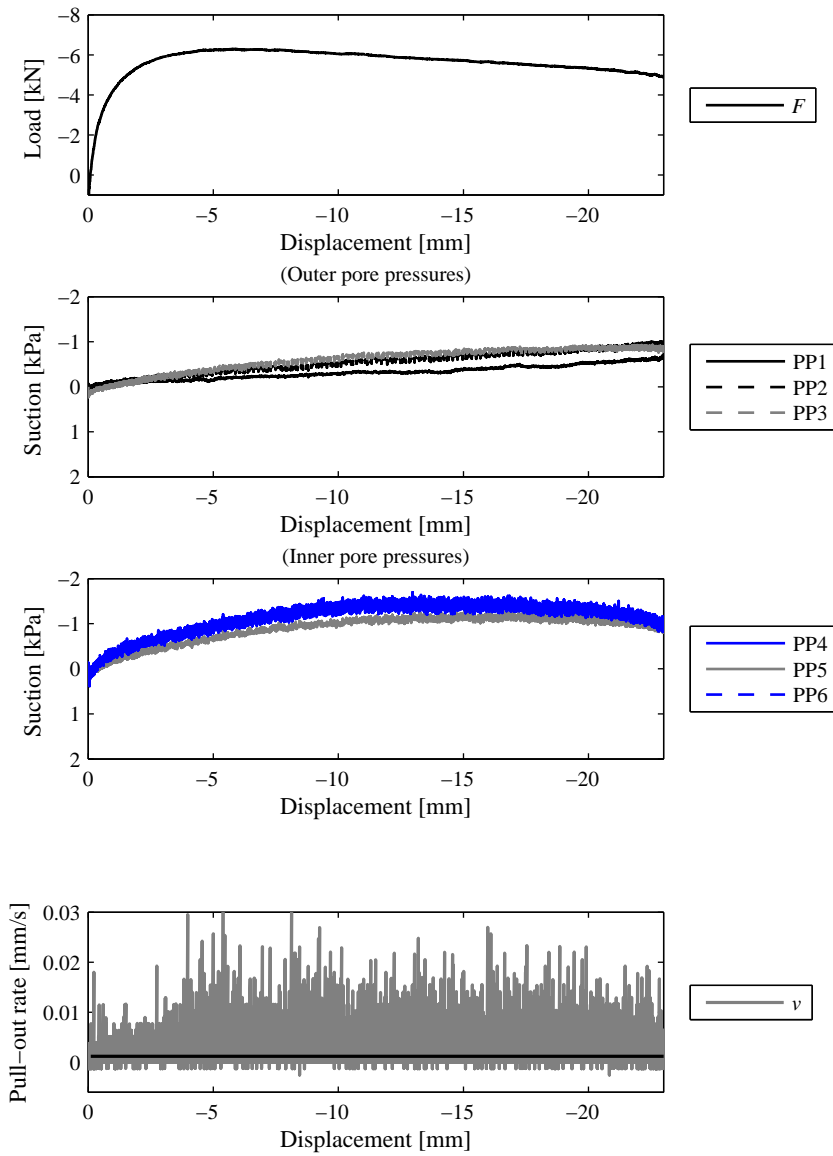


Figure G.88: Loading 13.02.07.

G.3.8 Test 13.02.08

Soil properties			Loading			Installation		
D_R	[%]	84.3	F_T	[kN]	-5.3	F_P	[kN]	49.5
σ of D_R	[%]	4.0	w_T	[mm]	-4.6	d_{inst}	[mm]	473.0
γ	[kN/m ³]	19.6	v	[mm/s]	0.002	Membrane pressure		
γ'	[kN/m ³]	9.6				p_m	[kPa]	0

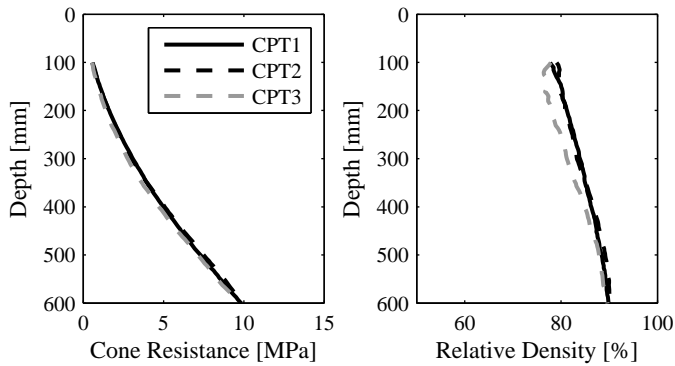


Figure G.89: CPT testing 13.02.08.

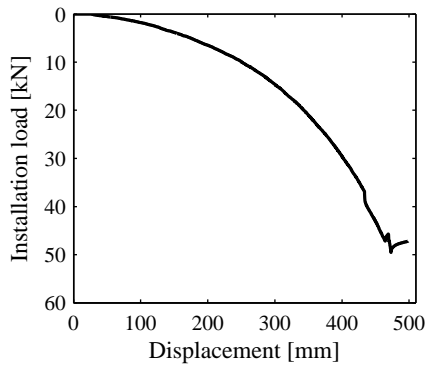


Figure G.90: Installation 13.02.08.

Comments:

Pore pressure transducer PP1 did not function.

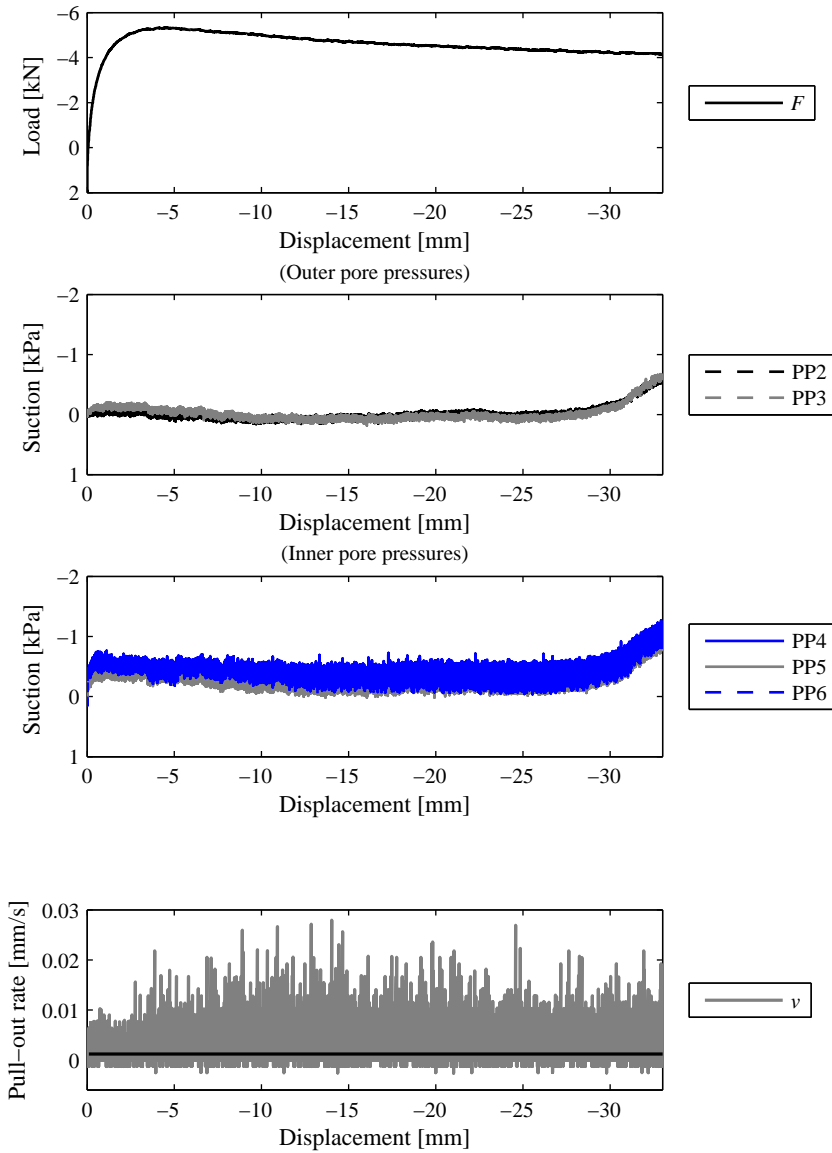


Figure G.91: Loading 13.02.08.

G.3.9 Test 13.02.09

Soil properties			Loading			Installation		
D_R	[%]	81.3	F_T	[kN]	-28.2	F_P	[kN]	68.3
σ of D_R	[%]	3.2	w_T	[mm]	-5.0	d_{inst}	[mm]	487.0
γ	[kN/m ³]	19.4	v	[mm/s]	0.001	Membrane pressure		
γ'	[kN/m ³]	9.4				p_m	[kPa]	41

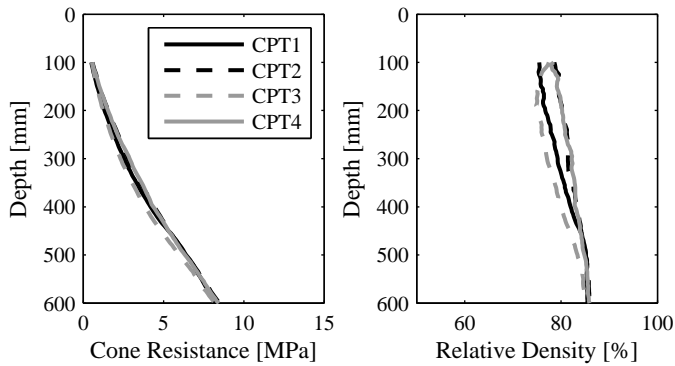


Figure G.92: CPT testing 13.02.09.

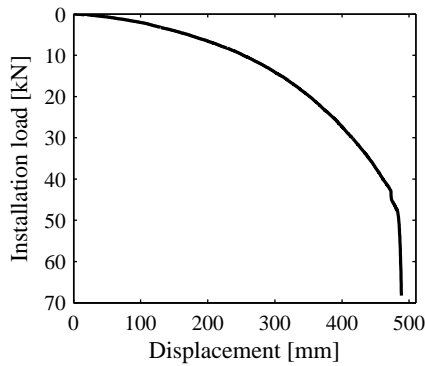


Figure G.93: Installation 13.02.09.

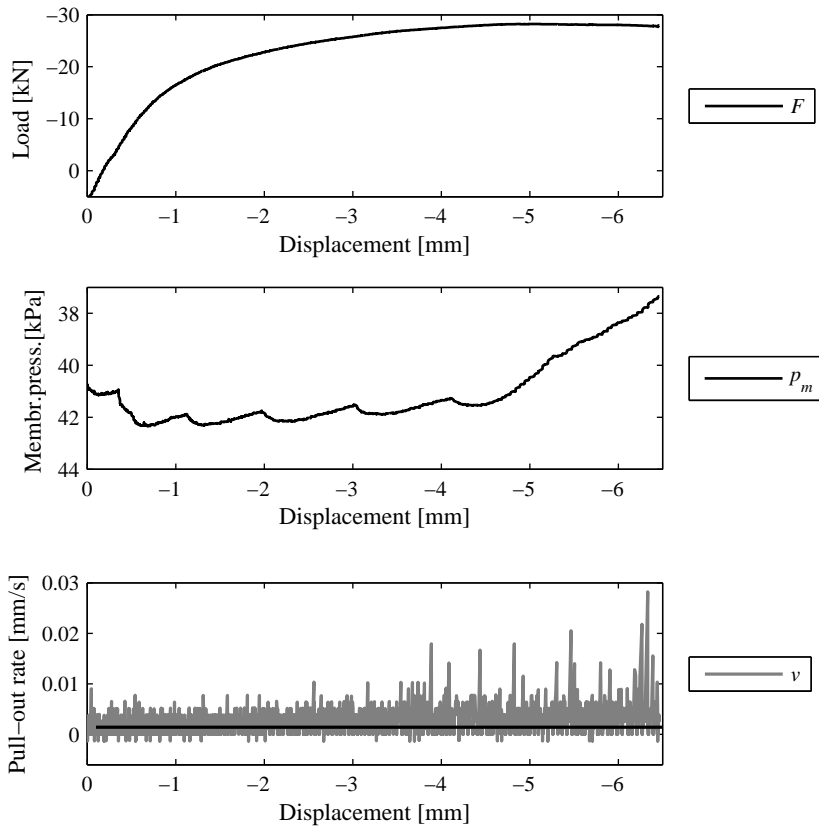


Figure G.94: Loading 13.02.09.

G.3.10 Test 13.02.10

Soil properties			Loading			Installation		
D_R	[%]	85.5	F_T	[kN]	-27.7	F_P	[kN]	203
σ of D_R	[%]	4.8	w_T	[mm]	-3.9	d_{inst}	[mm]	980.0
γ	[kN/m ³]	19.6	v	[mm/s]	0.001	Membrane pressure		
γ'	[kN/m ³]	9.6				p_m	[kPa]	0

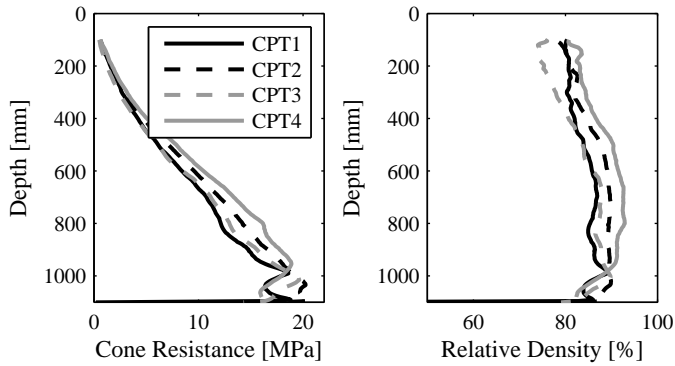


Figure G.95: CPT testing 13.02.10.

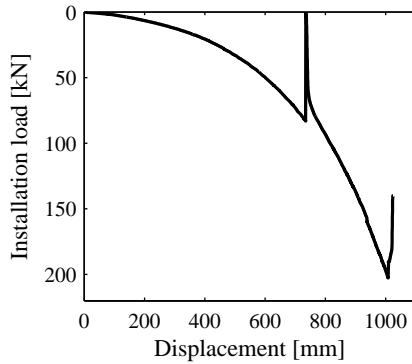


Figure G.96: Installation 13.02.10.

Comments:

Bucket $d/D = 1$. Installation performed in two steps due to insufficient piston length.

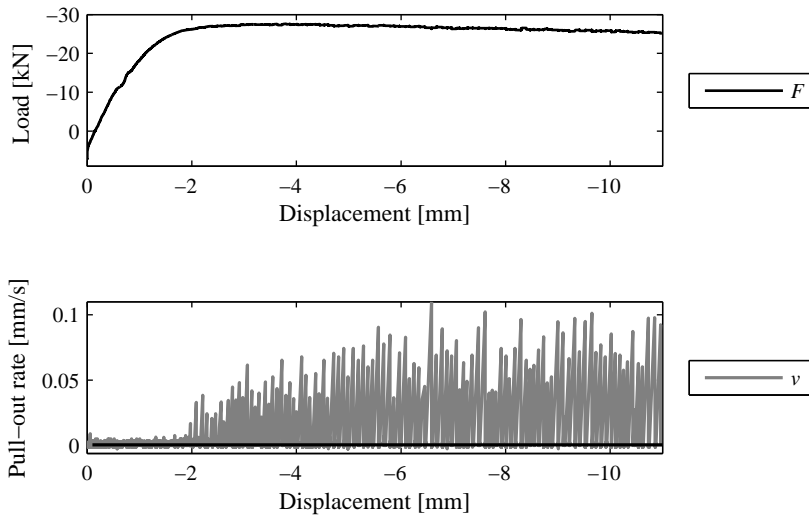


Figure G.97: Loading 13.02.10.

G.3.11 Test 13.02.11

Soil properties			Loading			Installation		
D_R	[%]	79.3	F_T	[kN]	-23.3	F_P	[kN]	57.3
σ of D_R	[%]	3.0	w_T	[mm]	-7.5	d_{inst}	[mm]	487.0
γ	[kN/m ³]	19.3	v	[mm/s]	0.002	Membrane pressure		
γ'	[kN/m ³]	9.3				p_m	[kPa]	20

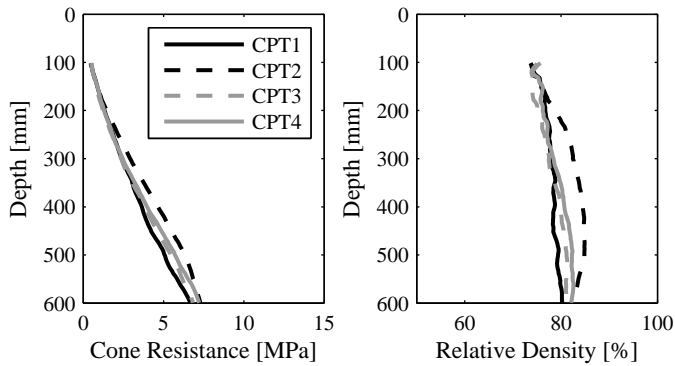


Figure G.98: CPT testing 13.02.11.

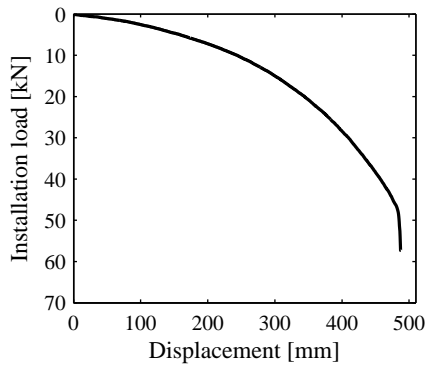


Figure G.99: Installation 13.02.11.

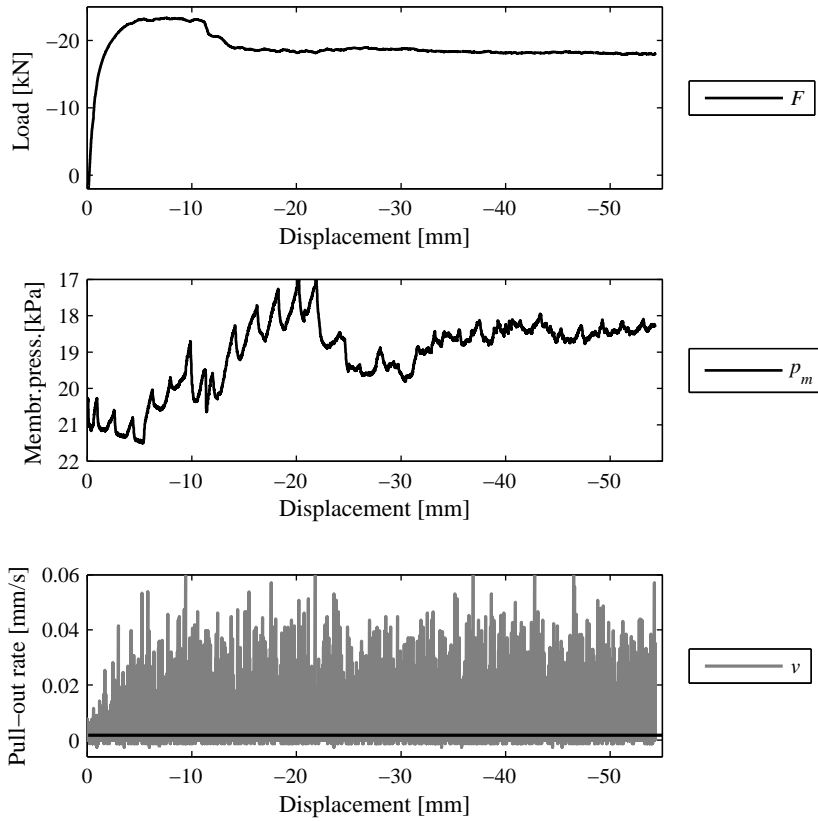


Figure G.100: Loading 13.02.11.

G.3.12 Test 13.02.12

Soil properties			Loading			Installation		
D_R	[%]	79.3	F_T	[kN]	-26.9	F_P	[kN]	72.8
σ of D_R	[%]	4.0	w_T	[mm]	-5.2	d_{inst}	[mm]	487.0
γ	[kN/m ³]	19.3	v	[mm/s]	0.002	Membrane pressure		
γ'	[kN/m ³]	9.3				p_m	[kPa]	40

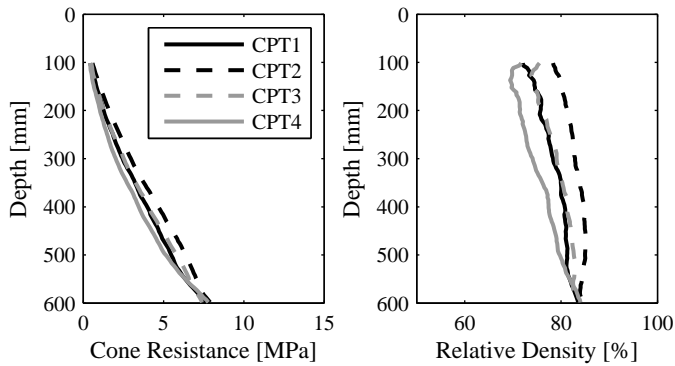


Figure G.101: CPT testing 13.02.12.

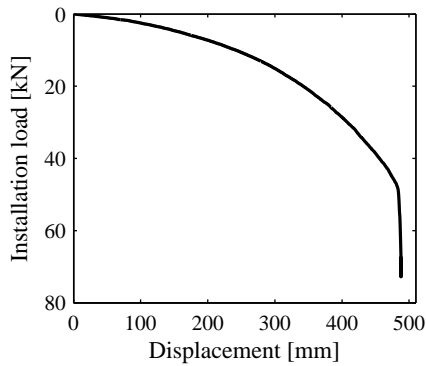


Figure G.102: Installation 13.02.12.

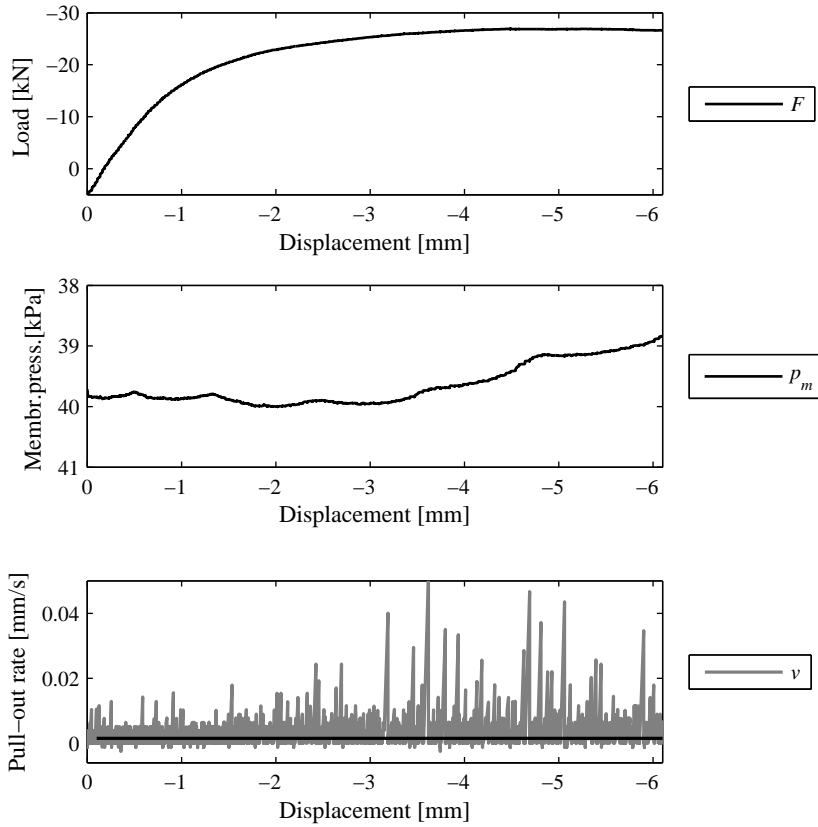


Figure G.103: Loading 13.02.12.

G.3.13 Test 13.02.13

Soil properties			Loading			Installation		
D_R	[%]	82.9	F_T	[kN]	-43.2	F_P	[kN]	70.1
σ of D_R	[%]	6.7	w_T	[mm]	-10.7	d_{inst}	[mm]	493.0
γ	[kN/m ³]	19.5	v	[mm/s]	0.002	Membrane pressure		
γ'	[kN/m ³]	9.5				p_m	[kPa]	68

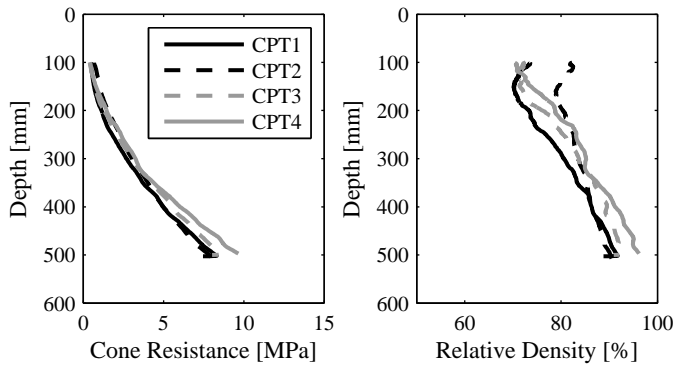


Figure G.104: CPT testing 13.02.13.

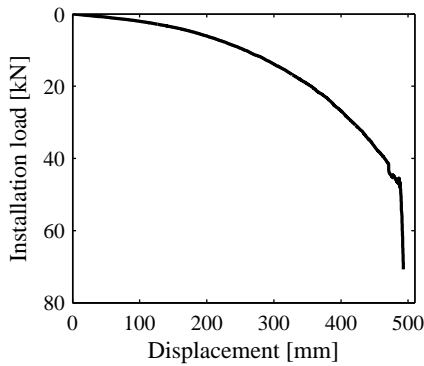


Figure G.105: Installation 13.02.13.

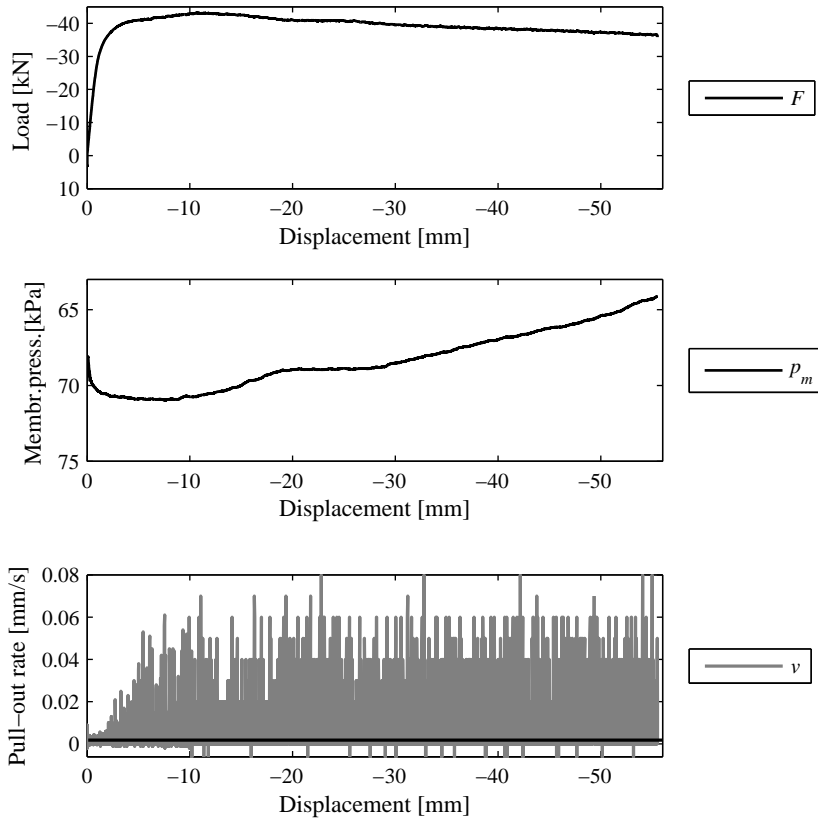


Figure G.106: Loading 13.02.13.

G.3.14 Test 13.02.14

Soil properties			Loading			Installation		
D_R	[%]	83.0	F_T	[kN]	-29.8	F_P	[kN]	220.0
σ of D_R	[%]	3.9	w_T	[mm]	-4.5	d_{inst}	[mm]	990.0
γ	[kN/m ³]	19.5	v	[mm/s]	0.001	Membrane pressure		
γ'	[kN/m ³]	9.5				p_m	[kPa]	0

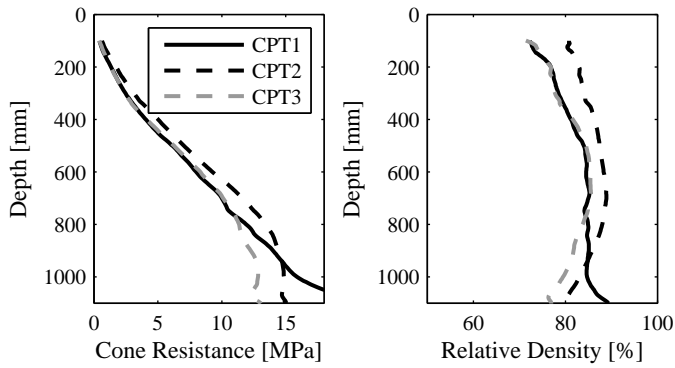


Figure G.107: CPT testing 13.02.14.

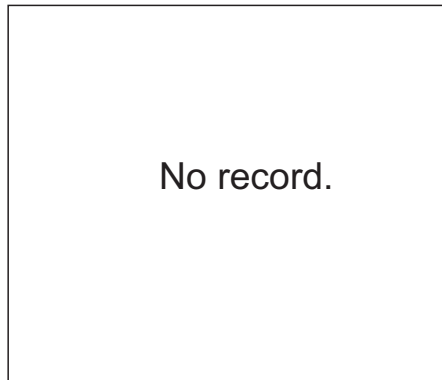


Figure G.108: Installation 13.02.14.

Comments:

Bucket $d/D = 1$. Installation was not recorded, but F_P and d_{inst} were visually observed in the computer screen.

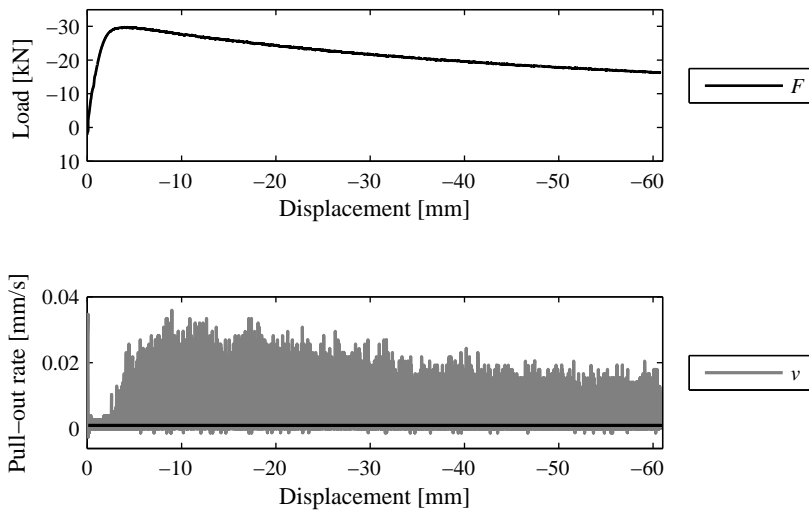


Figure G.109: Loading 13.02.14.

G.3.15 Test 13.02.15

Soil properties			Loading			Installation		
D_R	[%]	85.0	F_T	[kN]	-5.9	F_P	[kN]	73
σ of D_R	[%]	3.8	w_T	[mm]	-5.5	d_{inst}	[mm]	491.0
γ	[kN/m ³]	19.6	v	[mm/s]	0.002	Membrane pressure		
γ'	[kN/m ³]	9.6				p_m	[kPa]	0

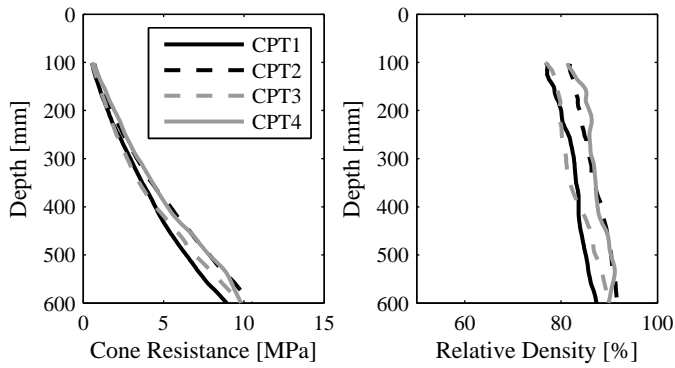


Figure G.110: CPT testing 13.02.15.

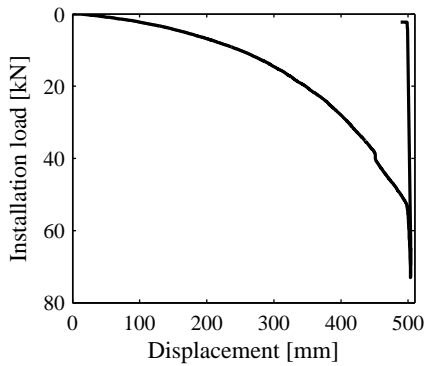


Figure G.111: Installation 13.02.15.

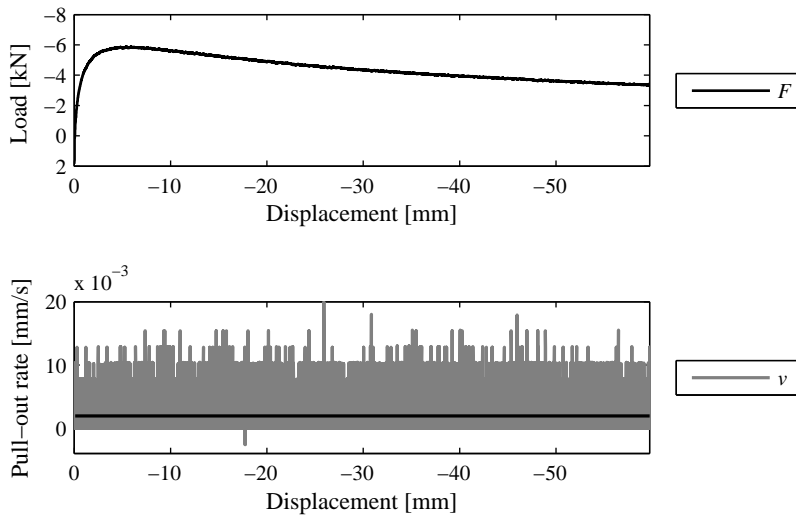


Figure G.112: Loading 13.02.15.

G.3.16 Test 13.02.16

Soil properties			Loading			Installation		
D_R	[%]	77.2	F_T	[kN]	-14.9	F_P	[kN]	70.5
σ of D_R	[%]	12.2	w_T	[mm]	-4.8	d_{inst}	[mm]	493.0
γ	[kN/m ³]	19.2	v	[mm/s]	0.002	Membrane pressure		
γ'	[kN/m ³]	9.2				p_m	[kPa]	0

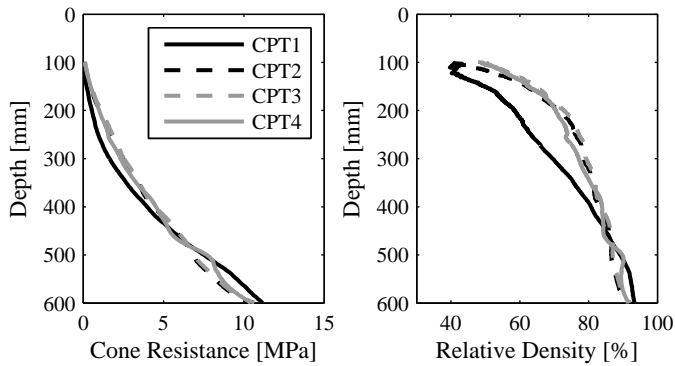


Figure G.113: CPT testing 13.02.16.

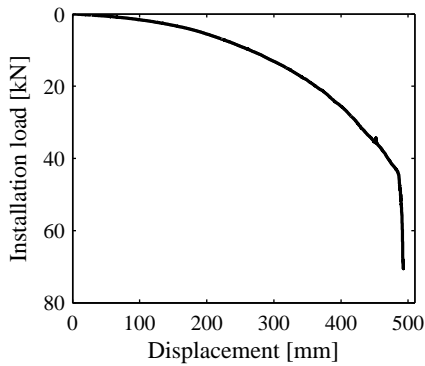


Figure G.114: Installation 13.02.16.

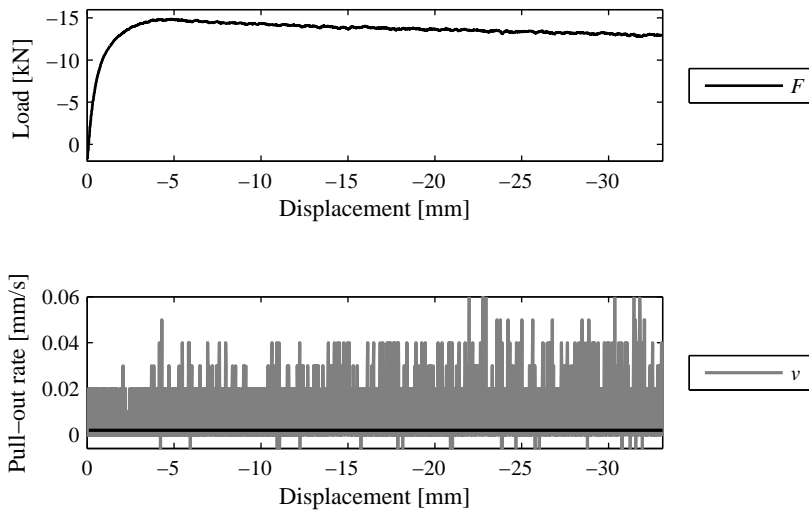


Figure G.115: Loading 13.02.16.

G.3.17 Test 13.02.17

Soil properties			Loading			Installation		
D_R	[%]	83.4	F_T	[kN]	-96.3	F_P	[kN]	74.0
σ of D_R	[%]	3.3	w_T	[mm]	-72.2	d_{inst}	[mm]	490.0
γ	[kN/m ³]	19.5	v	[mm/s]	0.002	Membrane pressure		
γ'	[kN/m ³]	9.5				p_m	[kPa]	73

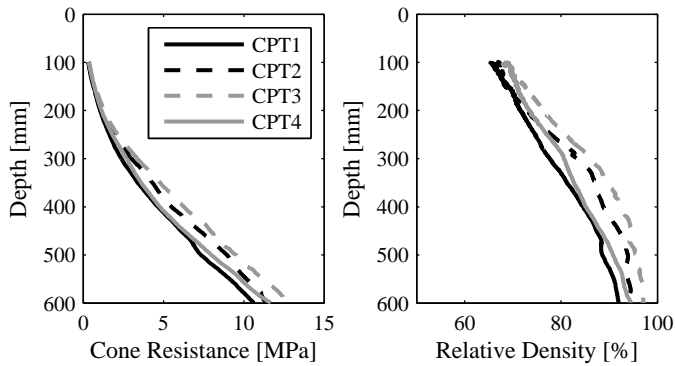


Figure G.116: CPT testing 13.02.17.

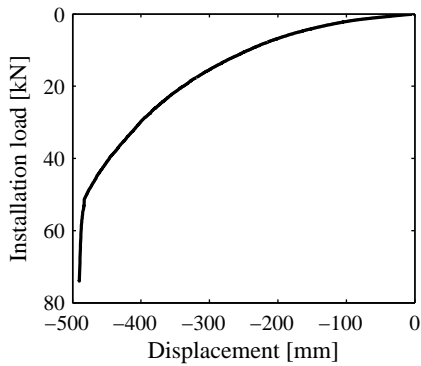


Figure G.117: Installation 13.02.17.

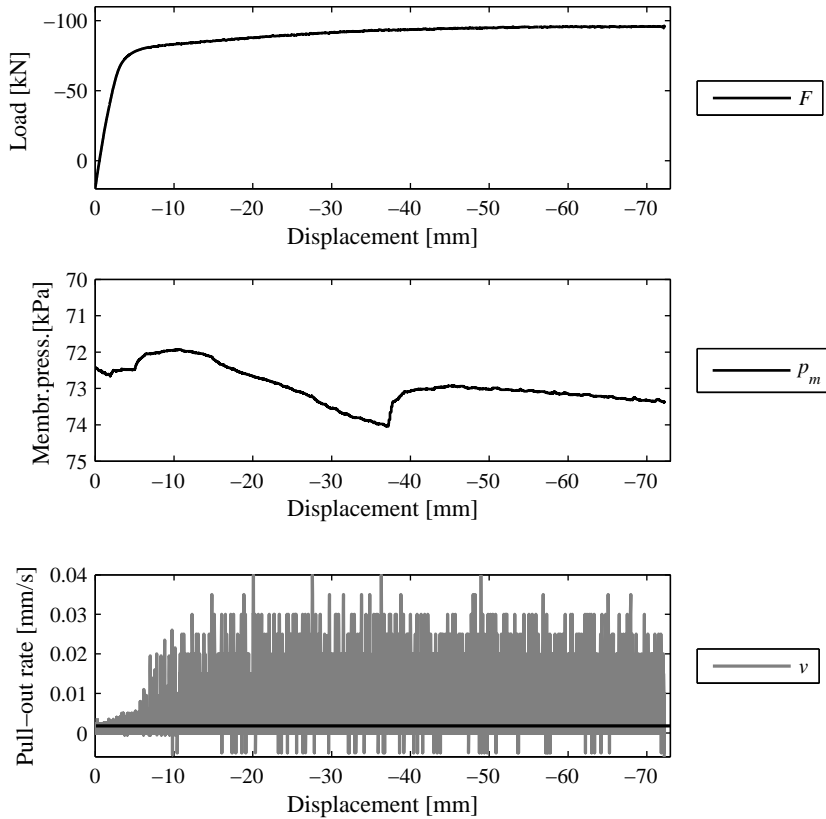


Figure G.118: Loading 13.02.17.

G.4 Test Series 13.03.XX Overview

Series 13.03.XX present cyclic loading tests on a bucket foundation model. This chapter provides the data of tests performed in the large yellow sand box. Bucket model dimensions were: 1.0 m in diameter D , 0.5 mm in skirt length d and 3 mm in skirt thickness t . Figure G.64 shows the test set-up. Figure G.66 shows the bucket foundation model. Figure G.65 shows the positions of the laboratory CPT samplings. Vaitkunaite 2015 described the testing procedure.

Table G.3: Test series 13.03.XX summary.

p_m [kPa]	Test No.	Cyclic loading				Post-cyclic load		D_R [%]	γ' [kN/m ³]
		F_{mean} [kN]	F_{cyc} [kN]	w_{cyc} [mm]	f [Hz]	F_{Pc} [kN]	w_{Pc} [mm]		
0	13.03.01	-2.11	1.02	-0.88	0.10	-5.34	-3.83	78	9.3
0	13.03.02	-2.05	1.93	-1.35	0.10	-5.95	-7.60	77	9.2
0	13.03.03	-2.05	3.85	-63.76	0.10	-	-	79	9.3
0	13.03.05	1.80	3.85	0.15	0.10	-	-	85	9.6
43	13.03.06	11.76	11.38	0.72	0.05	-31.33	-12.35	80	9.3
0	13.03.08	1.91	2.30	0.04	0.05	-5.03	-3.43	77	9.3
41	13.03.09	-13.03	18.37	-67.55	0.10	-	-	(75)	(9.1)
0	13.03.10	-2.05	1.93	-6.23	0.10	-4.74	-0.53	(75)	(9.1)
41	13.03.11	20.12	9.33	-63.81	0.10	-	-	82	9.4
0	13.03.12	-2.05	3.85	-65.80	0.10	-	-	(79)	(9.3)
71	13.03.13	2.01	29.38	0.74	0.05	-	-	82	9.5
70	13.03.14	1.92	29.30	1.25	0.10	-93.26	-28.29	82	9.4
73	13.03.15	-22.39	23.08	0.10	0.10	-93.90	-26.53	87	9.7
71	13.03.16	-51.67	24.49	-75.01	0.10	-	-	79	9.3
71	13.03.17	-50.61	45.78	-81.90	0.10	-	-	81	9.4
0	13.03.19	-0.30	1.66	-0.64	0.10	(-3.49)	-8.66	79	9.3
0	13.03.20	1.80	3.85	0	0.10	-4.85	-1.30	81	9.4
0	13.03.21	0	1.00	-0.29	0.10	-4.86	-4.84	81	9.4

G.4.1 Test 13.03.01

Soil properties			Loading		
D_R	[%]	77.8	F_{mean}	[kN]	-2.11
σ of D_R	[%]	5.5	F_{cyc}	[kN]	1.02
γ	[kN/m ³]	19.3	w_{cyc}	[mm]	-0.88
γ'	[kN/m ³]	9.3	f	[Hz]	0.10
Installation			f_s	[Hz]	0.04-1
F_P	[kN]	52.4	N	[-]	39,592
d_{inst}	[mm]	486	F_{Pc}	[kN]	-5.34
Membrane pressure			w_{Pc}	[mm]	-3.83
p_m	[kPa]	0	v	[mm/s]	0.002

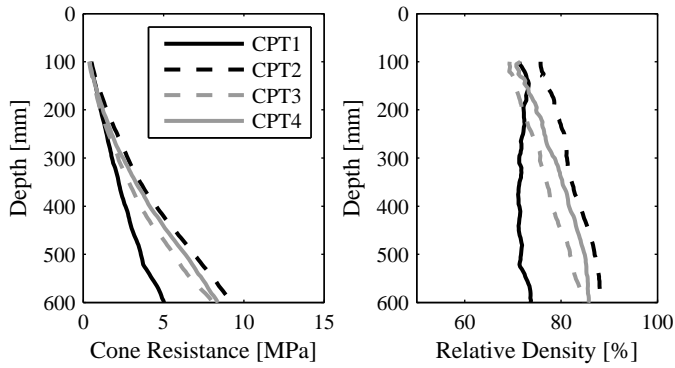


Figure G.119: CPT testing 13.03.01.

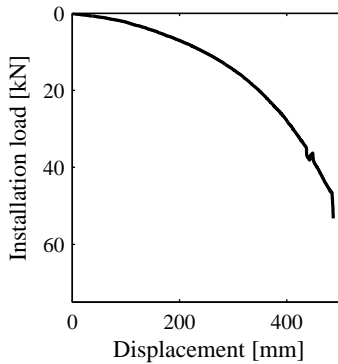


Figure G.120: Installation 13.03.01.

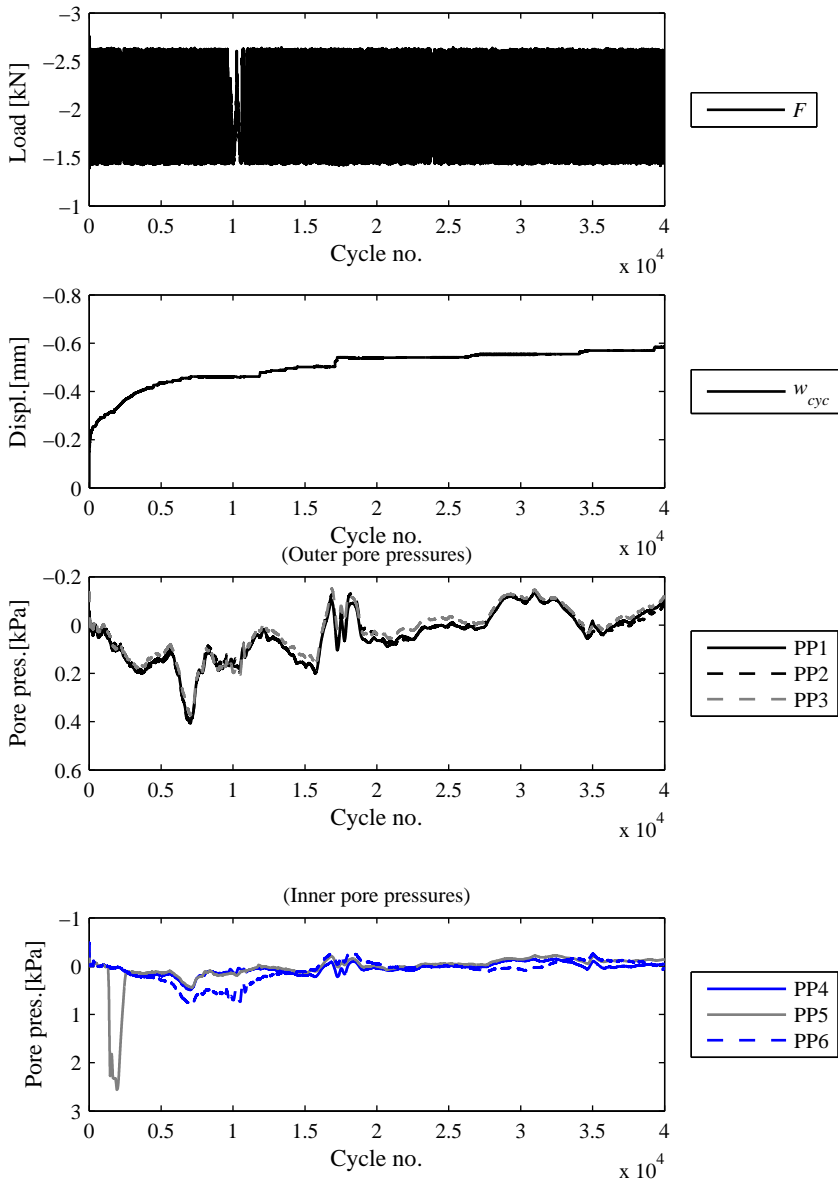


Figure G.121: Cyclic loading part 13.03.01.

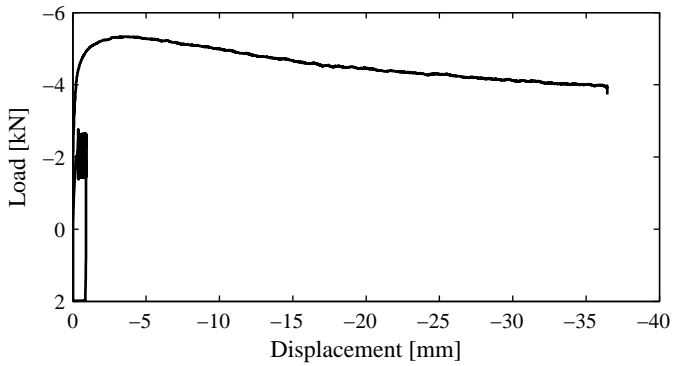


Figure G.122: Full loading vs. displacement 13.03.01.

Comments:

Problems in data sampling caused by an error in the data acquisition system. After cyclic loading the equipment stopped (unloading). Some hours later, the post-cyclic loading started.

G.4.2 Test 13.03.02

Soil properties			Loading		
D_R	[%]	76.9	F_{mean}	[kN]	-2.05
σ of D_R	[%]	5.3	F_{cyc}	[kN]	1.93
γ	[kN/m ³]	19.2	w_{cyc}	[mm]	-1.35
γ'	[kN/m ³]	9.2	f	[Hz]	0.10
Installation			f_s	[Hz]	0.05-1
F_P	[kN]	71	N	[-]	38,227
d_{inst}	[mm]	-	F_{Pc}	[kN]	-5.95
Membrane pressure			w_{Pc}	[mm]	-7.60
p_m	[kPa]	0	v	[mm/s]	0.002

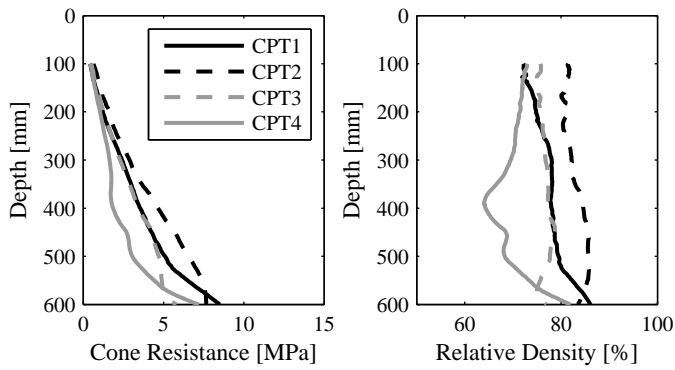


Figure G.123: CPT testing 13.03.02.

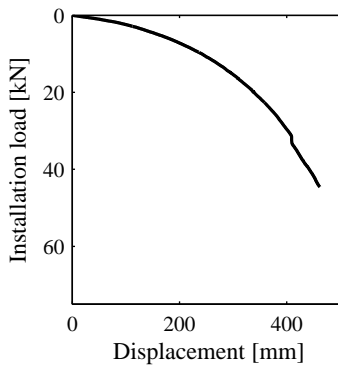


Figure G.124: Installation 13.03.02.

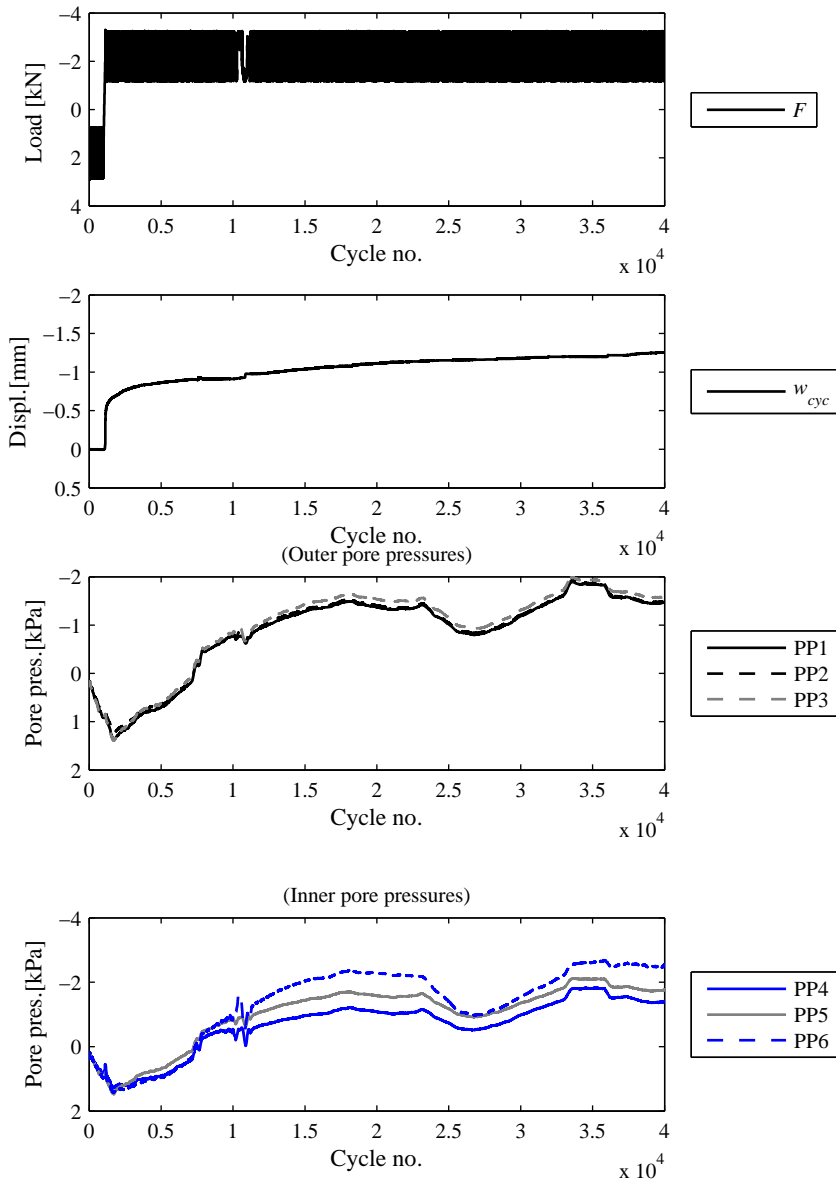


Figure G.125: Cyclic loading part 13.03.02.

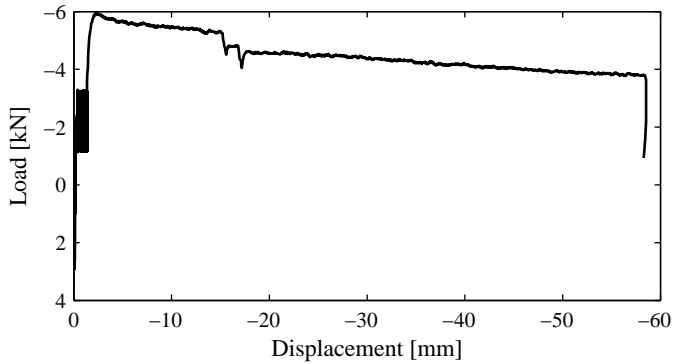


Figure G.126: Full loading vs. displacement 13.03.02.

Comments:

Installation response is not full, the final pre-load was observed in the computer screen. During the first 950 cycles, the cyclic mean load was +2.05 kN (compressive). Problems in data sampling caused by an error in the data acquisition system.

G.4.3 Test 13.03.03

Soil properties			Loading		
D_R	[%]	78.7	F_{mean}	[kN]	-2.05
σ of D_R	[%]	4.8	F_{cyc}	[kN]	3.85
γ	[kN/m ³]	19.3	w_{cyc}	[mm]	-63.76
γ'	[kN/m ³]	9.3	f	[Hz]	0.10
Installation			f_s	[Hz]	0.1-1
F_P	[kN]	71	N	[-]	8,100
d_{inst}	[mm]	492	F_{Pc}	[kN]	-
Membrane pressure			w_{Pc}	[mm]	-
p_m	[kPa]	0	v	[mm/s]	-

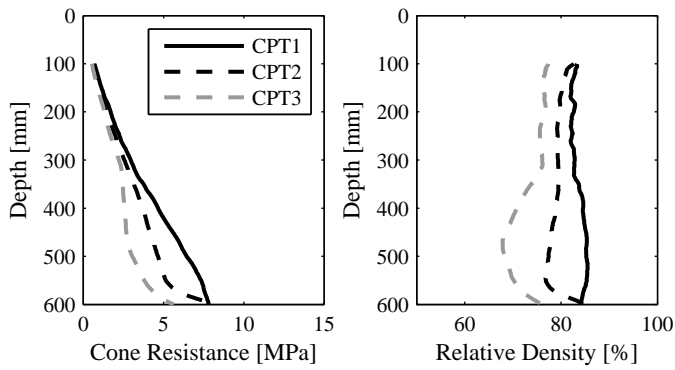


Figure G.127: CPT testing 13.03.03.

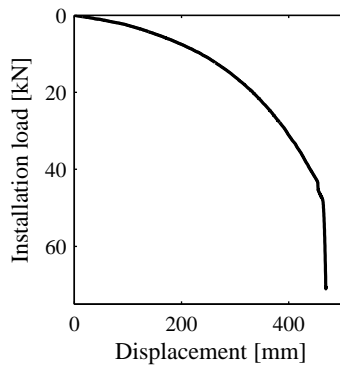


Figure G.128: Installation 13.03.03.

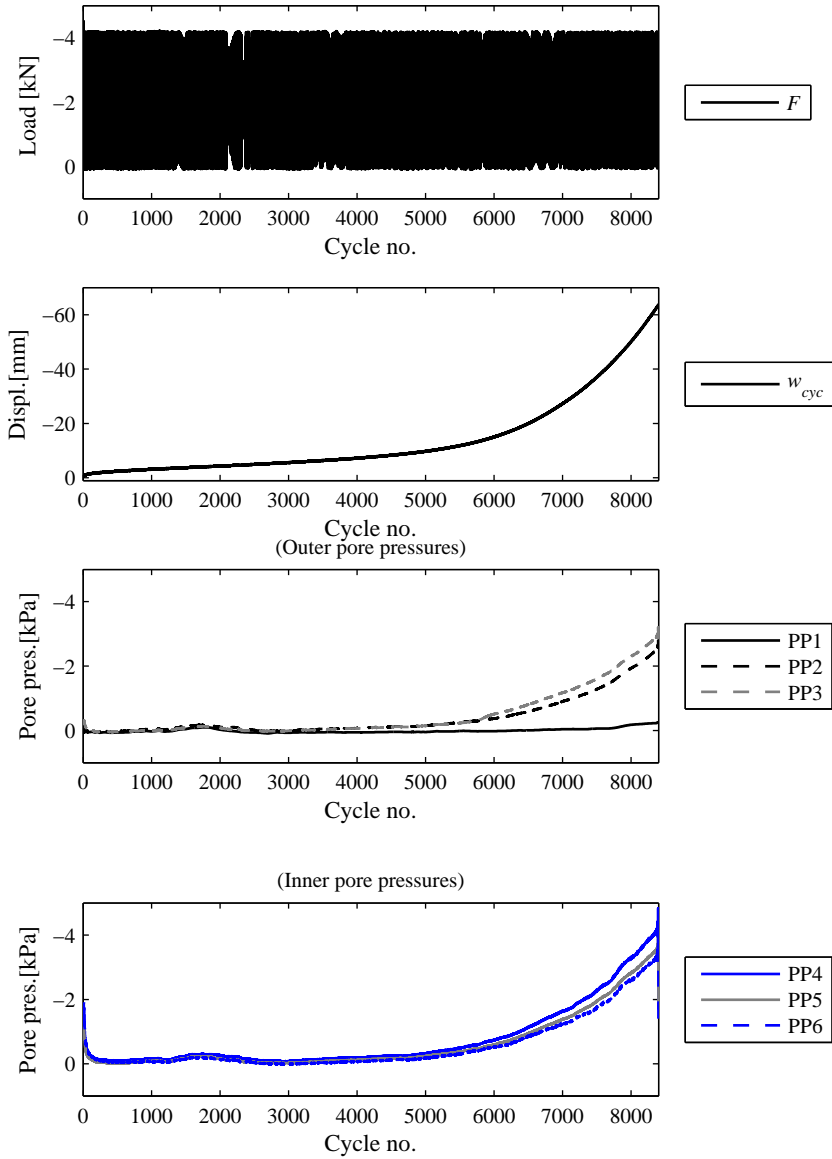


Figure G.129: Cyclic loading part 13.03.03.

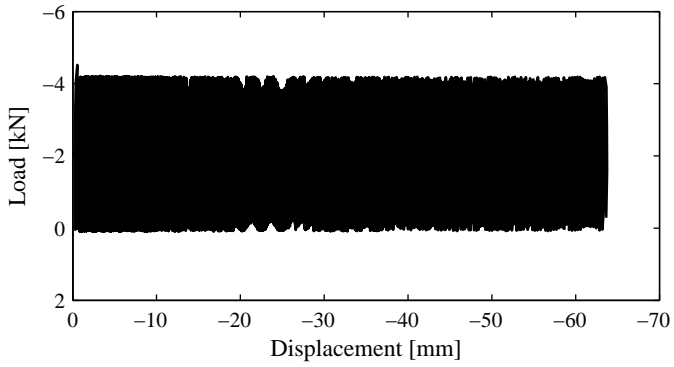


Figure G.130: Full loading vs. displacement 13.03.03.

Comments:

Problems in data sampling caused by an error in the data acquisition system.

G.4.4 Test 13.03.05

Soil properties			Loading		
D_R	[%]	85.3	F_{mean}	[kN]	1.80
σ of D_R	[%]	3.8	F_{cyc}	[kN]	3.85
γ	[kN/m ³]	19.6	w_{cyc}	[mm]	0.15
γ'	[kN/m ³]	9.6	f	[Hz]	0.1
Installation			f_s	[Hz]	2
F_P	[kN]	72	N	[-]	28,263
d_{inst}	[mm]	482	F_{Pc}	[kN]	-
Membrane pressure			w_{Pc}	[mm]	-
p_m	[kPa]	0	v	[mm/s]	0.002

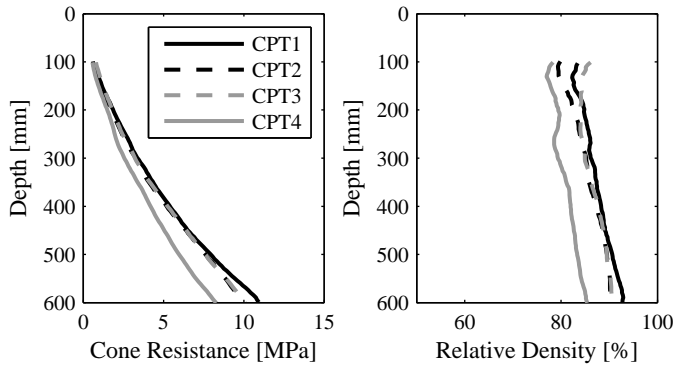


Figure G.131: CPT testing 13.03.05.

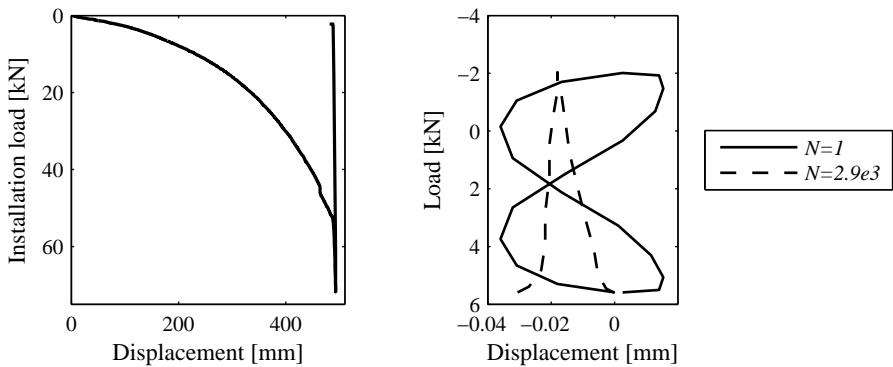


Figure G.132: Installation 13.03.05.

Figure G.133: Cyclic behaviour 13.03.05.

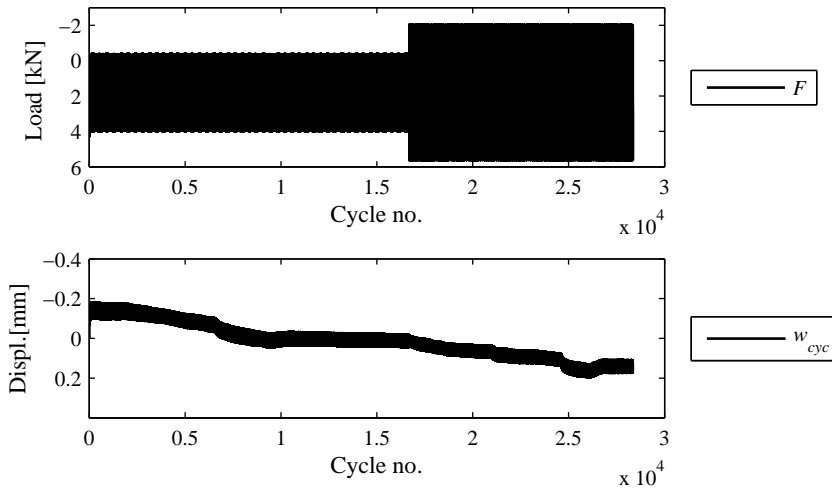


Figure G.134: Cyclic loading part 13.03.05.

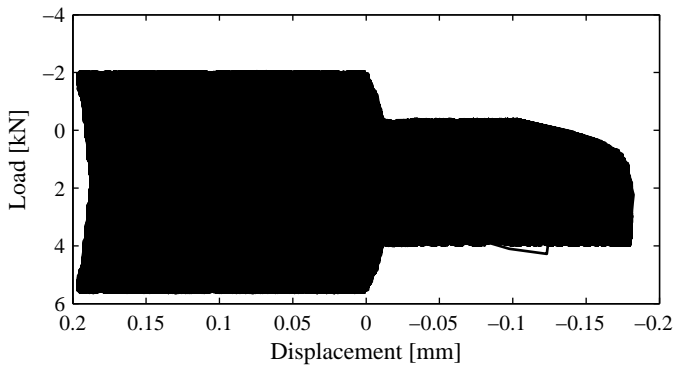


Figure G.135: Full loading vs. displacement 13.03.05.

Comments:

A sudden pull-out after 28,263 cycles, must be some technical mistake.

G.4.5 Test 13.03.06

Soil properties			Loading		
D_R	[%]	79.9	F_{mean}	[kN]	11.76
σ of D_R	[%]	4.3	F_{cyc}	[kN]	11.38
γ	[kN/m ³]	19.3	w_{cyc}	[mm]	0.72
γ'	[kN/m ³]	9.3	f	[Hz]	0.05
Installation			f_s	[Hz]	2
F_P	[kN]	70.9	N	[-]	19,900
d_{inst}	[mm]	493	F_{Pc}	[kN]	-31.33
Membrane pressure			w_{Pc}	[mm]	-12.35
p_m	[kPa]	43	v	[mm/s]	0.002

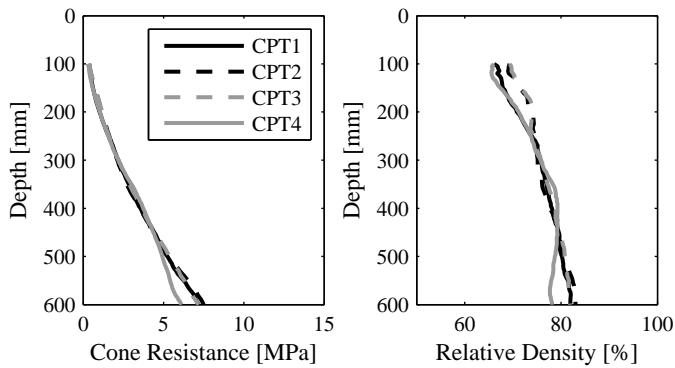


Figure G.136: CPT testing 13.03.06.

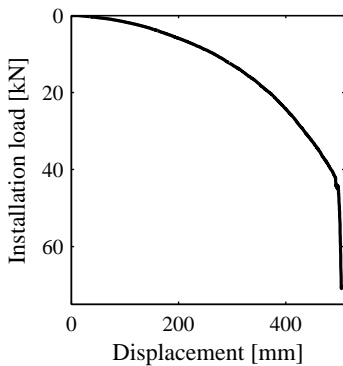


Figure G.137: Installation 13.03.06.

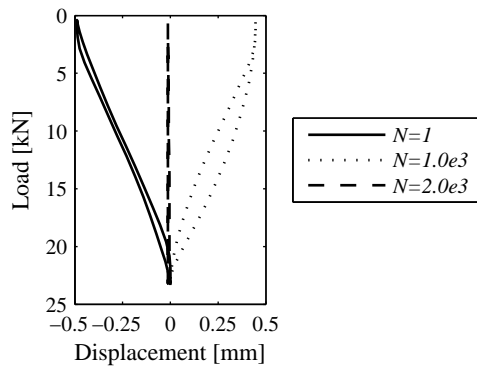


Figure G.138: Cyclic behaviour 13.03.06.

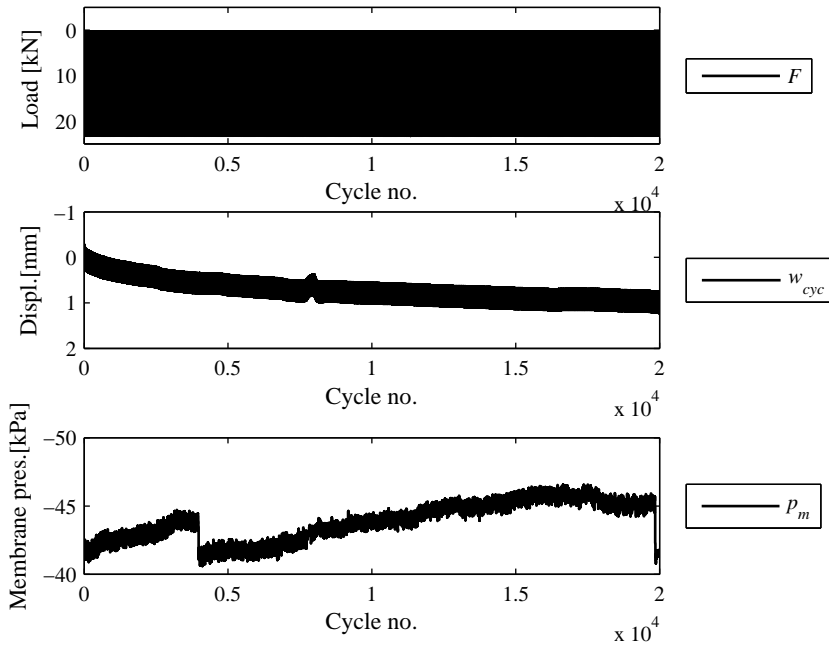


Figure G.139: Cyclic loading part 13.03.06.

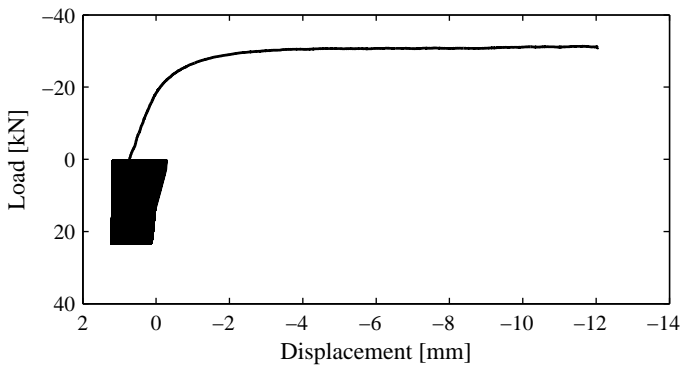


Figure G.140: Full loading vs. displacement 13.03.06.

G.4.6 Test 13.03.08

Soil properties			Loading		
D_R	[%]	76.9	F_{mean}	[kN]	1.91
σ of D_R	[%]	8.1	F_{cyc}	[kN]	2.30
γ	[kN/m ³]	19.3	w_{cyc}	[mm]	0.04
γ'	[kN/m ³]	9.3	f	[Hz]	0.05
Installation			f_s	[Hz]	2
F_P	[kN]	70.4	N	[-]	19,629
d_{inst}	[mm]	493	F_{Pc}	[kN]	-5.03
Membrane pressure			w_{Pc}	[mm]	-3.43
p_m	[kPa]	0	v	[mm/s]	0.002

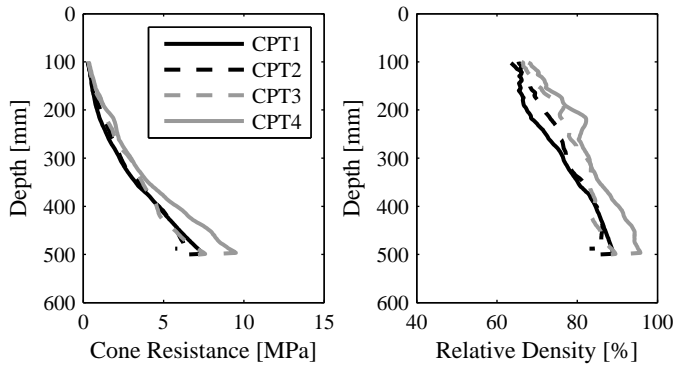


Figure G.141: CPT testing 13.03.08.

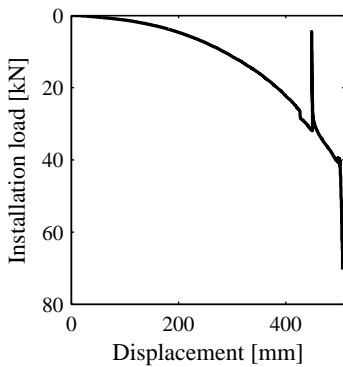


Figure G.142: Installation 13.03.08.

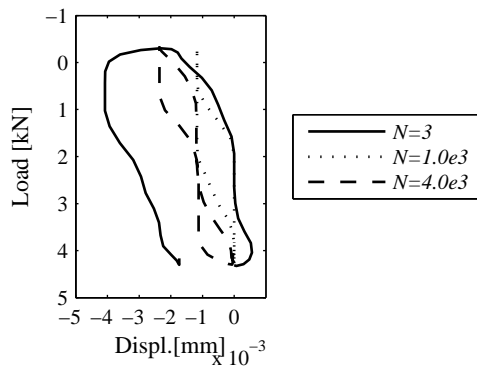


Figure G.143: Cyclic behaviour 13.03.08.

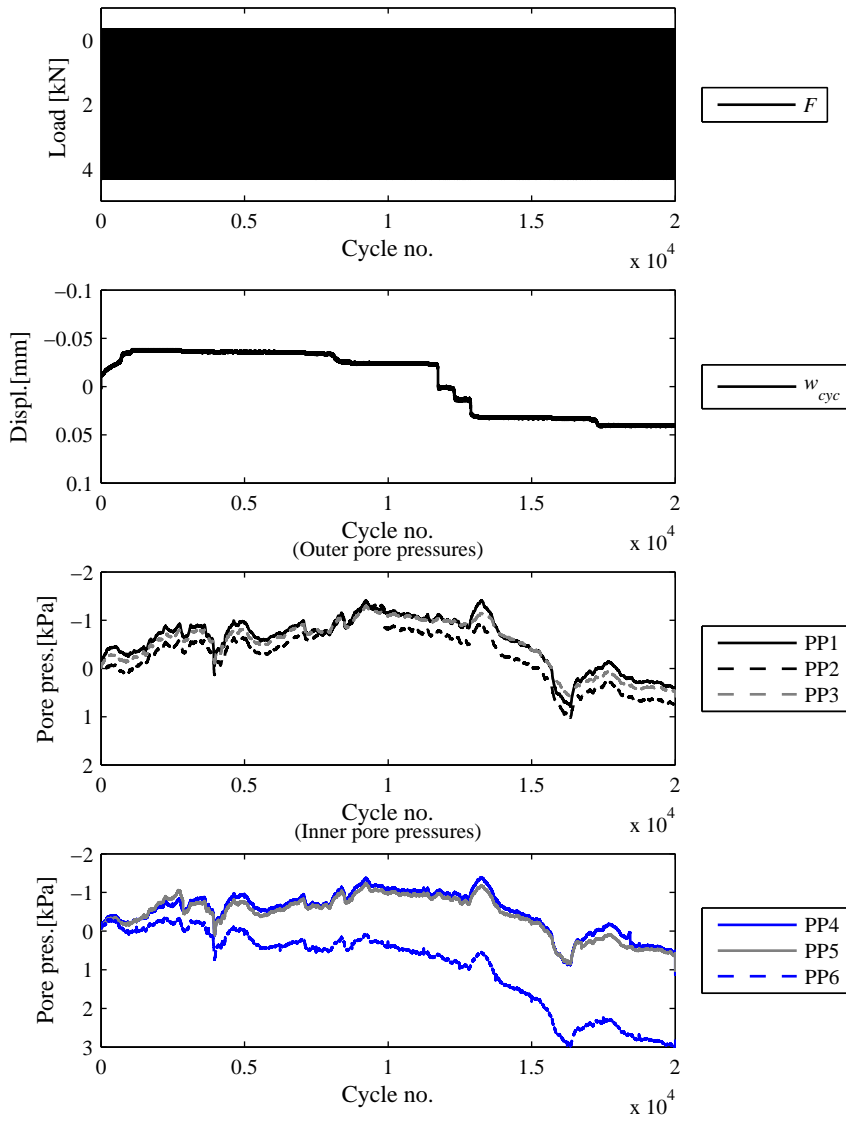


Figure G.144: Cyclic loading part 13.03.08.

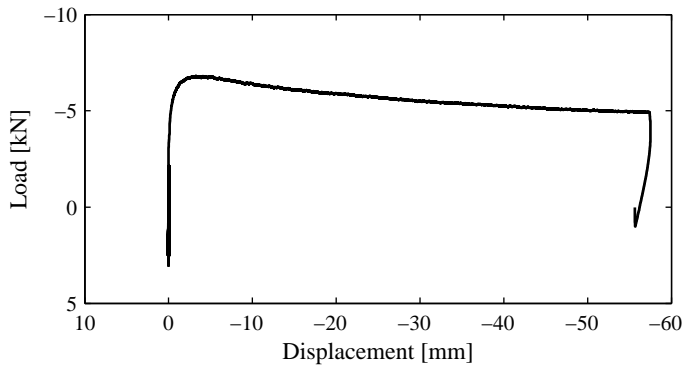


Figure G.145: Full loading vs. displacement 13.03.08.

Comments:

Problems in data sampling caused by an error in the data acquisition system: load and displacement signals were not taken at the very same moment. Thus, cyclic behaviour cannot be assessed precisely.

G.4.7 Test 13.03.09

Soil properties			Loading		
D_R	[%]	(75)	F_{mean}	[kN]	-13.03
σ of D_R	[%]	-	F_{cyc}	[kN]	18.37
γ	[kN/m ³]	(19.1)	w_{cyc}	[mm]	-67.55
γ'	[kN/m ³]	(9.1)	f	[Hz]	0.1
Installation			f_s	[Hz]	2
F_P	[kN]	70.6	N	[-]	67
d_{inst}	[mm]	488	F_{Pc}	[kN]	-
Membrane pressure			w_{Pc}	[mm]	-
p_m	[kPa]	41	v	[mm/s]	-

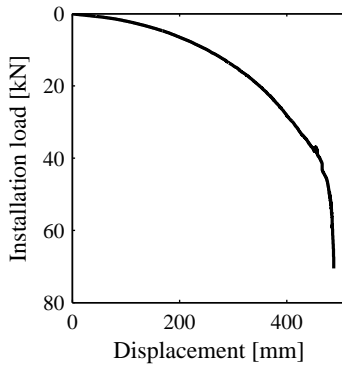


Figure G.146: Installation 13.03.09.

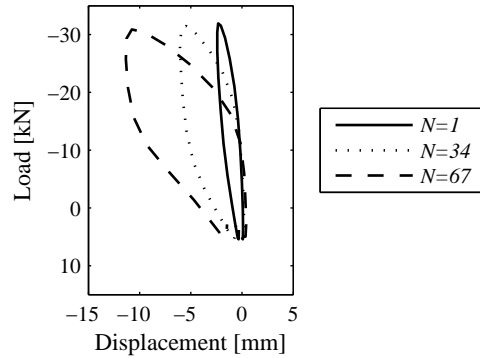


Figure G.147: Cyclic behaviour 13.03.09.

Comments:

CPT was not performed due to technical problems, approximate properties are estimated from the installation response.

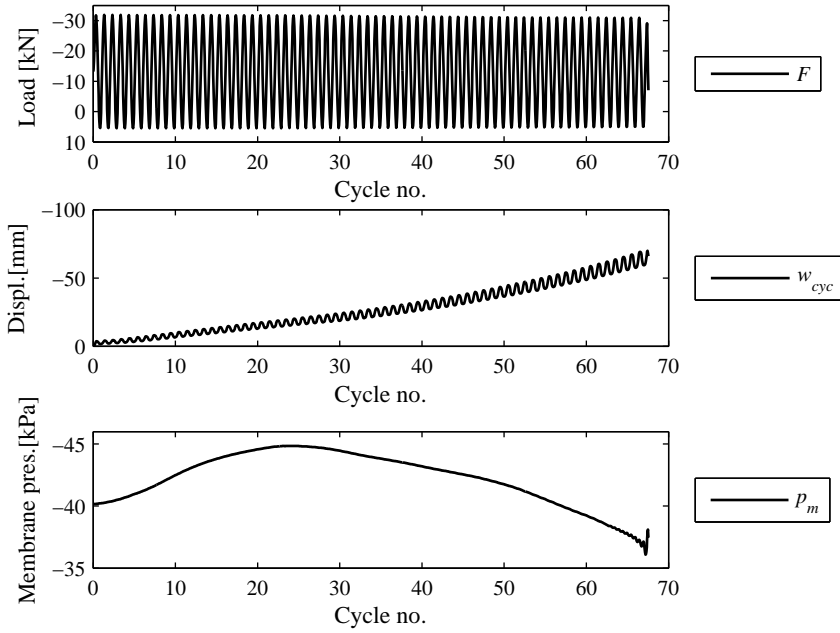


Figure G.148: Cyclic loading part 13.03.09.

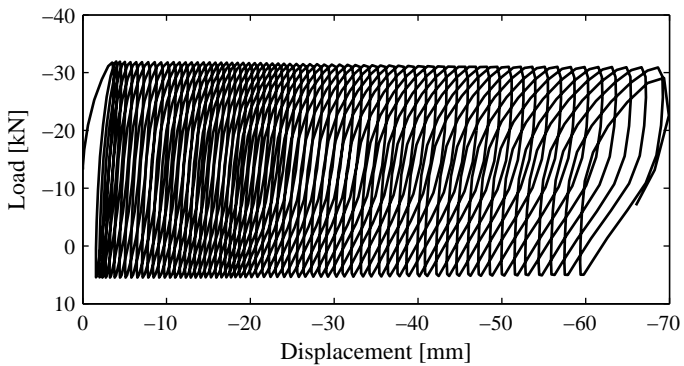


Figure G.149: Full loading vs. displacement 13.03.09.

G.4.8 Test 13.03.10

Soil properties			Loading		
D_R	[%]	(75)	F_{mean}	[kN]	-2.05
σ of D_R	[%]	-	F_{cyc}	[kN]	1.93
γ	[kN/m ³]	(19.1)	w_{cyc}	[mm]	-6.23
γ'	[kN/m ³]	(9.1)	f	[Hz]	0.10
Installation			f_s	[Hz]	2
\bar{F}_P	[kN]	70.5	N	[-]	39,753
d_{inst}	[mm]	495	F_{Pc}	[kN]	-4.74
Membrane pressure			w_{Pc}	[mm]	-0.53
p_m	[kPa]	0	v	[mm/s]	0.002

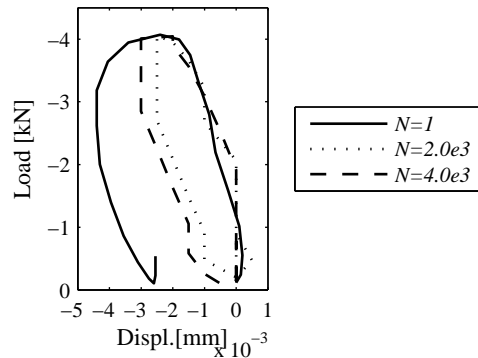
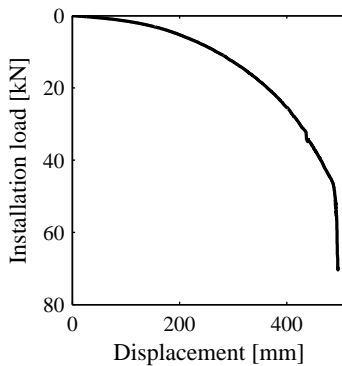


Figure G.150: Installation 13.03.10.

Figure G.151: Cyclic behaviour 13.03.10.

Comments:

CPT was not performed due to technical problems. Problems in data sampling caused by an error in the data acquisition system: load and displacement signals were not taken at the very same moment. Thus, cyclic behaviour cannot be assessed precisely.

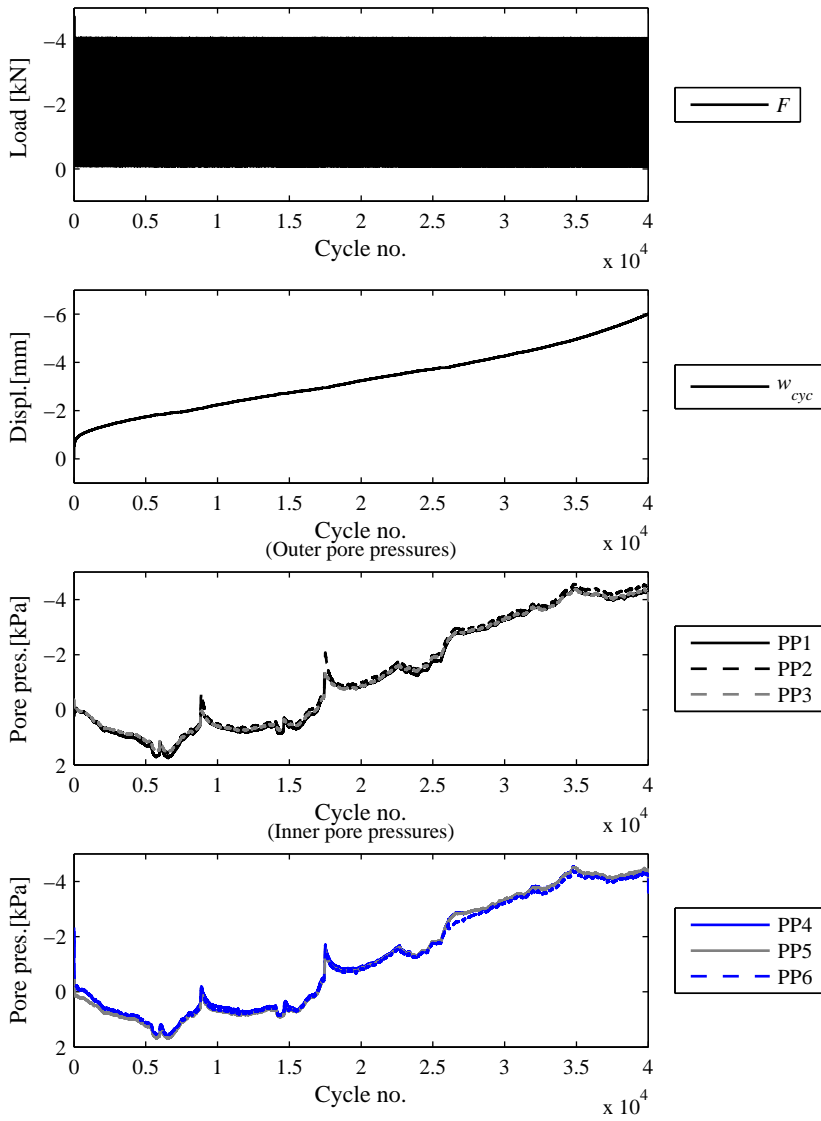


Figure G.152: Cyclic loading part 13.03.10.

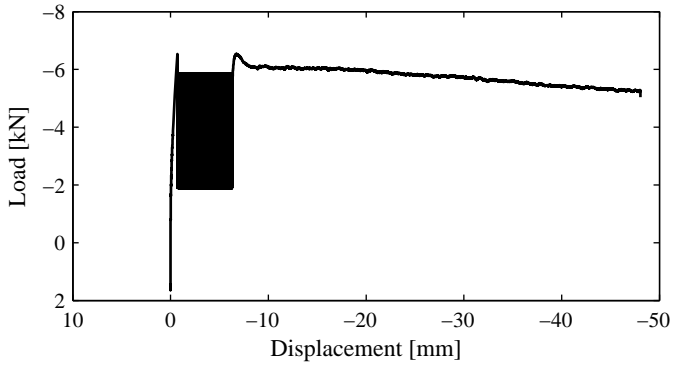


Figure G.153: Full loading vs. displacement 13.03.10.

G.4.9 Test 13.03.11

Soil properties			Loading		
D_R	[%]	81.9	F_{mean}	[kN]	20.12
σ of D_R	[%]	8.2	F_{cyc}	[kN]	9.33
γ	[kN/m ³]	19.4	w_{cyc}	[mm]	-63.81
γ'	[kN/m ³]	9.4	f	[Hz]	0.1
Installation			f_s	[Hz]	2
F_P	[kN]	71.2	N	[-]	202
d_{inst}	[mm]	492	F_{Pc}	[kN]	-
Membrane pressure			w_{Pc}	[mm]	-
p_m	[kPa]	41	v	[mm/s]	-

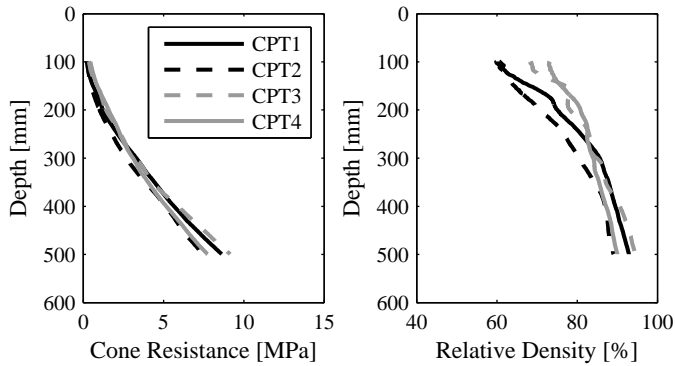


Figure G.154: CPT testing 13.03.11.

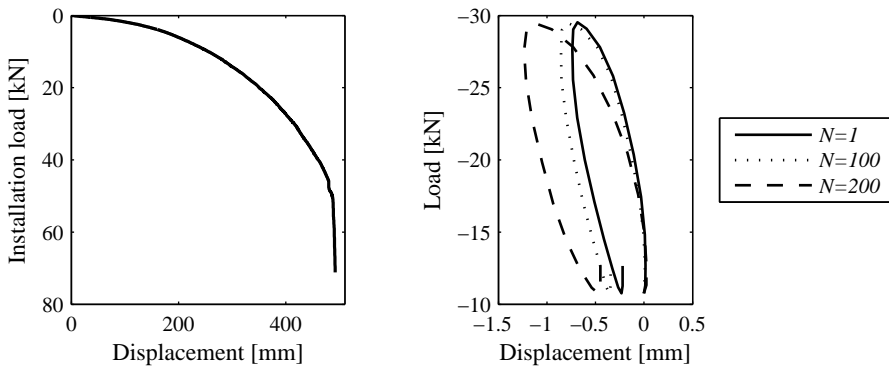


Figure G.155: Installation 13.03.11.

Figure G.156: Cyclic behaviour 13.03.11.

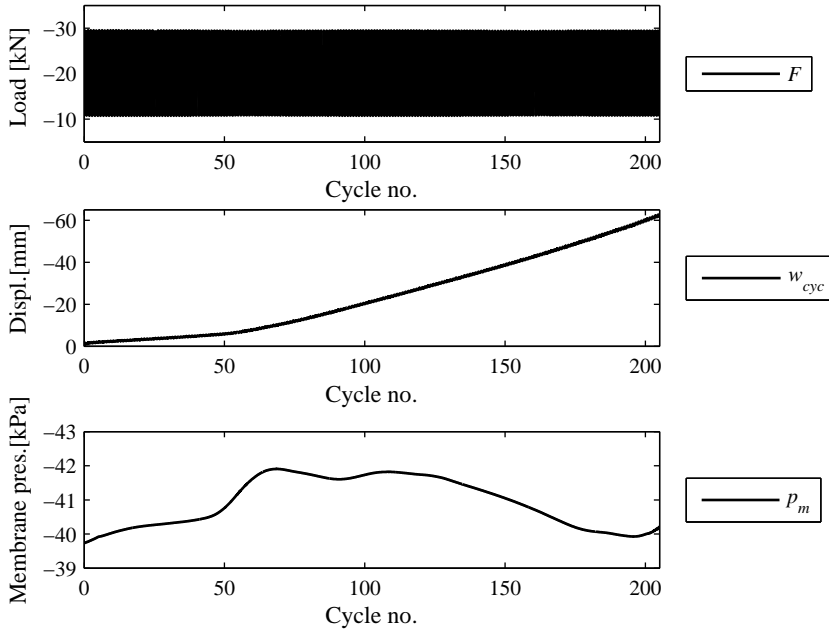


Figure G.157: Cyclic loading part 13.03.11.

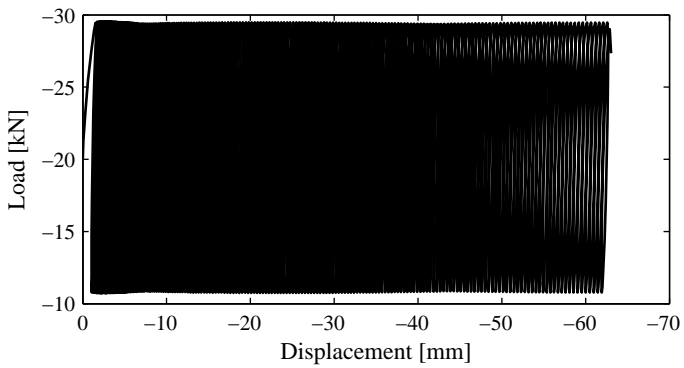


Figure G.158: Full loading vs. displacement 13.03.11.

G.4.10 Test 13.03.12

Soil properties			Loading		
D_R	[%]	(79)	F_{mean}	[kN]	-2.05
σ of D_R	[%]	-	F_{cyc}	[kN]	3.85
γ	[kN/m ³]	(19.3)	w_{cyc}	[mm]	-65.80
γ'	[kN/m ³]	(9.3)	f	[Hz]	0.10
Installation			f_s	[Hz]	2
F_P	[kN]	71.2	N	[-]	1,285
d_{inst}	[mm]	499	F_{Pc}	[kN]	-
Membrane pressure			w_{Pc}	[mm]	-
p_m	[kPa]	0	v	[mm/s]	-

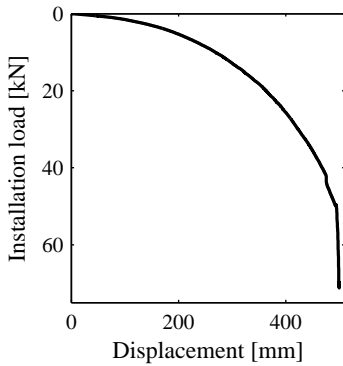


Figure G.159: Installation 13.03.12.

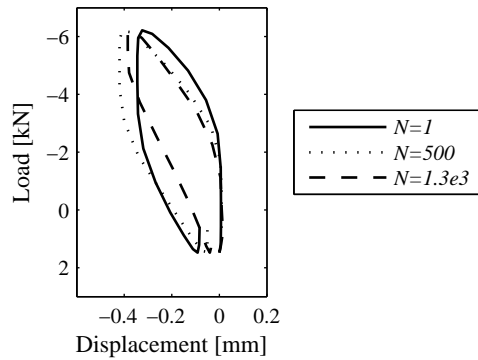


Figure G.160: Cyclic behaviour 13.03.12.

Comments:
 Pore pressure transducer PP2 did not function.

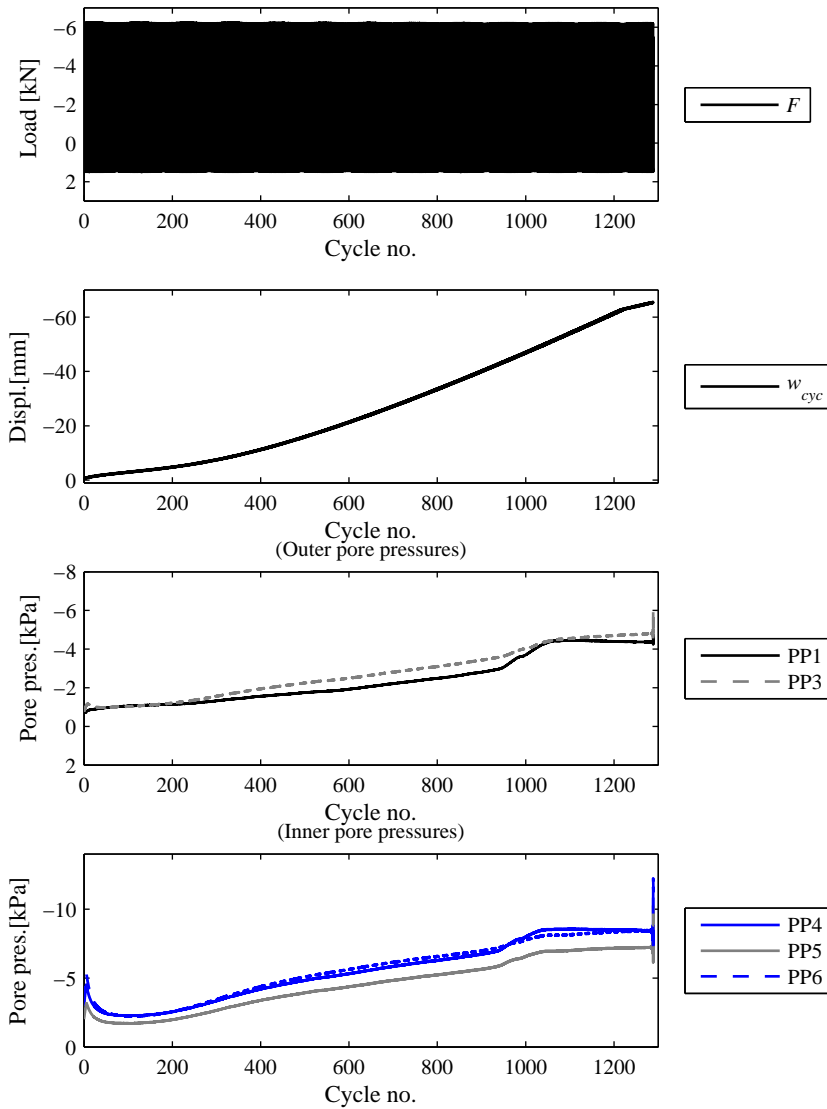


Figure G.161: Cyclic loading part 13.03.12.

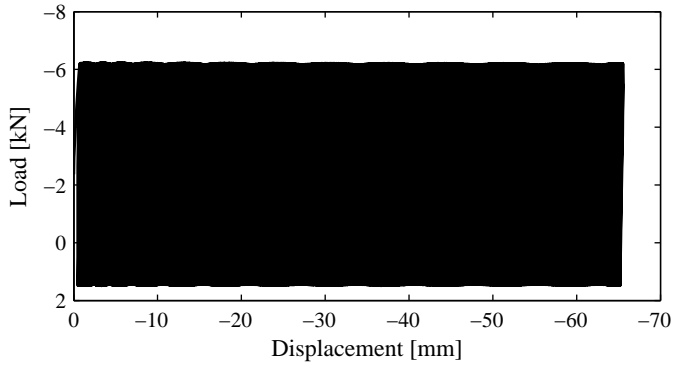


Figure G.162: Full loading vs. displacement 13.03.12.

G.4.11 Test 13.03.13

Soil properties			Loading		
D_R	[%]	82.4	F_{mean}	[kN]	2.01
σ of D_R	[%]	11.2	F_{cyc}	[kN]	29.38
γ	[kN/m ³]	19.5	w_{cyc}	[mm]	0.74
γ'	[kN/m ³]	9.5	f	[Hz]	0.05
Installation			f_s	[Hz]	2
F_P	[kN]	74.6	N	[-]	19,970
d_{inst}	[mm]	484	F_{Pc}	[kN]	-
Membrane pressure			w_{Pc}	[mm]	-
p_m	[kPa]	71.4	v	[mm/s]	-

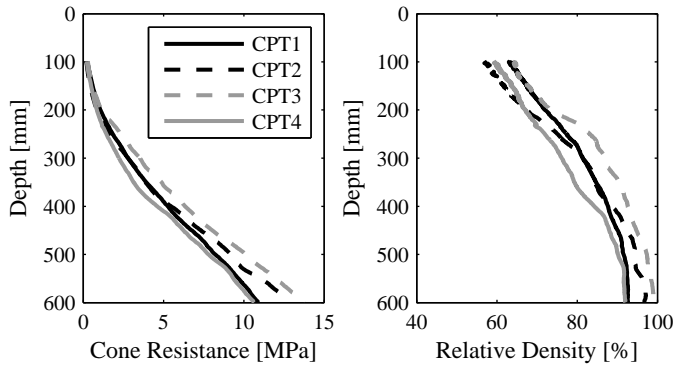


Figure G.163: CPT testing 13.03.13.

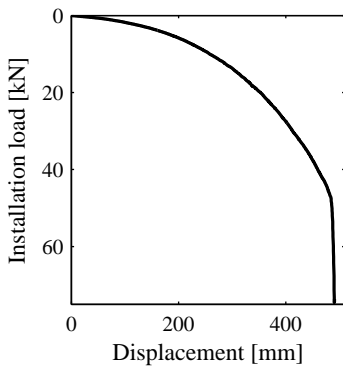


Figure G.164: Installation 13.03.13.

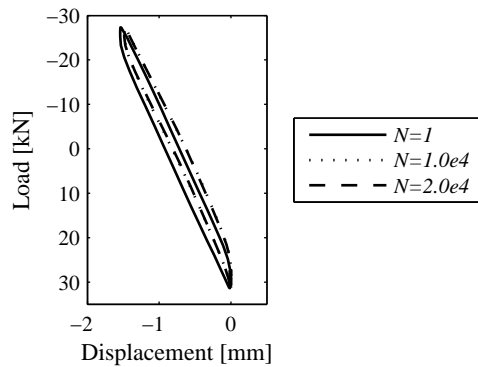


Figure G.165: Cyclic behaviour 13.03.13.

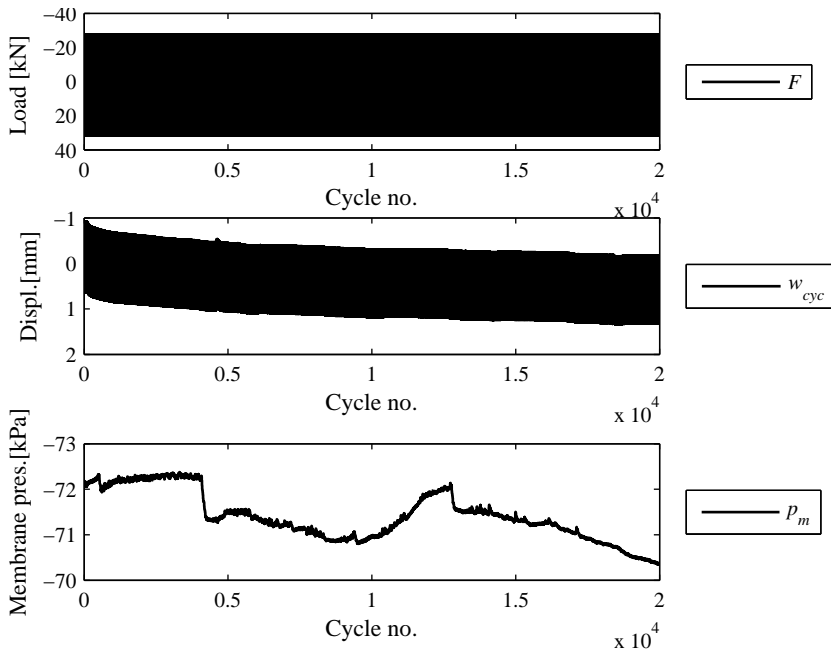


Figure G.166: Cyclic loading part 13.03.13.

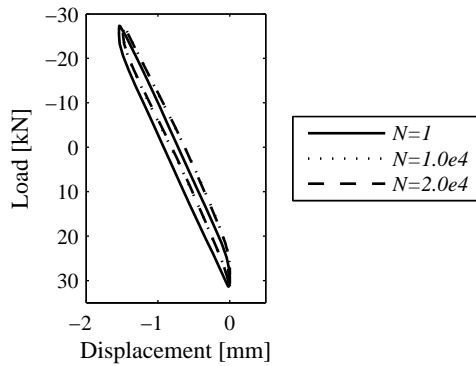


Figure G.167: Cyclic behaviour 13.03.13.

Comments:

Sand in the first 0.3-0.4 m was less dense than in the deeper layer. Probably, the soil was strongly disturbed due to another testing program in the same sand box and due to membrane pressure applications that create the upward gradient.

G.4.12 Test 13.03.14

Soil properties			Loading		
D_R	[%]	81.5	F_{mean}	[kN]	1.92
σ of D_R	[%]	9.8	F_{cyc}	[kN]	29.30
γ	[kN/m ³]	19.4	w_{cyc}	[mm]	1.25
γ'	[kN/m ³]	9.4	f	[Hz]	0.10
Installation			f_s	[Hz]	2
F_P	[kN]	73.3	N	[-]	40,867
d_{inst}	[mm]	491	F_{Pc}	[kN]	-93.26
Membrane pressure			w_{Pc}	[mm]	-28.29
p_m	[kPa]	70	v	[mm/s]	0.002

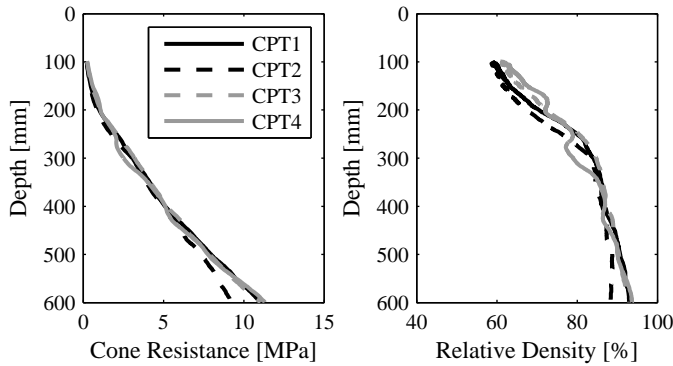


Figure G.168: CPT testing 13.03.14.

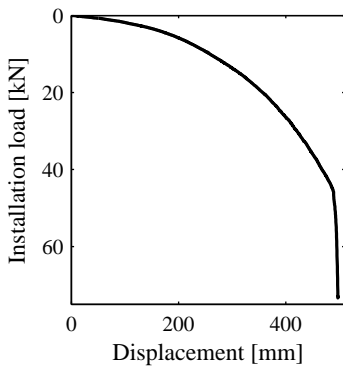


Figure G.169: Installation 13.03.14.

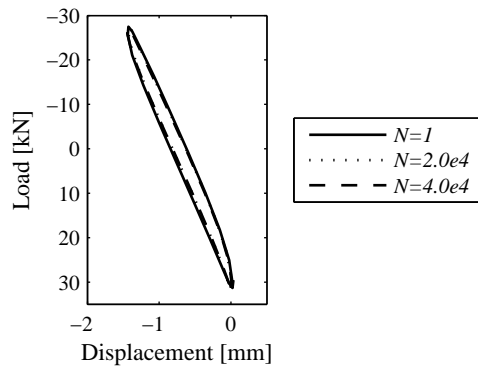


Figure G.170: Cyclic behaviour 13.03.14.

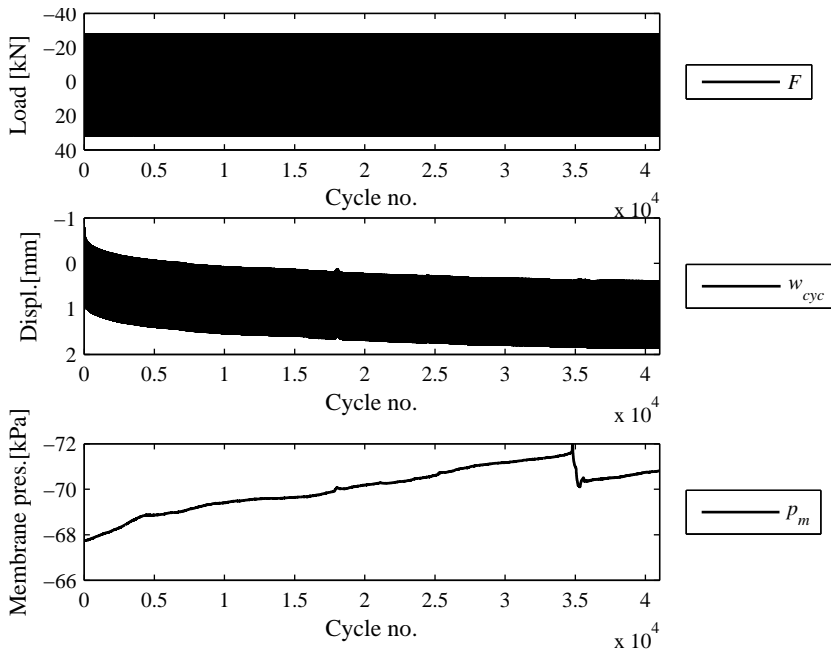


Figure G.171: Cyclic loading part 13.03.14.

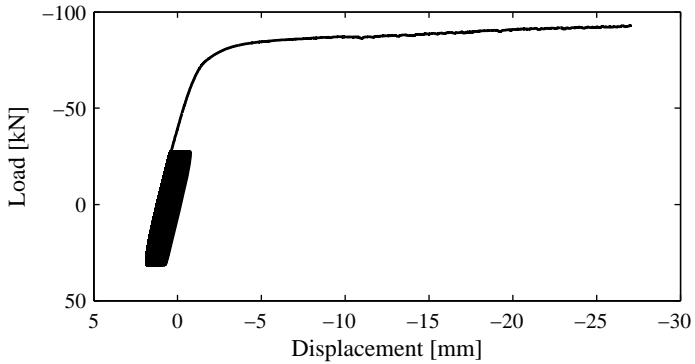


Figure G.172: Full loading vs. displacement 13.03.14.

Comments:

Sand in the first 0.3-0.4 m was less dense than in the deeper layer. Probably, the soil was strongly disturbed due to another testing program in the same sand box and due to membrane pressure applications that create the upward gradient.

G.4.13 Test 13.03.15

Soil properties			Loading		
D_R	[%]	87.1	F_{mean}	[kN]	-22.39
σ of D_R	[%]	6.8	F_{cyc}	[kN]	23.08
γ	[kN/m ³]	19.7	w_{cyc}	[mm]	0.10
γ'	[kN/m ³]	9.7	f	[Hz]	0.10
Installation			f_s	[Hz]	2
F_P	[kN]	83.1	N	[-]	31,619
d_{inst}	[mm]	492	F_{Pc}	[kN]	-93.90
Membrane pressure			w_{Pc}	[mm]	-26.53
p_m	[kPa]	73	v	[mm/s]	0.002

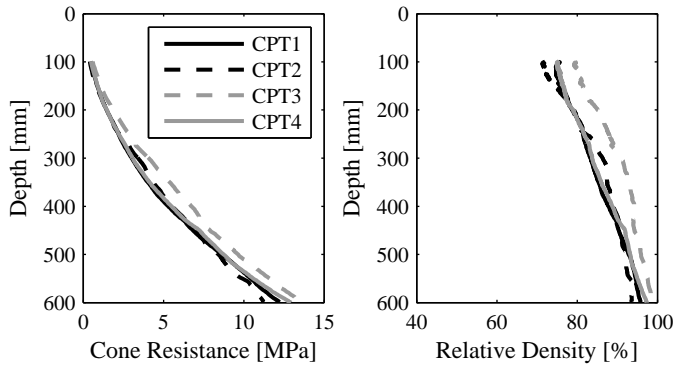


Figure G.173: CPT testing 13.03.15.

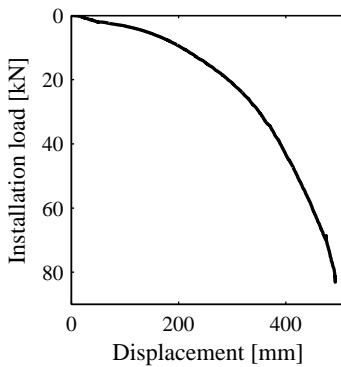


Figure G.174: Installation 13.03.15.

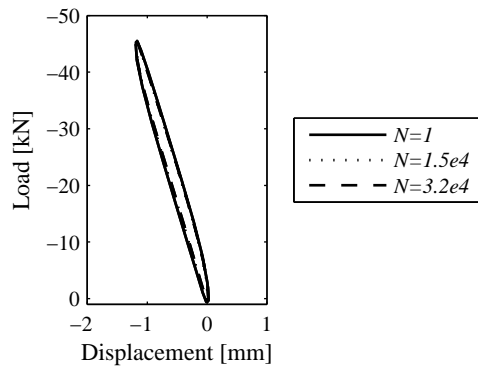


Figure G.175: Cyclic behaviour 13.03.15.

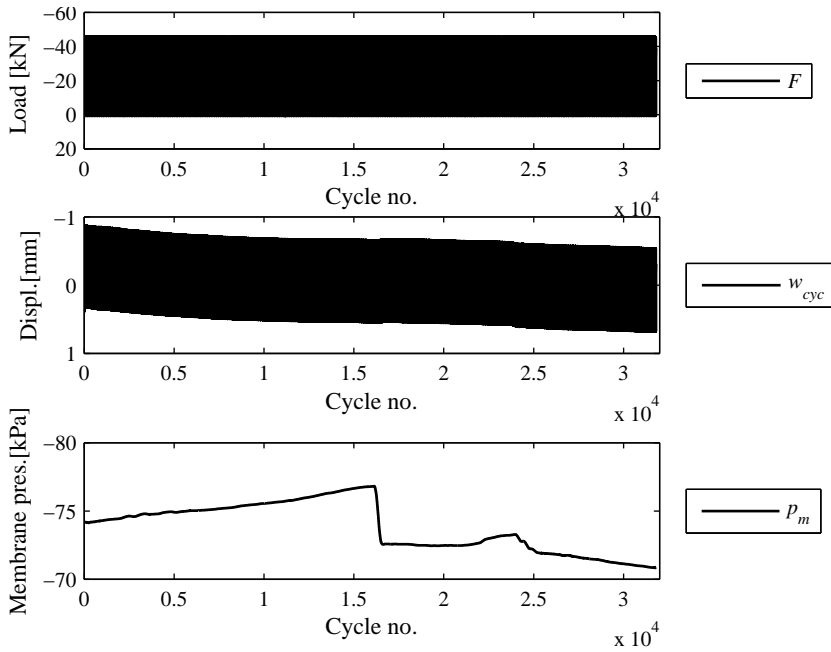


Figure G.176: Cyclic loading part 13.03.15.

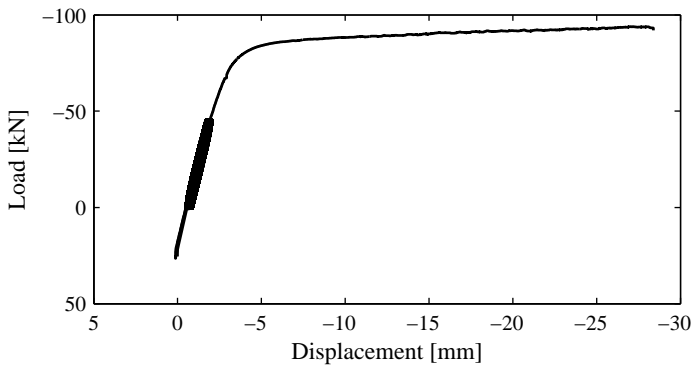


Figure G.177: Full loading vs. displacement 13.03.15.

G.4.14 Test 13.03.16

Soil properties			Loading		
D_R	[%]	79.3	F_{mean}	[kN]	-51.67
σ of D_R	[%]	10.1	F_{cyc}	[kN]	24.49
γ	[kN/m ³]	19.3	w_{cyc}	[mm]	-75.01
γ'	[kN/m ³]	9.3	f	[Hz]	0.10
Installation			f_s	[Hz]	2
F_P	[kN]	75.7	N	[-]	19,081
d_{inst}	[mm]	489	F_{Pc}	[kN]	-
Membrane pressure			w_{Pc}	[mm]	-
p_m	[kPa]	71	v	[mm/s]	-

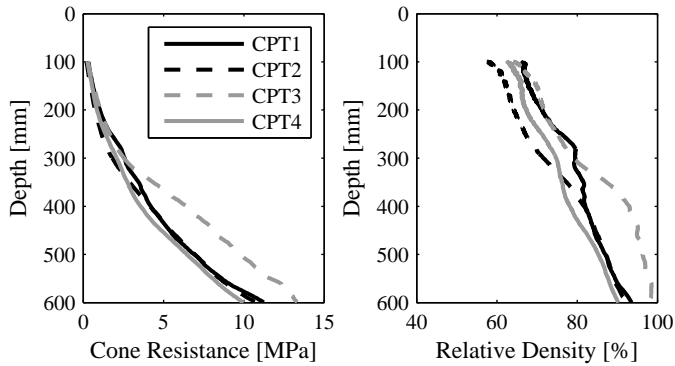


Figure G.178: CPT testing 13.03.16.

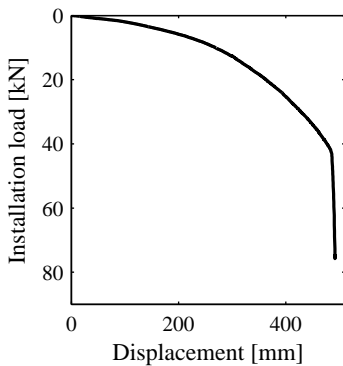


Figure G.179: Installation 13.03.16.

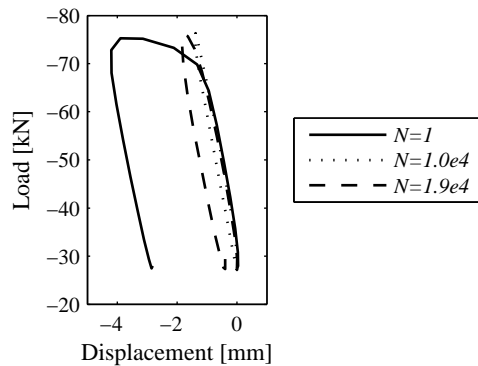


Figure G.180: Cyclic behaviour 13.03.16.

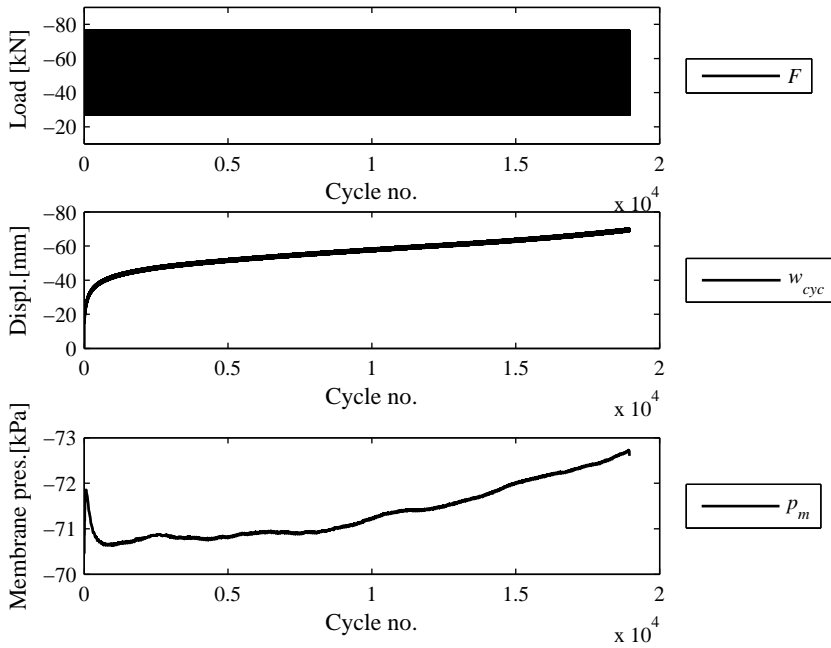


Figure G.181: Cyclic loading part 13.03.16.

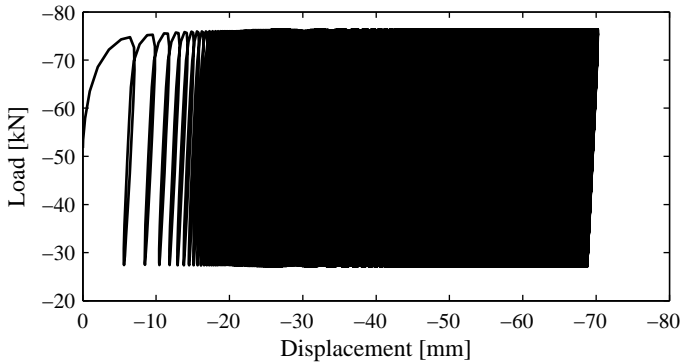


Figure G.182: Full loading vs. displacement 13.03.16.

Comments:

Sand in the first 0.3-0.4 m was less dense than in the deeper layer. Probably, the soil was strongly disturbed due to another testing program in the same sand box and due to membrane pressure applications that create the upward gradient.

G.4.15 Test 13.03.17

Soil properties			Loading		
D_R	[%]	81.2	F_{mean}	[kN]	-50.61
σ of D_R	[%]	7.8	F_{cyc}	[kN]	45.78
γ	[kN/m ³]	19.4	w_{cyc}	[mm]	-81.90
γ'	[kN/m ³]	9.4	f	[Hz]	0.10
Installation			f_s	[Hz]	2
F_P	[kN]	74	N	[-]	5
d_{inst}	[mm]	489	F_{Pc}	[kN]	-
Membrane pressure			w_{Pc}	[mm]	-
p_m	[kPa]	71	v	[mm/s]	-

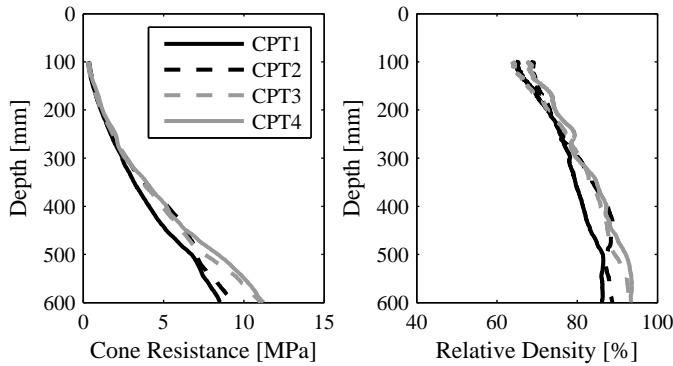


Figure G.183: CPT testing 13.03.17.

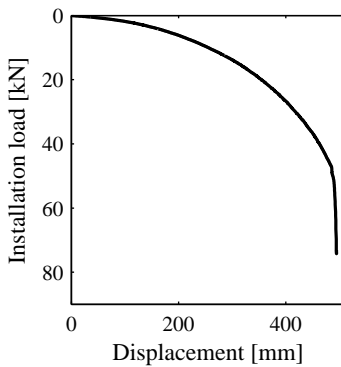


Figure G.184: Installation 13.03.17.

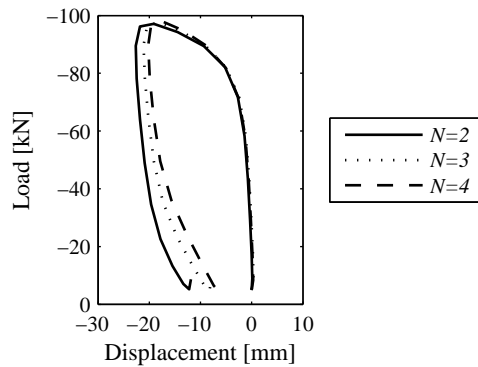


Figure G.185: Cyclic behaviour 13.03.17.

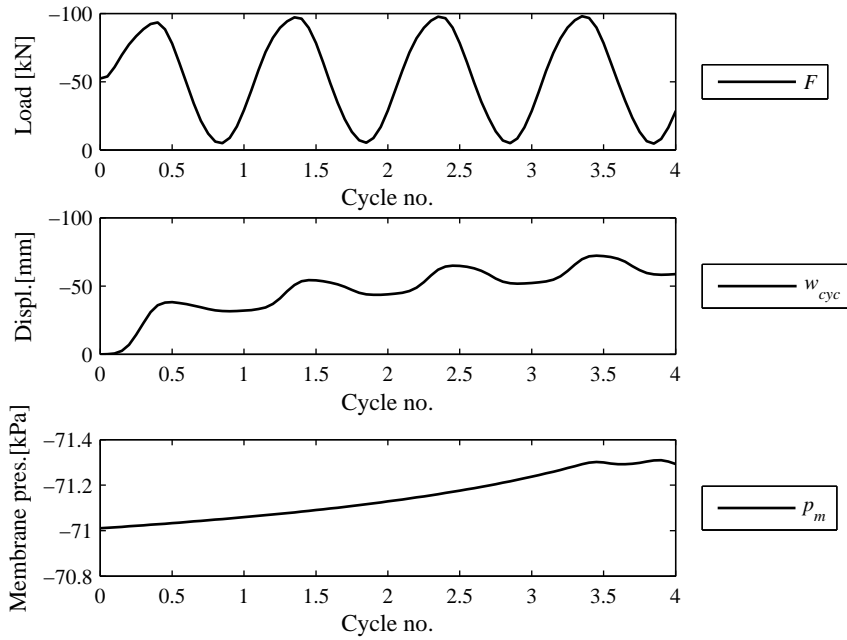


Figure G.186: Cyclic loading part 13.03.17.

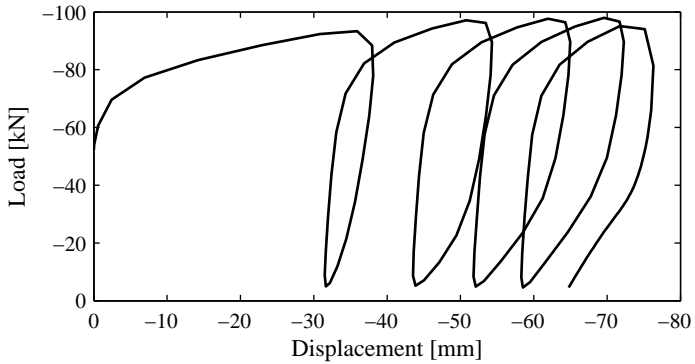


Figure G.187: Full loading vs. displacement 13.03.17.

Comments:

Sand in the first 0.3-0.4 m was less dense than in the deeper layer. Probably, the soil was strongly disturbed due to another testing program in the same sand box and due to membrane pressure applications that create the upward gradient.

G.4.16 Test 13.03.19

Soil properties			Loading		
D_R	[%]	79.0	F_{mean}	[kN]	-0.30
σ of D_R	[%]	8.8	F_{cyc}	[kN]	1.66
γ	[kN/m ³]	19.3	w_{cyc}	[mm]	-0.64
γ'	[kN/m ³]	9.3	f	[Hz]	0.10
Installation			f_s	[Hz]	2
F_P	[kN]	(72.5)	N	[-]	39,729
d_{inst}	[mm]	(488)	F_{Pc}	[kN]	(-3.49)
Membrane pressure			w_{Pc}	[mm]	-8.66
p_m	[kPa]	0	v	[mm/s]	0.002

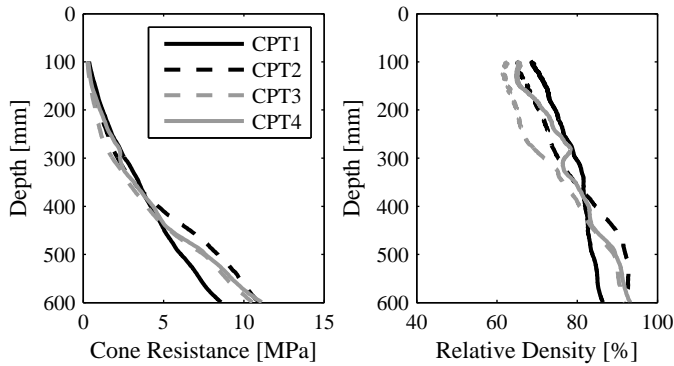


Figure G.188: CPT testing 13.03.19.

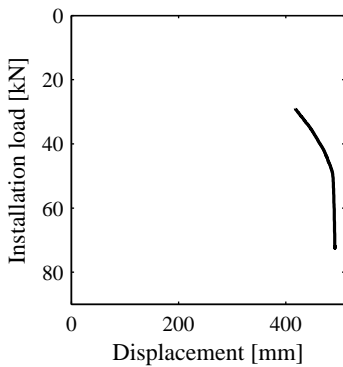


Figure G.189: Installation 13.03.19.

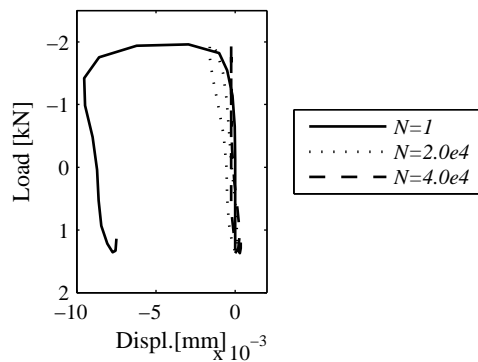


Figure G.190: Cyclic behaviour 13.03.19.

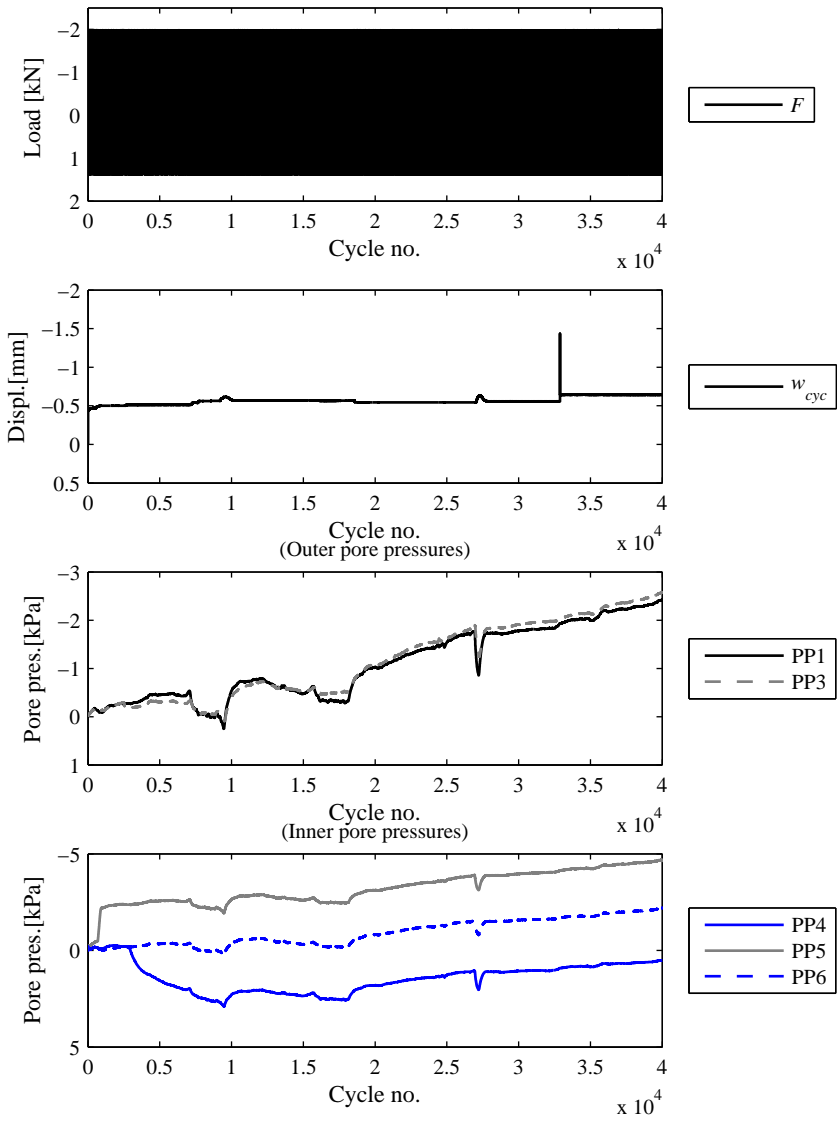


Figure G.191: Cyclic loading part 13.03.19.

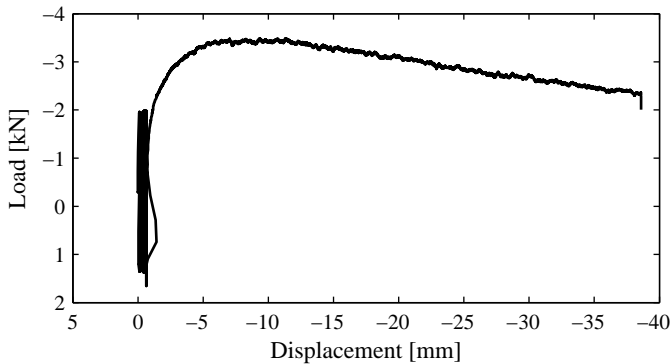


Figure G.192: Full loading vs. displacement 13.03.19.

Comments:

Only the last part of installation was recorded. Problems in data sampling caused by an error in the data acquisition system: load and displacement signals were not taken at the very same moment. Thus, cyclic behaviour cannot be assessed precisely. Sand in the first 0.3-0.4 m was less dense than in the deeper layer. Probably, the soil was strongly disturbed due to another testing program in the same sand box and due to membrane pressure applications that create the upward gradient. Post-cyclic pull-out should be ignored, because it was interrupted at the very beginning. Possible problems with pore pressure transducer calibration (settings in the computer program).

G.4.17 Test 13.03.20

Soil properties			Loading		
D_R	[%]	81.3	F_{mean}	[kN]	1.80
σ of D_R	[%]	11.7	F_{cyc}	[kN]	3.85
γ	[kN/m ³]	19.4	w_{cyc}	[mm]	0
γ'	[kN/m ³]	9.4	f	[Hz]	0.10
Installation			f_s	[Hz]	2
F_P	[kN]	69.2	N	[-]	39,980
d_{inst}	[mm]	490	F_{Pc}	[kN]	-4.85
Membrane pressure			w_{Pc}	[mm]	-1.30
p_m	[kPa]	0	v	[mm/s]	0.002

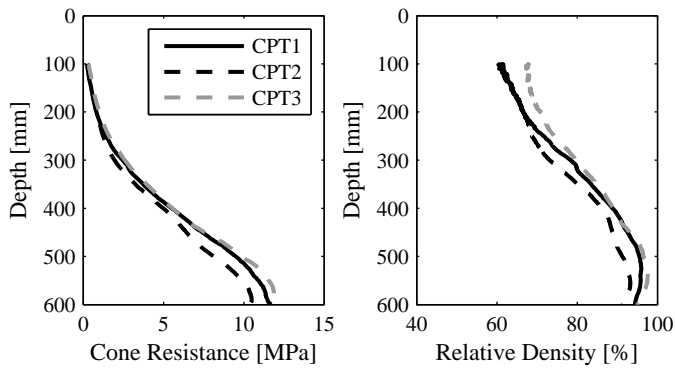


Figure G.193: CPT testing 13.03.20.

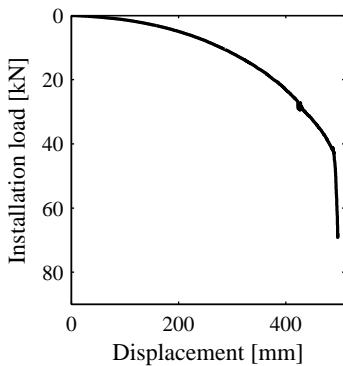


Figure G.194: Installation 13.03.20.

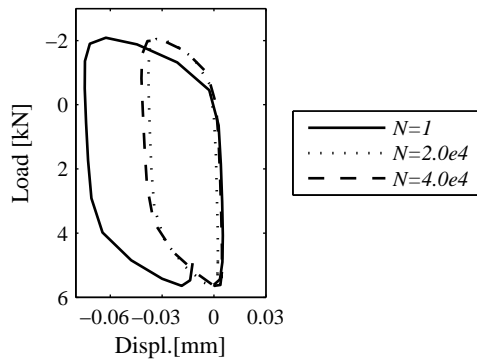


Figure G.195: Cyclic behaviour 13.03.20.

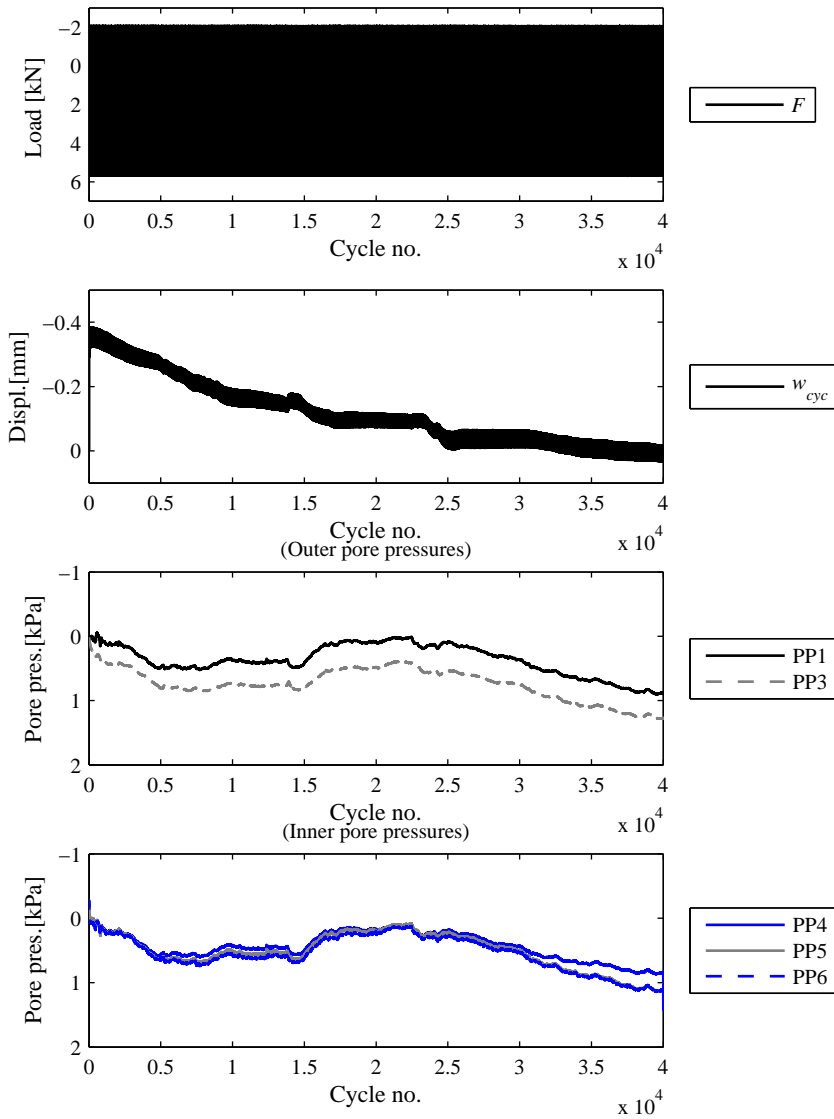


Figure G.196: Cyclic loading part 13.03.20.

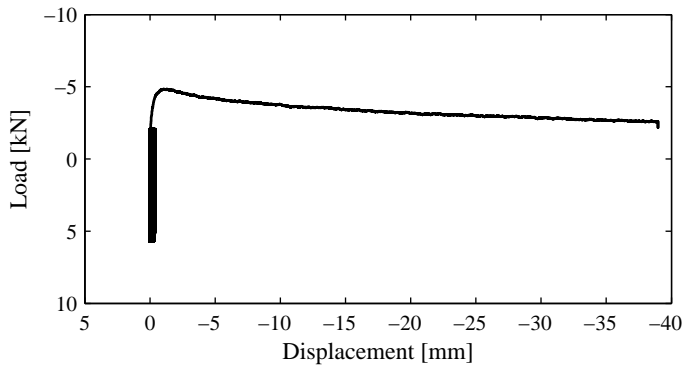


Figure G.197: Full loading vs. displacement 13.03.20.

Comments:

Sand in the first 0.3-0.4 m was less dense than in the deeper layer. Probably, the soil was strongly disturbed due to another testing program in the same sand box and due to membrane pressure applications that create the upward gradient.

G.4.18 Test 13.03.21

Soil properties			Loading		
D_R	[%]	80.5	F_{mean}	[kN]	0
σ of D_R	[%]	11.1	F_{cyc}	[kN]	1.00
γ	[kN/m ³]	19.4	w_{cyc}	[mm]	-0.29
γ'	[kN/m ³]	9.4	f	[Hz]	0.10
Installation			f_s	[Hz]	2
F_P	[kN]	(70)	N	[-]	40,020
d_{inst}	[mm]	(490)	F_{Pc}	[kN]	-4.86
Membrane pressure			w_{Pc}	[mm]	-4.84
p_m	[kPa]	0	v	[mm/s]	0.002

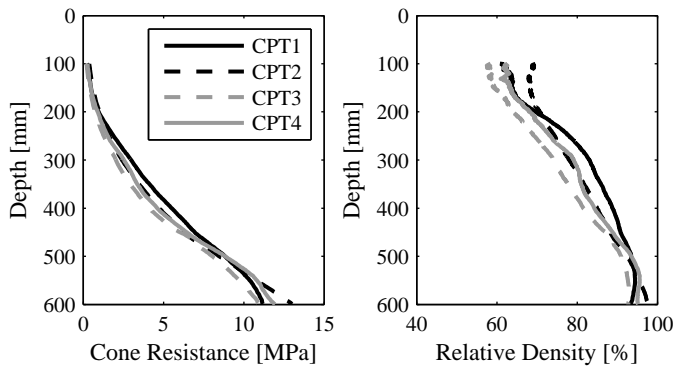


Figure G.198: CPT testing 13.03.21.

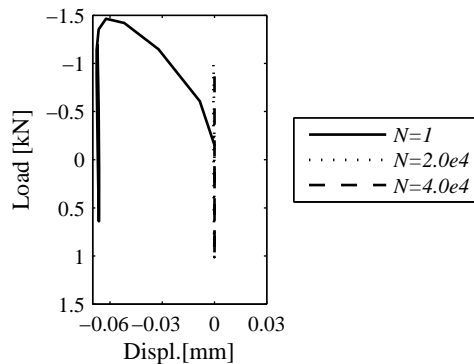


Figure G.199: Cyclic behaviour 13.03.21.

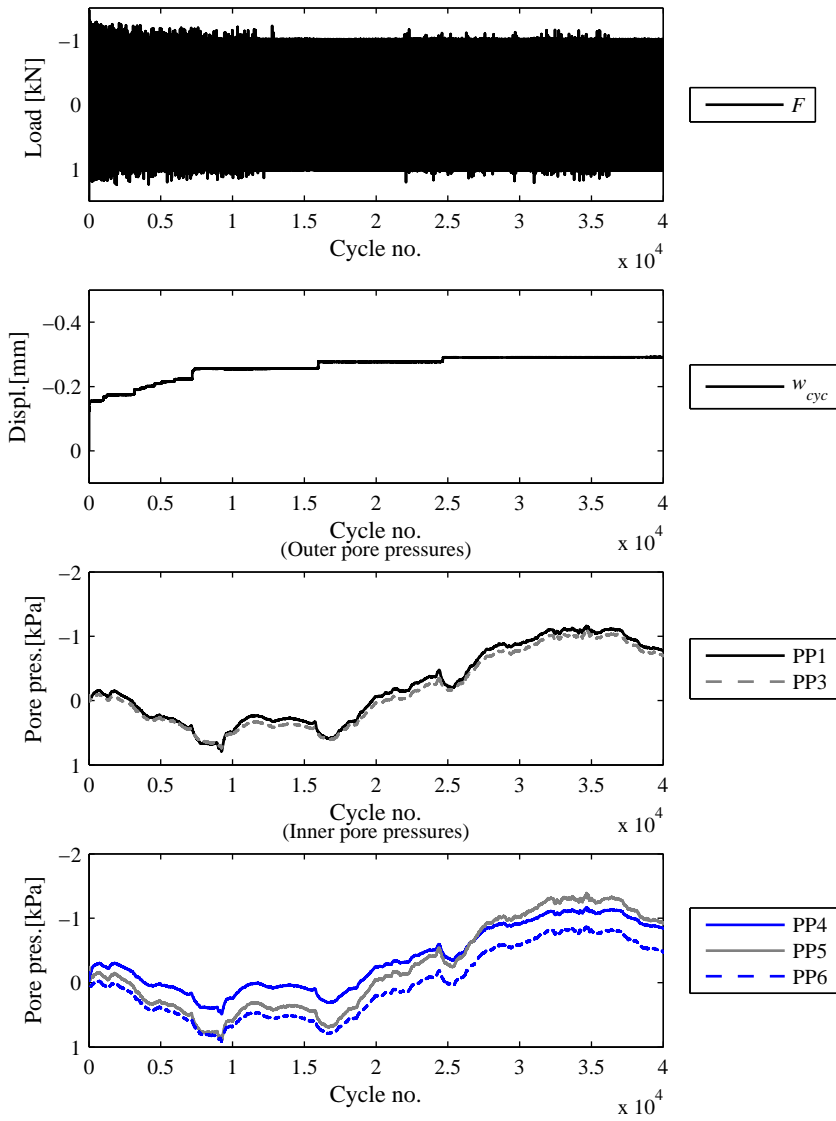


Figure G.200: Cyclic loading part 13.03.21.

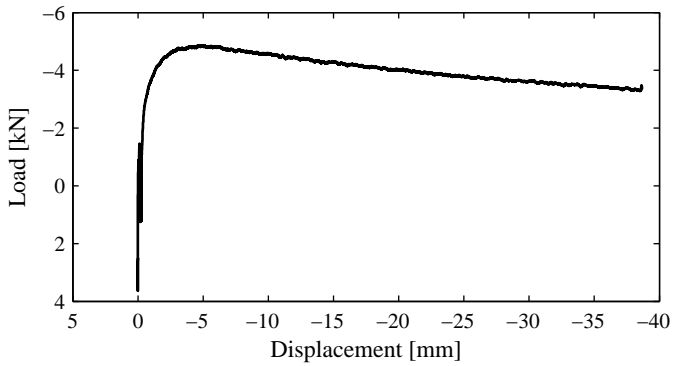


Figure G.201: Full loading vs. displacement 13.03.21.

Comments:

Sand in the first 0.3-0.4 m was less dense than in the deeper layer. Probably, the soil was strongly disturbed due to another testing program in the same sand box and due to membrane pressure applications that create the upward gradient.

Bibliography

- Hedegaard, J. and Borup, M. (1993). *Klassifikationsforsøg med Baskarp Sand No. 15*. Aalborg University Center, Aalborg University, Denmark.
- Ibsen, L.B. and Bødker, L. (1994). *Baskarp Sand No. 15: data report 9301*. Geotechnical Engineering Group, Aalborg University, Denmark.
- Sørensen, S.P.H. and Ibsen, L.B. (2012). Experimental comparison of non-slender piles under static loading and under cyclic loading in sand. *Proceedings of the 22nd International Ocean and Polar Engineering Conference*.
- Vaitkunaite, E. (2015). *Test Procedure for Axially Loaded Bucket Foundations in Sand (Large Yellow Box)*. Department of Civil Engineering, Aalborg University, Denmark. DCE Technical Memorandum no. 51, ISSN 1901-7278.

SUMMARY

Compared to oil and gas structures, marine renewable energy devices are usually much lighter, operate in shallower waters and are subjected to severe cyclic loading and dynamic excitations. These factors result in different structural behaviours. Bucket foundations are a potentially cost-effective solution for various offshore structures, and not least marine renewables.

The present thesis focuses on several critical design problems related to the behaviour of bucket foundations exposed to tensile loading. Among those are the soil-structure interface parameters, tensile loading under various displacement rates and tensile cyclic loading.

A new laboratory testing facility is constructed allowing large scale foundation model testing under long-term cyclic loadings. Another test set-up - a pressure tank – is employed for the displacement rate analysis. The extensive testing campaign provides valuable data about the effects of tensile loading.